EINSTEIN X-RAY OBSERVATIONS OF GALAXIES

by

VAUGHAN JOHN STANGER

Thesis submitted to the University of Leicester

for the degree of Doctor of Philosophy

February 1985

X-ray Astronomy Group
Department of Physics
University of Leicester

ProQuest LLC
789 East Eisenhower Parkway
P.O. Box 1346
Ann Arbor, MI 48106-1346


UNIVERSITY LIBRARY LEICESTER

Declaration

I hereby declare that no part of this thesis has been previously submitted to this or any other University as part of the requirement for a higher degree. The work described herein was conducted by the undersigned except for the contributions from colleagues and other workers which are acknowledged in the text, and in the following note on publications.

V.J. Stanger

February 1985

Publications

Some of the work reported in this thesis has either been published or submitted for publication elsewhere, as follows:

Watson, M.G., Stanger, V.J., Griffiths, R.E., 1984, Ap.J., 286, 144. "X-ray Emission from M82". (Chapter Three).

Stanger, V.J., Schwarz, J., 1984, Submitted to Ap.J. "The X-ray Properties of Early Type Galaxies". (Chapters Four and Five).

Stanger, V.J., Warwick, R.S., Schwarz, J., 1984, Proceedings of Symposium X-ray Astronomy '84, in press. "High Resolution X-ray and Radio Maps of the Giant Elliptical Galaxies NGC 4636 and NGC 4649". (Chapter Six).

This thesis is dedicated to

Mum, Dad

and

All who helped

Acknowledgements

Many people, by way of practical advice or simple encouragement, have in some way contributed to this thesis and the work it contains; it is a pleasure to express my thanks to all concerned. Mike Watson deserves particular credit; three years ago he took pity on a confused and somewhat naive postgraduate student, and showed him a few intriguing pictures of M82. Mike was thus directly responsible for stimulating the research interests which are reflected in this work, and I have benefited considerably from his continued interest in my subsequent activities. Bob Warwick, my supervisor, also provided a great deal of practical advice during the course of my research; furthermore, he successfully negotiated the thankless task of reading the preliminary drafts of this thesis, which without his thoughtful criticism would never have been completed satisfactorily.

Much of the work presented herein was initiated during a two month visit to the Harvard-Smithsonian Center for Astrophysics during the winter of 1982/83. It is a pleasure to acknowledge the generous help and support provided by everyone at CFA, particularly Joe Schwarz - who acted as my guide and mentor throughout - and also Martin Elvis and Pepi Fabbiano.

Thanks are also due to Dick Willingale for some fine software and valuable advice on many aspects of data analysis, Kev Poyner for a great deal of help with various recalcitrant computers, Ian McHardy for help with the analysis of VLA data, Bob Hall for moral support and some regrettably unpublishable jokes, Rosemary Littler for help with diagrams, and in particular Sharon Hood for her colossal typing efforts.

Finally, sincere thanks are due to Ken Pounds for allowing me to pursue my research project within the X-ray Astronomy Group, and also to the SERC for financing my research studentship.

Abstract

The high sensitivity and precise imaging provided by the Einstein Observatory instrumentation has enabled detailed X-ray studies of a variety of astrophysical phenomena to be performed. In this thesis Einstein observations are used to investigate the characteristic X-ray properties of galaxies, thus allowing a galaxy's X-ray emission to be related to the properties and evolution of its stellar population(s).

Analysis of Einstein HRI data for M82 - an archetypal peculiar galaxy - reveals complex structure both in the "starburst" nuclear region and in the galaxy's halo. The nuclear region's X-ray morphology corresponds closely with Population I optical features, thus linking the emission directly to the intense star formation activity. Moreover, the halo of diffuse X-ray emission distributed along the minor axis of M82 indicates thermal emission from outflowing hot gas, which is maintained by starburst-induced supernova heating; rapid cooling near shock fronts probably causes the observed correlation with the famous Hα filament system.

The majority of this thesis is devoted to an investigation of the X-ray properties of early type galaxies. Analysis of luminosity correlations displayed by the class as a whole, complemented by detailed studies of individual galaxies, confirms previous suggestions that for many early type galaxies, thermal emission from hot gas is the dominant X-ray emission mechanism. Supernova-driven hot winds keep some galaxies essentially gas free; their X-ray emission originates principally from stellar sources. In other galaxies hot gas generated by stellar evolution is retained and possibly incorporated into cooling flows. High resolution X-ray and radio

studies of NGC 4636 and NGC 4649 confirm that cooling flow scenarios are viable for the central regions of both galaxies, thus explaining the fueling of the observed radio sources.

Finally, the possibilities for further research presented by both current and future observational facilities are discussed.

Contents

CHAPTER ONE : INTRODUCTION

1.1 A Historical Perspective

Prior to the launch of the Einstein Observatory in 1978, and the consequent 1000-fold improvement in source detection sensitivity due to the use of imaging X-ray optics and detectors, the study of the X-ray properties of normal galaxies was essentially restricted to observations of the various discrete sources which contribute to the integrated X-ray luminosity of our own galaxy and the Magellanic Clouds. Almost without exception the identified extragalactic X-ray sources in the Uhuru and Ariel 5 catalogues (Forman et al. 1978, McHardy et al. 1981) are either active galactic nuclei or clusters of galaxies. Of all the individual galaxies detected in these early surveys only M31 and M82 could not reasonably be classified as AGNs. This essentially negative result was important, however, because it established an effective upper limit to the X-ray luminosity associated with the stellar population(s) and associated diffuse matter of a typical (ie. normal) galaxy. The failure to detect normal galaxies located within a sphere bounded by the Virgo Cluster at a typical survey's flux limit of $\sim 3 \times 10^{-11}$ erg $cm^{-2} s^{-1}$ implied characteristic X-ray luminosities $\lesssim 10^{42}$ erg s^{-1}. This result is not in any way surprising; the 2-10 keV luminosity of our own spiral galaxy, estimated by integrating the contributions from known discrete X-ray sources, is only $\sim 2 \times 10^{39}$ erg s^{-1} (e.g. Long and Van Speybroeck 1983).

The importance of the increase in sensitivity of the Einstein instrumentation relative to its predecessors is almost impossible to

over-emphasize. A typical Einstein observation attained a source detection sensitivity corresponding to a 0.2-4.0 keV flux of $\sim 1 \times 10^{-13}$ erg cm^{-2} s^{-1}, which is similar to the predicted flux from a galaxy identical to our own situated in the Virgo Cluster ($D \sim 15$ Mpc). With this quantum leap in sensitivity the study of the X-ray properties of normal galaxies, both as a class and as individual objects, becomes feasible.

Before its demise in 1981 Einstein observed several hundred individual galaxies, including examples of both "normal" and "active" species. The research reported in this thesis was performed during the period 1982 to 1984 and forms a part of a long-standing collaboration between members of the Leicester University X-ray Astronomy Group and the Harvard-Smithsonian Center for Astrophysics (a member group of the Einstein Observatory consortium). A large proportion of the relevant Einstein observations were unavailable for use in this research project. Instead of attempting a widely based study of all types of galaxy, we have restricted our attention to a rather limited sample of normal and mildly active galaxies which belong to specific morphological categories. Our principal aims are to determine the basic X-ray properties of these galaxies; examine the relationship between their X-ray emission and the fundamental properties of their stellar populations; and to perform detailed, high resolution studies of a few individual galaxies of particular interest.

On what basis should we select galaxies for inclusion in this study? As we have already noted, the availability of suitable data has proved to be the primary consideration. A more fundamental selection problem

does exist, however; namely, to what extent can we distinguish between "normal" and "active" galaxies? The standard definition for a normal galaxy envisages an ensemble of $\gtrsim 10^8$ stars plus associated diffuse matter (gas and dust) which has evolved by thermal equilibrium processes in a gravitationally stable configuration. In contrast, a galaxy is active if it exhibits non-thermal radiative phenomena and/or evidence of gravitational disequilibrium. A significant fraction of all galaxies are therefore active, with the classical AGNs occupying the extreme end of the activity scale. Since we are hoping to study the relationship between the X-ray properties of a galaxy and the properties of its stellar population(s) and interstellar medium, it is obviously sensible to exclude galaxies which have a large fraction of their X-ray luminosity generated by a single nuclear source. Seyfert I galaxies are therefore excluded, as are all other classical AGNs. In contrast, a galaxy like M82, which displays an unusual morphology and radiates copious quantities of non-thermal emission, falls within the compass of this thesis because it lacks a dominant nuclear X-ray source.

Although the results presented in this thesis do not impinge directly upon the observed properties and derived physics of AGNs, it is important to remember that in recent years the distinction between normal and active galaxies has started to blur. It is increasingly evident that a broad and continuous spectrum of activity exists among galaxies, with the classical normal galaxies and AGNs at the extremes of the distribution. Several examples exist of morphologically normal galaxies with very modest X-ray luminosities which display optical characteristics usually associated with Seyfert nuclei and QSOs (Elvis

and Van Speybroeck 1982, Elvis et al. 1984). These micro-quasars or mini-AGNs may eventually prove to be common, indicating that the AGN phenomenon spans many decades of luminosity. We should not exclude the possibility that all galaxies undergo one or more active phases during their evolution.

1.2 Pre-Einstein Results

As we have already noted, normal and weakly active galaxies are almost entirely absent from the Uhuru and Ariel 5 X-ray source catalogues. There are, however, several observational results from the pre-Einstein era which have considerable bearing on the characteristic X-ray properties of galaxies.

The principal result is rather obvious, as is its implication, although they are both still worth stating. Our galaxy contains $\sim$200 discrete X-ray sources at or above the sensitivity limit of the 4U catalogue (Forman et al. 1978). X-ray surveys of galactic sources are complete above a 2-10 keV luminosity of 5×10^{36} erg s^{-1}, so the high luminosity region of the X-ray source luminosity function for our galaxy is reasonably well established. Many of these high luminosity sources are members of binary star systems and are inferred to be very compact on the basis of their short timescale X-ray variability. Compact sources can crudely be separated into two categories; some are objects associated with old, low-mass Population II stars, located in the galactic bulge region or in globular clusters; the remainder are associated with high mass extreme Population I stars, located in the star-forming regions of spiral arms. Supernova remnants, specifically the ISM material swept up and heated to X-ray emitting temperatures by

the passage of a SN shock wave, are a further class of persistent galactic X-ray source. The handful of X-ray sources detected in the SMC and LMC share similar X-ray properties with the equivalent high luminosity objects in our galaxy (Clark et al. 1978, Bradt and McClintock 1983). It is therefore reasonable to assume that because the various classes of X-ray binaries and SNRs are the result of normal stellar evolution processes, they will contribute some fraction of the X-ray luminosity of all galaxies. Indeed, one might naively assume that such objects would be the only significant contributors to the X-ray luminosity of a galaxy which does not exhibit AGN characteristics. The X-ray observations presented in this thesis allow us to test this hypothesis, and to demonstrate that it is invalid for at least some galaxies.

A second highly significant result concerns X-ray emission from clusters of galaxies; at least 45 of which are known to be the counterparts of 4U sources. Analysis of these non-imaging observations indicated the presence of extended X-ray emission with a scale size similar to the optical size of the cluster (eg. Lea et al. 1973), but with a total luminosity greatly exceeding that predicted from integrating the likely contributions from individual member galaxies. Cluster X-ray spectra have been shown to be consistent with thermal bremsstrahlung emission from plasmas with temperatures between 2×10^7 K and 1×10^8 K. The detection of iron emission lines at 6.7 keV has proved that the plasma element abundances are near-solar, and hence the bulk of this hot intra-cluster medium has been reprocessed via stellar evolution within individual galaxies (eg. Serlemitsos et al. 1977). The discovery that hot, reprocessed plasma pervades the

gravitational potential well of a typical cluster raised the possibility that a similar situation, albeit on a much smaller scale, might exist within individual galaxies. Could a significant proportion of the X-ray emission from a normal galaxy be due to gravitationally confined hot plasma? Partial support for this idea came from the discovery of a hot phase within the interstellar medium of our own galaxy (eg. Shapiro and Field 1976, Fried et al. 1980). The vastly improved sensitivity and higher angular resolution of the Einstein instrumentation allows the possibility that individual galaxies have accumulated substantial quantities of hot gas to be addressed in detail for the first time.

1.3 Einstein Results

It is not intended that this section should provide a detailed review of the history of X-ray astronomy in the Einstein era. Nevertheless, we consider it worthwhile to highlight certain important observational results and briefly establish their significance in relation to the properties of normal galaxies.

1.3.1 Resolved X-ray Sources in Nearby Galaxies

For galaxies situated within the Local Group, Einstein observations enable detailed X-ray source surveys to be performed with a sensitivity comparable to the Uhuru and Ariel 5 surveys of sources within our galaxy. A significant fraction of the high luminosity sources observed in the Local Group spiral galaxies are associated with Population I dominated regions, eg. HII regions within spiral arms; while others, particularly those associated with the bulge region of M31, are probably older Population II objects (Long and Van Speybroeck 1983). Among the well studied galaxies the observed number

of high luminosity X-ray sources ($L_X \gtrsim 10^{37}$ erg s^{-1}) scales linearly with galactic mass, and the number of sources of a given type is consistent with the proportion of total galactic mass contributed by its parent stellar population. The obvious implication, which should apply to all galaxies, is that the evolution of a specific stellar population will yield a characteristic set of discrete X-ray sources, which will contribute some fraction of the integrated X-ray luminosity of the galaxy which contains that population. On this basis, we would not expect to find high mass Population I binaries contributing significantly to the X-ray luminosity of an old, Population II dominated system (eg. an elliptical galaxy).

1.3.2 The Normal Galaxy Survey

Long and Van Speybroeck (1983) examined a representative sample of ~70 morphologically normal galaxies. Although these authors did not attempt a detailed analysis, they did identify a reasonably well defined correlation between X-ray and optical luminosities, with no compelling evidence for a strong dependence on galaxy type. The existence of this correlation provides firm evidence that the X-ray properties of a normal galaxy are directly linked to the properties and evolution of its stellar component.

1.3.3 The X-ray Properties of Peculiar Galaxies

Fabbiano et al. (1982) examined a sample of 33 galaxies which possess abnormal colours and morphologies but lack AGN characteristics. As well as the predictable correlation between X-ray and optical luminosities, this sample of peculiar galaxies also exhibited an even stronger correlation between X-ray and radio luminosities. This,

coupled with their abnormally blue colours and high values of L_X/L_V, has been interpreted as evidence for the occurrence of intense bursts of star formation in these galaxies, resulting in an excess of Population I X-ray sources.

1.3.4 X-ray Emission from Main Sequence Stars

Einstein observations have clearly established that main sequence stars are a pervasive class of low luminosity X-ray sources (Vaiana et al. 1981). Coronal X-ray emission has been detected from stars along the entire main sequence. Early type stars have X-ray luminosities in the range 10^{31} - 10^{34} erg s^{-1}, whereas late type stars exhibit much lower luminosities, ie. 10^{26} - 10^{30} erg s^{-1}. The X-ray luminosity function for normal stars is not currently well established, but it is plausible that low mass dwarfs could contribute significantly to the integrated X-ray luminosity of a normal galaxy. An ad-hoc population of $\sim 10^{11}$ K-type dwarfs, each having $L_X \sim 3 \times 10^{27}$ erg s^{-1} (eg. Vaiana et al. 1981), could generate $\sim 3 \times 10^{38}$ erg s^{-1} of integrated X-ray luminosity, ie. $\sim$10% of the X-ray luminosity of our own galaxy.

1.3.5 X-ray Haloes Associated with Galaxies in Clusters

One of the most important and striking Einstein results has been the discovery that several early type galaxies situated near the core regions of rich clusters are surrounded by extended haloes of X-ray emission (Forman et al. 1979, Bechtold et al. 1983). Their high luminosity ($\sim 10^{41}$ erg s^{-1}), physical extent ($\gtrsim$ 10 kpc) and lack of direct association with powerful radio sources argues against non-thermal emission mechanisms; thermal bremsstrahlung from a hot plasma is the most likely origin of the halo X-ray emission. Studies of X-ray haloes are important because they allow the relative influence of

environmental factors and processes intrinsic to galaxies to be evaluated. It is clearly of considerable importance to ascertain whether X-ray haloes are a general property of normal galaxies.

1.3.6 Cooling Flows in Clusters of Galaxies

Einstein imaging observations have considerably extended our knowledge of the structure and evolution of the X-ray emitting matter within clusters of galaxies (eg. Jones and Forman 1984). Detailed analysis of X-ray surface brightness profiles has resulted in the derivation of accurate central temperatures and densities for the hot gas detected in $\sim$40 clusters. The radiative cooling times for the central gas in half of these clusters are less than a Hubble time. Unless heating processes are efficient, and current evidence suggests otherwise, the gas will cool and flow inwards towards the core of the cluster, possibly resulting in low-mass star formation and the fueling of radio sources (Cowie and Binney 1977, Fabian and Nulsen 1977, Stewart et al. 1984). The concept of a cooling accretion flow is important because it emphasizes that hot gas trapped within a gravitational potential well need not be completely static; dynamical evolution is likely to occur. Cooling flows may also be important within individual galaxies, since they can in principle occur in any sufficiently dense concentration of gravitationally confined gas which is allowed to cool radiatively.

1.4 Outline of Thesis

To conclude this introductory chapter we will outline the topics to be covered in the remainder of this thesis.

Chapter Two: the design, performance and sensitivity of the relevant Einstein Observatory instruments are briefly reviewed.

Chapter Three: the results of a high resolution study of the X-ray emission associated with M82 - an archetypal peculiar galaxy - are presented. The data are interpreted in the context of an enhanced Population I content generated by an intense burst of star formation, which has also given rise to an extensive X-ray halo.

Chapter Four: the basic X-ray properties of a sample of eleven early type galaxies are derived using Einstein data. X-ray fluxes and luminosities are determined for all of the members of the sample, and an analysis is performed of the spectral and surface brightness properties of those galaxies which emit sufficiently high X-ray fluxes.

Chapter Five: the sample of early type galaxies is extended to include all galaxies for which an Einstein-derived X-ray flux has been published. Correlations between integrated properties are examined and conclusions drawn regarding the relative importance of contributions from discrete X-ray sources and thermal emission from hot gas. The results are discussed with particular reference to plausible models for the dynamical evolution of hot gas, including both inflow and outflow processes.

Chapter Six: high resolution X-ray and radio maps of two giant, morphologically normal elliptical galaxies are presented and analysed. The X-ray emission displays a complex morphology, which is interpreted as evidence for the existence of "structure" in the spatial distribution of hot gas (which is the dominant component of the X-ray emission of these galaxies). There is ample evidence for the existence of a cooling flow in at least one of these galaxies; the possibility that cooling flows fuel the observed low luminosity nuclear radio sources while the remaining hot gas confines the extended radio structures is therefore investigated.

Chapter Seven: the results of the research presented in this thesis are briefly reviewed and placed in an appropriate general context. Considerable scope exists for further observations in all wavebands, and particular emphasis is placed on the possibilities arising from the next generation of X-ray astronomy satellites.

Appendix: various data analysis techniques which are directly relevant to the analysis and interpretation of the Einstein X-ray data presented in this thesis are discussed, and suitable definitions and nomenclature established.

CHAPTER TWO : THE EINSTEIN OBSERVATORY

2.1 Introduction

The Einstein Observatory, also known as HEAO 2, was successfully launched on November 13th 1979. For a period of just over two years it provided a facility capable of performing detailed studies of cosmic X-ray sources with a sensitivity roughly a factor of 10^3 superior to that achieved by previous X-ray astronomy experiments. The analysis and interpretation of Einstein data forms the fundamental element of the work presented in this thesis, hence it seems appropriate to briefly review the performance characteristics and scientific capabilities of the Einstein X-ray instrumentation. (Various aspects of data analysis techniques directly relevant to the analysis of Einstein X-ray data are discussed in an appendix at the end of this thesis).

2.2 The Characteristics and Performance of the Einstein X-ray Instruments

2.2.1 Overview

The launch and subsequent successful operation of the Einstein Observatory provided the astronomical community with the first in-orbit, fully imaging X-ray telescope, capable of an angular resolution of a few arcseconds within a field of view of ~20 arcminutes, and a rather more modest ~ arcminute resolution over the full 1° FOV. Incorporated within the satellite were a high resolution X-ray telescope, an aspect reconstruction system and a focal plane assembly capable of positioning at the telescope focus one of four primary instruments: a high resolution imager (HRI), a broad FOV imaging

proportional counter (IPC), a solid state spectrometer (SSS) and a Bragg crystal spectrometer (FPCS). Subsidiary instruments included a broad band filter system (BBFS) and two objective grating spectrometers (OGS), both for use with the HRI. A conventional, non-imaging monitor proportional counter (MPC) was also included in the instrument complement, its pointing axis coaligned with the telescope. The configuration of the various Einstein instruments is shown in Figure 2.1a.

The extragalactic objects which are the subject of this thesis are typically quite faint X-ray sources which yield fluxes below the sensitivity thresholds of the higher resolution spectrometers (eg. SSS, FPCS and OGS). Discussion of instrumental characteristics and performance will therefore be limited to the HRI, IPC and MPC. Detailed information relating to the full complement of instrumentation is available elsewhere (eg. Giacconi et al. 1979a). Relevant instrument parameters are summarized in Table 2.1; the quoted values for source detection sensitivities are representative, but should be used with caution as they depend critically on factors like the duration of the observation, and the angular extent and spectral properties of the X-ray source being observed.

2.2.2 The High Resolution Mirror

The Einstein telescope design utilizes the classic Wolter type-I geometry, incorporating a paraboloidal first element and a confocal and coaxial hyperboloidal second element (see Figure 2.1b). Efficient reflection of X-rays with energies in the 0.1 - 4.5 keV Einstein band requires a $\sim 1^\circ$ grazing angle relative to the mirror surfaces. The

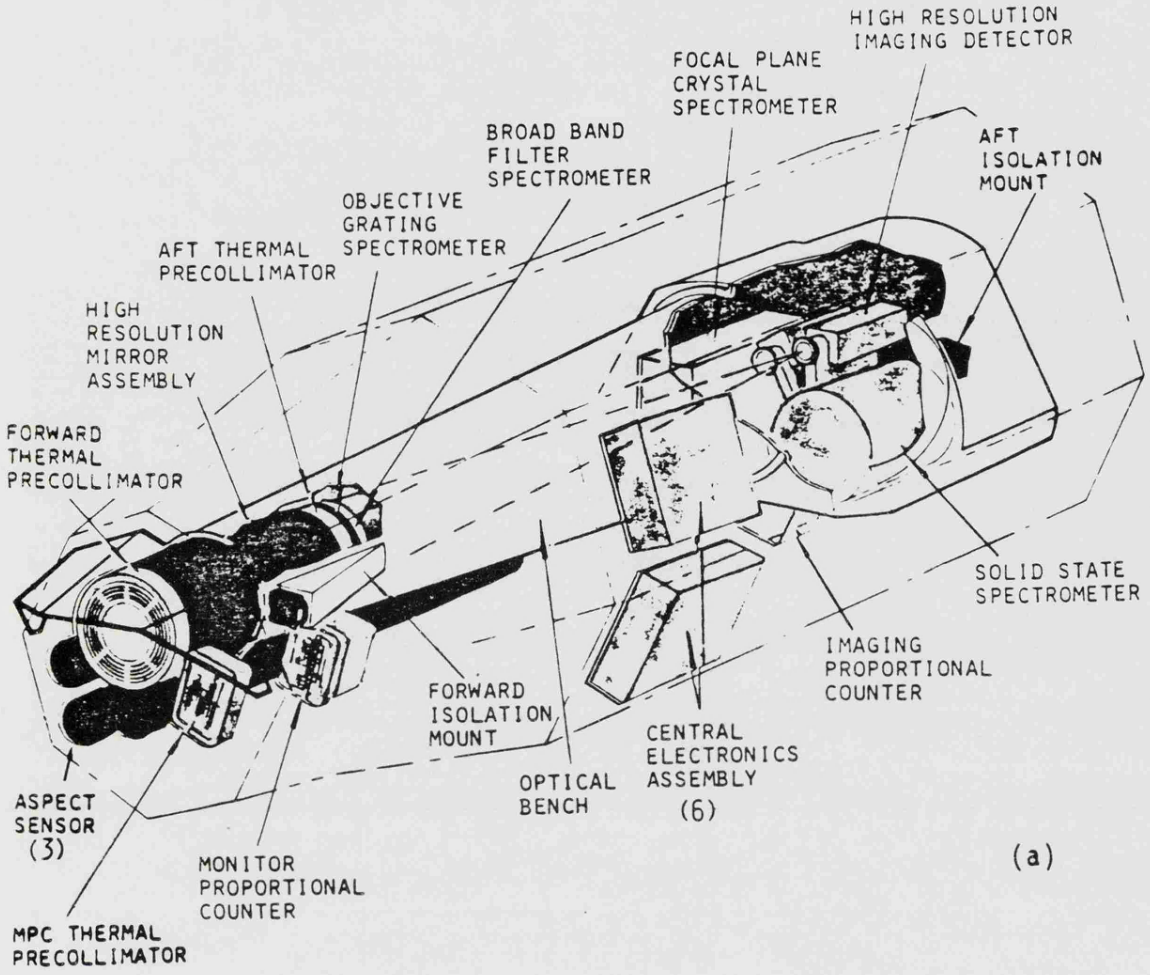

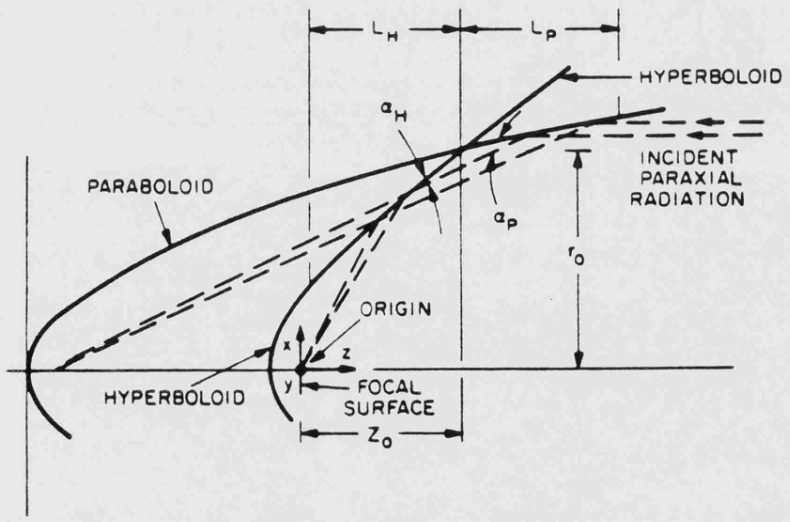

Figure 2.1 (a) Configuration of the Einstein Observatory.

(b) Wolter type I X-ray telescope geometry.

Table 2.1 : Summary of Instrumental Characteristics

Instrument	Field of View	Pixel Size	Angular Resolution (on-axis)	Aspect Solution	Effective Area	Energy Resolution and Range	Background Count Rate	Point Source Sensitivity (10000 sec exposure)
HRI	25' (diameter)	0.5"	4"	3.5"	10 cm^2 (at 1 keV)	none (0.1-3.0 keV)	1.3×10^{-6} ct s^{-1} $arcsec^{-2}$	0.008 Uhuru ct s^{-1}
IPC	75'x75'	8"	1'	20"	100 cm^2 (at 1 keV)	$E/\Delta E \sim 1$ (1 keV) (0.1-4.5 keV)	8×10^{-7} ct s^{-1} $arcsec^{-2}$	0.005 Uhuru ct s^{-1}
MPC	1.5°x1.5°	-	FWFM Collimated	-	667 cm^2 (at 6 keV)	$E/\Delta E \sim 5$ (6 keV) (1.5-20 keV)	10 ct s^{-1}	0.3 Uhuru ct s^{-1}

mirror system achieves an on-axis angular resolution of ~4 arcsec FWHM, or ~8 arcsec for the half-power beam diameter. The FWHM parameter effectively represents the size of the high resolution core of an image, and hence is indicative of the best attainable resolution for high contrast features; whereas the half-power diameter is energy dependent and is required for the calculation of the detectability of faint sources. Utilization of a four-nested mirror system results in a theoretical effective area of between 400 cm^2 at 0.25 keV and 30 cm^2 at 4.0 keV.

2.2.3 The Aspect System

The satellite aspect system consists of an assembly of reference calibration lights and three optical star trackers (one aligned with the telescope axis, the other two offset by 2°). Each star tracker has a 2°x2° FOV, and is sensitive to stars which are brighter than 9th magnitude. When in a locked-on mode they allow active positioning of the telescope axis to within ~1 arcminute of the required celestial coordinates. It was hoped that subsequent processing of star tracker data would allow the X-ray telescope's absolute pointing position to be determined to an accuracy of ~1 arcsec. Unfortunately this has proved to be impractical; aspect uncertainties for fully-processed Einstein HRI observations are ~3.5 arcsec (90% confidence).

2.2.4 The High Resolution Imager (HRI)

The HRI is a digital X-ray camera which provides high spatial and temporal resolution over the central 25 arcminutes of the telescope focal plane. It essentially consists of two microchannel plates operating in cascade and a 2-D charge detection read-out grid. A single X-ray photon passes through a UV shield and strikes the MgF_2

coating on the first MCP and produces one electron; subsequent multiplication within the channels of both MCPs results in a short duration pulse of $\sim 5 \times 10^7$ electrons ejected from the rear of the second MCP. The electron burst is collected by the crossed-grid charge detector, and the position and time of the electron event (and hence the X-ray photon) are determined by electronic signal processing. Although it lacks any spectral discrimination (essentially because the electron multiplication process is independent of the energy of the incident X-ray photon), the HRI is capable of very high temporal and spatial resolution. Indeed, the angular resolution of the Einstein mirror/HRI combination is limited by the roughness properties of the mirror surface rather than the intrinsic properties of the detector.

2.2.5 The Imaging Proportional Counter (IPC)

The IPC is a position sensitive proportional counter which provides full focal plane coverage with moderate spatial and energy resolution. A predominantly argon gas mixture is maintained at constant density and composition within a counter body which houses a plane of anode wires centrally located between two planes of cathode wires. An incident X-ray photon interacts with a gas atom, producing an electron which in turn initiates an avalanche of electrons at the anode wires, the resultant signal being detected at the cathodes. Rise time measurements define the original location of the incident photon to within ~ 1 arcminute over virtually the whole FOV. Signal processing yields timing information and 32 channels of energy resolution over the energy range 0.1 - 4.5 keV.

2.2.6 The Monitor Proportional Counter (MPC)

The MPC is a non-imaging proportional counter located outside the X-ray telescope assembly. It consists of two argon-CO_2 gas cells with a 1.5 mm beryllium entrance window and an external collimator. The effective area of the MPC is 667 cm^2, and the collimator provides a 1.5° FWFM circular field of view. Incident X-ray photons generate electron pulses which are detected at one of the four anodes; these signals are then amplified, integrated and pulse-height analysed in eight energy channels between 1.5 and 20 keV. The MPC therefore considerably extends the useful energy range of the Einstein instrumentation, allowing spectral and timing studies to be performed for relatively bright X-ray sources at energies beyond the range of the imaging detectors.

2.2.7 Instrument Sensitivities

Crude sensitivity estimates for the IPC and HRI, as a function of both exposure time and source detection cell size, are displayed in Figure 2.2a. The smallest detection cells, 3x3 arcmin (IPC) and 12x12 arcsec (HRI), are representative of the optimum cell sizes for the detection of faint, unresolved X-ray sources. Allowance has been made for effects due to instrumental resolution, the scattering properties of the mirror, and typical in-orbit background count rates (including contributions from instrument calibration sources and the cosmic soft X-ray background). To facilitate comparison with previous X-ray astronomy experiments the source strengths are represented by equivalent Uhuru detector count rates. It is important to emphasize that the IPC and HRI have significantly softer responses compared to the Uhuru instrument; they are sensitive to X-rays with energies in

(a)

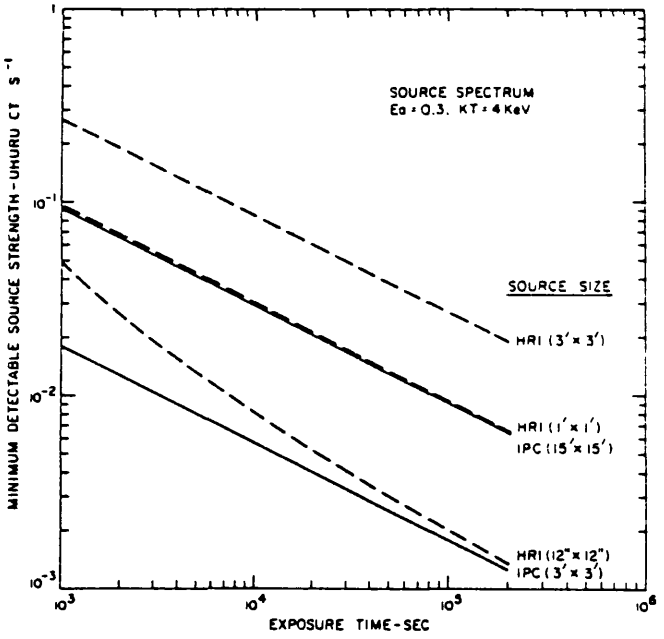

(b)

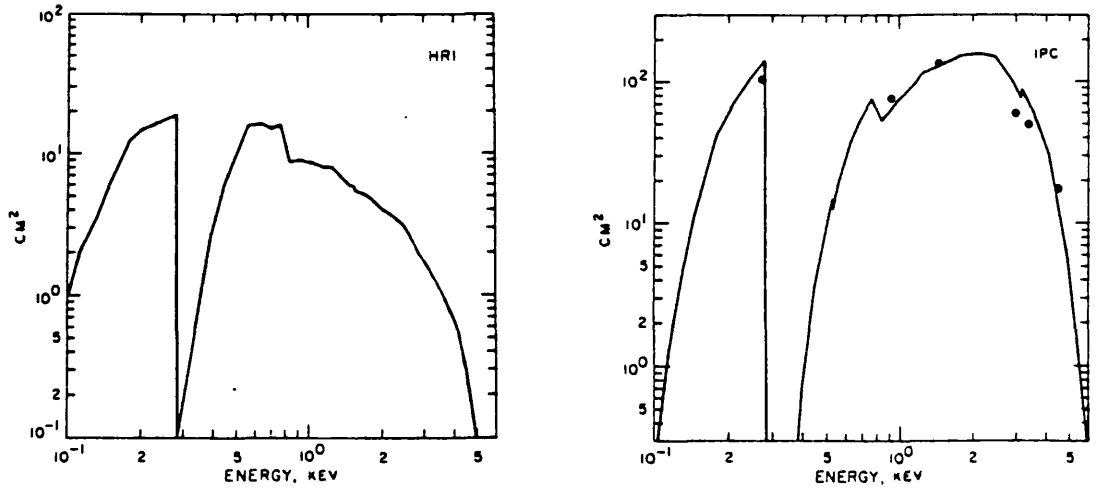

Figure 2.2 (a) Sensitivity of the Einstein imaging instruments.

(b) Effective area curves for HRI and IPC.

the range 0.1-4.5 keV, whereas the Uhuru energy band is 2-6 keV. The relative instrumental sensitivities are therefore a strong function of the adopted low energy cut-off. For the assumed thermal bremsstrahlung spectrum, with kT = 4 keV and cut-off energy Ea = 0.3 keV, the corresponding conversion factors are:

$$1 \text{ IPC ct s}^{-1} \simeq 0.1 \text{ HRI ct s}^{-1} \simeq 1 \text{ Uhuru ct s}^{-1}.$$

Figure 2.2a demonstrates that for practical observation times the HRI is less sensitive than the IPC for source detection. Comparison of the effective area curves (Figure 2.2b) shows that the HRI has a significantly softer response than the IPC, hence the ratio of HRI to IPC count rates is a function of the X-ray source spectrum.

2.3 In-Flight Performance and Status of Observation Processing

For both the HRI and the MPC in-flight performance proved to be entirely within specification. The situation with the IPC was rather less satisfactory: although the IPC's imaging capabilities and overall sensitivity met design specifications, gas leakage through porous plugs resulted in significant gain fluctuations on timescales upwards of a few hours, particularly during the early phases of the mission. Final calibration of detector gain for each individual IPC observation is underway, but is not complete as of late 1984 (Schwarz, private communication). The IPC observations presented in this thesis are therefore not in a definitive, fully processed form. Deductions regarding the spectral properties of X-ray sources based on IPC data alone should be treated with some caution, as the results can not yet be regarded as definitive (see Appendix A.3). HRI observations are now in a fully processed form and are routinely made available to the general astronomical community via a data bank service organized by

the Center for Astrophysics. It is anticipated that all IPC observations will become similarly available by the end of 1985.

CHAPTER THREE : THE X-RAY PROPERTIES OF M82

3.1 Introduction

The nearby galaxy M82 has been a favourite object of study since it was proposed as an "exploding galaxy" by Lynds and Sandage (1963). M82 is a nearly edge-on system with an inclination angle of $\sim 10°$; a member of the M81 group, it is situated at an estimated distance of 3.25 Mpc from our galaxy (Tammann and Sandage 1968). The galaxy, classified as Irr II (Sandage 1961) or IO (de Vaucouleurs et al. 1976), has approximate optical dimensions of 13x8 arcminutes, corresponding to a physical size (12x7.5 kpc) somewhat smaller than our galaxy. The nuclear region, with dimensions $\sim$ 50x15 arcsec elongated along the plane of the galaxy, is considerably larger than the corresponding region of our galaxy (see Solinger et al. 1977); and the integrated radio and infra-red luminosities, estimated to be $L_{RAD} \sim 10^{39}$ erg s^{-1} and $L_{IR} \sim 10^{44}$ erg s^{-1} (Hargrave 1974, Rieke et al. 1980), are also much larger. Optically and in the near-IR the nuclear region is dominated by high surface brightness star clusters and giant HII regions (eg. O'Connell and Mangano 1978), several of which are partially obscured by prominent dust clouds (see Figure 3.1a). The observed radio and far-IR emission from M82 is strongly concentrated in the nuclear region, and has a complex, clumpy morphology dominated by a compact, non-thermal source known as 41.9+58 (eg. Rieke et al. 1980, Kronberg et al. 1981) which lies 10 arcsec away from the well defined optical nucleus (see Figure 3.1b).

The many unusual features of the nuclear region of M82 have generally been attributed to an intense burst of star formation initiated 10^7 -

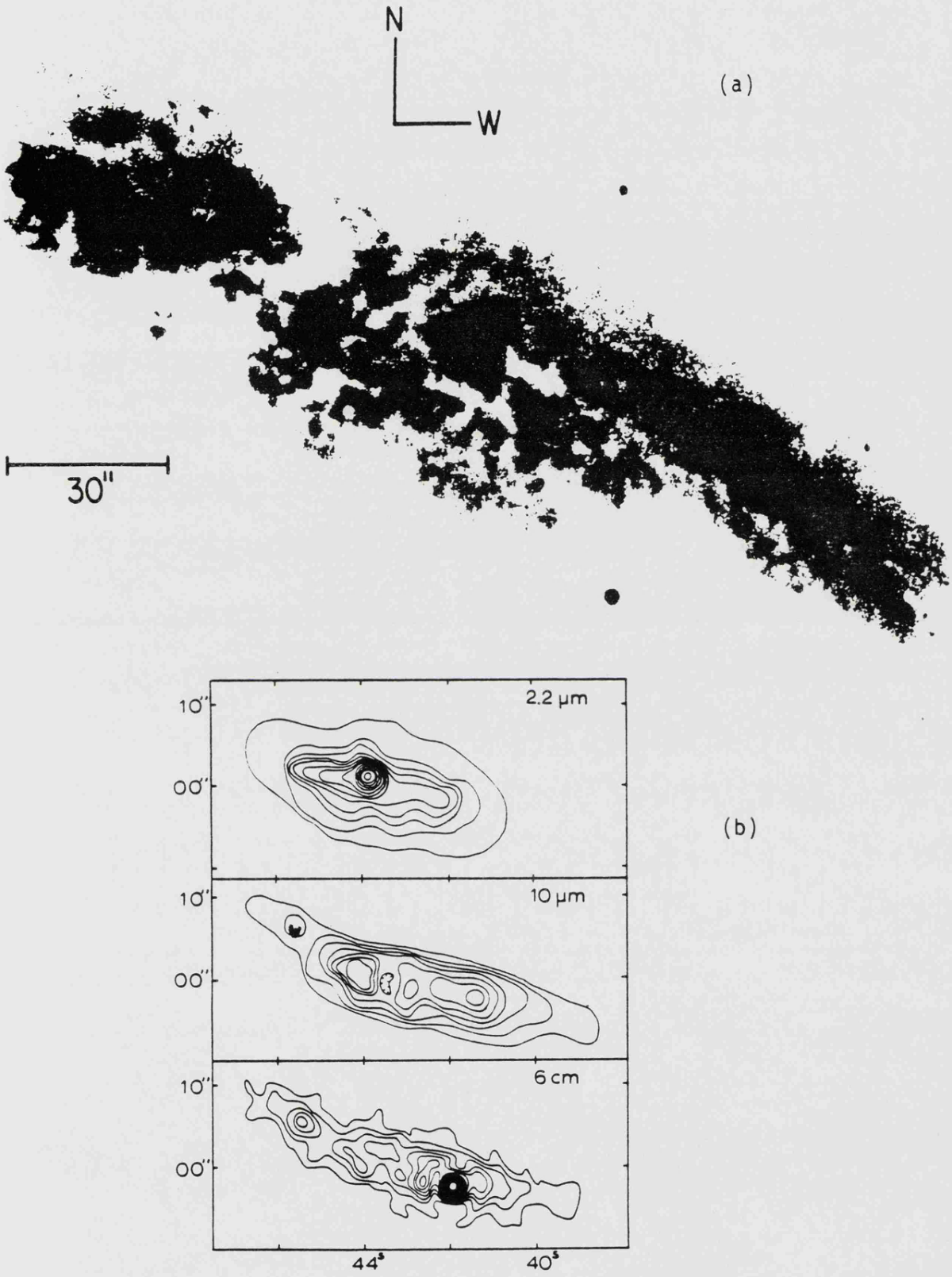

Figure 3.1 (a) Optical photograph of centre of M82, from O'Connell and Mangano (1978); (b) IR and radio maps of centre of M82, from Rieke et al. (1980). Coordinates are relative to RA = $9^h\ 51^m$ and DEC = +69° 55'.

10^8 years ago and possibly continuing into the current epoch (eg. O'Connell and Mangano 1978). HI aperture synthesis maps of the M81-M82 group provide compelling evidence that the M82 "starburst" was triggered by a tidal interaction with M81 (Cottrell 1977).

Beyond the nuclear region the galactic disk is similar to that of a normal spiral galaxy, but in optical continuum and Hα plates the appearance of M82 is dominated by an elongated halo which extends for several arcminutes along the minor axis of the galaxy. In Hα the halo displays a complex filamentary structure including components with radial and tangential orientations. Spectroscopic measurements reveal radial velocity differences of roughly 100 km s^{-1} between the filaments to the north and south of the nucleus. This velocity field was originally interpreted as evidence for an outflow along the minor axis with space velocities of $\sim$1000 km s^{-1} (hence the "exploding galaxy"; Lynds and Sandage 1963, Burbidge et al. 1964). The discovery of significant polarisation in the emission lines observed in optical spectra from parts of the filamentary system, and the well-ordered pattern of broad-band polarisation (Visvanathan and Sandage 1972, Visvanathan 1974, Bingham et al. 1976) led Solinger et al. (1977) to reinterpret the optical halo as being due to the scattering of light from the nuclear region into the line of sight by dust, thus removing any need to invoke high velocity outflow from the nucleus. Spectroscopic work by Axon and Taylor (1978) at least partially contradicts this result; their observations of line-splitting in the halo indicate that some form of outflow may indeed by occurring. Additional support for the outflow scenario is provided by the spectroscopic work of O'Connell and Mangano (1978), which demonstrated

that the line emission from the inner regions of the halo (ie. $R \lesssim 0.6$ kpc) is dominated by ionized plasma rather than cool scattering dust.

M82 was the suggested identification for a weak X-ray source which appeared in both the Uhuru and Ariel 5 catalogues (Forman et al. 1978, McHardy et al. 1981), and the identification was confirmed by HEAO 1 modulation collimator observations (Griffiths et al. 1979). In this chapter we present observations of M82 performed with the Einstein Observatory soft X-ray imaging instruments, which because of their superior sensitivity and angular resolution allow the first detailed study of the X-ray emission properties of this enigmatic galaxy.

3.2 X-ray Observations

Two Einstein observations of M82 were performed during 1979; the first was a 4292 sec. IPC exposure during April 8-9, which was followed by a 1311 sec. HRI exposure during May 3-6. The IPC image shows a bright extended source coincident with M82; M81 is also visible near the edge of the FOV. Although the angular resolution of the IPC is too coarse to determine the morphology of the X-ray emission associated with M82, the instrument does provide useful spectral information. The HRI image reveals a complex emission region centred near the nucleus of the galaxy, with significant emission over a region of several arcminutes extent (Figures 3.2 and 3.7). Complementary spectral information in the 1.5-20 keV band is provided by data from the MPC.

3.3 Analysis and Results

3.3.1 X-ray Spectra and Fluxes

We have performed spectral analysis of background subtracted IPC and MPC data using model X-ray spectra corresponding to optically thin

thermal and power law forms, in both cases including absorption by cold matter distributed along the line of sight. (For details of background subtraction and spectral fitting techniques refer to Appendix A.3). The results, summarized in Table 3.1, indicate a characteristic temperature of ~3 keV for thermal emission models or a correspondingly steep slope for power law models. Neither spectral form can be rejected on statistical grounds since both give acceptable fits.

We note in passing that given the uncertainties in the derived spectral parameters it is not possible to distinguish the X-ray spectrum of M82 from that of a typical AGN (ie. photon index ~1.7, Mushotzky 1980), even though the emission processes are probably very different. The best-fit column densities have a wide range and differ systematically according to which spectral model is selected. Use of the total HRI count rate as an additional constraint to spectral shape further restricts the range of allowed column densities to 3×10^{20} - 2×10^{21} cm^{-2}.

In order to calculate X-ray fluxes and luminosities, a thermal spectrum with kT = 3 keV and $N_H = 6 \times 10^{20}$ cm^{-2} has been assumed. The derived fluxes and luminosities are particularly sensitive to larger values of N_H, but are relatively insensitive to the assumed temperature. For the assumed spectral parameters, the HRI flux exceeds the IPC value (for the same energy band) by 17%. If this discrepancy is not due to systematic errors in the flux calibrations it could imply a composite X-ray spectrum for M82, with one component (eg. the halo discussed below) having a softer and/or less absorbed spectrum. The reddening in the direction of M82, estimated from the

Table 3.1 : Summary of Einstein X-ray Measurements of M82

	IPC	MPC	HRI
Total count rate (count s^{-1})	0.51 ± 0.01	0.39 ± 0.04	0.16 ± 0.006
X-ray Spectrum:			
(i) thermal			
kT (keV) (1)	3 (+2, -1.2)	5 (+2, -0)	-
N_H (10^{20} cm^{-2})	6 (+8, -3)	< 40	-
(ii) power law			
alpha (2)	-2.3 (+1, -1)	-2.2 (+0.3, -0.2)	-
N_H (10^{20} cm^{-2})	21 (+11, -15)	< 80	-
Fluxes (3) (erg cm^{-2} s^{-1})	1.8×10^{-11} (0.2 - 4 keV)	8.5×10^{-12} (2 - 6 keV)	2.1×10^{-11} (0.2 - 4 keV)
Luminosities (3) (erg s^{-1}, D = 3.25 Mpc)	2.3×10^{40} (0.2 - 4 keV)	1.1×10^{40} (2 - 6 keV)	2.7×10^{40} (0.2 - 4 keV)

Notes to Table 3.1

Errors quoted in brackets are for the 90% confidence interval appropriate to a 2-parameter spectral fit. For the IPC spectra the errors include appropriate allowance for the uncertainties in detector gain and background subtraction. The errors for the MPC spectral fits are purely statistical and probably underestimate the true uncertainties.

(1) Simple bremsstrahlung plus Gaunt factor spectrum fitted to the MPC data.

(2) Photon number index.

(3) Fluxes and luminosities are corrected for an assumed line of sight column density of $N_H = 6 \times 10^{20}$ cm^{-2}.

E(B-V) maps of Burstein and Heiles (1982), is $A_V \sim 0.1^m$, corresponding to $N_H \sim 2.5 \times 10^{20}$ cm^{-2} using the calibrations of Jenkins and Savage (1974) and Seaton (1979). The best-fit N_H for both types of model spectra is higher, probably indicating a modest amount of cool absorbing matter within M82 itself. Star clusters within the nuclear region of M82 have been found to exhibit optical extinction as high as $A_V \sim 5$. Although X-ray emission from such regions is likely to account for only a small fraction (<10%) of the total X-ray flux, we are unable to rule out the possibility that major sources of X-ray emission within M82 also suffer an equivalent degree of optical extinction, corresponding to a column density of $\sim 10^{22}$ cm^{-2}. This would lead to higher values for the X-ray luminosity of individual sources.

3.3.2 X-ray Morphology

The HRI image of M82 (Figures 3.2 and 3.3, see also Figure 3.7) displays two distinct components; (1) a complex central region containing several local maxima in X-ray surface brightness over a region ~ 1 arcminute in extent; (2) a halo of patchy, diffuse X-ray emission extending several arcminutes along the minor axis of the galaxy both north and south of the nuclear region. Detailed examination of the IPC data also reveals the presence of the extended halo, although the feature is not sufficiently well resolved to enable useful comparison with the HRI data.

Analysis of the variance of the HRI data demonstrates that the clumpy appearance of the nuclear region X-ray emission is not an artefact of photon noise. This suggests that the emission is dominated by a small

Figure 3.2 (Plate)

Einstein HRI image of M82 with pixel size 2 arcsec displayed as a linear greyscale. The image has been smoothed with the HRI point response function.

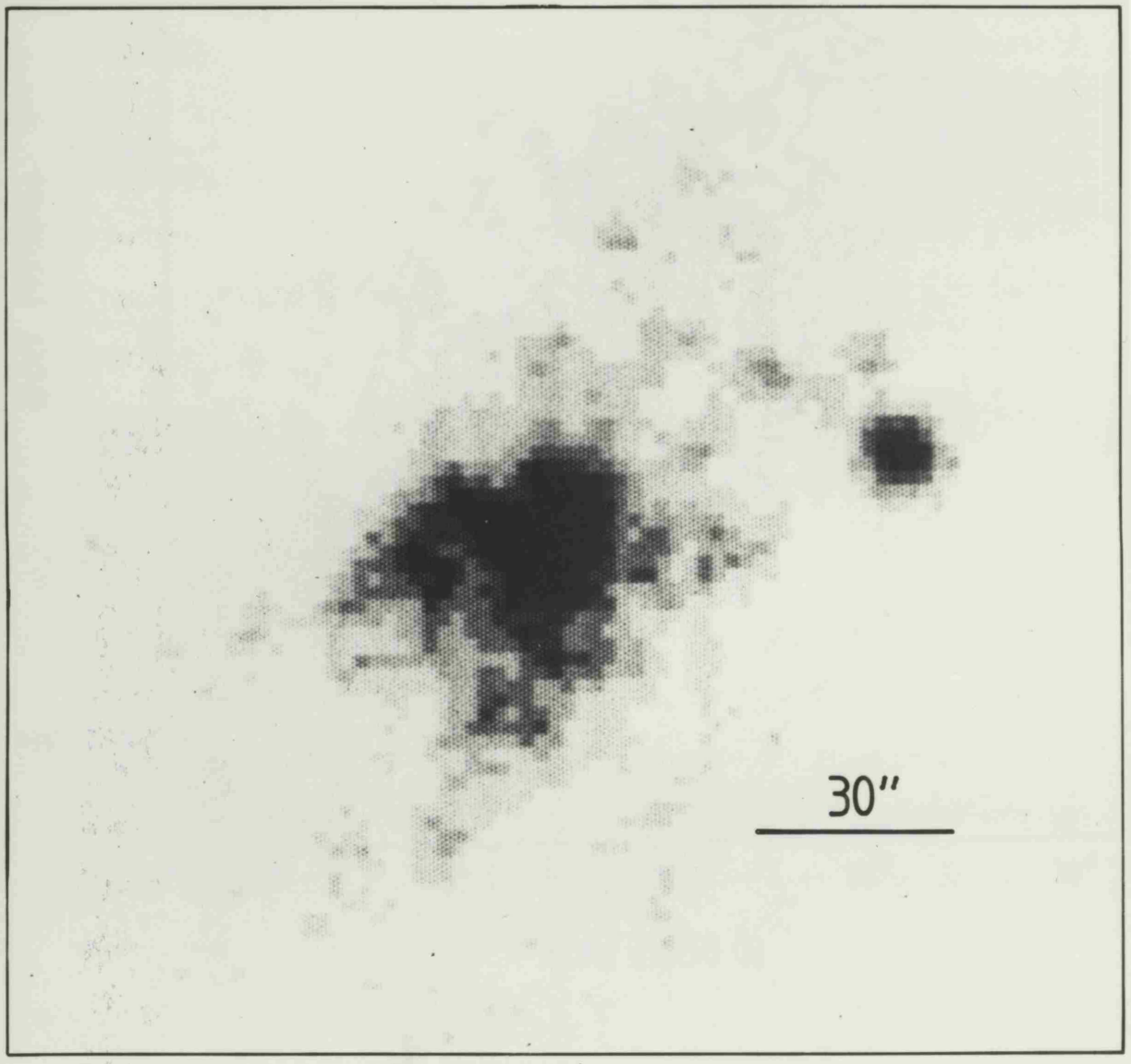
30″

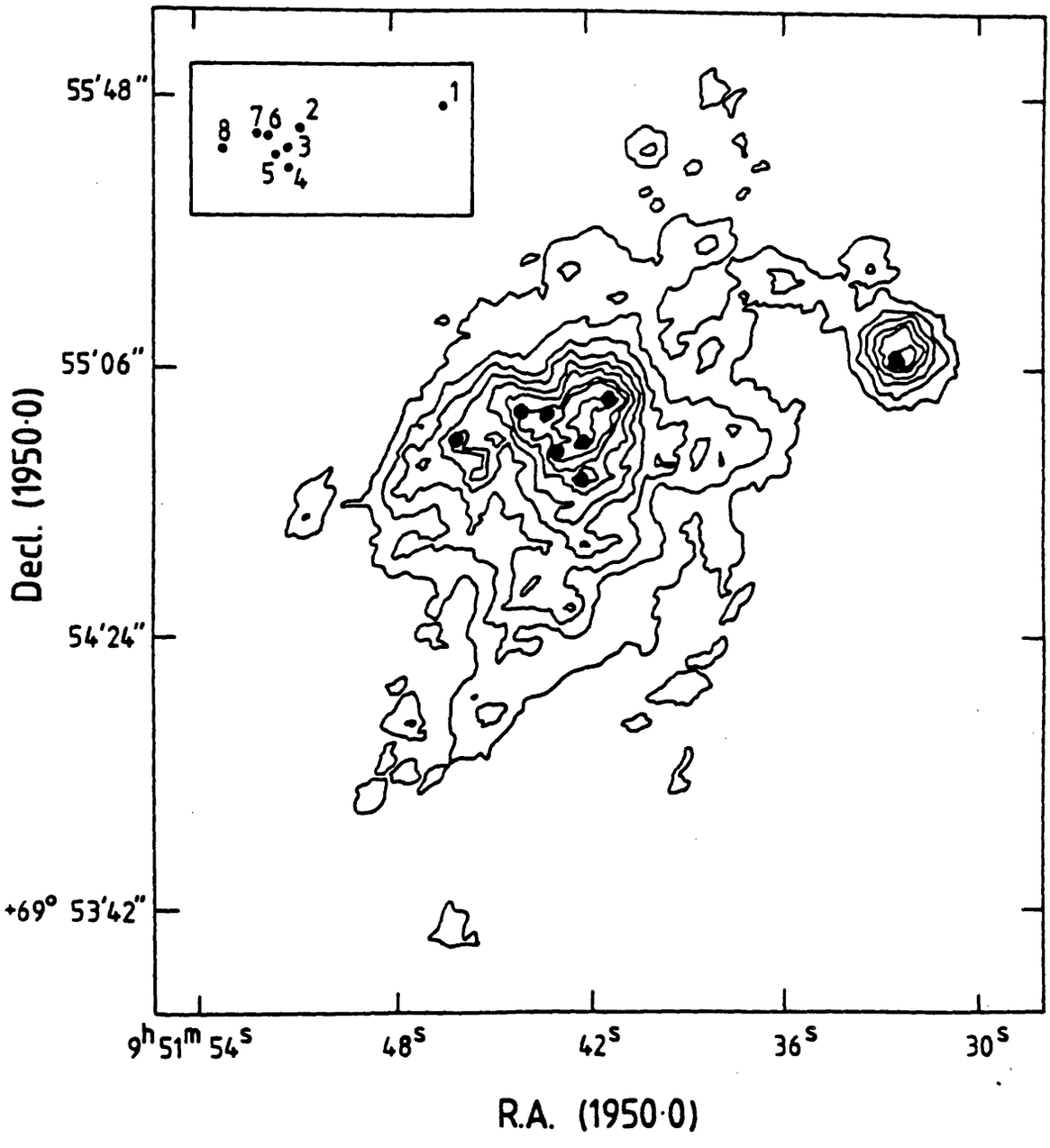

Figure 3.3 Einstein HRI image of M82 with pixel size 2 arcsec and smoothed with the instrumental PRF. The lowest contour level is 7.6×10^{-6} ct s^{-1} arcsec^{-2}, or 7 sigma above background. The remaining contours increment by 3.5 sigma. Eight unresolved sources are shown as filled circles and the inset shows the reference numbers used in the text.

number of unresolved sources, which are either genuine discrete X-ray emitting objects or bright knots in the ambient emission with scale sizes similar to the HRI point response function (ie. 4 arcsec $\simeq$ 60 pc). We have analysed the HRI data using the cross-correlation algorithm discussed in the appendix A.4 in order to locate possible unresolved sources in the presence of a non-uniform diffuse emission component. Eight unresolved sources are found by this technique above a 5 sigma significance threshold. Seven are apparently located in the bright nuclear region, and the eighth lies $\sim$1 arcminute to the west. Their positions, approximate count rates and luminosities are listed in Table 3.2 (see also Figure 3.3). If the unresolved sources are physically associated with M82, and assuming the best-fit IPC spectral parameters are applicable, they have soft X-ray luminosities in the range $5\text{-}10 \times 10^{38}$ erg s^{-1}.

In Figure 3.4 we show profiles of the X-ray surface brightness through the centre of M82 in two orthogonal directions corresponding to the major and minor axes of the galaxy. These profiles clearly demonstrate the presence of the diffuse X-ray halo extending along the minor axis out to at least 2.5 arcmin in the south-east and 2.0 arcmin in the north-west, whereas along the major axis the half-width of the emission is $\lesssim$ 1.4 arcmin. The halo merges into the emission from the nuclear region, with some indication of a change in the gradient of the surface brightness profile along the minor axis (Figure 3.4a) at radii of $\sim$30 arcsec (NW side) and $\sim$60 arcsec (SE side). For the purpose of discussion we define the nuclear region to be inside a 30 arcsec radius; all X-ray emission exterior to this boundary is considered to belong to the halo. Estimates of the X-ray count rates

Table 3.2 : X-ray Sources Within M82

Component	R.A.	Decl.	I_X(2)	L_X(3)	Comments
1	$9^h51^m32.4^s$	69°55'07"	4.4	8×10^{38}	~1 arcmin W of nuclear region
2	9 51 41.3	69 55 01	5.4	9×10^{38}	41.4+59 2 arcsec S; OM 'E' 2.3 arcsec E.
3	9 51 42.1	69 54 55	5.1	9×10^{38}	41.9+58 3 arcsec N; OM 'C' 2 arcsec SW.
4	9 51 42.1	69 54 49	4.0	7×10^{38}	
5	9 51 42.9	69 54 53	4.4	8×10^{38}	
6	9 51 43.3	69 54 59	4.3	7×10^{38}	43.1+60 1.5 arcsec NW; KPV 'A' 3 arcsec SE.
7	9 51 44.0	69 54 59	3.7	6×10^{38}	44.0+60 1.5 arcsec N; OM 'A' (nucleus?) 1 arcsec NW.
8	9 51 46.0	69 54 55	2.9	5×10^{38}	
Peak Region	9 51 41.7	69 54 58	7.3	1.2×10^{39}	Region 10x12 arcsec, includes 41.9+58
Nuclear Region	-	-	43.7	7.4×10^{39}	R < 30 arcsec
X-ray Halo	-	-	116.4	2.0×10^{40}	30 ⩽ R ⩽ 300 arcsec
TOTAL	-	-	160.1	2.7×10^{40}	

Notes to Table 3.2

(1) Errors in positions of the unresolved sources are dominated by the systematic uncertainty in satellite attitude. 90% confidence radius is ~4 arcsec in both coordinates.

(2) Background subtracted HRI count rates (x 10^{-3} ct s^{-1}). For the unresolved sources the intensities are equivalent point source values; for other components the values are directly measured for the regions specified, and hence slightly underestimate the true flux because the HRI point response function has broad wings. This is not an important effect for extended emission. Because the wings of the HRI are broad, some of the unresolved sources effectively overlap and hence "share" flux. In consequence the contribution of the point sources to the total flux seen in the central region is not simply given by the sum of the values for the sources.

(3) Soft X-ray luminosities (erg s^{-1}; 0.2 - 4.0 keV) derived assuming spectral parameters quoted in text.

(4) Possible identifications with radio and optical features within 3 arcsec radius (see text). aa.a+bb notation = Kronberg and Wilkinson (1975); OM = O'Connell and Magnano (1978); KPV = Kronberg et al. (1972).

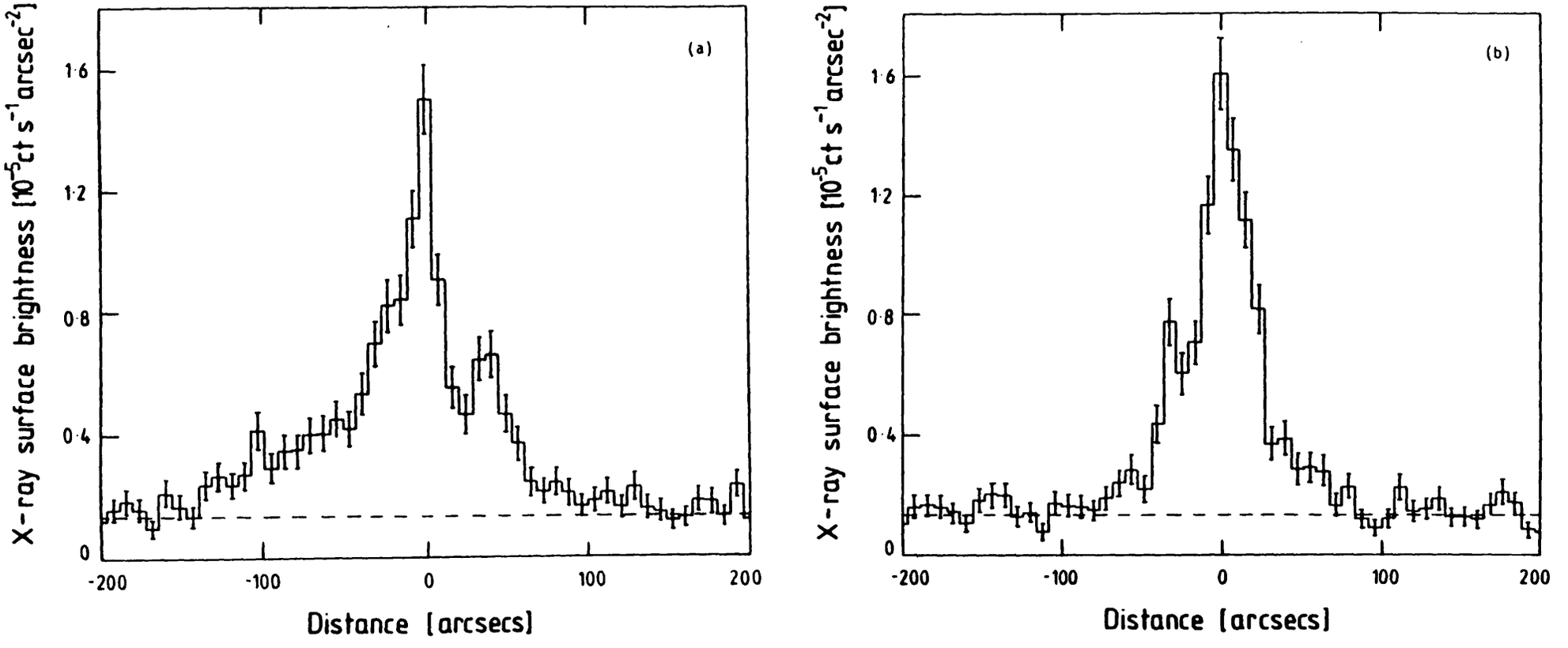

Figure 3.4 Cuts through M82 in two orthogonal directions; the value in each bin corresponds to the average X-ray surface brightness integrated across a strip 2 arcminutes wide. (a) profile at p.a. 150° (SE-NW along minor axis of galaxy); (b) profile at p.a. 60° (NE-SW along major axis of galaxy). Background levels are indicated by the dashed lines.

and luminosities associated with these two distinct regions are included in Table 3.2. The X-ray halo, although of low surface brightness, contributes ~70% of the X-ray flux emitted by M82 in the HRI energy band. A separate flux value has also been derived for a small region near the X-ray emission peak which includes souces 2 and 3 and the position of the compact radio source 41.9+58. The seven unresolved sources located in the nuclear region contribute a large proportion (~50%) of the flux emitted within 30 arcsec of the nucleus (see also the notes to Table 3.2). The remaining flux is probably due to a population of less luminous discrete sources which are not individually resolved by the HRI observation, although a contribution from a genuinely diffuse component (eg. an extension of the halo emission into the nuclear region) is not excluded by the data.

3.3.3 The Identification of the Unresolved X-ray sources

We have looked for possible identifications for the unresolved X-ray sources listed in Table 3.2 using the positions of optical features (star clusters, HII regions) from Kronberg et al. (1972) and O'Connell and Mangano (1978), and the positions of compact radio features given by Kronberg and Wilkinson (1975). Given the high source density in the radio and optical bands, the chance association rate must be quite high. Nevertheless, we list in Table 3.2 possible identifications with features located within 3 arcsec of the X-ray positions. Two particularly interesting associations are apparent:

(1) Source 7 lies within 1 arcsec of star cluster 'A' of O'Connell and Mangano; this cluster is generally thought to be associated with the nucleus of M82. The position of the X-ray source also agrees with the position of the 2.2μ nucleus given by Rieke et al. (1980). Thus

source 7 could be the nuclear X-ray source of the galaxy. If this is the case the X-ray luminosity quoted in Table 3.2 would probably be an underestimate, since optical and IR studies have revealed very high local absorption in the vicinity of the nucleus.

(2) Although the compact radio source 41.9+58 is not coincident with any of the detected X-ray sources, it is situated very near the peak of the X-ray emission region, midway between sources 2 and 3, along a ridge which is more or less aligned with the minor axis of M82. This raises the intriguing possibility that we are seeing an exceptionally luminous extended feature associated with this compact radio source (see also 3.4.1). It is interesting to note that the extended X-ray ridge has a linear dimension of $\sim$160 pc, very similar to the physical extent of the double lobe structure associated with the extraordinary galactic X-ray source SS433 (Watson et al. 1983). We estimate the soft X-ray luminosity of any unresolved source coincident with 41.9+58 to be $L_X \lesssim 3 \times 10^{38}$ erg s^{-1}.

Source 1 lies completely outside the nuclear region and is probably associated with the halo of M82. Analysis of the radial surface brightness profile of source 1 shows it to be completely consistent with an unresolved source. A recent VLA map fails to reveal the presence of a radio counterpart (E. Seaquist, private communication), and no optical counterparts are visible on available plate material; the magnitude limit derived from a deep CCD exposure obtained by J. Stocke is $m_R \gtrsim 22.5^m$ (this limit being set by the presence of diffuse light from the halo of M82), giving an implied X-ray to optical flux ratio $f_x/f_{opt} \gtrsim 200$. This value is somewhat uncertain because of

unknown reddening and bolometric corrections. Such an extreme flux ratio has only been observed for low mass Population II X-ray binaries (eg. Patterson 1981) and for the bizarre gamma ray source Geminga (Bignami et al. 1983). We do not favour the alternative possibility of identification with a background QSO with anomalously high reddening, since none of the QSOs identified in the Einstein Medium and Deep surveys (Stocke et al. 1983, Griffiths et al. 1983) have shown such an extreme flux ratio. Source 1 is therefore almost certainly an ultra-luminous low mass X-ray binary located in the halo region of M82. Its soft X-ray luminosity exceeds that of any established (or putative) system in our galaxy by almost an order of magnitude (Bradt and McClintock 1983). Exceptionally luminous unresolved sources have also been observed in several other nearby galaxies (Long and Van Speybroeck 1983), but they are invariably located in the outer spiral arm regions, and thus are probably associated with young Population I objects. This source, if located in M82, may be of particular interest as a possible Population II object associated with the halo region of a galaxy.

Another possible interpretation, that the source is a foreground object, can probably be ruled out, since in order for it to be located within our galaxy its intrinsic luminosity would have to be $L_X \lesssim 10^{34}$ erg s^{-1}, which is at least two orders of magnitude lower than any known low mass binary. In addition the optical luminosity distribution for low mass binaries is quite narrow, with a mean value equivalent to $M_V \sim 1$ (van Paradijs and Verbunt 1981); if this value applies to source 1 then we estimate a distance $\gtrsim$ 200 kpc, which places it well beyond our galaxy.

The relative X-ray source positions are determined to an accuracy of $\sim$1 arcsec, but are subject to an additional systematic error of $\sim$ 4 arcsec (90% confidence) arising from the uncertainty in the absolute pointing axis of the Einstein telescope. Any definite identification of an individual X-ray source could be used to refine the remaining source positions. In the absence of such an identification it should be noted that only a few of the associations listed in Table 3.2 are likely to be correct, since the position differences range from 0.5 to 3.0 arcsec in random directions.

3.4 Discussion

3.4.1 The Nuclear Region

In Figures 3.5 and 3.6 we compare the HRI X-ray image of M82 with radio (8 GHz) and optical maps of the galaxy (see also Figure 3.1). The X-ray image shows very little similarity with the high frequency radio map. Radio emission is strongly concentrated in a narrow strip more or less aligned with the plane of the galaxy, whereas the X-ray emission has a much more extended distribution principally aligned with the minor axis. A number of authors have pointed out the possibility of generating a high X-ray luminosity in M82 via inverse compton scattering of IR photons by the relativistic electrons associated with the non-thermal radio emission from the nuclear region (eg. Hargrave 1974, Rieke et al. 1980). The predicted X-ray luminosity from this process is $\sim 10^{40}$ erg s^{-1}, which is a significant fraction of the observed luminosity. Because of the complete lack of correlation between the X-ray and radio morphologies we suggest that the inverse compton process is not the dominant X-ray emission mechanism in M82; this may be the case if the ambient magnetic field

Figure 3.5 (Plate)

Composite radio/X-ray map of M82. Details of greyscale X-ray image as for Figure 3.2. Radio contours are schematic and are based on the 8085 MHz map of Kronberg and Clarke (1978), which has 2.2 arcsec resolution.

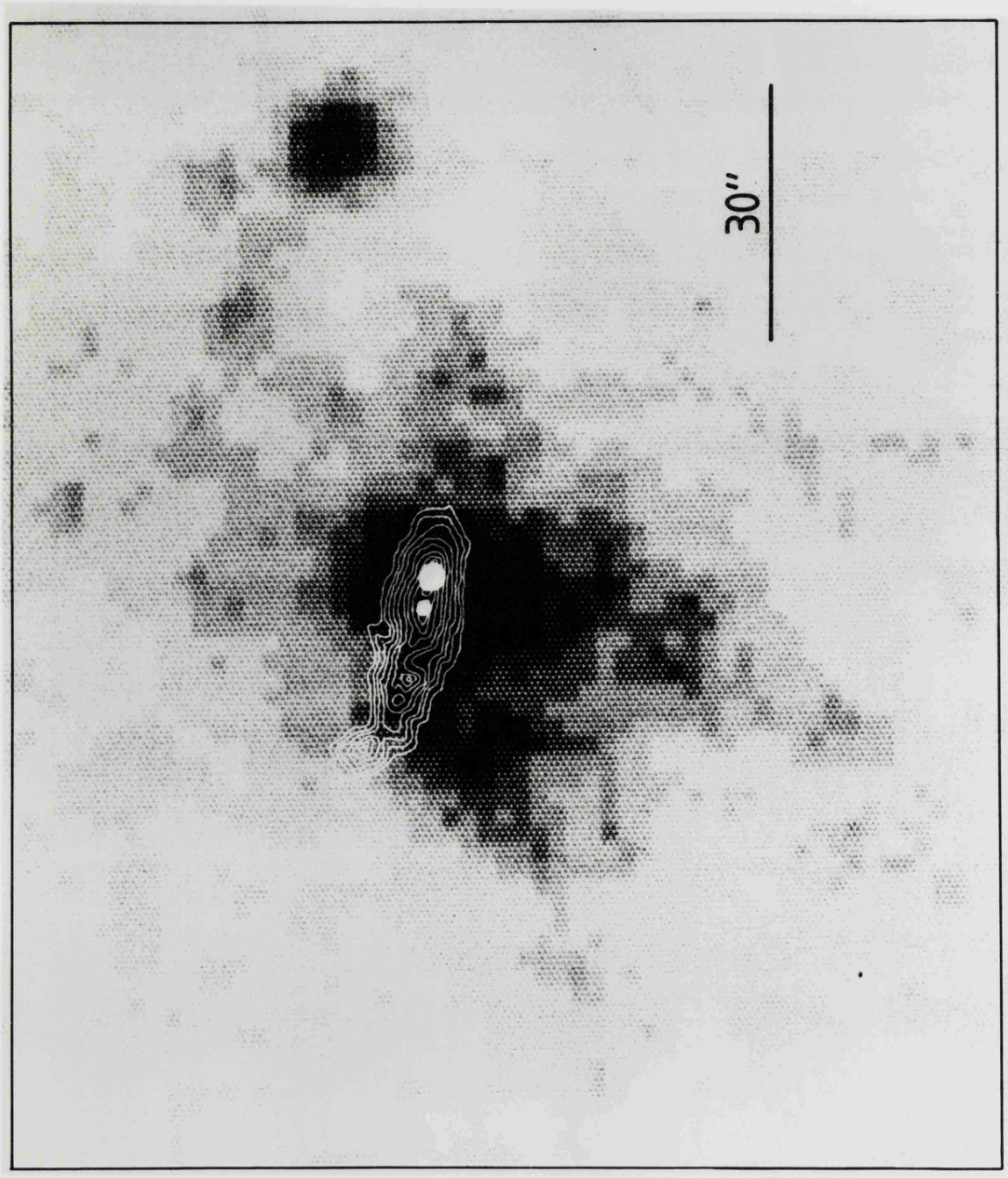
30"

is actually higher than the equipartition value ($B_{eq} \sim 3.5 \times 10^{-5}$ Gauss), since the inverse compton flux varies as $B^{-(1+\alpha)}$, where α is the low frequency radio spectral index ($\sim$0.3, Hargrave 1974). Indeed, the only way of understanding the X-ray morphology if the bulk of the emission had an inverse compton origin would be to hypothesise a remarkably different spatial distribution for the relativistic particles responsible for the X-rays ($\gamma \sim 100$) to that inferred for the particles which give rise to the high frequency radio emission ($\gamma \sim 10^3$ - 10^4).

The nature of the compact radio source 41.9+58 is still the subject of some debate (eg. Kronberg et al. 1981, Kronberg and Biermann 1983). Three possible models for 41.9+58 have been proposed; firstly it could be the true nucleus of M82, although it is located $\sim$10 arcsec west of the optical nucleus; the alternative suggestions are an ultra-luminous SNR or, perhaps more plausibly, an SNR in which a luminous young pulsar is embedded. In each case the radio emission is likely to be synchrotron in origin, and a naive extrapolation of the continuum spectrum with a measured index $\alpha = 0.9$ (Kronberg and Biermann 1983) to the X-ray band yields a predicted luminosity of $\sim 10^{38}$ erg s^{-1} (0.2-4.0 keV), assuming no break in the spectrum between radio and X-ray wavelengths. Thus the lack of an unambiguous detection of 41.9+58 at X-ray wavelengths is completely consistent with the spectral extrapolation. We have already discussed in section 3.3.3 the possibility that 41.9+58 is associated with the luminous ridge feature which extends N-S through part of the nuclear region. Higher resolution X-ray observation are required to confirm or refute this proposed association.

Comparison of the X-ray image with an R-band CCD exposure (Figure 3.6) shows that there is a significant correlation with the optical emission from the central regions of M82. The absence of X-ray emission from the part of the galaxy bisected by the broad dust lane - prominent in Figures 3.1a and 3.6 - probably indicates strong attenuation of the X-ray emission by the large column density associated with the dust. It is clear that the bulk of the nuclear region X-ray emission is of Population I origin, since it is well established that the optical light is dominated by HII regions, early-type stars etc, which are a direct result of the recent burst of star formation in the galaxy (eg. O'Connell and Mangano 1978). Although the optical light from the nuclear region is intrinsically quite blue, the R-band image shows the distribution of the optical emission equally well because of the effects of local extinction.

Given the enhanced Population I content and activity of the nuclear region of M82, it seems most likely that the bulk of the X-ray emission is associated with Population I objects. The possibilities are:

(1) High mass X-ray binaries. These systems have typical luminosities between 10^{35} and 10^{37} erg s^{-1} in our galaxy and up to 10^{39} erg s^{-1} in the Magellanic Clouds (Bradt and McClintock 1983, Clark et al. 1978). In contrast, low mass X-ray binaries, which dominate the bulge regions of our galaxy and M31, have luminosities up to $\sim 10^{38}$ erg s^{-1} (Bradt and McClintock 1983, Van Speybroeck et al. 1979, Vader et al. 1982). Source 1 in M82 may be an example of an exceptionally luminous low mass binary (see section 3.3.3).

Figure 3.6 (Plate)

Composite optical/X-ray map of M82. Details of greyscale X-ray image as for Figure 3.2. Optical contours shown are based on a R-band CCD observation made by J. Huchra and A. Lawrence using the Mt. Hopkins 24 inch telescope.

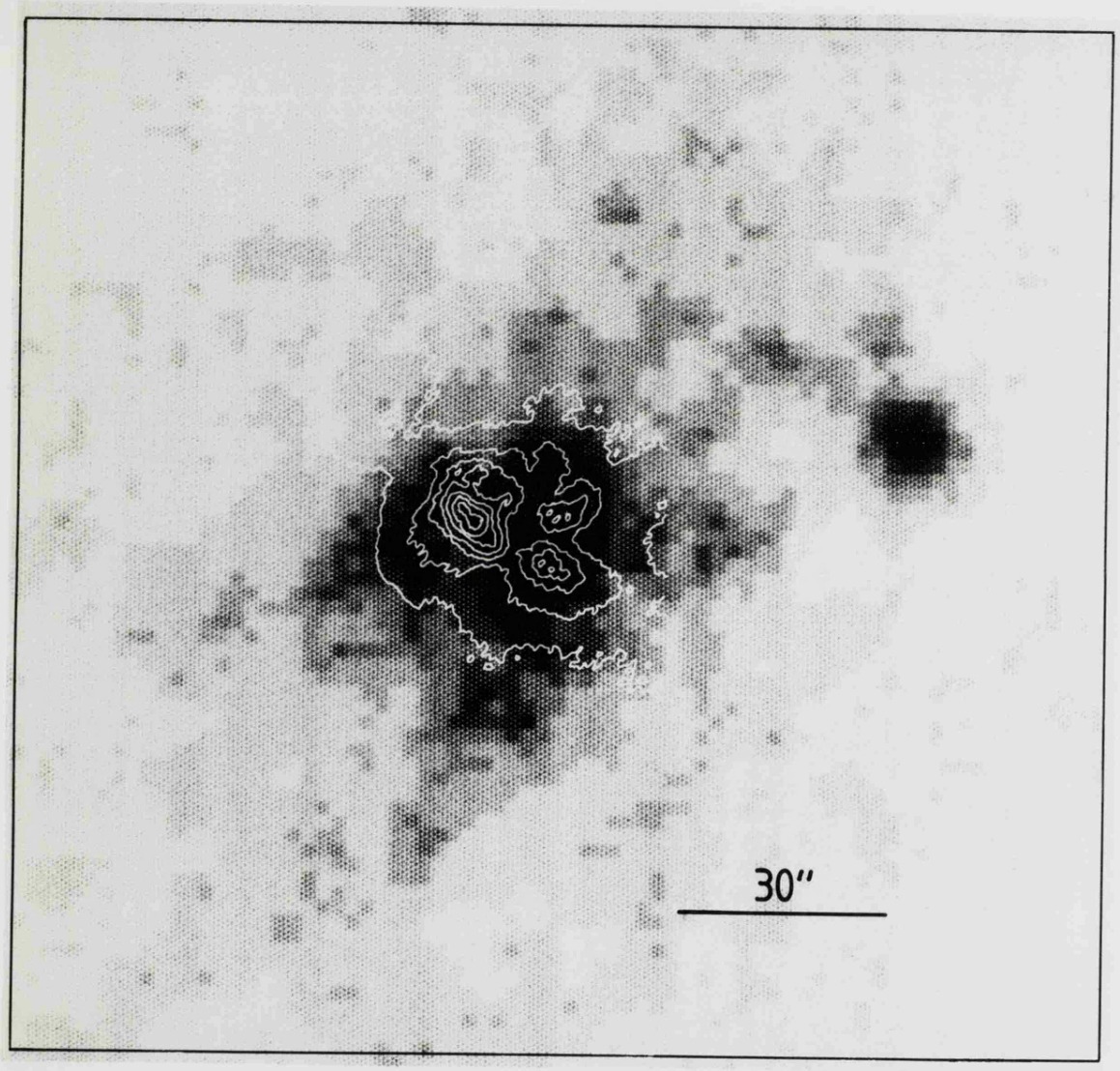
30″

(2) Supernova remnants. SNRs have luminosities in the range 10^{33}-10^{36} erg s^{-1} in our galaxy, but somewhat higher luminosities in the Magellanic Clouds, possibly due to a denser ambient ISM (Long and Helfand 1979, Seward and Mitchell 1981). There is evidence that in rare cases soft X-ray luminosities as high as 10^{39} erg s^{-1} may be attained, an example being the object tentatively identified as an SNR in NGC 4449 (Blair et al. 1983).

(3) Early-type stars. The soft X-ray luminosities associated with coronal activity in O-B stars can reach $L_x \sim 10^{33}$ erg s^{-1} (Vaiana et al. 1981).

The discrete X-ray sources detected in M82 have such high X-ray luminosities that if they are single objects they can be plausibly identified only with high mass X-ray binaries. (The alternative, that these sources are ultra-luminous SNRs, similar to the object in NGC 4449, can be discounted given their lack of association with known compact radio sources in M82.) If this is the case, the much higher incidence of such systems than is found in our galaxy is in accord with the enhanced star formation rate, and consequent over-abundance of massive stars. Note that this explanation requires that these sources have soft X-ray luminosities above the Eddington limit for accretion by solar mass compact objects. This need not be a fatal objection since several sources in the Magellanic Clouds also have super-Eddington luminosities (Clark et al. 1978), and the solar mass Eddington limit can be exceeded in a number of ways (eg. element abundance effects, anisotropic emission or trivially by increasing the mass of the compact object). The alternative, that these sources are

low mass Population II X-ray binaries, as might be expected by analogy with the equivalent bulge region of our galaxy or M31, would imply that the total number of this type of object in M82 is similar to that found in our galaxy and M31. This can almost certainly be discounted because Population II content is roughly proportional to total galactic mass (Long and Van Speybroeck 1983), and M82 is considerably less massive than either of these galaxies. Indeed, on the basis of galactic mass considerations we would expect the total contribution to the X-ray luminosity of M82 from Population II objects to be $\sim 10^{38}$ erg s^{-1}.

The possibility also exists that some of the discrete sources detected in M82 might be associated with compact star clusters. The most luminous clusters in M82, regions 'A' and 'C' of O'Connell and Mangano (1978), have estimated masses of $\sim 10^{7}$ $M_{\odot}$ and mass to light ratios indicating that they are dominated by massive young stars. Thus it is plausible that the X-ray emission from these regions could be due to the integrated emission of the 10^{5}-10^{6} stars in each cluster, resulting in total soft X-ray luminosities in the range 10^{38}-10^{39} erg s^{-1}.

A significant fraction of the total X-ray luminosity from the nuclear region of M82 is not resolved into discrete sources by the HRI. Although this component could be genuinely diffuse in nature (perhaps related to the halo emission), it seems more likely that it is due to a population of less luminous X-ray sources. X-ray binaries, SNRs and O-B stars will all contribute to the integrated luminosity. Young SNRs may be particularly important if their average X-ray luminosity

is higher than in our galaxy because of the greater density of the M82 ISM (eg. Rieke et al. 1980). Indeed all of the nuclear region X-ray luminosity could be explained by SNRs with $< L_X > \sim 10^{37}$ erg s^{-1} and lifetimes of ~3000 years, if the supernova rate is ~0.3 $year^{-1}$. Such a high rate might be expected in a region displaying a high density of Population I objects; and indeed, SN rates of 0.1-0.3 $year^{-1}$ are predicted by the starburst models of Rieke et al. (1980). Individual SNRs are probably insufficiently luminous to be detected in the HRI observation, and in any case none of the known compact radio sources, most of which are likely to be young SNRs (Kronberg and Biermann 1983), have convincing X-ray counterparts.

Thus, it seems probable that the nuclear region of M82 is very different from the equivalent region of our galaxy, being dominated by emission from Population I objects. Our interpretation finds general support from the work of Fabbiano et al. (1982), who have investigated the X-ray properties of a sample of 33 peculiar galaxies (see also Chapter One, 1.3.3). These authors have established that X-ray flux correlates with both B-band optical and radio fluxes; this they interpret in terms of enhanced star formation rates resulting in increased Population I content for many peculiar galaxies.

3.4.2 The X-ray Halo

In Figure 3.7 the HRI X-ray image is compared with a deep $H\alpha$ plate of M82. The X-ray and optical haloes have similar dimensions, and both extend further to the SE than the NW. There is significant correlation between features in the X-ray halo and the optical filamentary structure, strongly suggesting some physical connection between the

Figure 3.7 (Plate)

Composite Hα/X-ray map of M82. The X-ray image (shown in contour map form) has 4 arcsec pixels and has been smoothed with a 2-D gaussian function with σ = 4 arcsec. The Hα photograph is taken from Lynds and Sandage (1963).

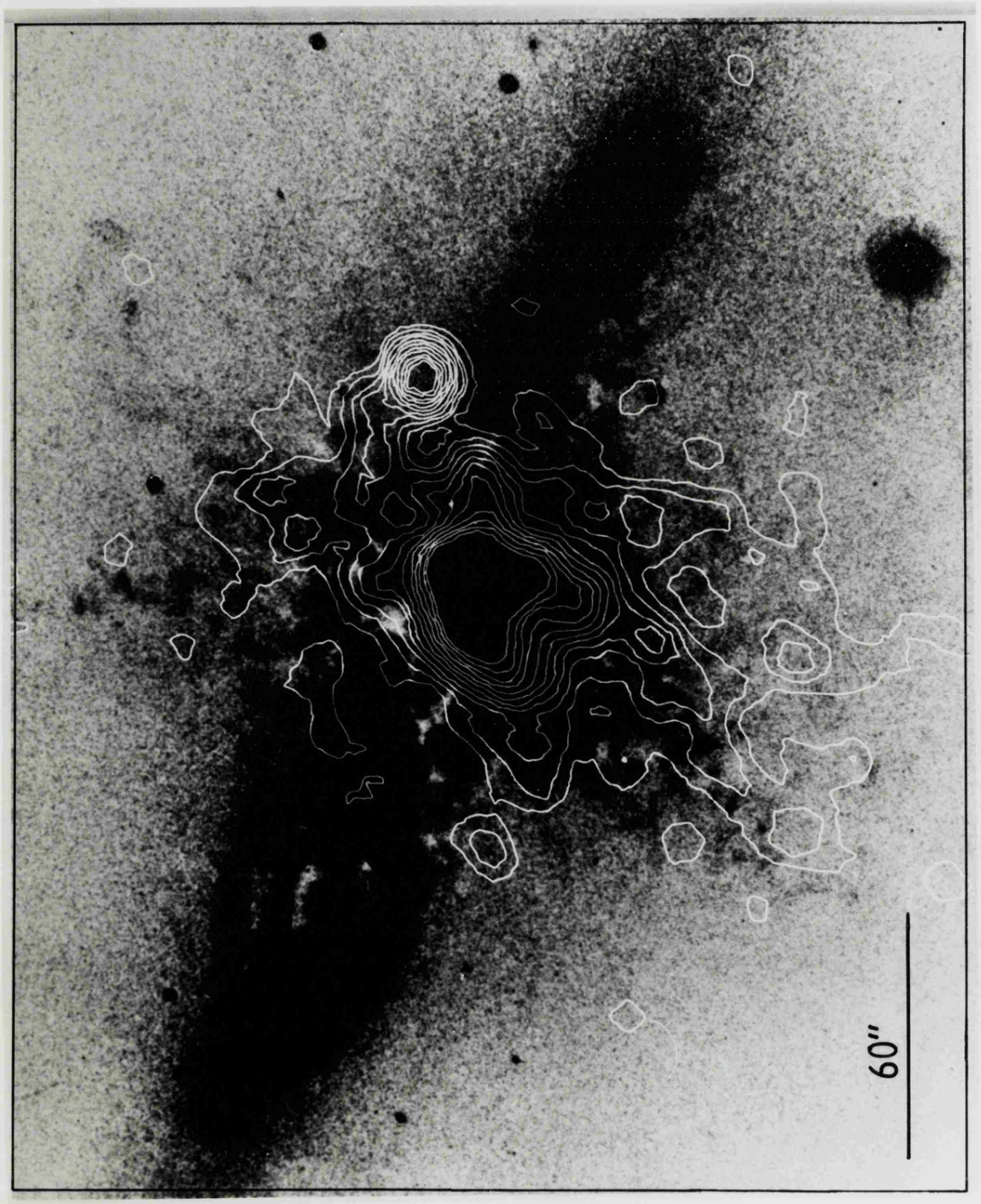
60"

two. We have also compared the X-ray data with a new high quality Hα plate kindly supplied by Dave Axon and find additional correlation with features not apparent on the Lynds and Sandage plate.

The X-ray halo is unlikely to arise from non-thermal processes since the radio flux from the halo region is a very small fraction of the total for M82 (Hargrave 1974), implying relativistic particle densities too low to yield the observed X-ray flux by either synchrotron or inverse compton mechanisms, even if the required energy densities in magnetic fields or photons were available. This conclusion would be invalid if the relativistic particles with the required energies ($\gamma \sim 100$ for inverse compton scattering of IR photons, or $\gamma \sim 10^7$ - 10^8 for synchrotron emission) have substantially different spatial distributions and energy densities compared to those particles responsible for the radio emission. We therefore believe that the X-ray emission from the halo is almost certainly due to thermal emission from hot gas.

Using the surface brightness profiles shown in Figure 3.4 we have estimated the full angular extent of the halo. We have assumed a slab geometry, with the halo thickness along the line of sight equal to the observed width of the halo, and estimate the total volume to be $V_{halo} \sim 6 \times 10^{65} f$ cm^3, where f is the volume filling factor. Because of the patchiness of the halo emission (clearly evident in Figures 3.3 and 3.7) we assume f = 0.1, although higher or lower values are obviously not ruled out (especially the latter, if the halo is thin along the line of sight). In order to derive accurate gas parameters we require a realistic estimate of the halo temperature. We have no direct way of determining this from the X-ray data, although we

require $T_{halo} > 10^6$ K for it to be observable with the HRI in the presence of $N_H > 2.5 \times 10^{20}$ cm^{-2} column density. The comparison between IPC and HRI fluxes for M82 as a whole provides some evidence that T_{halo} is less than the global value of 3 keV. In Table 3.3 we tabulate relevant thermal parameters for isothermal haloes with temperatures 3×10^6, 1×10^7 and 3×10^7 K, each yielding the measured HRI count rate in the presence of column density $N_H = 6 \times 10^{20}$ cm^{-2}. The column density internal to the halo is unknown, although the presence of considerable quantities of HI and dust suggests that it may be significant. Altering the assumed value of N_H by up to a factor of two changes the derived halo parameters by $\sim$30%. Our results indicate that the total mass of hot gas associated with M82 is $\sim 10^7$ M_o, considerably less than is contained in the extensive haloes which surround some early type galaxies (eg. Forman et al. 1979, Biermann and Kronberg 1983, this work - Chapter Five). The energy content of the gas contained in the M82 halo is equivalent to that released by $\sim 10^4$ supernovae, and its cooling time is similar to the estimates of the time elapsed since the start of the starburst (Rieke et al. 1980). The X-ray halo's complex morphology, unknown temperature and the ill-determined gravitational potential which it responds to, all tend to exclude the possibility of attempting a detailed deprojection of the X-ray data (cf. NGC 1275, Fabian et al. 1981); although we note that the radial emission profile of the halo appears to be relatively flat (see Figures 3.4 and 3.7), implying a weak dependence of electron density on distance from nuclear region.

The escape velocity within the halo of M82, inferred from the total galactic mass $M \sim 10^{10}$ M_o (Cottrell 1977), is $\sim$200 km s^{-1}. This

Table 3.3 : Thermal Parameters for the M82 X-ray Halo

T	L_x	Emission Measure	$\langle n_e \rangle$	M_{gas}	E_{gas}	$\langle t_{cool} \rangle$
[K]	[erg s^{-1}]	[cm^{-3}]	[cm^{-3}]	[$M_\odot$]	[ergs]	[years]
$3x10^6$	$1.5x10^{40}$	$5.4x10^{62}$	0.095	$2.9x10^6$	$7.1x10^{54}$	$1.5x10^7$
$1x10^7$	$1.3x10^{40}$	$4.6x10^{62}$	0.087	$2.6x10^6$	$2.2x10^{55}$	$5.2x10^7$
$3x10^7$	$2.1x10^{40}$	$1.8x10^{63}$	0.172	$5.2x10^6$	$1.3x10^{56}$	$1.9x10^8$

Notes to Table 3.3

(1) All calculations assumed an isothermal halo of volume $6x10^{65}$f cm^3, where f is the volume filling factor (assumed equal to 0.1), and an absorbing column density of $N_H = 6x10^{20}$ cm^{-2}, in each case resulting in a count rate of 0.1164 counts s^{-1} in the HRI band.

(2) The plasma is assumed to have solar abundances and emits an optically thin thermal spectrum (eg. Raymond and Smith) at the appropriate temperature.

implies that a halo with mean temperature $T \gtrsim 2 \times 10^6$ K would not be bound to M82; the hot gas would escape on a timescale of $\sim 10^7$ years assuming a halo scale size of ~ 2 kpc. The inferred cooling time for the hot gas is greater than the escape timescale, so radiative cooling is unimportant on a global scale for the halo gas observed with the HRI. We have no direct measurement of the temperature of the halo gas, but it is almost certainly hot enough to be unbound. The detection of an X-ray halo provides compelling evidence for the existence of mass outflow in the halo region of M82.

The existence of a halo of hot outflowing gas in M82 poses two interesting questions:

(1) What is the origin of the halo, and how is energy supplied to heat the gas?

(2) How are the X-ray and optical haloes physically linked?

The general properties of hot gaseous haloes around late type galaxies have been discussed by many authors (eg. Bregman 1978, 1980; York 1982, and references therein). In some respects, the halo observed in M82 resembles the models of Bregman (1980), but with one clear difference in that it is localised to a region near the minor axis, whereas Bregman's models (and most previous work) involve haloes of large scale height extending over the entire galactic disk. This difference can easily be understood if the M82 halo is linked to star formation occurring in the galaxy. Since the enhanced stellar activity in M82 is strongly concentrated within the nuclear region, we would expect the X-ray halo's morphology to reflect this concentration of activity. To be more specific, we suggest that much of the hot gas

now observed in the X-ray halo was originally infalling neutral gas (supplied by the ambient HI cloud in which M82 is embedded), some of which was consumed in fueling the rapid star formation in the nuclear region; the remainder has been heated to X-ray emitting temperatures by the passage of supernovae shock fronts outward from the nuclear region and thus incorporated into a general outflow of gas along the minor axis. The supernovae rate in the nuclear region may be sufficiently high for supernovae ejecta to also contribute significantly to the mass of hot gas in the halo. The energetics of the proposed supernovae heating are plausible: if the energy release per SN is $\sim 3 \times 10^{50}$ ergs (eg. Blair 1981), and the SN rate is 0.3 year^{-1} over a timescale of 3×10^{7} years (typical M82 starburst values, Rieke et al. 1980), then only $\sim 1\%$ of the total energy release is required to explain the current energy content of the X-ray halo. If the halo is unbound it would have to be completely replenished ~ 3 times during this period, since the escape timescale is $\sim 10^{7}$ years. The total SN heating rate in the nuclear region is $\sim 3 \times 10^{42}$ erg s^{-1}, which therefore greatly exceeds the radiative cooling rate of the X-ray halo ($L_X \sim 2 \times 10^{40}$ erg s^{-1}). Clearly, radiative cooling is unlikely to be important on a global scale within the M82 halo (in any case much of the gas will escape before it can cool radiatively), although we can certainly not exclude the possibility that cooling is locally important in small regions of unusually dense gas. In such regions dust may possibly play an important role by providing a shield against the effects of heating. The enormous discrepancy between the available heat input from supernovae and the actual energy content of the halo suggests that dissipative processes are highly efficient,

both within the nuclear region and the halo. The passage of SN shock waves through dense ISM clouds within the galaxy itself may actually initiate further star formation; the starburst may therefore be in some sense self-perpetuating. Energy dissipation in the halo may arise from the heating and consequent destruction of dust grains.

At present there are two more or less contradictory views on the nature of the optical halo and filaments: either they indicate the presence of line-emitting gas flowing outwards with space velocities of 400-600 km s^{-1} (Axon and Taylor 1978; Axon 1983, private communication), or they could arise from slowly drifting dust which scatters optical light originating in the nuclear region into our line of sight ("moving mirrors", Solinger et al. 1977). The timescale for the destruction of dust grains by thermal sputtering in a 10^7 K plasma is very short, $\sim 2\times10^5$ years for electron densities $n_e \sim 0.1$ cm^{-3} (Draine and Saltpeter 1977). This is difficult to reconcile with the existence of copious quantities of dust (and associated HI) in the same general region as the X-ray emitting gas, unless the halo region is highly inhomogeneous or the dust is continuously re-supplied from outside the halo. Neither possibility is excluded by currently available data. In contrast, if the filaments are line-emitting regions with substantial velocities with respect to the nucleus of M82, the significant correlation between the halo X-ray emission and the optical filaments can perhaps be plausibly explained by analogy with SNRs.

X-ray emission from SNRs originates in shock-heating of the ISM as the ejected shell moves outwards with velocities $\sim 10^2$-10^3 km s^{-1}. Hα filaments form in older SNRs (eg. Cygnus Loop, IC443) when radiative

losses lead to rapid cooling and hence fragmentation of the denser parts of the shock front (eg. Cox 1972). This can lead to overall correlation between the morphologies of the optical filaments and the X-ray emission, as is observed, since X-ray emission is also generated near the shock boundary. We envisage that a similar mechanism occurs in the halo of M82; the optical filaments therefore trace the positions of outflowing shocks. The complex morphology of the halo in this interpretation is then a direct result of the very complex velocity field of the outflowing gas, for which there is ample evidence from the many spectroscopic studies of M82 (eg. Williams et al. 1983). A major problem for our proposed interpretation is that both the morphology and the spectra of the optical filaments observed in the halo of M82 differ significantly from those of filaments observed in typical SNRs. It is conceivable that this discrepancy reflects the highly complex energetics and velocity structure of the halo region. Whatever the exact mechanism required to explain the properties of the optical filaments, we believe that the detection of the X-ray halo adds strong support to the contention that the inner parts of the M82 halo are dominated by outflow from the nuclear region.

Evidence for large quantities of dust is, however, overwhelming; particularly in the outer halo. This can be reconciled with the presence of the X-ray halo most naturally if the X-ray emitting gas and cold dust occupy spatially distinct regions. Our conclusions regarding the importance of outflow in the inner halo are supported by the work of O'Connell and Mangano (1978), which demonstrates that the line-emitting filaments in the inner region of the halo are dominated

by ionized plasma (as opposed to scattering dust). In the most detailed spectroscopic study to date, Williams et al. (1983) imaged the ionized hydrogen distribution associated with M82; their data indicate that infalling neutral gas (from the cloud in which M81 and M82 are immersed) fuels intense star formation in the nuclear region, the resulting outflow being responsible for the formation of the filaments. These authors also find evidence for gas in polar orbits about the galaxy, some of which may be accreting onto M82 at the current epoch. Clearly the dynamics of gas in the vicinity of M82, whether neutral, ionized or X-ray emitting plasma, must be highly complex. It is encouraging that several parallel lines of inquiry seem to be leading towards similar conclusions regarding the physical nature of the halo region of M82.

3.5 Conclusions

The main conclusions of our detailed study of the X-ray properties of M82 are as follows:

(1) The X-ray emission associated with M82 is not dominated by a single AGN-type nuclear source. Almost a third of the X-ray emission emanates from a complex region extending for $\sim$1 kpc and centred near the optical nucleus. Several discrete sources have been detected within the nuclear region, all of which have luminosities exceeding $\sim 5 \times 10^{38}$ erg s^{-1}. One of these sources is probably associated with the optical nucleus itself. A ridge of emission situated near the peak of the X-ray emission, aligned N-S along the minor axis of the galaxy, could be an extremely luminous extended feature associated with the compact radio source 41.9+58.

(2) On larger scales we have detected a halo of diffuse X-ray emission which extends for several kpc north and south of the nuclear region, roughly aligned with the galaxy's minor axis. Features in the X-ray halo are well correlated with the Hα filamentary system which is embedded in the optical halo.

The nuclear component of the X-ray emission can most readily be understood in terms of the integrated emission from Population I objects, such as high mass X-ray binaries, SNRs, O-B stars and associations thereof. Several of the nuclear region X-ray sources may in fact be ultra-luminous binary systems. The enhanced Population I content of the nuclear region has arisen from an intense burst of star formation initiated between 10^7 and 10^8 years ago. The same starburst activity, particularly supernova explosions, has created a mass outflow from the nuclear region which manifests itself as the X-ray halo: a $T \sim 10^7$ K plasma shock-heated by the outflow. If this interpretation is correct, the detection of an X-ray halo is important in enabling us to distinguish between the expulsion hypothsis, which appears to be valid for the inner halo, and the dust-scattering interpretation, which successfully accounts for the polarisation properties of the outer halo. There are important implications for our understanding of the dynamics of the gas flows in the vicinity of this most unusual galaxy.

Despite its extraordinary properties, it would be foolish to regard M82 as a unique galaxy. Several other galaxies share at least some of its characteristics; prominent examples include NGC 253 and NGC 3077. The former is a nearby, nearly edge-on spiral galaxy which possesses a

starburst nucleus; the latter is an Irr II galaxy with an optical morphology remarkably similar to M82, which by a curious coincidence happens to reside in the same physically associated group of galaxies. Do these galaxies also share the X-ray characteristics of M82? Their integrated properties are compared in Table 3.4.

NGC 253 has recently been the subject of a detailed X-ray study by Fabbiano and Trinchieri (1984); their analysis of HRI data reveals features remarkably similar to those we have observed in M82. Eight high luminosity ($\gtrsim 10^{38}$ erg s^{-1}) X-ray sources have been detected, some probably associated with the nuclear region, which on the basis of radio and IR measurements is known to be undergoing intense star formation. Fabbiano and Trinchieri also find evidence for a diffuse emission region associated with the nucleus, which they interpret as shock heated gas as a result of mass outflow from the starburst nucleus. This feature is less extensive and less luminous than the X-ray halo of M82, but in all other respects equivalent. In the case of NGC 253 there is no evidence that the starburst was triggered by tidal interaction with another galaxy; instead it may have been initiated by the accumulation of a critical quantity of gas slowly accreting from the galactic disk (as a result of normal stellar evolution).

In contrast, NGC 3077 is a galaxy which is morphologically similar to M82 and has clearly undergone tidal interaction with a neighbouring galaxy (M81, see Cottrell 1976), but which lacks obvious signs of intense star formation in its nuclear region. Cottrell (1976, 1977) has mapped the HI distributions around both NGC 3077 and M82, and has confirmed that the dynamics of the tidal interaction of each galaxy

Table 3.4 : Integrated Properties of M82 compared with NGC 253 and NGC 3077

NGC	TYPE	D [Mpc]	M_{DYN} [M_o]	L_x [erg s^{-1}]	L_{1415} [erg s^{-1} Hz^{-1}]
253	Sc	3.4	1.1×10^{11}	5.6×10^{39}	8.0×10^{28}
3034 (M82)	Irr II	3.25	1×10^{10}	2.7×10^{40}	1.1×10^{29}
3077	Irr II	3.25	6×10^{9}	1.9×10^{38}	2.7×10^{26}

Notes to Table 3.4

(1) Dynamical masses from Cottrell (1976), except for NGC 253 which was calculated on the basis of integrated optical luminosity and standard M/L for galaxy type. All masses must be considered to be highly uncertain.

(2) X-ray luminosities for NGC 253 and NGC 3077 are from Fabbiano and Trinchieri (1984) and Long and Van Speybroeck (1983) respectively.

(3) Monochromatic radio luminosity at 1415 MHz from Second Reference Catalogue of Bright Galaxies (de Vaucouleurs et al. 1976).

with M81, and the elapsed time since it occurred, are very similar. Both galaxies have similar masses ($\sim 10^{10}$ $M_{\odot}$) and are associated with complex systems of Hα filaments, yet NGC 3077 is underluminous by a factor of ~ 100 in both the X-ray and radio bands relative to M82. This discrepancy might seem to cast doubt on our interpretation of the X-ray properties of M82. A detailed examination of the HI maps of NGC 3077 and M82 does, however, suggest an explanation. Cottrell's map of NGC 3077 clearly demonstrates that very little of the neutral hydrogen associated with the NGC 3077 system is actually contained within the optical bounds of the galaxy. The obvious implication is that most of the gas deposited in the galaxy after the tidal interaction with M81 has already been used up in star formation. We conclude that unlike M82, where copious quantities of neutron hydrogen are still present within the galaxy, the starburst in NGC 3077 has subsided due to lack of fuel and presumably any associated outflow has been switched off. We note that there is no direct observational evidence for outflowing hot gas in this case, as there is no HRI data for NGC 3077; the low X-ray luminosity of NGC 3077 (Table 3.4) argues against the presence of substantial quantities of hot gas anyway. Further evidence that the starburst has subsided is provided by the very low radio luminosity, implying a relative dearth of SNRs compared with M82, and therefore a low current supernova rate. The continued presence of an Hα filament system in NGC 3077 presumably indicates that the (hypothetical) mass outflow due to starburst activity has only recently terminated in this galaxy. M82 and NGC 253 are examples of galaxies where starbursts are occurring at the current epoch.

CHAPTER FOUR : THE EINSTEIN-CFA SURVEY OF EARLY TYPE GALAXIES

4.1 Overview

In this chapter we present the results of a survey of eleven nearby early type galaxies observed with the X-ray imaging instrumentation on board the Einstein Observatory. The galaxies included in the survey have been selected on the basis of being isolated or weakly clustered; they are not members of the dense core regions of rich clusters of galaxies. Studies of relatively isolated galaxies should yield information relating to physical processes intrinsic to the galaxies themselves rather than the environmental processes which tend to dominate in cluster cores (eg. Fabian et al. 1980, Bechtold et al. 1983). Any attempt to determine the general X-ray properties of early type galaxies as a class requires the analysis of a galaxy sample significantly larger than the one under consideration here; we defer such an analysis to Chapter Five. Our immediate aims are therefore restricted to determining the basic observational X-ray properties of each individual member of the galaxy sample. Although the total number of objects is small, they are representative local examples of their class, thus the study of their properties should yield information of more general relevance. Analysis of Einstein image data will enable the derivation of an accurate soft X-ray flux for each galaxy in the sample; if an observed flux is sufficiently high we can expect to obtain additional information relating to the morphological and spectral properties of the X-ray emission.

4.2 Early Type Galaxies

4.2.1 Classification

The classification of galaxies as early type and late type species is a direct result of Hubble's classification scheme (Hubble 1936, also Sandage 1961). Hubble's scheme relied entirely on the visual appearance of a galaxy on a photographic plate. The resultant "tuning fork" diagram of morphological types was initially interpreted as an evolutionary sequence. Elliptical galaxies, lacking any evidence of recent star formation, were therefore designated early type galaxies. Subsequent work has demonstrated that all galaxies, irrespective of morphological type, display underlying old stellar populations. Late type galaxies, such as our own spiral system, possess an additional young stellar population. The Hubble classification scheme does not reflect an evolutionary sequence as was originally suggested, rather it is a conservation classification; a galaxy's morphology, and hence its location in the sequence of morphological types, reflects the proportion of star-forming matter consumed during the initial evolution of the galaxy (first 10% of its lifetime). This proportion is essentially 100% for most early type galaxies.

Although in a sense obsolete, the description early type galaxy has been retained. It is routinely applied to all galaxies which display elliptical (E) or lenticular (L or SO) morphologies, and in some cases also to bulge-dominated spirals (Sa). For the purposes of this study we classify galaxies as early type if they are listed in the Second Reference Catalogue of Bright Galaxies (de Vaucouleurs et al. 1976, hereafter 2RCBG) with Hubble type classification parameter $T < 0$. Galaxies classified as $T = 0$ are usually morphologically peculiar (eg.

have prominent dust lanes); we include them in the early type galaxy category if their underlying optical morphology and colours are normal for an early type galaxy.

Hubble subdivided elliptical galaxies according to the ratio of the observed (not necessarily intrinsic) dimensions of their major and minor axes. An elliptical galaxy is classified as En, where n = 10(a-b)/a and a/b is the ratio of the major and minor axes. No elliptical galaxies with $a/b \gtrsim 3$ are known, and the distribution of observed ellipticities is consistent with a relatively flat distribution of intrinsic ellipticities.

The classification lenticular galaxy was introduced by Hubble in 1936 to describe galaxies with a morphology intermediate between the flattest ellipticals (E7) and the bulge-dominated spirals (Sa). Lenticular galaxies are characterised by a disk-like appearance without obvious spiral arm structure. Apart from their morphologies, lenticular galaxies exhibit properties similar to those of elliptical galaxies: predominantly old stellar populations and considerably less gas and dust than is observed in spiral galaxies. Unlike elliptical galaxies, the majority of lenticular galaxies are probably intrinsically quite flat stellar systems.

For many years the observational evidence reinforced the view that early type galaxies were dynamically simple stellar systems consisting of an old population of predominantly low mass dwarf stars, and little else. Recent observational and theoretical work has indicated that view is overly simplistic. It has been established that elliptical galaxies possess a wide range of geometries, including spherical,

prolate, oblate and even triaxial examples; and the velocity distributions of stars within some early type galaxies show evidence of anisotropy (for a review, see Illingworth 1983). Indeed, the flattened structure of at least some early type galaxies may be due to their anisotropic velocity distributions rather than the effects of rotation. Recent observations also demonstrate that a small, but significant, minority of early type galaxies do contain measurable quantities of neutral gas and dust; albeit considerably less than is observed in spiral galaxies of comparable mass. The gas content of early type galaxies is a topic of considerable current interest; we will therefore review the observational evidence and discuss its implications in the next section.

4.2.2 The Gas Content of Early Type Galaxies

Stellar evolution in the form of mass loss from stars is expected to generate $\sim 0.015\ (L_V/10^9 L_\odot)\ M_\odot\ \text{year}^{-1}$ of gas in typical early type galaxies (Faber and Gallagher 1976). If we naively assume that no internal or external processes continually deplete the gas we would expect observable quantities of gas ($\gtrsim 10^9\ M_\odot$) to accumulate during the lifetime of a galaxy. What would be the physical state of the gas? There is strong observational evidence for the existence of a multiple phase ISM in our own spiral galaxy, including a high temperature component ($T \gtrsim 10^6$ K) observable in the soft X-ray band (eg. Fried et al. 1980). This has prompted several authors, including Bregman (1980), to propose models for hot X-ray emitting gas distributed in haloes of large scale height around our own and other galaxies. Such models are loosely based on the "galactic fountain" model for the ISM in our galaxy (eg. Shapiro and Field 1976).

The first attempts to detect gas in early type galaxies focussed on the possibility that these systems had accumulated and retained substantial quantities of neutral hydrogen. Surveys at 21cm indicate that only a small proportion of nearby early type galaxies have detectable quantities of neutral hydrogen, ie. $M_{HI}/D^2 \gtrsim 10^6\ M_o\ Mpc^{-2}$ (eg. Gallagher et al. 1975, Knapp et al. 1978). Indeed, extremely low mass limits have been established for certain galaxies, eg. $M_{HI} \lesssim 10^7\ M_o$ for NGC 4251 (Bieging and Biermann 1977). Sanders (1980) suggested that the distribution of observed HI masses among elliptical galaxies is bimodal, with $\lesssim$ 25% of systems being HI-rich ($M_{HI}/L_V \gtrsim 0.01$) and the remainder HI-poor ($M_{HI}/L_V \lesssim 0.003$). Whether lenticular galaxies share this behaviour is not clear, although it may be premature to attribute bimodality to elliptical galaxies given the present sparseness and poor sensitivity of the HI data. Neutral hydrogen observations have rarely attained sufficient sensitivity or angular resolution to map individual early type galaxies in any detail. Where HI has been detected, it is usually found to be distributed in an extended disk (eg. NGC 1052, Fosbury et al. 1978) or a clumpy ring (eg. NGC 4278, Raimond et al. 1981).

There is some evidence for the existence of a correlation between HI-richness and the presence of weak nuclear activity in elliptical galaxies (Dressel et al. 1982). Non-thermal radio emission and emission lines in the optical spectrum of the nuclear region are the most common signatures of activity. Examples of HI-rich, weakly-active elliptical galaxies include NGC 1052 and NGC 4278. Several authors have suggested that the correlation between these properties may imply a causal link; for example, the neutral gas might accrete

onto a massive, pre-existing central object and hence fuel the nuclear activity (eg. Hummel et al. 1983).

The demonstrable absence of significant quantities of neutral gas in most early type galaxies prompted several authors to examine mechanisms for either removing the gas or storing it in some "unobservable" form. Gisler (1976) noted that ram pressure stripping, caused by a galaxy's motion relative to a static IGM, would be an important gas depletion process for galaxies situated in, or passing through, the core regions of rich clusters. The efficiency of this process depends on the density of the ambient IGM and a galaxy's velocity relative to it. (Of course, the properties of a cluster IGM are at least partially determined by the evolution of the individual member galaxies.) Relatively isolated galaxies are also frequently observed to be gas-poor; since ram pressure stripping is unlikely to be significant for these galaxies, it would seem to be necessary to invoke efficient internal gas depletion mechanisms.

Star formation has been proposed as a possible sink for the missing neutral gas. High conversion efficiency (> 90%) would be required otherwise observable quantities of neutral gas would still remain in typical early type galaxies. A very steep or truncated IMF would also be necessary in order to avoid over-production of massive stars and hence anomalously blue colours. Faber and Gallagher (1976) favoured hot galactic winds as the most plausible gas depletion mechanism likely to operate in early type galaxies. In the hot wind scenario gas generated by stellar evolution is injected at a temperature consistent with the local stellar motion ($T \sim 4 \times 10^6$ K). Supernova

heating causes the gas to become unbound with respect to the galaxy's gravitational potential well and it escapes as a steady wind (eg. Mathews and Baker 1971). Hybrid models involving cycles of gas accumulation, rapid star formation and a subsequent supernova-driven wind have also been proposed (eg. Sanders 1981). The particular importance of the various wind models is that they imply the existence of hot gas within early type galaxies, admittedly in the process of being expelled. If the gas becomes sufficiently dense it ought to be detectable in the soft X-ray band.

4.2.3 Early Type Galaxies as X-ray Sources

It is clearly of considerable importance to establish the X-ray properties of this class of galaxy, and in particular to determine whether typical early type galaxies accumulate and retain significant quantities of hot gas. Only with the advent of the Einstein Observatory have observations with the required sensitivity and angular resolution proved feasible.

Several normal and weakly active early type galaxies have been detected in the soft X-ray band, with lumonisities in the range 10^{39} - 10^{42} erg s^{-1} (Forman et al. 1979, Long and Van Speybroeck 1983, Bechtold et al. 1983). Few detailed studies have been performed, but in cases where extended X-ray emission has been detected it has always been interpreted as due to substantial quantities of hot gas. Examples include M86 in the Virgo Cluster (Forman et al. 1979) and the isolated elliptical galaxy NGC 1395 (Nulsen et al. 1984). The hot gas hypothesis clearly has merit, but it is obvious that discrete X-ray sources (eg. low mass binaries, SNRs and even main sequence stars) must also contribute to the X-ray luminosity of an early type galaxy,

just as they do in M31 and our own galaxy, and may even provide the dominant contribution in some cases. By examining the detailed properties of a few typical galaxies (Chapters Four and Six) and the integrated properties of a much larger sample (Chapter Five), we should be able to determine the relative importance of X-ray emission from discrete sources and hot gas.

4.3 The Galaxy Sample

Our sample of eleven early type galaxies can be considered to be a set of reasonably representative local examples of their class. The sample consists of five normal ellipticals, four lenticulars, one dwarf elliptical (NGC 205, a companion of M31) and one peculiar galaxy (NGC 4753; classified I0 or T = 0, it has the visual appearance of a normal elliptical galaxy partially bisected by a dust lane). Optical and radio data for the members of this sample have been assembled in Table 4.1. The radio and HI data are dominated by upper limits, reflecting the low detection rate which applies even to relatively nearby early type galaxies at currently attainable instrumental sensitivities. NGC 4636 and NGC 4649 are the only galaxies in our sample definitely detected at GHz frequencies in radio continuum surveys; while NGC 5102 is the only galaxy for which a completely reliable HI detection exists. All data have been adapted from the listed references and rescaled to the distances established in Table 4.1. A Hubble constant of 75 km s^{-1} Mpc^{-1} has been assumed throughout.

Our interests are biased towards the intrinsic properties of early type galaxies; thus strongly clustered galaxies are excluded from our

Table 4.1 : General properties of Survey Galaxies

NGC	TYPE	D (Mpc)	B_T^o	$(B-V)_T^o$	L_v (erg s^{-1})	L_{Radio} (erg s^{-1} Hz^{-1})	M_{HI} (M_o)	References
205	E5	0.7	8.44	0.75	1.47×10^{42}	$<2.35\times10^{24}$	3.0×10^{5}	Radio 1, HI 2
1332	S0	20.3	10.84	0.81	1.41×10^{44}	$<4.93\times10^{27}$	$[5.3\times10^{8}]$	Radio 3, HI 4
1533	S0	7.5	11.58	0.89	1.08×10^{43}	$<1.01\times10^{27}$	-	Radio 5
3379	E1	10.4	10.00	0.89	9.42×10^{43}	$<1.29\times10^{27}$	$<2.9\times10^{7}$	Radio 1, HI 6
3585	E7	16.5	10.64	0.87	1.21×10^{44}	$<3.26\times10^{27}$	$<7.6\times10^{8}$	Radio 1, HI 7
4251	S0	12.3	11.25	0.81	3.56×10^{43}	$<1.81\times10^{27}$	$<1.3\times10^{7}$	Radio 3, HI 8
4291	E2	26.2	11.85	0.87	1.00×10^{44}	$<8.21\times10^{27}$	-	Radio 1
4636	E0	14.3	10.29	0.89	1.29×10^{44}	1.10×10^{28}	$<3.3\times10^{7}$	Radio 1, HI 9
4649	E2	15.0	9.62	0.95	2.96×10^{44}	6.73×10^{27}	$<1.2\times10^{8}$	Radio 1, HI 6
4753	I0	15.2	10.43	0.85	1.21×10^{44}	$<1.38\times10^{28}$	$<6.5\times10^{8}$	Radio 10, HI 7
5102	S0	4.2	9.86	0.58	1.06×10^{43}	$[1.69\times10^{26}]$	3.3×10^{8}	Radio 11, HI 7

Notes to Table 4.1

Column 1

Morphological type from second Reference Catalogue of Bright Galaxies (de Vaucouleurs et al. 1976; 2RCBG).

Column 2

Distances calculated from corrected redshift in 2RCBG, or from mean system redshift if member of a group or cluster (Sandage and Tammann 1975, de Vaucouleurs 1975). H_o = 75 km s^{-1} Mpc^{-1} assumed.

Columns 3 and 4

B_T^o and $(B-V)_T^o$ are corrected face on values from 2RCBG. $(B-V)_T^o$ was not available for NGC 4251 and NGC 4291; mean values for their morphological types were assumed.

Column 5

Visual luminosity calculated from B_T^o, $(B-V)_T^o$ and a suitable bolometric correction.

Column 6

Monochromatic radio luminosity at a frequency of 1.4 GHz except for NGC 1533 (2.7 GHz) and NGC 5102 (5.0 GHz). A value in brackets indicates that the result requires confirmation.

Column 7

Neutral hydrogen mass, adapted from listed references. A value in brackets indicates that the result requires confirmation.

References for Radio and HI Data

1. Hummel et al. (1983)
2. Unwin (1980)
3. Hummel and Kotanyi (1982)
4. Balkowski (1979)

5. Sadler (1984)
6. Knapp et al. (1978)
7. Gallagher et al. (1975)
8. Bieging and Biermann (1977)
9. Thonnard (1982)
10. Hummel (1980)
11. Disney and Wall (1977)

sample, whereas isolated or weakly clustered galaxies (eg. members of small groups or the outer regions of rich clusters) are included since they are unlikely to be subject to severe environmental influences. Seven of the galaxies included in our sample were also members of the widely-based survey of normal galaxies performed by Long and Van Speybroeck (1983); they in effect comprise the completed portion of the CFA-Einstein survey of early type galaxies, which was originally intended to encompass observations of twenty galaxies. Long and Van Speybroeck did not attempt detailed studies of the X-ray properties of individual galaxies, but instead presented an analysis of the properties of the sample of all types of normal galaxies as a whole, based on crude X-ray fluxes derived from IPC observations. In addition to the seven galaxies included in the original survey, we have acquired Einstein data for four extra galaxies; one was detected as a serendipitous source in an IPC observation of a quasar, the other three were targets of various observations which have been made available by the Einstein data bank service.

4.4 Observations and Results

4.4.1 Source Detection and Identification

The Einstein observations of the eleven early type galaxies in our sample are summarised in Table 4.2. Seven of the galaxies have been detected at a formal statistical significance greater than 3 sigma (and five of these at a significance greater than 5 sigma). For each detection, measurements indicate that the centroid of the X-ray emission and the optical centre of the galaxy have celestial coordinates which correspond to within an accuracy of ~ 1 arcmin. Since a typical galaxy has an optical extent of ~ 5 arcmin, and the

Table 4.2 : Summary of X-ray Observations

NGC	(1) SEQ	(2) EXPOSURE TIME (secs)	(3) DETECTION CELL	(4) COUNT RATE (10^{-3} ct s^{-1})	(5) STATISTICAL SIGNIFICANCE (Sigma)
205	H2730	23744.0	10' x 10'	3.8	0.8
1332	I7028	14296.0	4' radius	19.7	13.1
1533	I7030	13813.8	3' radius	5.0	4.5
3379	I2110	959.7	3' radius	8.0	2.0
3585	I7034	8977.9	3' radius	4.7	3.9
4251	I7036	12015.7	3' radius	1.4	1.4
4291	I5424	12825.9	3' radius	22.7	13.4
	H559	6020.8	3' x 3'	5.4	1.8
4636	I412	1317.1	4' radius	243.2	16.4
	H7038	32247.6	4' x 4'	56.4	37.6
4649	H2132	17272.3	4' x 4'	27.8	12.9
4753	I7039	12414.4	3' radius	7.3	6.1
5102	I7040	1990.4	3' radius	0.8	0.3

Notes to Table 4.2

Column 1

Observation sequence number. Prefix I = IPC, H = HRI.

Column 2

Observation exposure time.

Column 3

Detection cell used for determining count rates, detection significance and subsequent pulse-height analysis of IPC data.

Column 4

Background subtracted count rate, restricted to energy range ~0.5 to ~3.0 keV for IPC data. Dead time and quantum efficiency corrections have been applied.

Column 5

Statistical significance of detection.

aspect solutions of most IPC images are currently accurate to ~20 arcsec, we can be confident that the X-ray source identifications are secure.

Source detection was performed by sampling the relevant region of an image with a range of detection cells, using the automatic scientific analysis results as a guide (see Appendix A.2). For IPC images a circular cell of radius 3 arcmin was usually selected, this being an acceptable compromise between the optical extent of a typical galaxy and the requirements for optimum source detection imposed by the properties of the instrumental PRF. Larger detection cells were adopted for the definitive analysis of count rates and pulse-height spectra if there was any evidence of extended X-ray emission. Count rates for X-ray sources observed in HRI images were derived using detection cells optimized for the observed shape and angular extent of the emission (if resolved). If no X-ray source was detected, a 3 sigma upper limit to the count rate was derived using a cell roughly equivalent to the angular extent and shape of the "optical" galaxy.

4.4.2 Spectral Analysis and Flux Calibration

Only three of the galaxies detected in IPC observations yielded a sufficient number of counts to warrant a spectral analysis of the pulse-height data. Background subtracted pulse-height spectra were extracted from the source detection cells listed in Table 4.2. Details of the background subtraction procedure and the various corrections which are required in order to obtain the best estimate of the source-only spectrum are given in Appendix A.3. The useful IPC energy range for the relatively weak X-ray sources discussed here is ~0.5-3.0 keV; beyond this energy range, which is weakly dependent on

the instrumental gain during a particular observation, the signal to noise of the background subtracted pulse-height data is usually very poor, and residual contamination from the cosmic soft X-ray background and the instrumental calibration source tends to dominate (see Appendix A.3). Spectral model fitting therefore has to be performed over a very limited energy range, which combined with the IPC's very coarse energy resolution severely inhibits our ability to derive precise values for spectral model parameters. In particular, it has proved difficult to simultaneously constrain parameters describing the shape of the X-ray continuum and the degree of low energy absorption. Further uncertainty is introduced by the necessity of performing the spectral analysis for a range of possible IPC gain values; the exact gain being poorly determined for non-reprocessed IPC observations (see Chapter Two, section 2.3; and Appendix A.3).

In the three cases where spectral fitting could sensibly be performed, both non-thermal power law models and optically thin thermal models (eg. Raymond and Smith 1977) produced statistically acceptable fits to the data, although the thermal models are slightly favoured due to their lower chi-squared values. The best-fit thermal models have low energy absorption consistent with the line of sight column density through our galaxy (eg. Heiles 1975), although the range of allowed parameter values does not explicitly rule out higher quantities of absorption. We feel that there is no compelling evidence for excess low-energy absorption intrinsic to individual galaxies in our sample. Biermann and Kronberg (1983) reached a similar conclusion for the giant elliptical galaxy NGC 5846 on the basis of a spectral analysis of IPC data. For the definitive spectral analysis results (Table 4.3)

we have fixed N_H at the appropriate value for the galactic column density, enabling the derivation of a 1-D 90% confidence range for the thermal temperature using the prescription of Lampton et al. (1976). The best-fit thermal model and the background subtracted pulse-height spectrum for one of the galaxies in our sample (NGC 4636) are shown in Figure 4.1.

The spectral fits for NGC 1332 and NGC 4636 indicate relatively low characteristic temperatures of $\sim$1 keV for thermal emission from an optically thin plasma with solar element abundances. If instead a power law model is selected, the derived photon number index is correspondingly steep ($\gtrsim$ 3). A somewhat higher temperature is derived for NGC 4291; the result is less reliable, however, since the source spectrum may be slightly contaminated by scattered photons from a very much brighter quasar located 6 arcmin from the galaxy. Also, because the galaxy is not situated at the centre of the IPC FOV, the local instrumental gain is less well determined, and the reliability of the spectral analysis results further reduced.

The IPC and HRI fluxes listed in Table 4.3 have been calculated for an assumed isothermal plasma with a characteristic temperature kT = 1 keV and solar element abundances. A correction for low energy absorption due to the column density of neutral gas along the appropriate line of sight through our galaxy has been applied in each case. The derived fluxes are relatively insensitive to the assumed thermal temperature; varying the thermal temperature between 0.5 keV and 3.0 keV alters the flux values by $\lesssim$ 30%, comparable to the systematic uncertainty introduced into IPC flux calculations by the poorly determined

Table 4.3 : Spectral Analysis and Flux Calibration

NGC	(1) IPC BAL	(2) N_H(galactic)	(3) Best Fit kT (keV)	(4) 90% limit kT (keV)	(5) Flux (erg cm^{-2} s^{-1})	(6) L_x (erg s^{-1})	(7) L_x/L_v
205	H	7.2×10^{20}			$<1.7\times10^{-12}$	$<1.0\times10^{38}$	$<7.0\times10^{-5}$
1332	16.7	2.8×10^{20}	1.1	0.8-1.8	5.1×10^{-13}	2.5×10^{40}	1.8×10^{-4}
1533	16.8	2.4×10^{20}			1.2×10^{-13}	8.0×10^{38}	7.4×10^{-5}
3379	12.7	3.3×10^{20}			$<2.9\times10^{-13}$	$<3.7\times10^{39}$	$<3.9\times10^{-5}$
3585	15.9	6.1×10^{20}			1.3×10^{-13}	4.3×10^{39}	3.6×10^{-5}
4251	16.1	3.0×10^{20}			$<1.3\times10^{-13}$	$<2.4\times10^{39}$	$<6.7\times10^{-5}$
4291	16.2	3.9×10^{20}	1.8	1.2-4.8	6.4×10^{-13}	5.3×10^{40}	5.3×10^{-4}
	H	"			$<9.5\times10^{-13}$	$<8.0\times10^{40}$	$<8.0\times10^{-4}$
4636	17.3	2.8×10^{20}	1.2	0.9-1.5	6.2×10^{-12}	1.5×10^{41}	1.2×10^{-3}
	H	"			5.6×10^{-12}	1.4×10^{41}	1.1×10^{-3}
4649	H	2.8×10^{20}			2.8×10^{-12}	7.5×10^{40}	2.5×10^{-4}
4753	15.6	2.8×10^{20}			1.6×10^{-13}	4.5×10^{39}	3.7×10^{-5}
5102	16.5	4.4×10^{20}			$<3.0\times10^{-13}$	$<6.0\times10^{38}$	$<5.7\times10^{-5}$

Notes to Table 4.3

Column 1

BAL is a measure of the gain of the IPC during the observation. "H" implies HRI observation.

Column 2

N_H due to column density through line of sight in our galaxy. Values for NGC 1533 and NGC 5102 are from Heiles and Cleary (1979), all others from Heiles (1975).

Columns 3 and 4

Best-fit and 90% confidence region for thermal temperature derived from spectral model fitting. N_H was fixed at value in column 2.

Column 5

Absorption-corrected X-ray flux in 0.5 to 3.0 keV band, calculated for ~1.0 keV thermal spectrum. Upper limits are 3 sigma.

Column 6

0.5 to 3.0 keV X-ray luminosities derived from fluxes in column 5 and distances in Table 4.1. Upper limits are 3 sigma.

Column 7

Ratio of X-ray and visual luminosities. Upper limits are 3 sigma.

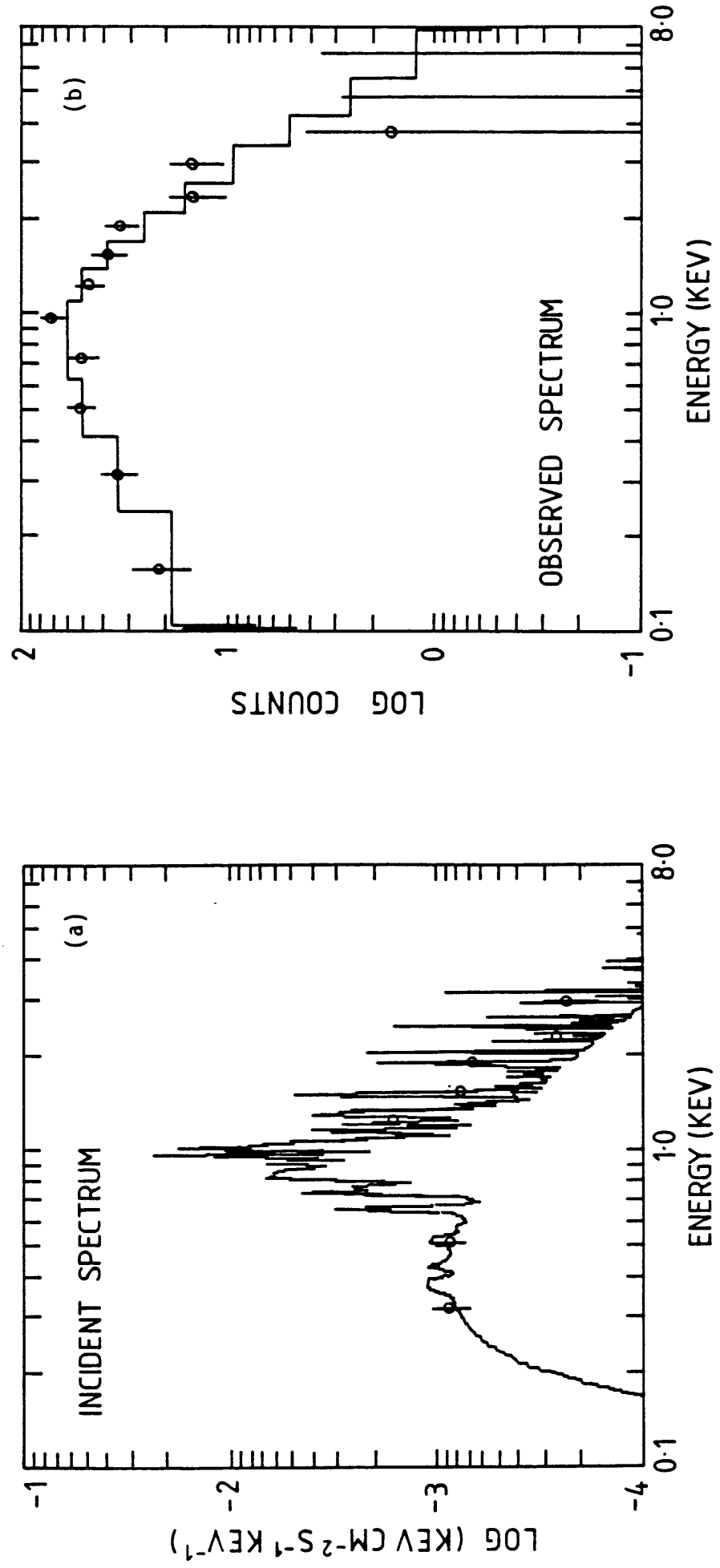

Figure 4.1 Best-fit thermal spectrum for NGC 4636 (kT = 1.2 keV, $N_H = 2.8 \times 10^{20}$ cm^{-2}) shown as (a) an incident energy spectrum and (b) compared with the background subtracted pulse-height data.

instrumental gain.

Our sample of early type galaxies exhibits a wide range of soft X-ray luminosities and X-ray to optical luminosity ratios (see Table 4.3). Several galaxies have soft X-ray luminosities below $\sim 10^{39}$ erg s^{-1}; whereas NGC 4636, with $L_x \sim 1.5 \times 10^{40}$ erg s^{-1}, is comparable to the most X-ray luminous early type galaxies previously reported (Forman et al. 1979, Biermann and Kronberg 1983, Nulsen et al. 1984). In the next section we will briefly discuss the X-ray properties of all the galaxies in our sample.

4.4.3 The X-ray Properties of Individual Galaxies

NGC 205

This dwarf elliptical companion of M31 has an optical extent of ~17x11 arcminutes and therefore occupies a substantial proportion of the HRI FOV. Analysis of the HRI data smoothed with a wide range of 2-D functions yields no evidence for extended, diffuse X-ray emission on angular scales $\lesssim$ 20 arcmin (~4 kpc). The mean image surface brightness is 1.3×10^{-6} ct s^{-1} $arcsec^{-2}$, a value typical for deep HRI exposures of high galactic latitude fields. Our three sigma upper limit to the X-ray flux (Table 4.3) implies a soft X-ray luminosity $L_x \lesssim 10^{38}$ erg s^{-1} for NGC 205.

The standard source detection algorithm applied to the HRI image during the post-observation automatic analysis detected three very faint X-ray sources near the edges of the instrument FOV. At least one spurious source (ie. an artefact of counting statistics) is expected per HRI field when this algorithm is used with a 24 x 24 arcsec detection cell; use of smaller cells resulted in no detections.

All three "sources" are situated well beyond the optical bounds of the galaxy, thus even if they are genuine X-ray sources (which is doubtful) they are almost certainly not associated with NGC 205. We therefore derive a three sigma upper limit to the X-ray intensity of any discrete objects located in NGC 205 of $\sim 3 \times 10^{-4}$ ct s^{-1}, corresponding to a 0.5-3.0 keV luminosity of $\sim 2 \times 10^{36}$ erg s^{-1}. This represents a well defined limit to the high L_X region of the X-ray luminosity function for discrete X-ray sources in NGC 205. We note that Long and Van Speybroeck (1983) have identified two discrete X-ray sources which are probably associated with M32 (NGC 221), another dwarf elliptical companion of M31. Although these authors did not provide details of fluxes, we would infer $2 \times 10^{36} \lesssim L_X \lesssim 2 \times 10^{37}$ erg s^{-1} for these sources if they are members of M32.

NGC 1332

Examination of contour maps of the smoothed IPC image indicates that the X-ray emission associated with this highly flattened (axial ratio 3.5) lenticular galaxy is approximately circular-symmetric and inconsistent with being an unresolved source. If a future high resolution observation confirms that the morphology of the X-ray emission is significantly different from the shape of the stellar component, it would provide compelling evidence that the bulk of the emission is generated by hot gas rather than main sequence stars and associated evolved objects. Further analysis of the properties of the extended X-ray emission associated with NGC 1332 is deferred to section 4.4.4.

NGC 1533, NGC 3585 and NGC 4753

Although all three galaxies have been detected by the IPC, their soft

X-ray fluxes are insufficient for useful spectral analysis to be performed. Indeed, the counting statistics are so poor that we are unable to determine whether or not the X-ray emission associated with these galaxies is extended. Perhaps the most interesting feature common to these three galaxies is that each has a very low X-ray to optical luminosity ratio (Table 4.3). This is most strikingly demonstrated by comparing NGC 3585 and NGC 4753 with NGC 4636. All three galaxies have similar optical luminosities, but NGC 4636 is a factor of $\sim$30 more luminous in the X-ray band than either NGC 3585 or NGC 4753.

NGC 3379, NGC 4251 and NGC 5102

None of these galaxies have been detected by the IPC, although in two cases, NGC 3379 and NGC 5102, the exposure time was rather short and the detection of X-ray emission correspondingly less likely. Even so, the three sigma upper limits derived for their X-ray to optical luminosity ratios indicate that these galaxies have X-ray properties which are comparable to the detected galaxies discussed in the previous section. Perhaps the most surprising non-detection is NGC 5102; this lenticular galaxy is quite unusual since its nuclear region is anomalously blue and contains young star clusters embedded in HII regions, and also substantial quantities of HI (van den Bergh 1976). Despite the evident star formation activity, the X-ray luminosity of NGC 5102 is very low ($\lesssim 10^{39}$ erg s^{-1}).

NGC 4291

Although this elliptical galaxy is relatively bright, the IPC data is probably contaminated by scattered photons from a very bright quasar centrally located in the detector FOV and displaced from the galaxy by

$\sim$6 arcminutes. We are therefore unable to derive detailed information about the angular extent and morphology of the X-ray emission associated with NGC 4291. Visual inspection of contour maps of the smoothed IPC image indicates approximate circular symmetry and an angular extent in the range 2 to 4 arcminutes. Although the short HRI observation failed to detect NGC 4291, the three sigma upper limit to the X-ray flux is entirely consistent with the measured IPC flux, assuming the X-ray emission has an angular exent of a few arcminutes. We can deduce from the HRI data that any purely nuclear X-ray source (ie. an AGN) associated with NGC 4291 has an X-ray luminosity $\lesssim 10^{40}$ erg s^{-1}.

NGC 4636 and NGC 4649

Given the existence of a deep HRI observation, a detailed analysis of the very short IPC observation of NGC 4636 might not seem particularly profitable. Examination of the IPC image clearly demonstrates that the X-ray emission is extended and highly asymmetric at low surface brightness levels (see Figure 4.2). A detailed analysis of the IPC radial surface brightness profile for NGC 4636 will be performed in section 4.4.4. The IPC data for NGC 4649 has only recently been released to the general astronomical community; we have not so far attempted a detailed analysis of the data, although output from the automatic scientific analysis indicates an angular extent of at least 1.5 arcmin for the X-ray emission associated with this galaxy. The automatic scientific analysis also indicates a soft X-ray flux roughly consistent with the HRI measurement (see Table 4.3). Similar consistency has already been demonstrated between the IPC and HRI fluxes emitted by NGC 4636. The deep HRI observations of NGC 4636 and

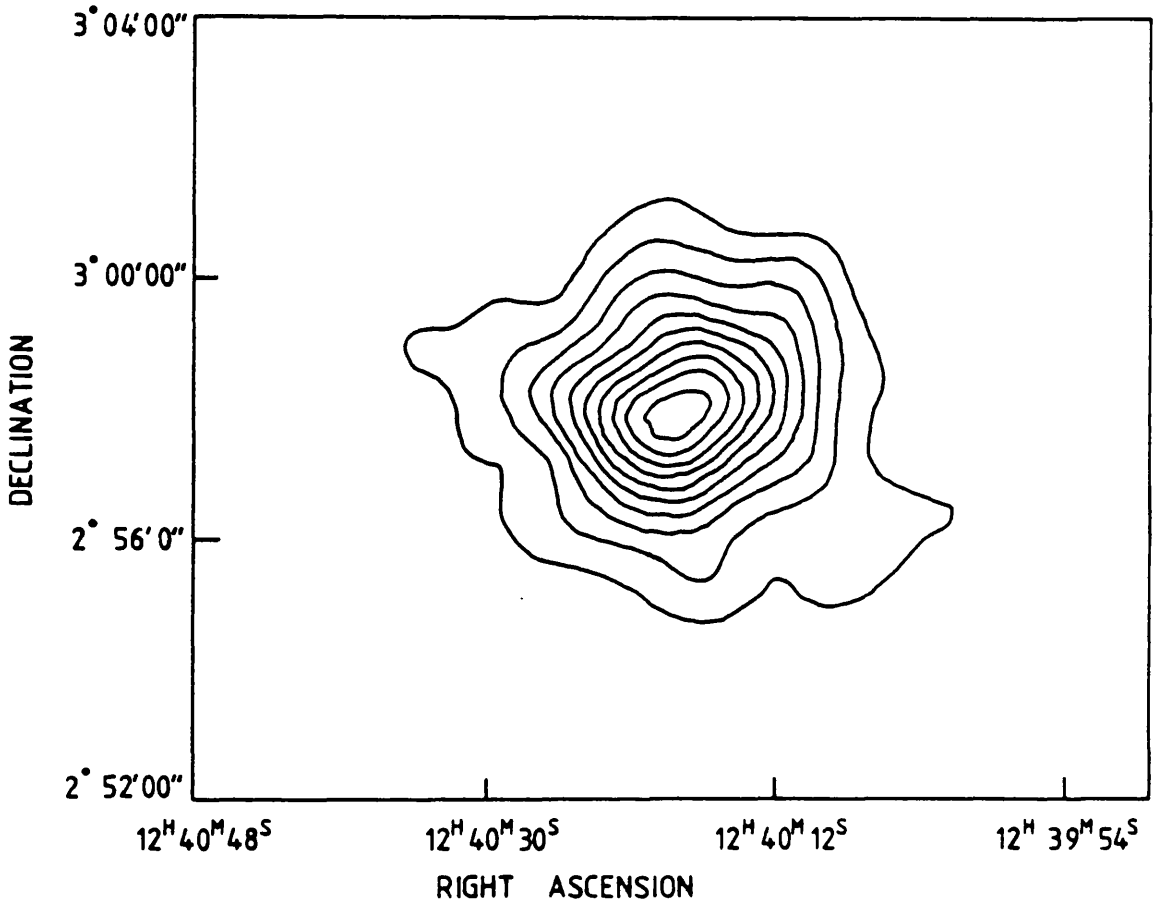

Figure 4.2 Contour map of NGC 4636 : the IPC data has been smoothed with a σ = 32 arcsec gaussian function and the contour levels correspond to 3, 6, 9.... sigma above background.

NGC 4649 yielded approximately 1800 and 500 source counts respectively; sufficient to map their complex central X-ray emission regions in some detail. A complete analysis of the HRI data for these two galaxies is beyond the scope of this chapter and is therefore deferred to Chapter Six, where we will also perform a complementary study of high resolution VLA radio data.

4.4.4 Analysis of IPC Radial Surface Brightness Profiles

Although the on-axis angular resolution of the IPC is a rather modest ~ 1 arcminute, it is possible to derive limited information about the angular extent and surface brightness properties of the X-ray emission associated with the brightest galaxies in our sample. Such an analysis might seem irrelevant for NGC 4636, given the availability of HRI data. The HRI is, however, intrinsically less sensitive to diffuse emission than the IPC; thus the IPC data allows us to trace the X-ray surface brightness of a galaxy like NGC 4636 out to larger radii. The radial profile analysis discussed below provides the simplest and most useful parameterization of the surface brightness properties of the X-ray emission detected by the IPC.

We have utilized a simple model-fitting technique to determine the angular extent and parameterize the surface brightness properties of X-ray sources displaying approximate circular symmetry detected in IPC (or HRI) images. This procedure is essentially analogous to spectral fitting for IPC pulse-height data. Simple geometrical models are convolved with a suitable representation of the instrumental point response function and tested (via the chi-squared statistic) against the background subtracted radial surface brightness profile of the X-

ray source. The radial profile is constructed by transforming the X-ray image into polar coordinates, with the origin at the X-ray source centroid, and rebinning the data into azimuthally averaged, concentric annuli. Only X-ray photons which have energies in the range $\sim$0.5-3.0 keV are included in the radial profile, since this is the energy range where the angular resolution of the IPC is optimum and where the surface brightness of the image background is at a minimum.

We have applied this technique to several IPC sources which HRI observations have confirmed are genuinely point-like; fitting to a gaussian model typically yields $\sigma \lesssim 15$ arcsec (90% confidence). It is our belief that this radial profile modelling technique gives reliable results for IPC sources which have angular extents equivalent to a gaussian width $\gtrsim$ 30 arcsec. Below this limit systematic errors due to inadequately determined IPC point response function parameters and residual jitter in the aspect solution (which tends to blur an unresolved source) seriously impair our ability to derive accurate model parameters.

Three simple models have been adopted for the analysis of IPC radial profiles:

(1) The gaussian model: $S(r) \propto \exp - (r^2/2\sigma^2)$. This model provides a useful parameterization of angular extent (σ, or some multiple thereof), but is not really physically meaningful because the X-ray surface brightness profiles of well-resolved galaxies are invariably non-gaussian.

(2) The power law model: $S(r) \propto r^{-\alpha}$. This model also lacks a direct physical justification, although it frequently provides an adequate

description of the X-ray surface brightness profile of a galaxy at large distances from the X-ray centroid.

(3) The isothermal gas sphere model; $S(r) \propto (1 + (r/a_x)^2)^{0.5-3\beta}$. This model essentially represents the observed (ie. projected) surface brightness distribution of an isothermal, spherically symmetric plasma (temperature T, mean atomic weight μ) in hydrostatic equilibrium with a gravitational potential field described by a King model. It is a standard formalism often used to parameterize the extended thermal X-ray emission associated with clusters of galaxies. It can in principle also be used to model similar emission associated with an individual galaxy. The parameter a_x is the core radius of the X-ray emission, and β is the ratio of the energy per unit mass associated with the hot plasma and the gravitating matter. For galaxy clusters β is theoretically equal to $\mu m_H \sigma^2/kT$, where σ is the velocity dispersion of the system. This definition also applies to an individual galaxy if the velocity dispersion of the stellar component (ie. its random motion) greatly exceeds the system's mean rotational velocity. This is certainly not true for all early type galaxies (eg. Illingworth 1983).

The results of the radial profile analysis of the IPC data for NGC 1332 and NGC 4636 are presented in Table 4.4. Only the power law model for NGC 4636 fails to provide an acceptable fit (ie. $\chi^2_\nu \lesssim 1.5$). Our inability to distinguish between the various models on statistical grounds is primarily due to the coarse resolution of the IPC. The derived gaussian width for NGC 1332, $\sigma = 30^{+10}_{-11}$ arcsec, is at the limit where systematic errors probably become important. This result

Table 4.4 Radial Profile Modelling of IPC Data

NGC	Model	Fitted Parameter	Best Fit and 90% Confidence Range	Reduced Chi-Squared
1332	Gaussian	σ (arcsec)	30^{+10}_{-11}	0.85
	Power Law	Index	$1.43^{+0.30}_{-0.18}$	0.77
	Isothermal Gas Sphere (β=0.5)	Core Radius (arcsec)	10^{+6}_{-5}	0.77
	Isothermal Gas Sphere (β=1.0)	Core Radius (arcsec)	50^{+18}_{-20}	0.82
4636	Gaussian	σ (arcsec)	72^{+9}_{-9}	0.96
	Power Law	Index	$1.40^{+0.10}_{-0.07}$	2.10
	Isothermal Gas Sphere (β=0.5)	Core Radius (arcsec)	33^{+7}_{-7}	0.72
	Isothermal Gas Sphere (β=1.0)	Core Radius (arcsec)	118^{+16}_{-16}	0.62

Notes to Table 4.4

Gaussian Model

$S(r) \propto \exp - r^2/2\sigma^2$, fitted parameter σ.

Power Law Model

$S(r) \propto r^{-\alpha}$, fitted parameter α .

Isothermal Gas Law Model

$S(r) \propto (1 + (r/a_x)^2)^{0.5-3\beta}$, β fixed, fitted parameter a_x.

therefore requires confirmation via a suitable high resolution X-ray observation. Results for NGC 4291 are not included in Table 4.4 because they are severely influenced by systematic errors due to contamination from the nearby QSO; we derive a formal gaussian width of ~ 45 arcsec, however the errors on this quantity are large and unknown.

A two parameter (a_x, β) isothermal gas sphere model provides a satisfactory fit to the IPC radial profiles of both NGC 1332 and NGC 4636. Unfortunately, the allowed ranges for both parameters are poorly constrained; the loci of parameter values within the 90% confidence contour is given by $a_x/\beta \simeq$ constant for values of $\beta \gtrsim 0.4$. The poorly constrained parameters are a consequence of the fairly low signal to noise and dynamic range of the data. In Table 4.4 we tabulate the model fitting results for β equal to 0.5 and 1.0 (the latter is the simplest form of the isothermal gas sphere, with the energy of the system equally distributed between the gas and the gravitating matter; eg. Lea et al. 1973). Data and best-fit $\beta = 1.0$ models for NGC 1332 and NGC 4636 are displayed in Figure 4.3. Early type galaxies with optical luminosities similar to NGC 1332 and NGC 4636 typically have velocity dispersions $\sigma \sim 200$-250 km s^{-1}, corresponding to $\beta \sim 0.3$ if the X-ray emitting gas has a temperature of ~ 1 keV and assuming rotation is unimportant. Models with such low values of β do <u>not</u> yield statistically acceptable fits to the IPC data, perhaps implying that rotation does contribute to the observed value of β. We conclude that although isothermal gas sphere models do provide an adequate description of the IPC data for NGC 1332 and NGC 4636, the allowed values of β are not directly predictable on the

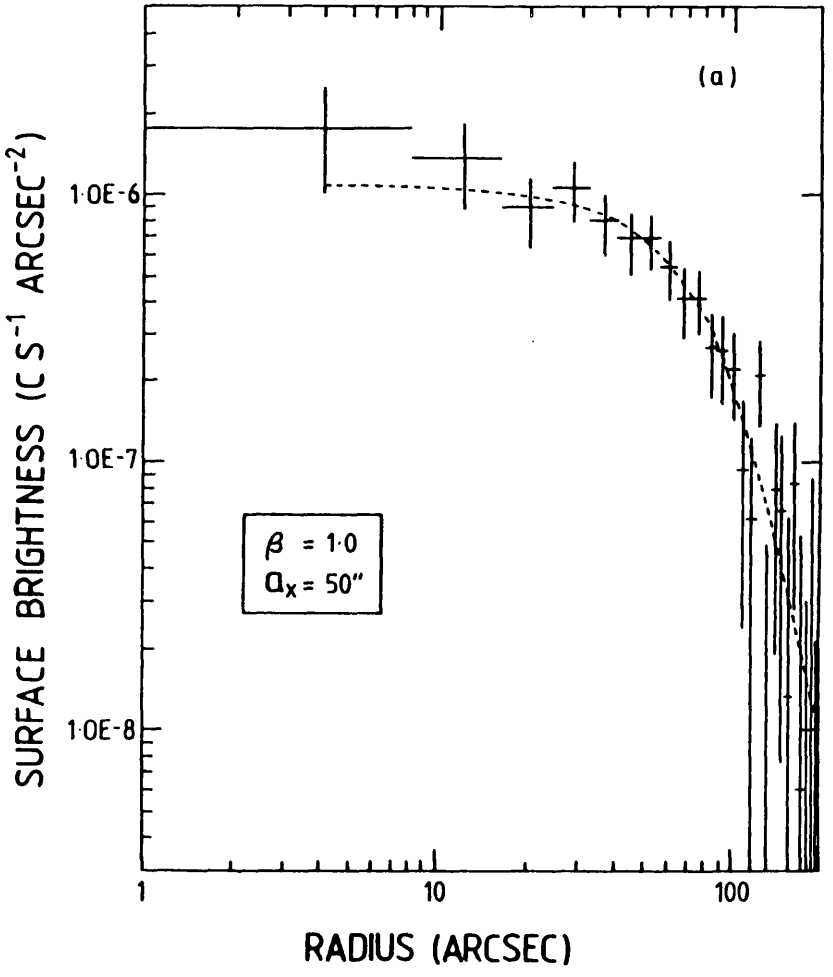

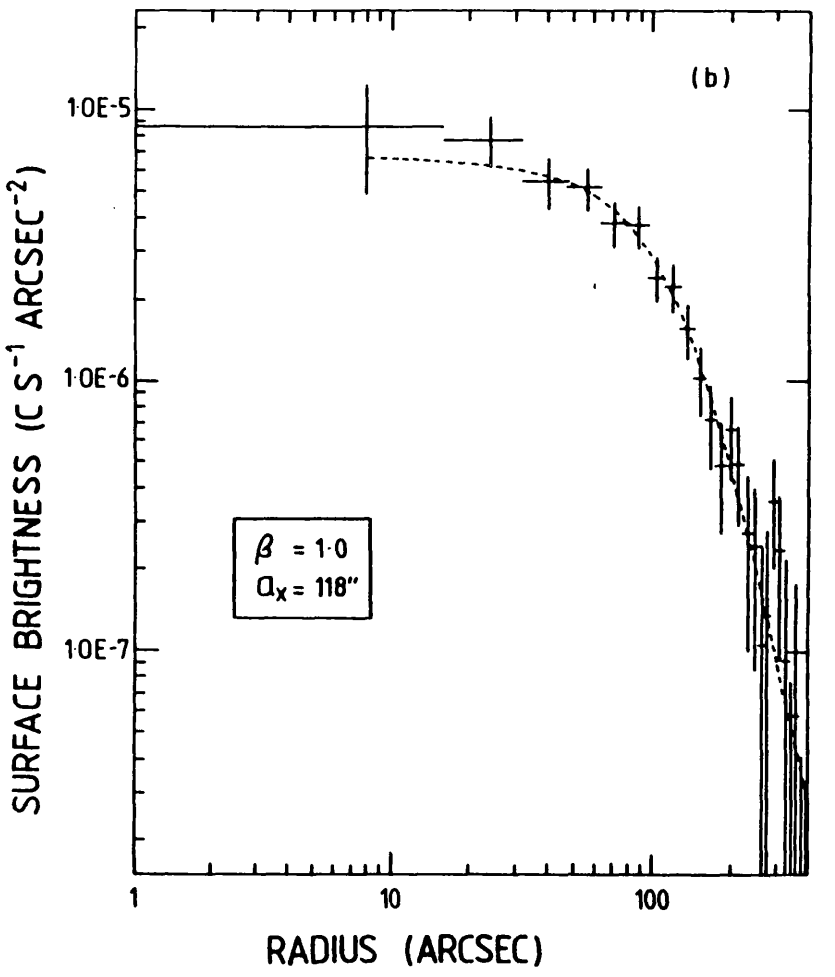

Figure 4.3 Background subtracted IPC radial profiles and best-fit isothermal gas sphere models for (a) NGC 1332 and (b) NGC 4636.

basis of other observable properties.

4.5 Conclusions

We have derived reliable X-ray fluxes, luminosities and X-ray to optical luminosity ratios for our representative sample of eleven nearby early type galaxies using IPC and HRI data. Limited spectral analysis has been performed for the three brightest galaxies detected in IPC observations. Their spectra are consistent with optically thin thermal emission with $kT \sim 1$ keV and no intrinsic low energy absorption. For two of these galaxies we have also derived information relating to their X-ray surface brightness profiles. Isothermal gas sphere models provide a good description of the radial profiles of NGC 1332 and NGC 4636, although gaussian models provide the simplest parameterization and a direct measure of the angular extent of the X-ray emission. If we define the characteristic X-ray radius to be $R_X = 3\sigma$ (where σ is the best-fit gaussian width), then NGC 1332 has $R_X \sim 9$ kpc and NGC 4636 has $R_X \sim 15$ kpc. These values are obviously only very crude estimates of the effective radius of the X-ray emission, since the gaussian model is unlikely to apply at large radii.

In Chapter Five we will examine the integrated properties of a larger sample of early type galaxies. Our principal aim will be to establish the relative contributions from stellar X-ray sources and thermal emission from hot gas to the X-ray luminosities of typical early type galaxies.

CHAPTER FIVE: THE INTEGRATED X-RAY PROPERTIES OF EARLY TYPE GALAXIES

5.1 Introduction

In Chapter Four we examined the observational X-ray properties of a small number of typical early type galaxies. The limited nature of this sample meant that we could not attempt to probe the possible relationships between X-ray and other integrated properties for this class of galaxy. By expanding the sample to include all early type galaxies for which reliable X-ray fluxes are available, and placing particular emphasis on the relationship between X-ray and optical luminosities, we should be able to determine the relative importance of the various X-ray emitting components within these systems. As we will shortly see, substantial quantities of hot, X-ray emitting gas are present in a significant number of early type galaxies; we therefore devote the second half of this chapter to a detailed analysis of its properties and possible evolution.

5.2 The Galaxy Sample

Compilation of a well defined galaxy sample is hindered by both the scarcity and non-uniformity of the available X-ray data. The absence of a uniform all-sky survey at Einstein sensitivities necessarily implies that any galaxy sample we formulate is incomplete, and neither X-ray flux limited nor optical magnitude limited in any strict sense. A detailed statistical analysis of sample properties will not be attempted, since any derived parameters would probably be influenced by the biases inherent in the sample. The galaxy sample which we study in this chapter should therefore be considered as representative rather than complete. It is, however, sufficiently large and widely

based that careful analysis should reveal interesting and generally applicable results.

The 40 galaxies listed in Table 5.1 form our basic sample. They have been selected using the following criteria; (a) inclusion in 2RCBG (de Vaucouleurs et al. 1976) with Hubble classification parameter $T < 0$ ($T = 0$ also accepted if the optical colours and underlying morphology of the galaxy are similar to early type galaxy norms); (b) availability of a reliable X-ray flux (or 3σ upper limit) derived from Einstein IPC or HRI observations. We have deliberately excluded the ~30 early type galaxies located in the rich cluster Abell 1367 which were discussed by Bechtold et al. (1983), as their inclusion would severely bias the sample towards strongly clustered galaxies. Another undesirable feature of the Abell 1367 sample is that virtually all of the galaxies were undetected, with flux limits which correspond to luminosities $\gtrsim 10^{41}$ erg s^{-1}. Their inclusion would severely distort the high luminosity region of the X-ray - optical luminosity relationship for early type galaxies discussed in this chapter. In contrast, galaxies associated with the Virgo Cluster have been included in our sample; they comprise only 20% of the total sample and thus are unlikely to influence its properties severely. Only two of the Virgo Cluster galaxies (NGC 4374 and NGC 4406) are thought to be physically associated with the core region of the cluster, and hence subject to significant environmental influences such as ram pressure stripping. Their inclusion in the sample is unlikely to lead to a significant bias.

Information relating to the methods adopted for deriving galaxy distances, fluxes and luminosities is provided in the notes

Table 5.1 : The Galaxy Sample

NGC	Group	Type	D(Mpc)	$(B-V)_T^o$	$Log_{10}\ L_V$	$Log_{10}\ L_X$	$Log_{10}\ L_{1415}$	$Log_{10}\ M_{HI}$	$Log_{10}\ L_X/L_V$	Refs
205	LOCAL	E5	0.7	0.75	42.15	<38.00	<24.37	5.48	<-4.15	2,9
221	LOCAL	E2	0.7	0.85	42.08	<37.81	<24.37		<-4.28	1,
524		L	34.6	0.88	44.49	40.72	<28.16	<8.26	-3.77	1,12
720		E5	24.3	0.86	44.31	40.77	<27.85	<8.69	-3.54	1,10
936		L	18.0	0.88	44.11	<40.47	<27.59		<-3.64	1,
1052	GROUP	E4	19.1	0.89	43.99	40.49	29.58	8.99	-3.51	7,10
1172		E1	21.6	0.81	43.50	<39.75			<-3.75	3,
1316	FORNAX I	Lp	21.8	0.83	44.80	41.14	31.78	<8.55	-3.66	1,15
1332	ERIDANUS	L	20.3	0.81	44.15	40.40	<27.69	8.72?	-3.75	2,14
1380		L	22.2	0.81	44.28	40.41			-3.87	1,
1395	ERIDANUS	E2	20.3	0.87	44.16	40.47	<27.69		-3.69	3,
1533	GROUP	L	7.5	0.89	43.03	38.91			-4.13	2,
1574		L	8.9	0.74	43.33	<39.39			<-3.94	1,
2859		L	22.1	0.85	44.04	<40.05	<27.77		<-3.99	1,
2974		E4	23.8	0.89	44.08	40.31	<28.23	8.48?	-3.78	3,10
3377	LEO I	E5	10.7	0.79	43.58	<39.46	<27.14	<7.06	<-4.12	1,10
3379	LEO I	E1	10.7	0.89	43.97	<39.60	<27.14	<7.49	<-4.37	2,10
3489	LEO I	L	10.7	0.74	43.57	<39.53	<27.14	<7.06	<-4.03	1,12
3585		E7	16.5	0.87	44.08	39.63	<27.51	<8.88	-4.46	2,10
3607	LEO I	L	10.7	0.88	43.67	39.91	<27.14	<6.57	-3.77	4,12
3818		E5	17.6	0.83	43.39	<40.09	<27.47		<-3.30	1,
3923		E4	20.6	0.91	44.26	40.48	<27.71	<9.02	-3.79	1,10
4251	COMA I	L	12.3	0.81	43.55	<39.37	<27.26	<7.15	<-4.18	2,13
4291	GROUP	E2	26.2	0.87	44.00	40.72	<27.91		-3.28	2,
4374	VIRGO	E1	15.7	0.92	44.29	40.20	30.26	<8.39	-4.08	5,16

NGC	Group	Type	D(Mpc)	$(B-V)_T^o$	$Log_{10}\ L_V$	$Log_{10}\ L_X$	$Log_{10}\ L_{1415}$	$Log_{10}\ M_{HI}$	$Log_{10}\ L_X/L_V$	Refs
4382	VIRGO	L	9.6	0.81	43.91	40.01	<27.04		-3.90	1,
4406	VIRGO	E3	15.7	0.89	44.33	41.34	<27.07	<8.36	-2.99	5,10
4459	VIRGO	L	13.9	0.88	43.77	<39.91	<27.36		<-3.86	1,
4472	VIRGO	E2	10.9	0.89	44.35	41.02	28.50	<7.62	-3.33	6,11
4636	VIRGO	E0	14.3	0.89	44.11	41.18	28.04	<7.52	-2.93	2,11
4638	VIRGO	L	13.4	0.78	43.41	39.03	<27.33		-4.38	1,
4649	VIRGO	E2	15.0	0.95	44.47	41.07	27.83	<8.07	-3.40	1,10
4697		E6	15.6	0.87	44.31	40.21	<27.46	<9.07	-4.09	1,10
4753		Lp	15.2	0.85	44.08	39.65	<27.44	<8.81	-4.44	2,13
5102	CAS A	L	4.2	0.58	43.03	<38.80		8.52	<-4.22	2,13
5532		L	94.7	0.90	44.82	41.39			-3.43	1,
5846	GROUP	E0	22.9	0.93	44.31	41.31	28.03	8.50?	-3.00	8,10
5866		L	11.7	0.74	43.81	39.71	27.42		-4.11	1,
5898		E0	28.4	0.95	44.04	40.16	<28.35		-3.88	1,
6876		E3	50.7	0.87	44.53	41.27			-3.26	3,

Notes to Table 5.1

Column 2

Physical grouping or cluster with which the galaxy is associated. "Group" refers to an anonymous system.

Column 3

Morphological type from 2RCBG.

Column 4

Best estimate of distance to galaxy, based on redshift listed in 2RCBG and H_o = 75 km s^{-1}. If galaxy is member of a group, the mean group redshift is adopted (Sandage and Tammann 1975). NGC 4374 and NGC 4406 are probably associated with the Virgo Cluster core; we have assumed the redshift of M87 applies to these two galaxies. NGC 4636 is associated with the G26-Virgo II complex, and we have adopted the distance derived by de Vaucouleurs (1975).

Column 5

Corrected value of $(B-V)_T^o$ from 2RCBG.

Column 6

Visual luminosity L_V has been calculated using B_T^o and $(B-V)_T^o$ from 2RCBG, and a suitable bolometric correction corresponding to B-V values for main sequence stars.

Column 7

Soft X-ray luminosity calculated from IPC or HRI measured flux in the $\sim$0.5-3.0 keV energy band, corrected for absorption along the line of sight through our galaxy.

References: (1) Long and Van Speybroeck (1983)

(2) This work - Chapter Four

(3) Nulsen, Stewart and Fabian (1984)

(4) Biermann, Kronberg and Madore (1982)

(5) Forman et al. (1979)

(6) Forman, Jones and Tucker (1983)

(7) Jones, Wrobel and Shaffer (1984)

(8) Biermann and Kronberg (1983)

Column 8

Monochromatic radio luminosity (erg s^{-1} Hz^{-1}) at a frequency near 1415 MHz. Data for all elliptical galaxies is from Hummel, Kotanyi and Ekers (1983); data for lenticular galaxies is from Hummel and Kotanyi (1982), except for NGC 1316 (2RCBG) and NGC 4753 (Hummel 1980).

Column 9

Neutral hydrogen mass derived from 21 cm data. Values followed by "?" are currently considered to be doubtful detections.

References: (9) Unwin (1980)

(10) Dressel, Bania and O'Connell (1982)

(11) Thonnard (1982)

(12) Biermann, Clarke and Fricke (1979)

(13) Gallagher, Faber and Balick (1975)

(14) Balkowski (1979)

(15) Jenkins (1983)

(16) Knapp, Kerr and Henderson (1979)

accompanying Table 5.1. Einstein X-ray fluxes have been obtained from several sources (see list of references); the authors of which have adopted a variety of energy ranges and spectral forms for their flux calculations. We have not attempted to standardize these fluxes, since utilization of a single spectrum and energy range typically alters a flux from its published value by no more than $\sim 30\%$. Such variations are unlikely to significantly influence the results of our essentially qualitative treatment of the galaxy sample. IPC-derived fluxes have been used in preference to HRI fluxes wherever possible, because the IPC is intrinsically more sensitive to the extended X-ray emission which is characteristic of early type galaxies. The wide range of IPC and HRI observation times (10^3 to 4×10^4 seconds) has resulted in a non-uniform detection sensitivity for the sample. The detection limit varies between 5×10^{-14} and 5×10^{-13} erg cm^{-2} s^{-1} in the 0.5 - 3.0 keV energy band.

The basic properties of the galaxy sample are displayed in Figure 5.1. Virtually all of the galaxies are fairly local; the mean distance of 18 Mpc is similar to distance of the Virgo Cluster. Inclusion of the two Local Group dwarf ellipticals, NGC 205 and NGC 221, has ensured that the distributions of both optical and X-ray luminosities are quite broad. The optical luminosity distribution shows quite a sharp cut-off at $\log_{10} L_V \sim 44.5$, indicating a lack of supergiant elliptical galaxies (cD types etc) in our sample. The distribution of X-ray luminosities peaks at $\log_{10} L_X \sim 40.0$, with an apparent cut-off at $\log_{10} L_X \sim 41.5$, perhaps denoting a real upper limit for galaxies of this type. An essentially similar galaxy located at the centre of the gravitational potential well of a rich cluster (eg. NGC 1275 in

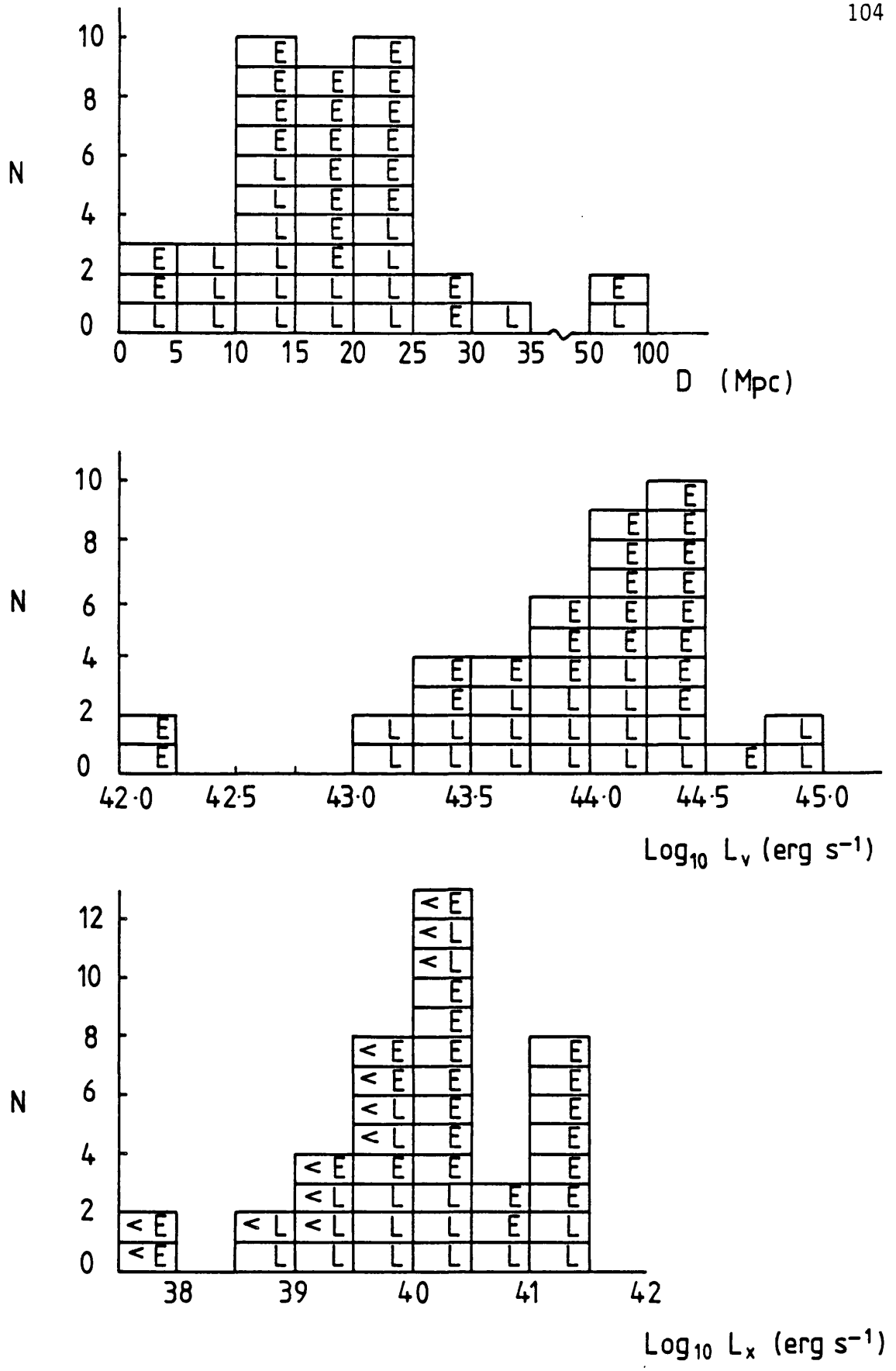

Figure 5.1 The general properties of the sample of early type galaxies. E = elliptical; L = lenticular; < denotes upper limit.

Perseus, M87 in Virgo) can attain a considerably higher X-ray luminosity. The X-ray emission from such galaxies is dominated by processes associated with the dynamical evolution of the whole cluster (eg. galactic cannabilism leading to the formation of cD galaxies which become the centre of pressure-driven cooling flows); we therefore exclude them from our sample.

Although the final galaxy sample is by no means ideal for the intended study, it is the largest representative set of early type galaxies at our disposal. We believe that the study of a large sample of galaxies, albeit incomplete and possibly biased by selection effects, is likely to prove worthwhile.

5.3 Relationships Between Integrated Properties

5.3.1 The Correlation Between X-ray and Optical Luminosities

In Figure 5.2 we present the fundamental result of our survey of early type galaxies: the soft X-ray and optical luminosities display a well defined correlation. Although considerable scatter is evident in the L_X - L_V relationship, it is clear that the most optically luminous galaxies also tend to be the most X-ray luminous. A least squares fit to the data has not been attempted, primarily because the low luminosity region is poorly determined, being dominated by upper limits derived from X-ray observations of varying sensitivity. It is obvious, however, that the slope of the L_X - L_V relationship is steeper than unity at least for high luminosities.

A generally similar correlation is evident for the corresponding X-ray and optical fluxes (Figure 5.3), although a somewhat greater degree of

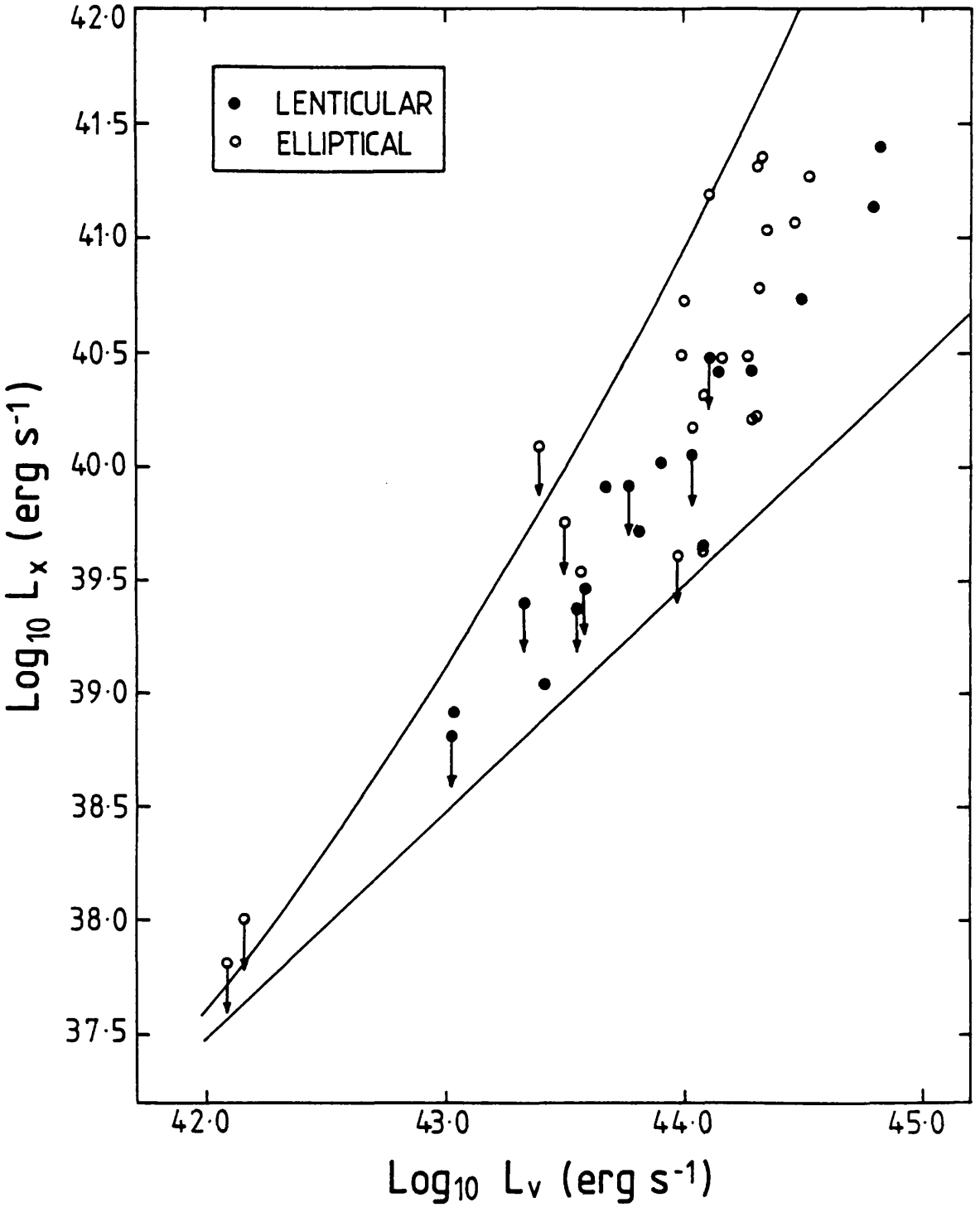

Figure 5.2 The relationship between X-ray luminosity and visual luminosity for early type galaxies. The two empirical luminosity functions discussed in the text are also displayed.

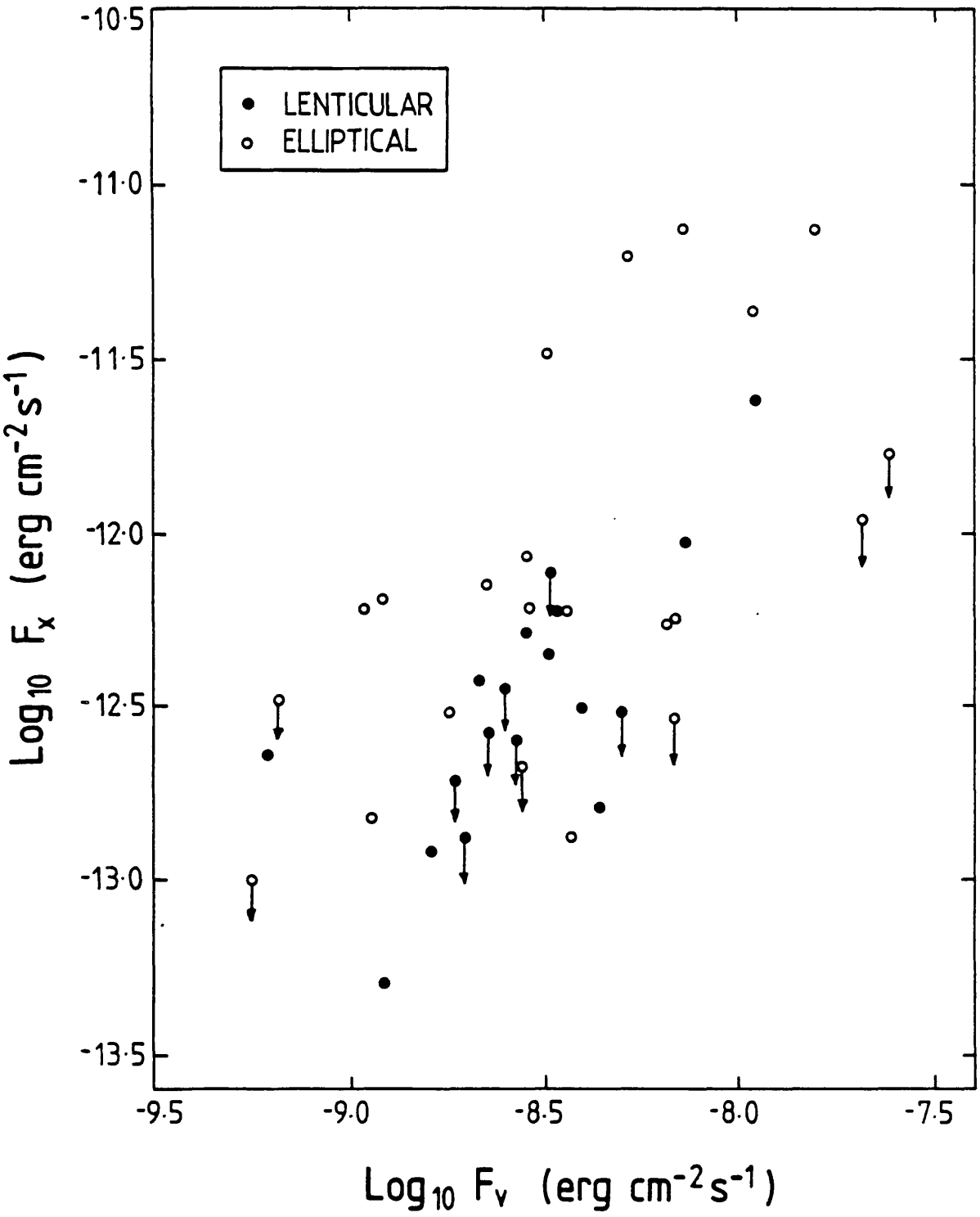

Figure 5.3 The relationship between X-ray flux and visual flux for early type galaxies.

scatter is apparent. It is worth noting that if a set of objects with widely varying distances are detected over a small range of apparent brightness in two separate wavebands, a correlation between absolute luminosities will be observed even if the corresponding fluxes are uncorrelated. For the present galaxy sample, a degree of correlation between X-ray and optical fluxes certainly exists; moreover, both sets of fluxes range over roughly two orders of magnitude. Figure 5.1 demonstrates that most of the galaxies in our sample have rather similar distances, hence the luminosity correlation is almost certainly genuine, as opposed to it being a spurious artefact. Long and Van Speybroeck (1983) noted the existence of an essentially similar correlation between X-ray and optical luminosities in their sample of ~70 normal galaxies of all morphological types. Given that some early type galaxies are common to both samples it is not entirely surprising that similar correlations exist.

The 22 elliptical galaxies and 18 lenticular galaxies in the current sample, considered independently, appear to display generally similar X-ray - optical luminosity functions, although the slope of the function is somewhat steeper at high luminosities for elliptical galaxies (see Figure 5.2). This result is consistent with the findings of Long and Van Speybroeck that the X-ray - optical luminosity functions for the various classes of normal galaxies are rather similar.

The existence of a well defined correlation between X-ray and optical luminosities has an obvious, but very important, implication for normal galaxies in general and early type galaxies in particular. X-ray emission associated with a particular galaxy must be generated by

processes which are a direct result of the normal evolution of its stellar population(s). In the case of an early type galaxy, X-ray emission can arise from main sequence stars, low mass X-ray binary systems, globular cluster sources, SNRs and thermal emission from hot gas. The last of these occurs because matter ejected from stars at various stages of their evolution is thermalized at X-ray emitting temperatures by random stellar motions and possibly supernova heating. Late type galaxies have an additional X-ray emission component associated with Population I objects, eg. O-B stars and high mass X-ray binaries.

If the X-ray emission associated with early type galaxies was simply generated by a large number of discrete objects (main sequence stars, SNRs, X-ray binaries) we would expect to find a well defined linear correlation, namely $L_X \propto L_V$, exhibiting relatively little intrinsic scatter. Galaxies with similar optical luminosities would be most unlikely to display a wide range of X-ray luminosities. Partial support for this hypothesis was provided by Long and Van Speybroeck (1983), who observed that the number of high luminosity ($L_X \gtrsim 10^{37}$ erg s^{-1}) discrete sources associated with a spiral galaxy in the Local Group is proportional to the galaxy's mass. Indeed, this relationship also extends to the two Local Group elliptical galaxies in our sample. NGC 205 and NGC 221 have masses of $\sim 4 \times 10^9$ $M_\odot$; comparison with M31 ($M_{gal} \sim 3 \times 10^{11}$ $M_\odot$, 80 objects with $L_X \gtrsim 10^{37}$ erg s^{-1}) leads to a prediction of one high luminosity object per galaxy. The observed X-ray source numbers, zero in NGC 205 (Chapter Four) and possibly two in NGC 221 (Long and Van Speybroeck 1983), are consistent with the prediction.

Early type galaxies in which the X-ray emission is predominantly due to hot gas might also be expected to follow a simple relationship, ie. $L_X \propto L_V^2$. This functional form follows from L_X (gas) $\propto \langle n_e \rangle^2 V_{gas}$, and the reasonable assumption that the total mass of gas generated by stellar mass loss is a linear function of the mass of the stellar component; hence $\langle n_e \rangle \propto L_V$. We have, of course, further assumed that the volume occupied by the gas is not a function of L_V; this may be unrealistic since V_{gas} could be determined by a galaxy's gravitational potential well, which is shaped by the stellar distribution and therefore related to L_V. We shall see, however, that the subsequent evolution of hot gas in an early type galaxy may be quite complex. The scatter in the high luminosity region of the L_X - L_V relationship could reflect a large variation in the amount of hot gas actually retained by galaxies of similar optical luminosity.

5.3.2 Analysis of X-ray - Optical Luminosity Ratios

The luminosities assigned to a particular galaxy are necessarily a strong function of the adopted distance, which due to uncertainty as to the correct value of H_o is obviously ill-determined. We therefore prefer to use the distance-independent ratio L_X/L_V as an indicator of relative X-ray power. The L_X/L_V values for the 40 galaxies in our sample (Table 5.1) range from 3×10^{-5} to 10^{-3}. The obvious implication is that some early type galaxies generate a considerably higher quantity of X-ray emission per unit mass of stellar population (hereafter, specific X-ray luminosity) than others.

The L_X/L_V distributions for the entire sample, and for the elliptical and lenticular species separately, are displayed in Figure 5.4.

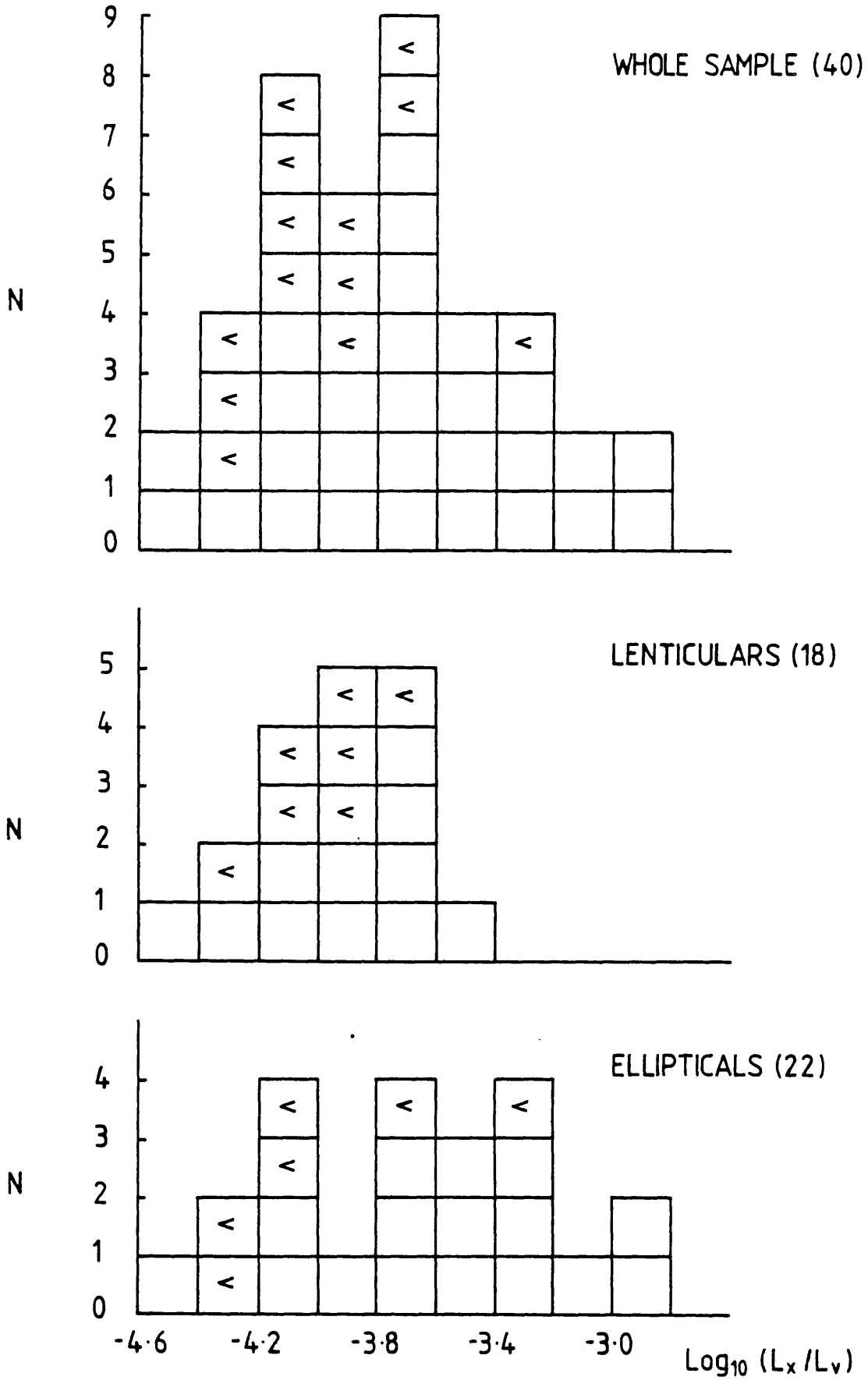

Figure 5.4 L_x/L_v distributions for the sample as a whole, and for lenticular and elliptical galaxies separately. < denotes upper limit.

Several interesting features are apparent.

(1) The distribution is not sharply peaked, and has a median value of $L_X/L_V \sim 10^{-4}$. Since upper limits to L_X comprise only about one third of the sample they are unlikely to severely distort the true shape of the distribution.

(2) Separation of the L_X/L_V distribution into the two galaxy species demonstrates that the distribution for lenticular galaxies is truncated at $L_X/L_V \sim 2.5 \times 10^{-4}$, whereas the distribution for elliptical galaxies extends to $\sim 1 \times 10^{-3}$. The most optically luminous elliptical galaxies appear to have significantly higher specific X-ray luminosities than the equivalent lenticular galaxies. Although this result might simply reflect the limitations of our sample, the total number of elliptical and lenticular galaxies is rather similar (22 and 18 respectively), which does provide some backing for this potentially important result. Selection effects can obviously not be ruled out, however, so a detailed analysis of a much larger sample of galaxies would be highly desirable. In Figure 5.5a L_X/L_V is plotted against L_V, clearly demonstrating that for high values of L_V the elliptical galaxies in our sample possess a wider range of specific X-ray luminosities than the lenticular galaxies. A plot of L_X/L_V versus L_X (Figure 5.5b) also confirms that high specific X-ray luminosities are associated with high L_X rather than low L_V.

(3) For both elliptical and lenticular galaxies the lowest observed values of L_X/L_V are $\sim 3.5 \times 10^{-5}$; there are also several three sigma upper limits below $\sim 6 \times 10^{-5}$. Obviously, all galaxies must have

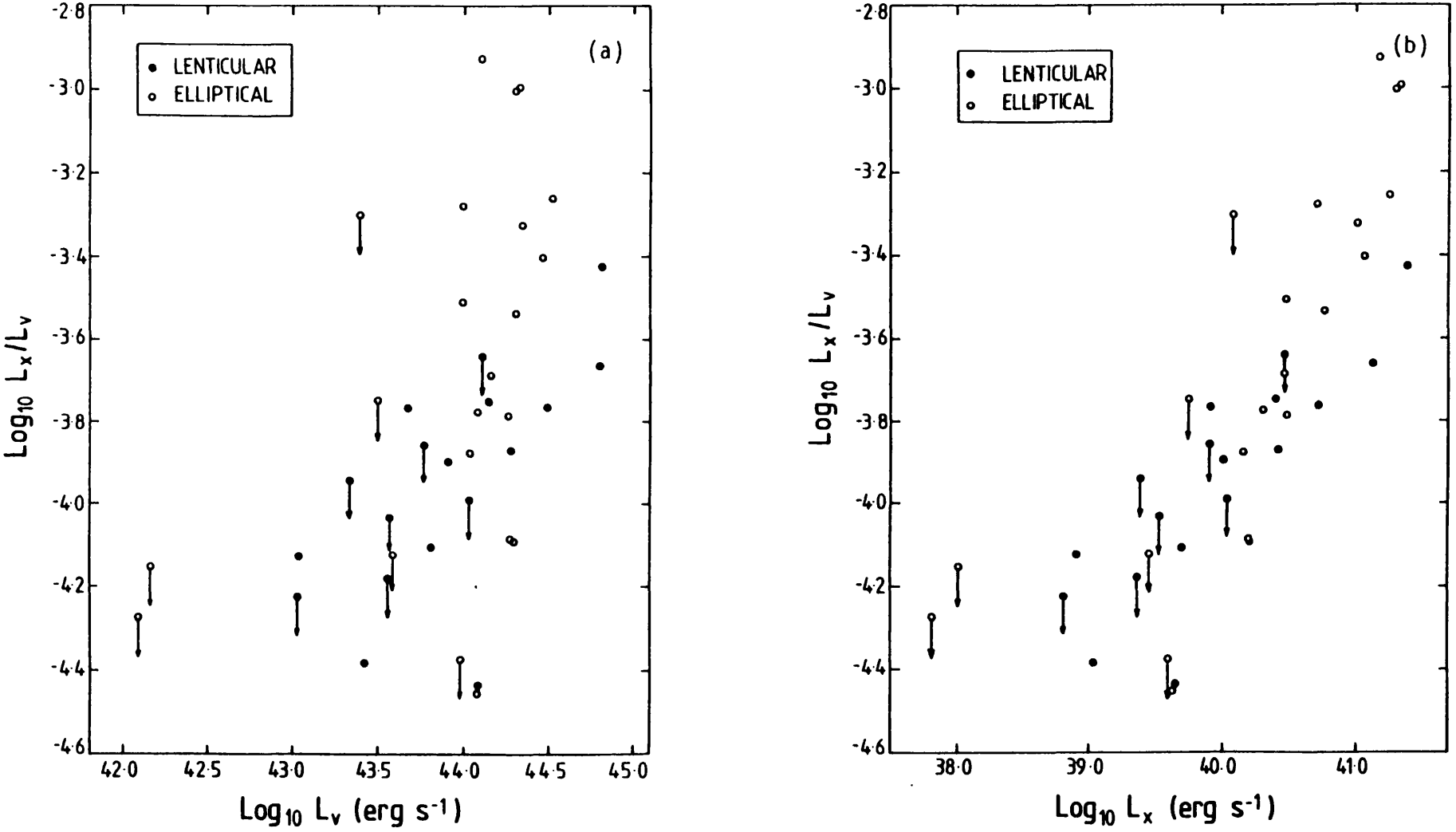

Figure 5.5 (a) L_x/L_v plotted as a function of L_v; (b) L_x/L_v plotted as a function of L_x.

$L_X/L_V > 0$, since even main sequence stars emit X-rays. Vaiana et al. (1981) derive $L_X/L_V \sim 10^{-5}$ - 10^{-4} for low mass main sequence stars. For a given stellar population (i.e. initial mass function, chemical composition and age specified) there should be a characteristic value for the specific X-ray luminosity, $(L_X/L_V)_*$, corresponding to X-ray contributions from main sequence stars and their evolved descendents - SNRs and X-ray binaries. The X-ray luminosity of this stellar component is proportional to the mass, and therefore optical luminosity, of a galaxy. We suggest that the minimum observed value of L_X/L_V for galaxies in our sample is a reasonable estimate of the quantity $(L_X/L_V)_*$ for early type galaxies. Henceforth, we will assume that $(L_X/L_V)_* \sim 3\times10^{-5}$ is applicable to the stellar populations of all the galaxies in our sample. The locus of $L_X/L_V = 3\times10^{-5}$ is plotted on the X-ray - optical luminosity diagram for the sample (Figure 5.2). It is interesting to note that our estimate for $(L_X/L_V)_*$ is very similar to the lowest observed values of L_X/L_V for the spiral galaxies included in the normal galaxy survey performed by Long and Van Speybroeck (1983). We would expect the bulge regions of spiral galaxies to have L_X/L_V values similar to our estimate of $(L_X/L_V)_*$ for eary type galaxies, since their stellar populations are thought to be very similar. Spiral galaxies also have a significant proportion of their X-ray luminosity generated by Population I objects associated with their spiral arm regions.

(4) Since the early type galaxies in our sample lack any obvious symptoms of strong activity, it is clearly unreasonable to attribute the high specific X-ray luminosities displayed by some galaxies to either AGN phenomena or starbursts. Furthermore, the concentration of

non-thermal radio sources (hence relativistic electrons) in the central 1-2 kpc of these galaxies excludes the possibility that the considerably more extensive X-ray emission is generated by synchrotron or inverse compton mechanisms. The only viable alternative is that high L_X/L_V early type galaxies have accumulated and retained substantial quantities of hot gas. A direct measure of the proportion of X-ray emission generated by thermal emission from hot gas is given by: $1 - ((L_X/L_V)_*/(L_X/L_V)_{obs})$. NGC 4636 is the galaxy in our sample which has the highest proportion of its X-ray emission generated by hot gas ($\sim$98%). The wide range of L_X/L_V values exhibited by the galaxies in our sample can be interpreted as variation in the proportion of hot gas actually retained by individual galaxies. Our results indicate that lenticular galaxies retain a systematically smaller fraction of the gas generated by stellar evolution than elliptical galaxies. We suggest that those galaxies with $L_X/L_V \sim (L_X/L_V)_*$ have lost virtually all of their gas, thus implying the existence of efficient gas depletion processes.

Given this possibly simplistic scenario we can derive an empirical relationship between L_X and L_V:

$$L_X = L_X \text{ (stellar)} + L_X \text{ (gas)} \simeq 3\times10^{-5}\ L_V + 8.9 \times 10^{-48}\ L_V^2;$$

the second term has simply been normalized with respect to NGC 4636. We have plotted this relationship, and also $L_X/L_V = 3\times10^{-5}$, on the observed $L_X - L_V$ distribution (Figure 5.2). Virtually all of the galaxies in our sample have locations intermediate between these two empirical relationships, which although not best-fitted to the data are clearly representative of the possible extreme cases.

5.3.3 Specific X-ray Luminosity as a Function of Stellar Content

Having explored the relationship between X-ray and optical luminosities, it would now seem appropriate to consider whether the X-ray properties of early type galaxies are a function of their current stellar content. Multi-colour optical photometry and accurate spectroscopy can, in principle, be used to generate models of the stellar content of a galaxy; an extremely sophisticated stellar evolution synthesis model would be required, however, in order to accurately predict the quantity of X-ray emission from main sequence stars, evolved objects and gas. This last component provides a particularly difficult problem; the gas is generated, and possibly depleted, thoughout the lifetime of the galaxy, hence it only indirectly reflects the properties of the current stellar population.

A complex synthesis approach is clearly beyond the scope of this work; we therefore resort to a simple study of observational properties. In Figure 5.6 we show L_X/L_V as a function of B-V for all the galaxies in our sample. This diagram can crudely be interpreted as displaying the relationship between relative X-ray power (ie. proportion of X-ray emission generated by hot gas) and mean stellar spectral type for early type galaxies. Two interesting features are apparent; firstly, although the range of B-V values is rather narrow there does appear to be an association of high L_X/L_V with high values of B-V (the ten galaxies with highest specific X-ray luminosities all have B-V $\geqslant$ 0.85); secondly, low values of L_X/L_V occur over the whole range of B-V for early type galaxies. Our interpretation of these results is dependent on what we believe the colour parameter B-V tells us about the stellar content of a galaxy; but it is clear that gas richness is

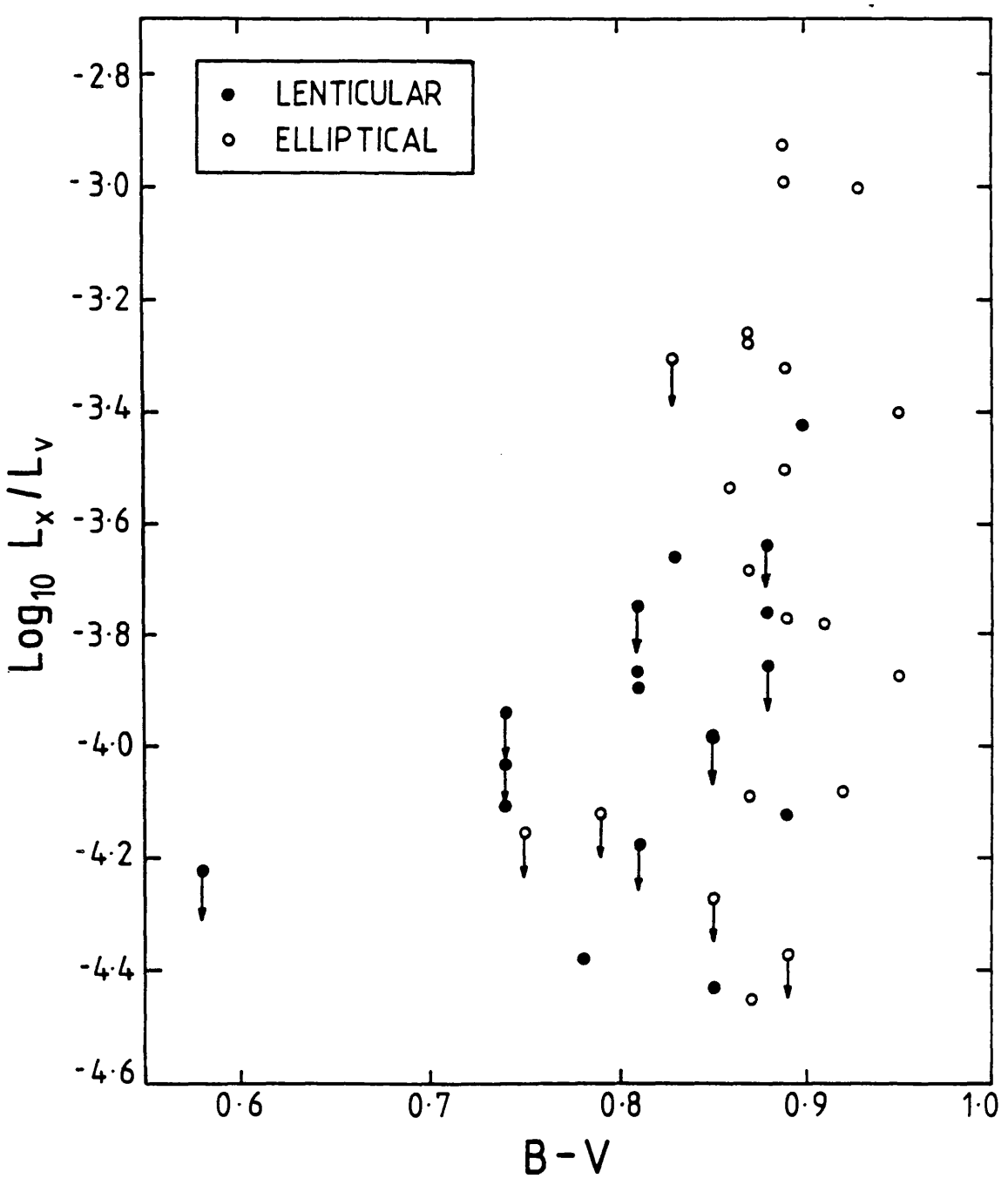

Figure 5.6 L_x/L_v plotted as a function of the optical colour parameter B-V.

associated with optical redness, at least for the galaxies in our sample. If B-V measures the relative abundance of cool low-mass dwarfs, then our results would seem to indicate that the gas richness (and hence specific X-ray luminosity) of an early type galaxy is partially dependent on the mass function of its stellar population. That this is not the only determining factor is evident from the large range of L_X/L_V displayed by galaxies with similar colours.

5.3.4 The Relationship Between X-ray and Radio Properties

Any attempt to derive information relating to a genuine correlation between X-ray and radio luminosities is influenced by the fact that the radio and optical luminosities of early type galaxies are strongly correlated (eg. Hummel and Kotanyi 1982, Hummel et al. 1983). We have already established a quite separate X-ray - optical correlation, thus it is not surprising to find that some degree of correlation exists between radio and X-ray luminosities for the 33 galaxies in our sample which have been observed at radio wavelengths (Figure 5.7). The L_X-L_{radio} distribution is dominated by upper limits, hence its true form is ill-determined. In our X-ray selected sample the proportion of radio detections (27%) is similar to the optically selected samples of Hummel et al. (1983), indicating that our sample is not strongly biased towards radio-powerful galaxies.

We have divided the galaxy sample into radio-weak and radio-powerful categories, and plotted their L_X/L_V distributions separately (Figure 5.8). The luminosity division occurs at $L_{1415} = 10^{27.5}$ erg s^{-1} Hz^{-1}, which corresponds to a typical survey detection limit of $\sim$10mJy (at 1415 MHz) for a galaxy situated in the Virgo Cluster. The radio-

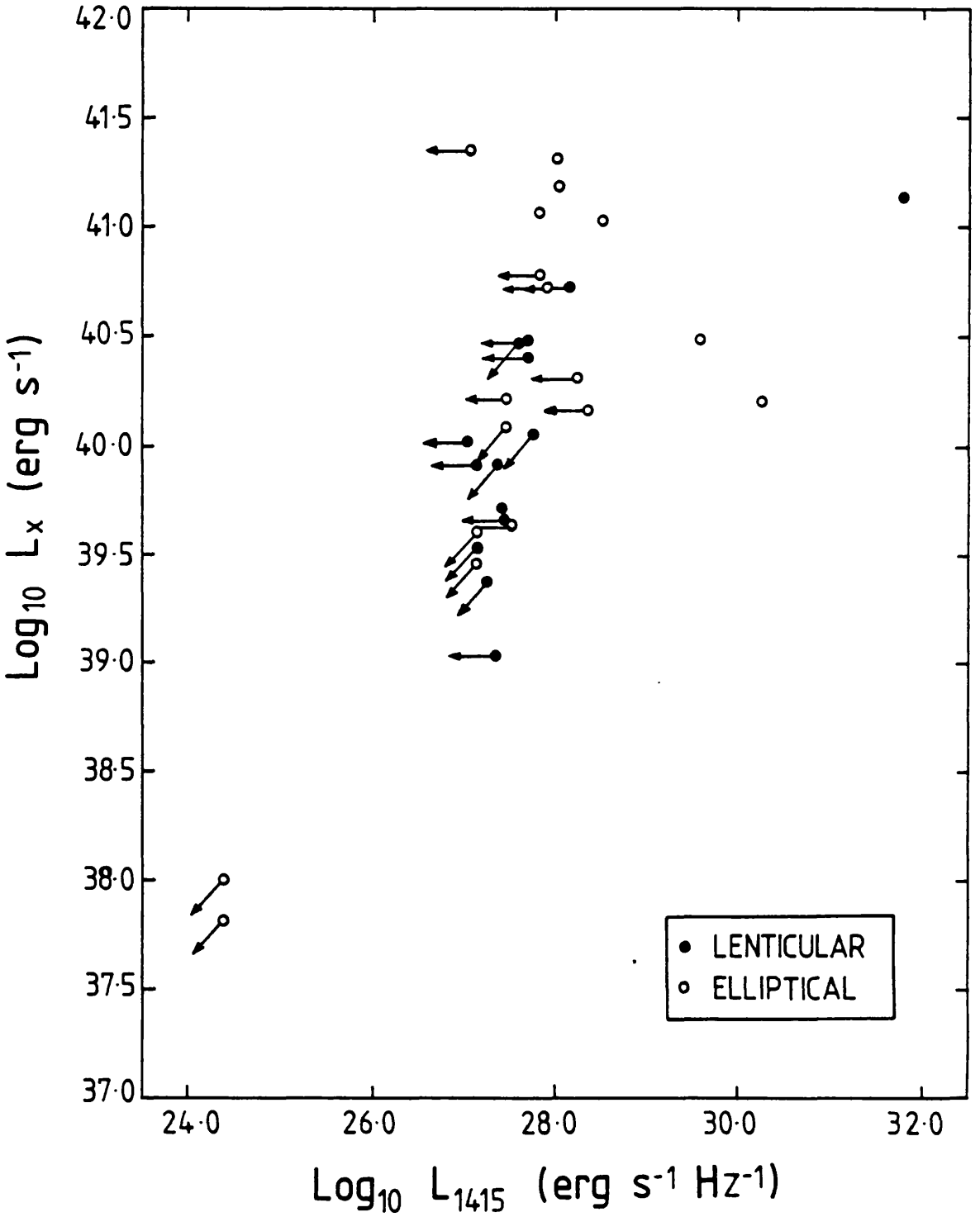

Figure 5.7 The relationship between X-ray luminosity and monochromatic radio luminosity (at 1.4 GHz) for galaxies in the sample which have been observed at radio wavelengths.

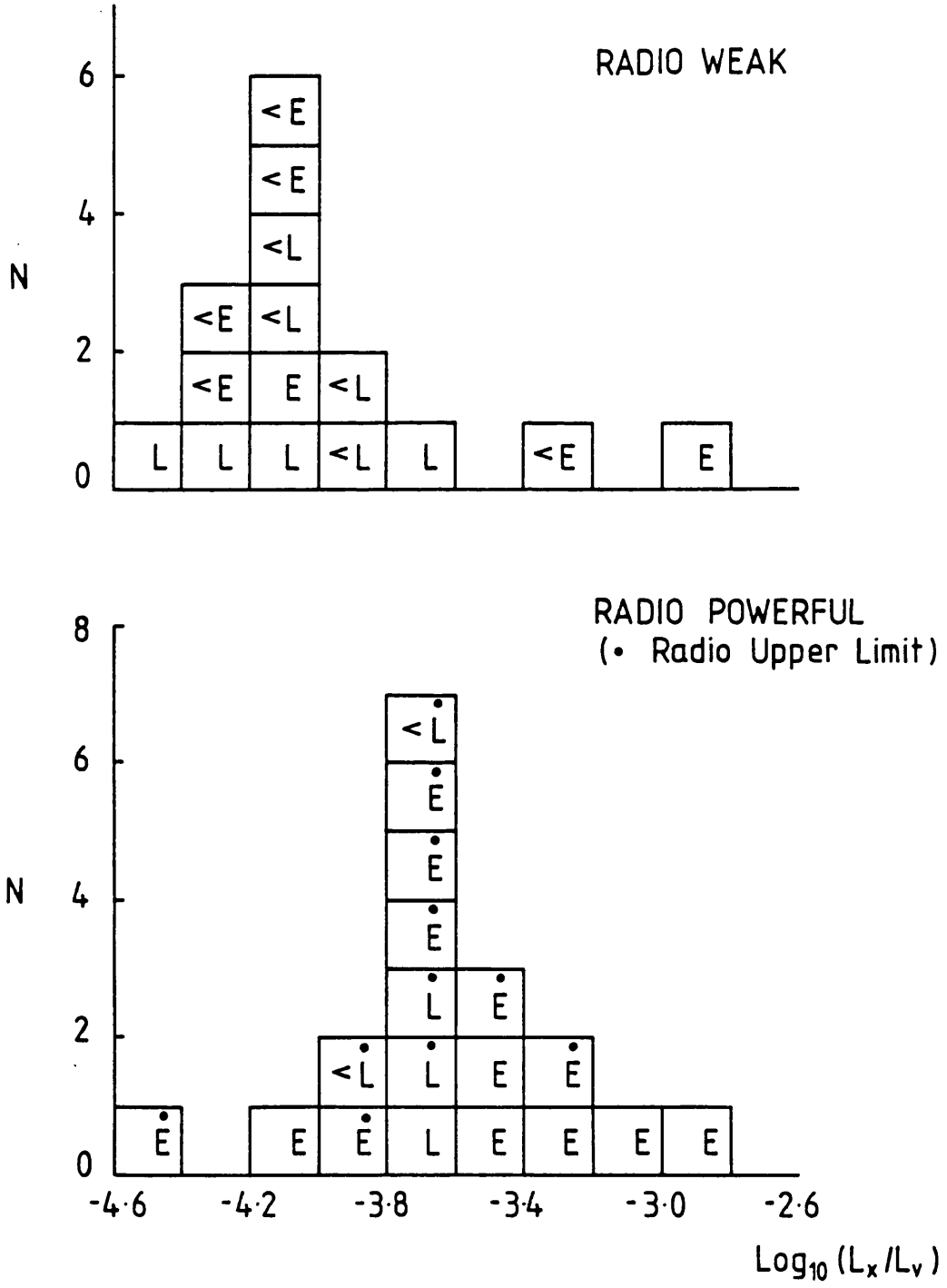

Figure 5.8 L_x/L_v distributions for radio-weak and radio-powerful sub-samples. The radio luminosity division occurs at $L_{1.4} = 10^{27.5}$ erg s^{-1} Hz^{-1}. < denotes L_x/L_v upper limit.

powerful galaxies appear to exhibit systematically higher values of L_X/L_V than their radio-weak counterparts. Dressel and Wilson (1983) reached a similar conclusion for a sample of radio selected early type galaxies (which have been excluded from our sample because the authors did not quote X-ray fluxes). This result may, of course, be understood as a correlation of L_X/L_V with L_V (Figure 5.5a) and hence, via the radio-optical luminosity correlation, with L_{1415}. We should also note that the L_X/L_V distribution for the radio-powerful galaxies is almost certainly distorted by the large number of L_{1415} upper limits which have been included. It is clear that a significant improvement in the sensitivity of radio surveys will be required before we are able to attempt a detailed analysis of the relationship between X-ray and radio luminosities.

Although the general trend is for high values of L_X/L_V and L_{1415} to be associated, several counter-examples exist. NGC 4406 (M86) has a high specific X-ray luminosity, but a very low limit has been derived for its radio luminosity; NGC 4374 has a considerably lower specific X-ray luminosity, but is associated with a very powerful radio source. Even so, the majority of the genuinely radio-powerful early type galaxies in our sample have high L_X/L_V values, and are therefore gas-rich. Perhaps the presence of substantial quantities of hot gas is a necessary, but not sufficient, condition for the existence of a radio source in an early type galaxy.

The radio luminosities of elliptical galaxies are strongly correlated with their roundness. No elliptical galaxies flatter than E4 have been detected in radio surveys (Hummel et al. 1983, Disney et al.

1984), a result which is reflected in a plot of L_{1415} versus ellipticity parameter (n, where n = 10(a-b)/a) for the elliptical galaxies in our sample (see Figure 5.9a). A similar plot of L_X/L_V versus ellipticity parameter (Figure 5.9b) shows no such trend, although relatively flat galaxies are poorly represented in our sample. Indeed, several counter-examples to the trend exist; NGC 720 is a relatively flat galaxy (E5) which has a high value of L_X/L_V; NGC 3379 is a quite round galaxy (E1) with a low value of L_X/L_V. Gas-richness is clearly not a strong function of the shape of elliptical galaxies, although it is interesting to speculate whether the systematically lower L_X/L_V values of the lenticular galaxies in our sample could be related to their intrinsic flatness.

Although radio and X-ray emission in early type galaxies may be linked in some indirect way (eg. fueling of a radio source by accretion of gas), a more direct link involving the generation of a substantial proportion of the observed X-ray emission by non-thermal processes can almost certainly be excluded, since the radio and X-ray emission invariably display dissimilar morphologies and physical extents. An extreme example is NGC 1316, which has exceptionally powerful radio lobes extending far beyond the optical (or X-ray) bounds of the galaxy (Ekers et al. 1983). No X-ray emission has been detected from the radio lobe regions. Other galaxies have compact radio sources confined to their core regions (eg. Hummel et al. 1983), whereas their X-ray emission extends for many kpc. Jones et al.(1984) proposed the inverse compton mechanism as a possible source of the 3×10^{40} erg s^{-1} of X-ray emission associated with NGC 1052, an elliptical galaxy possessing a powerful nuclear radio and IR source. We would wish to

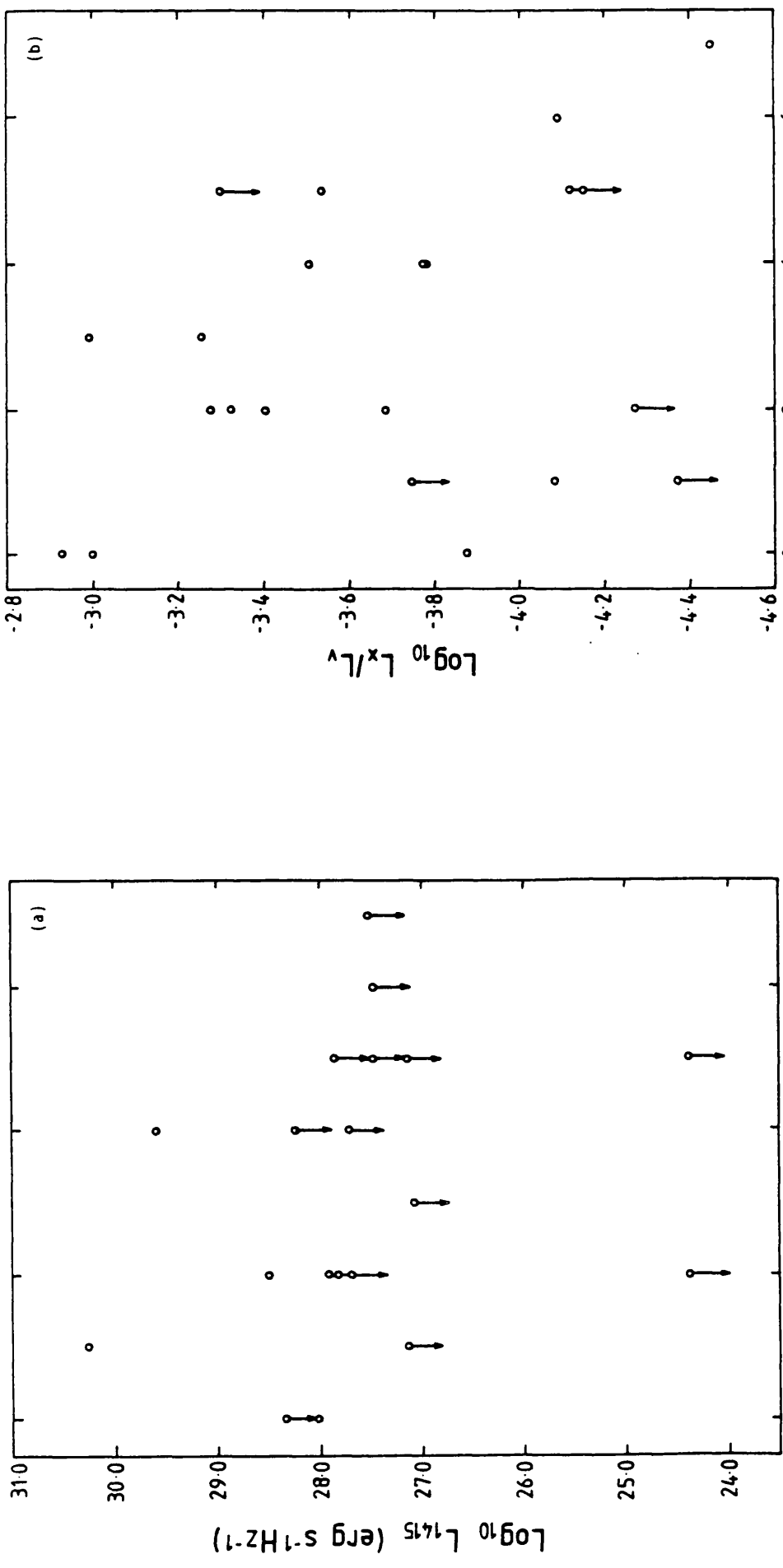

Figure 5.9 (a) Monochromatic radio luminosity versus ellipticity parameter for the elliptical galaxies in our sample; (b) L_x/L_v versus ellipticity parameter for the elliptical galaxies in our sample.

stress that the inverse compton process is most unlikely to be the dominant X-ray emission process, since the emission is known to extend throughout the galaxy (as Jones et al. readily admit), whereas the radio/IR nucleus is highly compact.

5.3.5 Relationships Between X-ray and Neutral Hydrogen Properties

The neutral hydrogen properties of early type galaxies were reviewed in Chapter Four (section 4.2.2). Our sample of galaxies reflects the general result that very few early type galaxies contain detectable quantities of HI. Indeed, there are only three secure detections among the 23 galaxies for which HI measurements exist. Since the HI data is dominated by non-uniform upper limits, little general information can be derived regarding possible links between X-ray properties and the presence or absence of neutral hydrogen. At least one galaxy, NGC 1052, has both a high specific X-ray luminosity and a relatively large mass of neutral hydrogen. High resolution X-ray and HI maps of NGC 1052 would allow the spatial relationship between the hot and cool gas to be examined. Neutral hydrogen has been detected in both NGC 205 and NGC 5102, but is associated with abnormal Population I activity and should probably be regarded as pathological (Hodge 1973, van den Bergh 1976).

Several authors have suggested that radio luminosity and HI mass are correlated, at least for elliptical galaxies (eg. Dressel et al. 1982). We are unable to test for such a correlation using our sample, although we could propose the radio-weak, HI-rich galaxy NGC 5102 as a counter-example. The recent tendency for galaxies previously classified as HI-rich to be reclassified as HI-poor, when reobserved

with more sensitive instrumentation (eg. Thonnard 1982, Knapp et al. 1983), suggests that this proposed correlation should be carefully reviewed.

5.3.6 The Influence of Clustering on the X-ray Properties of Early Type Galaxies

Are the X-ray properties of strongly clustered early type galaxies significantly different compared with those of their less clustered counterparts? This question is not easily addressed, primarily due to two observational problems:

(1) Very few galaxies are genuinely isolated, ie. have no neighbours within a few Mpc. Most galaxies in our current sample can be regarded as weakly clustered; they may be members of small groups, or perhaps located in the outskirts of rich clusters. Studies of genuinely isolated galaxies are of fundamental importance because their X-ray properties must be derived purely from the action of internal processes.

(2) At the other extreme, very few rich clusters of galaxies are near enough for detailed X-ray surveys of their members to be performed. Examples of early type galaxies having high specific X-ray luminosities have been identified in the Perseus Cluster (Fabricant et al. 1979) and Abell 1367 (Bechtold et al. 1983). At the distances of these clusters only the high luminosity region of the L_X/L_V distribution is sampled. The Virgo Cluster is the only system which is sufficiently close for detailed correlative studies to be attempted, but so far no X-ray survey of its early type galaxies has been published. The Virgo Cluster galaxies included in our sample

exhibit X-ray properties which are similar to those of the other galaxies.

At present we have to conclude that the degree of clustering experienced by an early type galaxy is not crucial in determining its X-ray properties, except perhaps for systems which are moving through the dense core of a rich cluster and are therefore subject to ram pressure stripping of gas (eg. Forman et al. 1979, Bechtold et al. 1983). Examples of gas-rich early type galaxies are found in a wide range of environments: central regions of rich clusters (NGC 4406 in Virgo, NGC 3852 in Abell 1367), cluster outskirts (NGC 4636 in Virgo), small groups (NGC 1052 and NGC 5846) and even in isolation (NGC 1395). Since thermal emission from hot gas provides the dominant X-ray emission component in many early type galaxies, we ought to examine the physical processes which determine its properties and evolution.

5.4 The Properties and Evolution of Hot Gas in Early Type Galaxies

5.4.1 Gas Properties

Despite the IPC's limitations as an X-ray spectrometer, it has proved possible to derive crude estimates of the effective temperature for the X-ray emission associated with several early type galaxies, including NGC 1332, NGC 4291 and NGC 4636 (Chapter Four), NGC 1395 (Nulsen et al. 1984) and NGC 5846 (Biermann and Kronberg 1983). In each case, the spectral data is consistent with optically thin thermal emission from a plasma with near solar element abundances and a temperature in the range 5×10^6 K to 2×10^7K. These galaxies all have high L_X/L_V values; thermal emission from hot gas therefore provides the dominant contribution to their X-ray luminosities.

In Chapter Four we used a simple isothermal gas sphere model to parameterize the surface brightness profiles extracted from the IPC data for NGC 1332 and NGC 4636. Although this model is arguably not completely realistic (hot gas is unlikely to be isothermal throughout the galaxy, and need not necessarily be in hydrostatic equilibrium either), it does provide a good fit to the data and can be used to derive physically meaningful gas parameters. Our basic requirement is to derive an estimate of the radial gas density profile $n_e(r)$. For an isothermal sphere of gas in hydrostatic equilibrium with a King model distribution of gravitating matter, the observed X-ray surface brightness profile is modelled as:

$$S(r) = S(0)\ (1 + (r/a_x)^2)^{0.5-3\beta} \qquad (1),$$

which is generated by an electron density profile:

$$n_e(r) = n_e(0)\ (1 + (r/a_x)^2)^{-3\beta/2} \qquad (2).$$

A shell of gas at radius r, volume dV(r), radiates an X-ray luminosity of:

$$L_x(r) \simeq n_e(r)^2\ F(T)\ dV(r) \qquad (3),$$

where F(T) is the cooling function for a $T \sim 10^7$ K plasma with solar element abundances (eg. Raymond and Smith 1977). Since we know the X-ray luminosity out to some limiting radius, we can integrate equation (3) and solve for $n_e(0)$, thus allowing us to calculate radiative cooling times and gas masses.

The results for NGC 1332 and NGC 4636, using the $\beta = 0.5$ and $\beta = 1.0$ models discussed in Chapter Four, are summarized in Table 5.2. Our estimates of the total mass of gas associated with each galaxy are a weak function of β (and the corresponding core radius a_x), but

Table 5.2: Thermal Parameters from IPC Data

	NGC 1332		NGC 4636	
	$\beta = 0.5$	$\beta = 1.0$	$\beta = 0.5$	$\beta = 1.0$
Isothermal Core Radius (kpc)	1.0	4.9	2.3	8.2
Core Electron Density (cm^{-3})	2.1×10^{-2}	8.9×10^{-3}	2.3×10^{-2}	1.1×10^{-2}
Core Cooling Time (years)	2.4×10^{8}	5.6×10^{8}	2.2×10^{8}	4.5×10^{8}
Hubble Cooling Radius (kpc)	14.2	11.9	29.6	21.4
Gas Mass (M_o)	2.8×10^{8}	2.2×10^{8}	8.3×10^{8}	1.1×10^{9}

Notes to Table 5.2

(1) The electron density is assumed to be due to an isothermal gas sphere distribution in hydrostatic equilibrium, with the form: $n_e(r) = n_e(o)\,[1 + (r/a_x)^2]^{-3\beta/2}$.

(2) Thermal temperature of X-ray emitting plasma is kT = 1.0 keV.

(3) The Hubble cooling radius is the radial distance at which $n_e(r)$ is low enough for the gas cooling time to exceed the Hubble Time ($\sim 10^{10}$ years).

(4) For mass calculations we assume that the outer radius of the distribution is 20 kpc, consistent with the observed radial X-ray extent of $\sim$200 arcsec for NGC 1332 and $\sim$300 arcsec for NGC 4636.

obviously a strong function of the assumed outer radius of the gas distribution. Neither parameter is well determined by the IPC data. We estimate that the mass of hot gas contained in NGC 1332 is $\sim 2\times10^{8}$ M_{o}, whereas NGC 4636 contains a considerably greater quantity, ie. $\sim1\times10^{9}$ M_{o}. Radiative cooling times are significantly less than a Hubble time throughout both galaxies, thus providing additional support for the hypothesis of Nulsen et al. (1984) that radiative cooling plays an important role in determining the evolution of hot gas in early type galaxies. A more detailed thermal modelling of the X-ray emission associated with NGC 4636 will be performed in Chapter Six using HRI data.

5.4.2 The Origin of Hot Gas in Early Type Galaxies

Observations of planetary nebulae within our own galaxy and other Local Group systems indicate that the stellar mass loss rate associated with old stellar populations is ~0.015 $(L_{V}/10^{9}$ $L_{o})$ M_{o} yr^{-1} (Faber and Gallagher 1976). We therefore predict current stellar mass loss rates of ~0.55 M_{o} yr^{-1} for NGC 1332 and ~0.50 M_{o} yr^{-1} for NGC 4636. Integrated stellar mass loss rates were almost certainly higher during earlier phases of galactic evolution (eg. MacDonald and Bailey 1981), hence we would expect at least 5×10^{9} M_{o} of gas to accumulate in NGC 1332 and NGC 4636 during a Hubble time. Observations indicate that the total mass of gas (HI, HII and 10^{7} K plasma) associated with either galaxy is no more than $\sim10^{9}$ M_{o}, significantly less than is predicted from stellar mass loss considerations. Nulsen et al. (1984) derived a similarly discrepant mass for the X-ray emitting gas associated with NGC 1395. The obvious implication is that gas depletion processes must operate even in these relatively gas-rich

early type galaxies. We note in passing that since stellar evolution is more than capable of supplying the observed gas, there is no need to consider more exotic gas-supply mechanisms, eg. infall from gas-rich companion galaxies or accretion from the IGM. The former process has occasionally been postulated as a mechanism capable of creating the tilted HI disks observed in a small number of early type galaxies (eg. NGC 1052, Jones et al. 1984).

Before proceeding to examine possible gas depletion mechanisms we should outline the processes which heat stellar ejecta to X-ray emitting temperatures. Random stellar motion will cause collisional heating resulting in thermalization of the gas at a temperature consistent with the velocity dispersion of the galaxy, ie. $T_i \simeq \mu m_H \sigma^2/k$ ($\sim 5\times10^6$ K for $\sigma \sim 250$ km s^{-1}). Although IPC-derived temperature measurements are rather imprecise, they do indicate gas temperatures in the range 5×10^6 - 2×10^7 K, marginally inconsistent with the probable injection temperature (T_i). Fabian et al. (1980) suggested that supernova heating could generate the required increase in global temperature. Following their terminology, we find:

$$T_x - T_i \simeq \alpha_{SN} T_{SN}/\alpha_s \quad ,$$

where T_x is the observed gas temperature, T_{SN} is the kinematic temperature of the supernova ($\sim 10^9$ K), and α_s and α_{SN} are the specific mass loss rates from stars and supernovae respectively. For NGC 4636 the required temperature increase is roughly 10^7 K. The integrated stellar mass loss rate is 0.5 $M_\odot$ yr^{-1}, corresponding to $\alpha_s \sim 1.5\times10^{-12}$ yr^{-1}. The required value for α_{SN} is therefore $\sim 1.5\times10^{-14}$ yr^{-1}, or roughly one supernova every 200 years. In contrast, Nulsen et al. (1984) have argued that radiative cooling is

more important than supernovae-induced heating, and suggest that adiabatic compression of gas in the resultant cooling flow maintains a suitably high gas temperature throughout typical early type galaxies.

Having derived the basic properties of the hot gas associated with early type galaxies, and also examined its origin, we are now able to study the physical processes which regulate its evolution. Successful evolutionary scenarios must explain why some early type galaxies are essentially devoid of hot gas, while others have accumulated and retained substantial quantities of gas, although still considerably less than is predicted from stellar evolution considerations. Most of the galaxies included in the sample discussed earlier in this chapter are only weakly clustered; environmentally-induced gas removal processes are therefore unlikely to be significant. Internal gas depletion processes are discussed in the following two sections; the evolution of gas in strongly clustered galaxies is reviewed in section 5.4.5.

5.4.3 Hot Galactic Winds and the Gravitational Confinement of Gas

The most frequently proposed mechanism for removing gas from early type galaxies is the hot galactic wind (eg. Mathews and Baker 1971, Faber and Gallagher 1976). Provided the integrated supernova rate is suitably high, gas shed by stars can be heated to temperatures where it no longer remains gravitationally bound to the galaxy. The gas flows out as a steady wind, continually replenished by stellar mass loss. Several authors have suggested that radiative cooling could induce thermal instabilities on both small and large scales in a galactic wind (eg. "The Cyclic Wind", Sanders 1981); although in the most detailed quantitative study to date, White and Chevalier (1983)

concluded that all elliptical galaxies are capable of maintaining steady winds.

Despite their predicted universality, it is very simple to demonstrate that hot galactic winds are incapable of generating the high X-ray luminosities associated with galaxies like NGC 4636. Gas flowing out in a steady wind escapes in a timescale,

$$t_{esc} \simeq R_{galaxy} / (kT/\mu m_H)^{1/2}.$$

Beyond the edge of the galaxy the gas undergoes free expansion and cools rapidly; the hypothetical wind-generated X-ray emission must therefore arise during the passage of the gas through the galaxy. The requirement is essentially that the observed X-ray emitting gas be replenished once per flow time; the required integrated stellar mass loss rate is therefore $\dot{M} \simeq M_{gas}/t_{esc}$. Using parameters derived for NGC 4636 (ie. $M_{gas} \sim 10^9$ M_o, $R_{galaxy} \sim R_{gas} \sim 20$ kpc, $T \sim 10^7$ K), we find that the outflow timescale is $t_{esc} \sim 5 \times 10^7$ years and the required mass loss rate is $\dot{M} \sim 20$ M_o yr^{-1}. This exceeds the predicted mass loss rate for NGC 4636 by a factor of 40! Nulsen et al. (1984) reached a similar conclusion in relation to a simple hot wind model for NGC 1395. A galaxy which fuels a wind via 0.5 M_o yr^{-1} of stellar mass loss would probably contain no more than $\sim 2.5 \times 10^7$ M_o of hot gas at any time. Such a low mass of gas, if contained within a typical galaxy in our sample, would not be detected by the IPC. It therefore seems reasonable to assume that early type galaxies which exhibit low values of L_X/L_V are kept essentially gas-free by the action of steady galactic winds. It is obvious, however, that simple wind models are inappropriate for NGC 4636 and other similarly X-ray luminous galaxies.

Clearly, in galaxies like NGC 4636 some process has suppressed a general wind. But what is the nature of this process and why does it only function in certain galaxies? Two possibilities have been suggested; either the outflow of hot gas is prevented by a physical confinement mechanism, or the energetics within some galaxies do not favour the existence of steady winds. As we shall see, currently available data does not exclude either possibility, and indeed both could occur simultaneously.

The most frequently proposed mechanism for retaining large quantities of hot gas within an early type galaxy is gravitational confinement by a massive and extensive halo of dark matter (eg. Fabian et al. 1980, Bechtold et al. 1983). In the simplest scenario, the dark halo acts as a potential barrier which the buoyant gas is unable to surmount. The hot gas is therefore confined to the galaxy; even so, it probably extends beyond the optical light distribution of the system, since the dark halo is required to be very extensive indeed. Provided that radiative cooling losses are offset by supernova heating, we would expect to observe quantities of gas very similar to that predicted from stellar evolution arguments. This does not appear to be the case for NGC 1332, NGC 1395 and NGC 4636, although the IPC-derived gas masses should be used with some caution as they are probably only accurate to a factor of about two.

The gravitational confinement scenario has recently been criticized by White and Chevalier (1983), who performed a detailed analysis of the effects of a wide range of halo models on a steady hot wind. They concluded that for all physically reasonable models, the presence of a

dark halo did not suppress a steady wind. A dark halo would tend to decelerate, and therefore cool, the outflowing hot gas; but not sufficiently to bind the gas to the galaxy. This view is by no means universally accepted (Forman 1984, private communication). Even if a dark halo can confine a substantial quantity of gas, it is not certain that supernova heating is sufficient to maintain it against cooling losses. For example, the total cooling rate for NGC 4636 is $\sim 1.5 \times 10^{41}$ erg s^{-1}, and the best available estimate for the SN rate is ~ 0.005 SN yr^{-1} (Tammann 1981). If we assume that each SN injects $\sim 3 \times 10^{50}$ ergs of energy into the ambient gas (eg. Blair 1981), we derive a total heating rate of $\sim 4.8 \times 10^{40}$ erg s^{-1}, ie. 30% of the cooling rate. Since all of these parameters are highly uncertain, it is quite conceivable that a relatively close balance exists between heating and cooling processes. Interestingly, we would expect the SN heating rate to be proportional to L_V, whereas the radiative cooling rate probably scales as a higher power of L_V (eg. L_V^2), hence cooling should become increasingly important as L_V increases. If cooling dominates, a radiatively driven cooling flow may occur, a possibility which will be discussed in detail in the next section (5.4.4).

Independent evidence for the general existence of massive dark haloes around early type galaxies is not yet compelling, although Space Telescope observations of the distribution of globular clusters around Virgo Cluster ellipticals may eventually settle the question. We can certainly not rule out the possibility that the presence or absence of a dark halo is one of the factors (perhaps the crucial one) which determines whether a galaxy blows a steady wind or accumulates a substantial quantity of hot gas.

Other physical confinement processes have occasionally been postulated, eg. pressure confinement by a hot, tenuous IGM (Fabian et al. 1980), but probably have only limited applicability (see section 5.4.5). It should be recognized, however, that it is not essential that the observed gas actually be confined by some independent mechanism. As we have already noted, the detailed balance between heating and cooling processes may favour the latter in certain galaxies. If radiative cooling is dominant, then the dynamical evolution of the gas generated by stellar evolution probably involves inflow rather than outflow.

5.4.4 Cooling Accretion Flows

If gas inflow is to occur within an early type galaxy, radiative cooling has to nullify the effects of heating processes. Nulsen et al. (1984) have cited the fairly short ($\lesssim 10^9$ years) cooling times inferred for the hot gas observed in early type galaxies as evidence for this scenario. White and Chevalier (1984) have examined several realistic models for the evolution of gas in elliptical galaxies and conclude that radiatively driven inflow is energetically favoured for at least a subset of such systems. As we have already demonstrated, a wind-type outflow could not generate the observed X-ray luminosity of NGC 4636.

Cooling accretion (in)flow models were first applied to those rich clusters of galaxies where the cooling time of the hot gas in the core region was found to be less than a Hubble time (Cowie and Binney 1977, Fabian and Nulsen 1977). Unlike rich clusters, a galaxy like NGC 4636 possesses a distribution of hot gas which has a radiative cooling time

less than H_o^{-1} throughout its entire physical extent (see Table 5.2). If widespread radiative cooling is not inhibited by supernova heating, a steady cooling flow can be achieved throughout the galaxy, with stellar mass loss exactly balancing the cooling rate (ie. the radiative regulation model of Cowie and Binney 1977). Even if the heating rate exceeds the radiative cooling rate integrated over the galaxy as a whole, the hot gas in the core region is likely to be sufficiently dense for cooling to be locally dominant; a small-scale cooling flow can therefore still occur. Nulsen et al. (1984) have performed a detailed study of the likely properties of a cooling flow occurring in an isolated elliptical galaxy. We will reiterate some of their principal findings in the context of the observed X-ray properties of early type galaxies in general.

Adiabatic compression caused by the flow of gas through a galaxy's gravitational potential field will maintain the hottest (X-ray emitting) gas at a temperature $T(r) \simeq GM(r)\mu m_H/kr$. In a typical galaxy, $T(r) \sim T_i$ (the injection temperature for the gas) in the outer regions, but increases to $\gtrsim 10^7$ K at a distance of a few optical core radii from the centre of the galaxy, decreasing sharply thereafter as the gravitational potential flattens. Local or large-scale heating may tend to modify the adiabatic temperature profile to some extent. Future X-ray observations with high spatial resolution and good spectral discrimination should allow us to derive an accurate temperature profile for a galaxy like NGC 4636. If T(r) is quasi-isothermal, a model featuring a gravitationally bound static distribution of hot gas is likely to apply; if T(r) decreases sharply near the core region, cooling flow models are probably appropriate.

In a steady cooling flow, the gas flow time is roughly equal to the cooling time throughout, so the stellar mass rate required to fuel the cooling flow is: $\dot{M} \simeq L_X/(5kT/2\mu m_H)$ (eg. Stewart et al.1984). For NGC 4636 (L_X (gas) $\sim 1.5 \times 10^{41}$ erg s^{-1}, $T_{gas} \sim 1.4 \times 10^7$ K) we find that the required integrated stellar mass loss rate is $\sim 0.49\ M_\odot\ yr^{-1}$. If the work done against the gravitatonal potential is also taken into account, the estimate of $\dot{M}$ would have to be revised upwards slightly, but even so is still in good agreement with the mass loss rate predicted from stellar evolution arguments ($\sim 0.5\ M_\odot\ yr^{-1}$).

It is obviously tempting to attribute the wide range of L_X/L_V displayed by the galaxies in our sample to the relative influence of heating and cooling processes. A galaxy with $0.5\ M_\odot\ yr^{-1}$ of stellar mass loss can presumably fuel a cooling flow, a static halo of gas, or an outflowing wind. The wind, however, yields a very low X-ray luminosity. We suggest that there are at least two determining factors involved: the presence or absence of a dark halo which gravitatonally binds the hot gas, and the detailed balance between radiative cooling and supernova heating. The extreme possibilities are: (a) heating dominant and no dark halo, resulting in a steady wind; (b) cooling dominant combined with the presence of dark halo, in which case the gravitationally bound gas is incorporated into a cooling flow. Intermediate possibilities such as non-cooling static haloes of bound gas are, of course, also allowed. Why dark haloes should only occur in a fraction of early type galaxies, as is required by this scenario, is by no means obvious.

Another evolutionary scenario which the present data does not exclude

is the cyclic hot wind model of Sanders (1981), which consists of phases of radiatively driven cooling flow, star formation from the accumulated cool gas (cf. the HI and Population I-rich lenticular galaxy, NGC 5102) and a supernova-driven hot wind. In this scenario the wide variation in L_X/L_V among early type galaxies would simply reflect different evolutionary phases within the cycle.

If all of the stellar mass loss within NGC 4636 is incorporated in a cooling flow we would predict that a large quantity of cool gas would be generated during a Hubble time (perhaps as much as 5×10^9 $M_\odot$). Sensitive observations indicate that NGC 4636, like most other early type galaxies, contains very little HI ($\lesssim 3\times10^7$ $M_\odot$, Thonnard 1982) and even less HII (Caldwell 1982). Since all of the integrated mass loss is required to fuel the cooling flow, we are unable to reinvoke a wind as a method for removing the excess cool gas. Star formation occurring continuously throughout the galaxy provides the only feasible mechanism for depleting the cool gas; although the IMF would be required to be either very steep relative to that of the solar neighbourhood or truncated at ~ 2 $M_\odot$, in order to prevent the colours of the galaxy becoming anomalously blue (O'Connell and Sarazin 1983). The Jeans critical mass for a self-gravitating blob of cool gas immersed in a hot ($T\sim10^7$ K), dense ($n_e \sim 0.01$ cm^{-2}) and dust-free medium is ~ 1 $M_\odot$, so low-mass star formation is not unreasonable (Spitzer 1978). Nulsen et al. (1984) suggest that star formation occurs diffusely throughout a galaxy undergoing a cooling flow, reflecting the distribution of stellar mass loss, and is rife within the core of the galaxy. In certain cases a transfer of angular momentum in the outer region of a galaxy may result in the ejection of

a disk of neutral hydrogen (cf. NGC 4278, Raimond et al. 1981).

Although star formation uses up virtually all of the available cool gas, sufficient quantities will still reach the centre of the galaxy to promote the fueling of a nuclear radio source; the remaining hot gas could pressure confine any resultant extended radio structures. Shocks probably occur within the inner regions of cooling flows, resulting in the formation of optical emission line regions (eg. Caldwell 1982). We suggest that gas-rich early type galaxies which have nuclear regions which exhibit radio emission and/or optical line emission are good candidates for the presence of cooling flows. Examples include NGC 4472, NGC 4636, NGC 4649 and NGC 5846.

5.4.5 The Evolution of Hot Gas in Highly Clustered Galaxies

The main aim of the second half of this chapter has been to identify the internal processes responsible for the evolution of gas in early type galaxies. External processes induced by environmental factors will inevitably be important (perhaps dominant) for galaxies located in or near the core regions of rich clusters, and are briefly reviewed in this section.

In their survey of the rich cluster Abell 1367, Bechtold et al. (1983) identified several early type galaxies, located near the centre of the cluster, which possess haloes of hot gas essentially similar to those associated with the more isolated galaxies which we have examined. How can a galaxy in a cluster core environment maintain a substantial quantity of hot gas against the effects of evaporation and ram pressure stripping? The authors estimated that $\sim$100 $M_{\odot}$ yr^{-1} of hot gas would be stripped from a galaxy moving through the centre of

A1367, and a further $\sim 50\ M_{\odot}\ yr^{-1}$ would be lost via evaporation. A galaxy like NGC 4636, if situated in such a region, would be almost completely devoid of gas after $\sim 10^7$ years. Two possibilities for maintaining a substantial quantity of gas against such efficient depletion processes have been considered:

(1) A galaxy possesses an extremely massive dark halo ($M \gtrsim 10^{13}\ M_{\odot}$) and/or a relatively strong magnetic field, both of which considerably inhibit the efficiency of stripping and evaporation processes. Ram pressure stripping also decreases in efficiency if a galaxy is relatively slow moving with respect to the ambient ICM (ie. $V_{galaxy} \ll$ cluster velocity dispersion).

(2) A galaxy is apparently associated with the core region of a cluster, but is in fact physically located outside the core and "seen" there only in projection. Ram pressure stripping efficiency decreases by a factor of ~ 10 as the distance from the centre of a rich cluster increases from zero to one optical core radius, due to the decrease in the density of the ICM (Bechtold et al. 1983). The elliptical galaxy M86, which possesses a prominent offset plume of X-ray emitting gas, is probably just re-entering the core region of the Virgo Cluster (Forman et al. 1981). It is likely that ram pressure stripping has recently been activated, and is beginning to remove the gas generated during a period of $\gtrsim 10^9$ years spent outside the core.

Fabian et al. (1980) suggested that the tenuous IGM in the outer regions of a cluster might exert sufficient pressure to confine hot gas within an early type galaxy, thus obviating the need for gravitational confinement by a dark halo. The characteristic

confinement radius for this process is $\sim$60 kpc, and is almost independent of the density and temperature of the ambient confining medium. The maximum radius of the hot gas associated with the weakly clustered galaxy NGC 4636 is 20-30 kpc, so it seems unlikely that pressure confinement is important in this case. The same is probably true for most other early type galaxies.

Clearly, galaxies which are located in the core regions of rich clusters, but which do, for whatever reasons, retain substantial quantities of hot gas, will be subject to evolutionary processes similar to those experienced by less clustered galaxies. Cooling flows will occur in those galaxies where global heating is relatively unimportant.

5.5 Conclusions

Although early type galaxies clearly display an overall correlation between X-ray and optical luminosities, the quantity of X-ray emission generated per unit mass of stellar population varies considerably among the galaxies in our sample. Our analysis of the properties of the sample provides strong support for previous suggestions that high L_X/L_V galaxies have accumulated substantial quantities of hot gas, although detailed measurements indicate that the mass of gas is considerably less than is expected to be generated by stellar evolution during a Hubble time. We suggest that hot galactic winds keep low L_X/L_V galaxies essentially gas-free, while the gas in high L_X/L_V galaxies is either gravitationally confined in a static halo or incorporated into a cooling accretion flow. The last possibility is particularly attractive because it provides a natural explanation for

the existence of weak radio sources in the central regions of some early type galaxies. In Chapter Six we will investigate the nature of the relationship between X-ray emitting gas and radio emission by performing the first high resolution X-ray and radio mapping of the elliptical galaxies NGC 4636 and NGC 4649.

CHAPTER SIX : HIGH RESOLUTION X-RAY AND RADIO OBSERVATIONS OF NGC 4636 AND NGC 4649

6.1 Introduction

In Chapter Five we examined the integrated properties of a large sample of X-ray selected early type galaxies. Our analysis of the luminosity relationships displayed by the sample clearly demonstrates that the most luminous galaxies contain substantial quantities of hot gas, and it is thermal emission from this diffuse component which provides the dominant contribution to their X-ray luminosities. In addition to the L_X-L_V relationship which we have identified, there exists a well established correlation between optical and radio luminosities for early type galaxies. It is therefore not surprising to find that gas-rich systems frequently contain nuclear radio sources. Nevertheless, it is interesting to ask whether the two properties, gas-richness and the presence of a nuclear radio source, occur independently (via completely separate correlations of X-ray and radio luminosities with optical luminosity) or alternatively are directly related, perhaps implying a causal or evolutionary link between the two. The data presented in Chapter Five are probably consistent with either possibility. We have previously argued that at least some gas-rich galaxies contain cooling flows; the resultant infall of cool gas into the core region of a galaxy provides an obvious explanation for the presence of nuclear activity, since the gas can accrete onto a pre-existing, massive black hole. The presence of substantial quantities of hot, X-ray emitting gas incorporated within a radiatively driven cooling flow may therefore be a necessary

condition for the existence of a nuclear radio source. To investigate this scenario in greater detail we need to determine the distribution of hot gas within the central regions of suitable early type galaxies, and examine its relationship to the morphological properties and energy requirements of their associated nuclear radio sources.

For a typical galaxy situated in the Virgo Cluster, the IPC's ~ 1 arcmin angular resolution corresponds to a spatial scale of ~ 5 kpc; this is clearly inadequate for detailed mapping purposes. Instead, we require the much finer resolution of the HRI (4 arcsec, or ~ 0.3 kpc at Virgo distances); although unfortunately, due to its lower quantum efficiency and higher internal background, the HRI is intrinsically less sensitive to diffuse X-ray emission than the IPC. Our experience indicates that a galaxy which yields an X-ray flux below $\sim 2 \times 10^{-12}$ erg cm^{-2} s^{-1} (in the 0.5-3.0 keV band) generates too few HRI counts to enable accurate mapping of extended emission. High sensitivity radio observations of early type galaxies, attaining an angular resolution comparable to the HRI in the soft X-ray band, can be performed with the Very Large Array facility at GHz frequencies using one of several antennae configurations.

Selection of galaxies suitable for high resolution studies was performed using the following criteria; (1) availability of a deep ($\gtrsim$ 15000 sec) HRI observation, (2) IPC-derived 0.5-3.0 keV flux $\gtrsim$ 2×10^{-12} erg cm^{-2} s^{-1}, (3) 1.4 GHz radio flux $\gtrsim$ 10 mJy, and (4) non-membership of the core regions of rich clusters of galaxies. This last criterion was adopted in order to reject those galaxies likely to be subject to severe environmental influences. Two giant elliptical galaxies, NGC 4636 and NGC 4649, met all our requirements and were

therefore selected for further study.

The properties of NGC 4636 and NGC 4649 are summarized in Table 6.1. Both galaxies are located in the outskirts of the Virgo Cluster; NGC 4636 is a member of the G26-Virgo II complex (de Vaucouleurs 1975), situated at a projected distance of $\sim$4.6 cluster core radii from M87; NGC 4649 is a locally dominant member of the main cluster, at a projected distance of $\sim$1.6 cluster core radii from the cluster centre. Their optical luminosities and photometric colours are quite typical for giant elliptical galaxies, and both exhibit regular (ie. undisturbed) optical morphologies. NGC 4649 is somewhat unusual in that it is a member of a close binary system; the less massive companion galaxy shows evidence of considerable tidal distortion, undoubtedly caused by NGC 4649.

The IPC-derived specific X-ray luminosities for NGC 4636 and NGC 4649 are sufficiently high that we can be certain that virtually all of the observed X-ray emission is due to hot gas. As much as 10^9 M_o of hot ($T\sim10^7$ K) gas is known to be associated with NGC 4636 (Chapter Five, 5.4.1); and although a detailed analysis of the IPC data for NGC 4649 has yet to be performed, we would expect the value for the total mass of hot gas to be broadly similar. HI observations indicate that very little neutral gas is associated with either galaxy. Until 1982 NGC 4636 was regarded as HI-rich (eg. Bottinelli and Gouguenheim 1978), but recent high sensitivity observations clearly refute this belief (eg. Thonnard 1982). The optical spectra of both galaxies reflect the properties of their predominantly old stellar populations, although some unusual features are evident. Several weak emission lines,

Table 6.1: Basic Properties of Galaxies

	NGC 4636	NGC 4649
D (Mpc)	14.3	15.0
B_T^o	10.29	9.62
$(B-V)_T^o$	0.89	0.95
L_V (erg s^{-1})	1.3×10^{44}	3.0×10^{44}
L_X (erg s^{-1})	1.5×10^{41}	* 1.2×10^{41}
L_X/L_V	1.2×10^{-3}	3.9×10^{-4}
L_{1415} (erg s^{-1} Hz^{-1})	1.1×10^{28}	6.7×10^{27}
M_{HI} (M_o)	$<3.3 \times 10^{7}$	$<1.2 \times 10^{8}$
λ3727 Equiv.Width	4Å	-
U.V. Excess	-	YES
Type	E0	E2

Notes to Table 6.1

References and derivation methods for D, L_V, L_X, L_{1415}, and M_{HI} are identical to those listed in Chapter Five, Table 5.1. B_T^o and $(B-V)_T^o$ are from 2RCBG (1976).

*X-ray luminosity for NGC 4649 is currently uncertain, due to the discrepancy between the IPC and HRI fluxes discussed in the text. The value quoted here is for the IPC measurement.

notably Hα and [OII], have been detected in the spectrum of NGC 4636, probably indicating the presence of ionized gas ($T \sim 10^4 K$) in the nuclear region, and perhaps a natural consequence of a cooling flow (see Nulsen et al. 1984). NGC 4649 is one of a small number of elliptical galaxies which exhibit a sharply rising UV flux at wavelengths less than 2500 Å. Bertola et al. (1982) suggest that the "hot" stars required to explain the UV excess are either evidence for a young, massive stellar population, or alternatively belong to an anomalously abundant population of evolved horizontal-branch stars. The near-IR (1-3μ) colours of both galaxies are consistent with a simple extrapolation of their optical spectra. No far-IR observations are currently available, although the results of the IRAS mini-survey (De Jong et al. 1984) suggest that "normal" elliptical galaxies are not detectable at $\lambda \gtrsim 10\mu$, and therefore contain negligible quantities of dust (which is consistent with the observed lack of neutral gas).

No high resolution radio maps of NGC 4636 and NGC 4649 have been published prior to the work reported in this chapter. Dressel and Condon (1978) concluded, on the basis of single dish 2.4 GHz measurements, that the weak radio source associated with NGC 4636 had an angular diameter of ~ 2.4 arcminutes. All other published radio observations of both galaxies have set upper limits of $\sim$1 arcmin for radio source extent, clearly demonstrating that the radio emission is confined well within the bounds of their stellar systems.

In section 6.2 we perform a detailed study of the X-ray morphologies of NGC 4636 and NGC 4649. A simple cooling flow model is constructed, and used to deproject the HRI data, thus allowing the radial dependence of gas parameters to be determined. An analysis of

recently acquired, high resolution VLA radio maps of both galaxies is presented in section 6.3. Radio and X-ray morphologies are compared, and the possible relationship between cooling flows and nuclear radio sources further investigated. In section 6.4 we examine physical processes which may tend to disrupt, or even completely suppress, cooling flows in NGC 4636 and NGC 4649.

6.2 High Resolution X-ray Observations - Analysis and Results

6.2.1 Overview

Relevant details of the HRI observations of NGC 4636 and NGC 4649, including exposure times and integrated count rates, are listed in Table 4.2 (Chapter Four). The soft X-ray fluxes listed in Table 4.3 were calculated for an assumed 1 keV thermal spectrum (eg. Raymond and Smith 1977). There is excellent agreement between the flux values derived for NGC 4636 using IPC and HRI data. We have not had the opportunity to perform a detailed analysis of the IPC data for NGC 4649, so we are unable to demonstrate a similar agreement between the IPC and HRI fluxes. Long and Van Speybroeck (1983) derived an X-ray flux of $\sim 4.3 \times 10^{-12}$ erg cm^{-2} s^{-1} for NGC 4649, based on an admittedly crude analysis of IPC data. This value exceeds our HRI flux by $\sim 50\%$, but is probably not inconsistent since Long and Van Speybroeck assumed a systematically higher thermal temperature. It is, of course, entirely possible that a 1 keV thermal spectrum is inappropriate for NGC 4649; detailed analysis of the IPC pulse-height spectrum should eventually resolve these ambiguities.

The HRI observations of NGC 4636 and NGC 4649 yielded ~ 1800 and ~ 500 net source counts respectively, thus allowing a reasonably detailed

map of the extended X-ray emission associated with each galaxy to be constructed. In both cases the peak of the X-ray surface brightness distribution is roughly coincident with the optical centroid of the galaxy.

6.2.2 Large Scale Morphology

To enable a detailed examination of the large-scale distribution of diffuse X-ray emission, we have rebinned the HRI data into 2 arcsec pixels and smoothed the resultant images with a $\sigma = 8$ arcsec 2-D gaussian function. It is experience that this procedure provides considerably enhanced sensitivity to extended emission, albeit at the expense of degraded resolution. Contour maps of the smoothed HRI images of NGC 4636 and NGC 4649 are displayed in Figure 6.1, and in a simplified form are superimposed upon the relevant regions of Palomar Sky Survey red plates in Figure 6.2.

NGC 4636

The lowest contour level reproduced in the HRI map of NGC 4636 represents a source surface brightness of 6.6×10^{-7} ct s^{-1} $arcsec^{-2}$, which corresponds to 5% of the peak value and is ~ 3 sigma above background. Levels 1-4 increment by 6% of the peak surface brightness value, while levels 5-10 increment by 12%. The NGC 4636 HRI map displays two striking features; firstly, a steep rise in surface brightness towards the centre of the galaxy; secondly, the outer contours exhibit a high degree of asymmetry.

The strong enhancement in X-ray surface brightness near the centre of NGC 4636 is a most unusual feature, reminiscent of the excess X-ray emission observed in the core regions of some clusters of galaxies

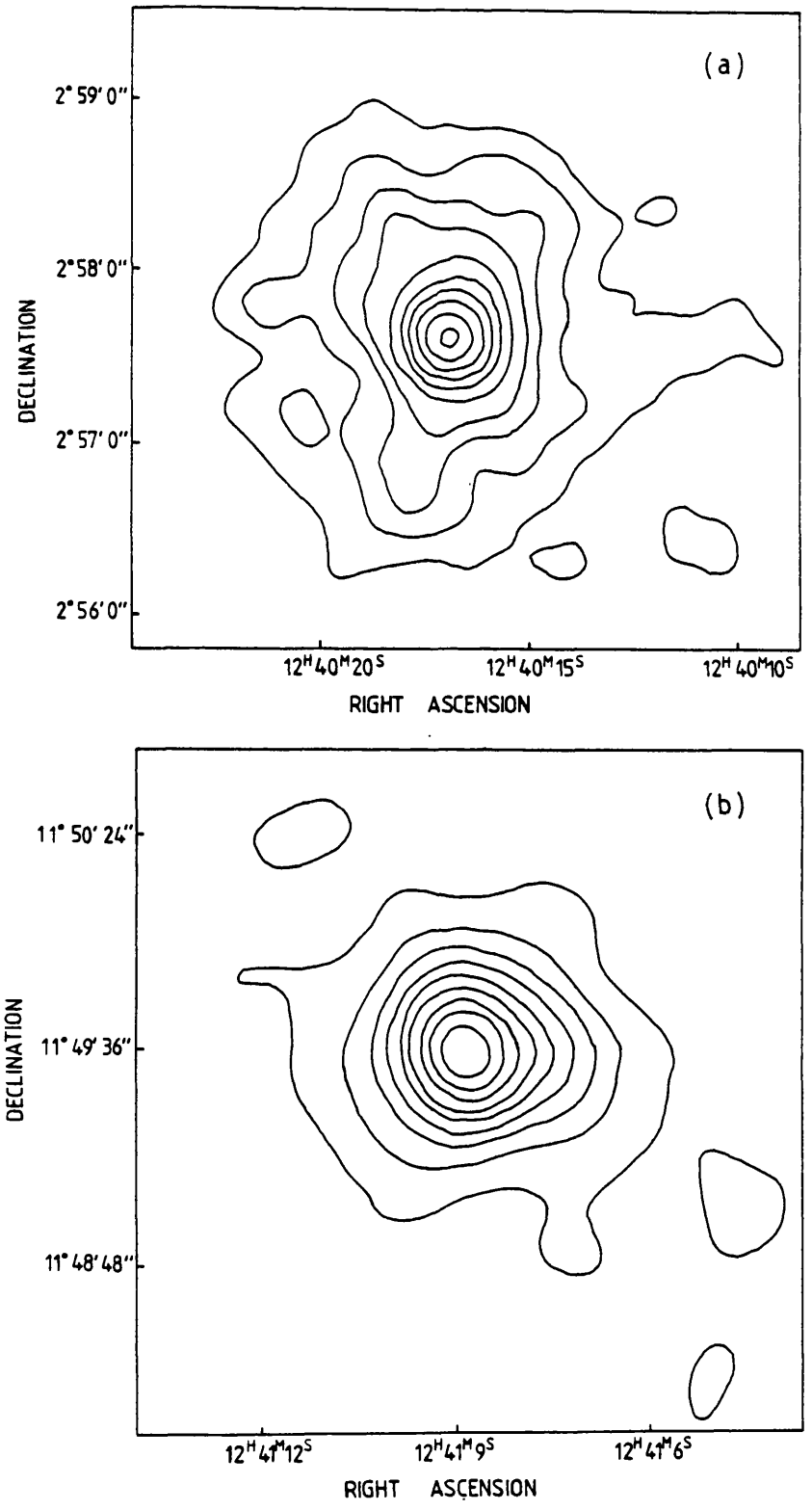

Figure 6.1 Contour maps of Einstein HRI images of (a) NGC 4636 and (b) NGC 4649. Each image has been smoothed with an 8 arcsec gaussian function, and the lowest reproduced contour level corresponds to 3 sigma above background.

Figure 6.2 (Plate)

(a) HRI X-ray contour map of NGC 4636 superimposed upon Palomar Sky Survey red plate. Lowest X-ray contour is 3 sigma above background. Plate scale is 5.5 arcsec/mm, thus 1 arcmin (or 4.2 kpc) corresponds to 10.9 mm.

(b) HRI X-ray contour map of NGC 4649 superimposed upon Palomar Sky Survey red plate. Lowest X-ray contour is 3 sigma above background. Plate scale is 5.5 arcsec/mm, thus 1 arcmin (or 4.4 kpc) corresponds to 10.9 mm.

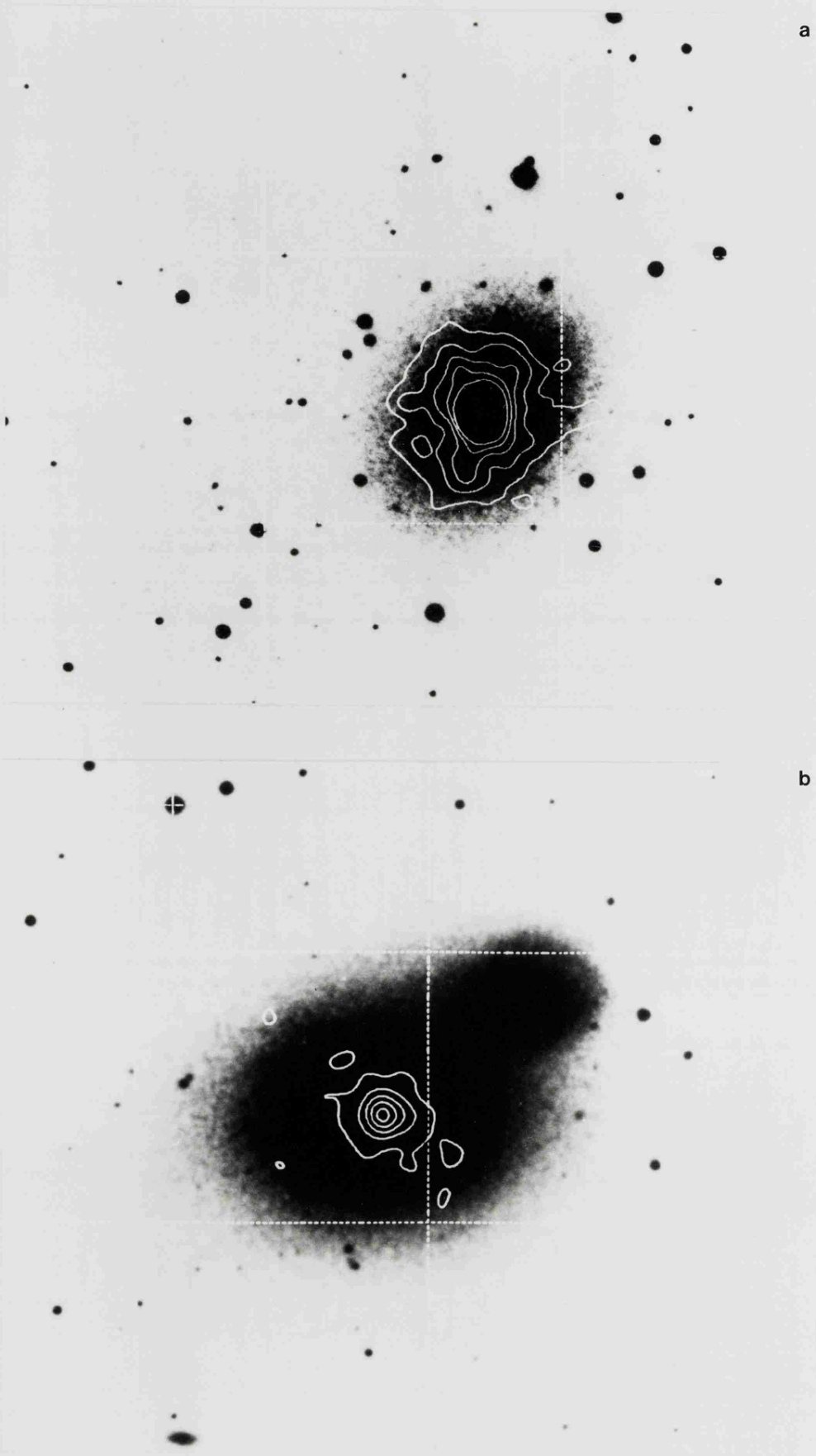
a
b

(Forman et al. 1984), but hitherto unknown among individual early type galaxies. We estimate that the central excess in NGC 4636 contributes roughly 25% of the total X-ray luminosity generated by the galaxy and has an angular extent of ~45 arcsec (FWZI). Since this excess is well resolved by the HRI, we can immediately reject the hypothesis that it is due to a low luminosity AGN situated in the nucleus of NGC 4636. Although the most probable explanation for the X-ray excess is that it represents a strong enhancement in the density of the ambient hot gas, we are unable to explicitly rule out more exotic scenarios, eg. the clumping together of a large number of very luminous discrete sources in the central 2 kpc of the galaxy. There is, however, no independent evidence supporting the latter explanation, and in Chapter Five we demonstrated that the discrete X-ray source contribution to the X-ray luminosity of NGC 4636 is probably no more than a few percent.

The mean radius of the outer (3 sigma) contour level is ~70 arcsec (5 kpc), but this does not represent an accurate measure of the effective radius of the distribution of X-ray emitting gas associated with NGC 4636, since the IPC data analysed in Chapter Four (section 4.4.4) indicates that the emission extends to at least 20 kpc. A detailed comparison between the HRI and IPC maps of NGC 4636 (Figures 6.1 and 4.2) is not particularly useful given their different resolutions, but it is obvious that both display similar large-scale asymmetry. Is the azimuthal asymmetry evident in the HRI data actually significant? The background subtracted azimuthal surface brightness profile for $28 < r \leqslant 72$ arcsec (ie. excluding the central excess), shown in Figure 6.3, is clearly inconsistent with a constant surface brightness model since it yields a chi-squared value of 21.7.

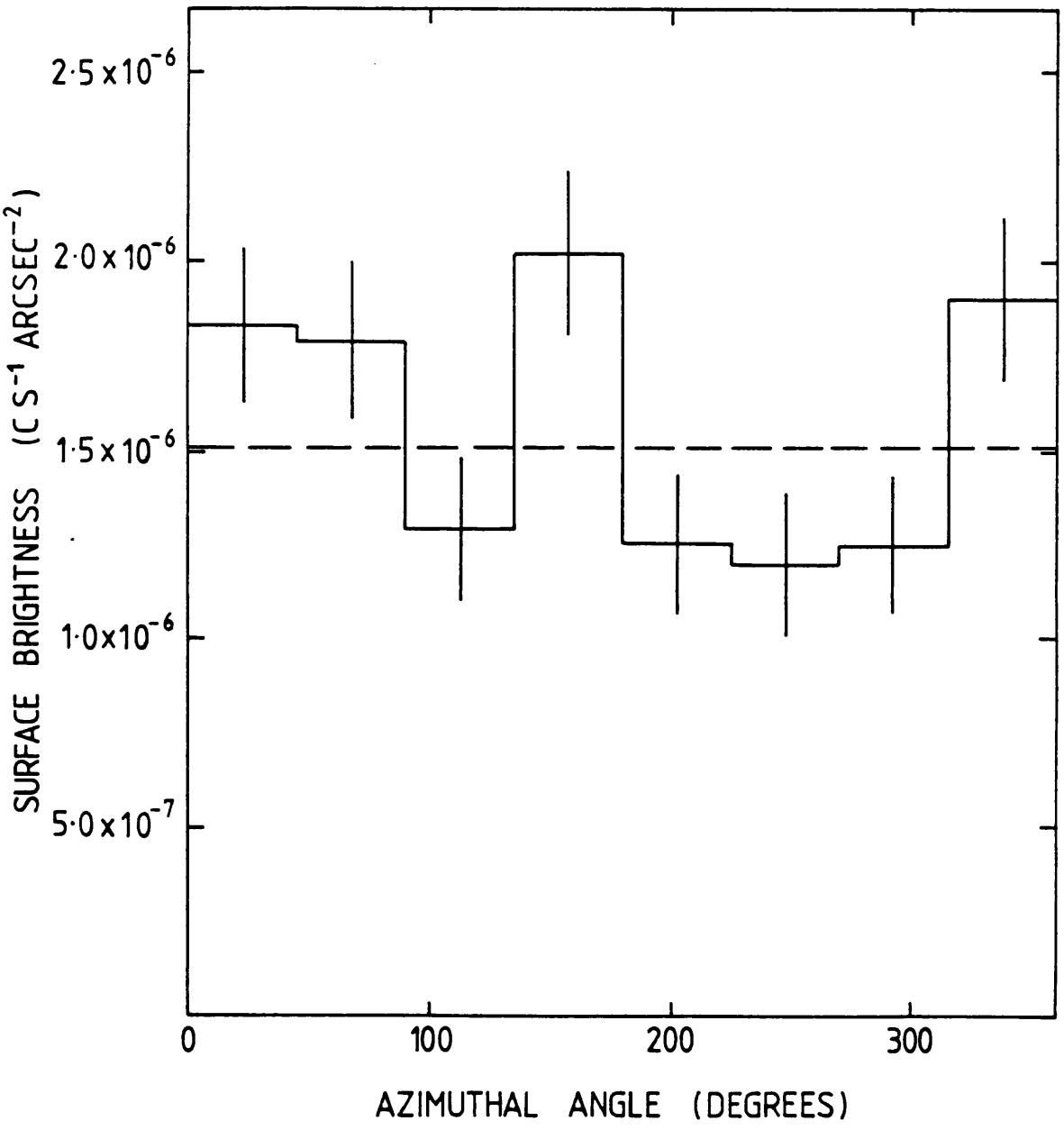

Figure 6.3 Background subtracted azimuthal surface brightness profile extracted from the HRI data for NGC 4636 (excluding the bright central excess).

NGC 4636 is classified as an E0 galaxy on the basis of its optical appearance (de Vaucouleurs et al. 1976). It is therefore reasonable to assume that this galaxy is a physical system which displays a fairly high degree of spherical symmetry. Optical photometry clearly demonstrates that the optical light from the stellar system follows a simple, smooth surface brightness distribution (King 1978). Since the hot gas which generates virtually all of the X-ray emission exists as a direct consequence of normal stellar evolution, we might expect that its spatial distribution would exhibit symmetry properties similar to those of the optical light. Figures 6.1a and 6.2a clearly demonstrate that this is not the case, thus indicating that the observed asymmetric gas distribution is the result of complex dynamical evolution. (Note that if the X-ray emission was composed entirely of contributions from main sequence stars and evolved objects, we would expect that the X-ray surface brightness distribution would closely mimic the optical light distribution of the parent stellar population.)

Ram pressure stripping of hot gas has occasionally been invoked to explain the asymmetric gas distributions observed in some early type galaxies. The most notable case is M86, where the discovery of a semi-detached plume of gas offset from the main body of the galaxy provides clear evidence of the recent onset of stripping as the galaxy re-enters the core region of the Virgo Cluster (Forman et al. 1981). NGC 4636 is located near the extreme edge of the Virgo Cluster, where the ambient IGM is probably extremely tenuous; furthermore, the galaxy's velocity differential relative to the cluster centroid is fairly modest (~ 0.5 x cluster dispersion), which would seem to

indicate that ram pressure stripping exerts negligible influence on the hot gas associated with NGC 4636. We note that Bechtold et al. (1983) concluded that a galaxy as massive as NGC 4636 would probably not undergo significant ram pressure stripping if located at more than one cluster core radius from the centre of a rich, unevolved cluster (eg. Virgo or Abell 1367).

Since we are unable to attribute the asymmetric gas distribution displayed by NGC 4636 to the action of external processes, we are forced to assume that internal processes are responsible. In Chapter Five we examined the possibility that the large quantity of hot gas contained in NGC 4636 (and similar galaxies) is gravitationally confined by an extensive halo of dark matter. If supernovae heating maintains the confined gas against the effects of radiative cooling, the gas temperature will be roughly constant throughout the galaxy, and its spatial distribution will be smooth and exhibit symmetry properties similar to the underlying gravitational potential field. A highly asymmetric gas distribution is a most unlikely result of this scenario. Alternatively, if radiative cooling dominates the evolution of the gas a steady cooling flow will occur, and again we would expect to observe a fairly regular and symmetric X-ray morphology. In Chapter Five we examined the global energetics of the hot gas in NGC 4636, and concluded that the heating and cooling rates could well be quite similar (except in the central region, where the gas density is very high). Given this possibly close balance between competing processes, it would seem plausible that the observed asymmetry simply indicates the presence of erratic, large-scale gas flows in the outer regions of the galaxy. Supernova heating may therefore be disrupting,

but not completely suppressing, a global cooling flow.

We have extracted an azimuthally averaged radial surface brightness profile from the raw HRI data, binned into 8 arcsec annuli in order to reduce the influence of instrumental resolution and photon noise. The radial profile of NGC 4636 (Figure 6.4a) clearly shows the pronounced central excess which is so prominent in the contour map. Despite the obvious azimuthal asymmetry evident in the 2-D data, it is still useful to model, and hence parameterize, the 1-D radial profile data. An isothermal gas sphere model of the form:

$$S(r) \propto (1 + (r/a_x)^2)^{0.5-3\beta},$$

does not provide a statistically acceptable fit to the data unless the three innermost bins are excluded. The low signal to noise and poor dynamic range of the radial profile data beyond the central excess do not enable significant constraints to be derived for the fitted parameters a_x and β. For statistically acceptable fits we find $a_x/\beta \simeq$ constant, with a_x = 75 arcsec for a β = 1.0 model (see Figure 6.4a). Addition of a simple gaussian component to the basic isothermal gas sphere model allows the central excess to be modelled successfully, but does not readily permit a physically meaningful interpretation of the distribution of the hot gas. Although we could use the radial profile models to calculate gas parameters (see Chapter Five, 5.3.1), we prefer to use a less model-dependent deprojection technique (see section 6.2.4).

NGC 4649

The lowest contour level reproduced in the HRI map of NGC 4649 (Figure 6.1b) represents a source surface brightness of 1.01×10^{-6} ct s^{-1}

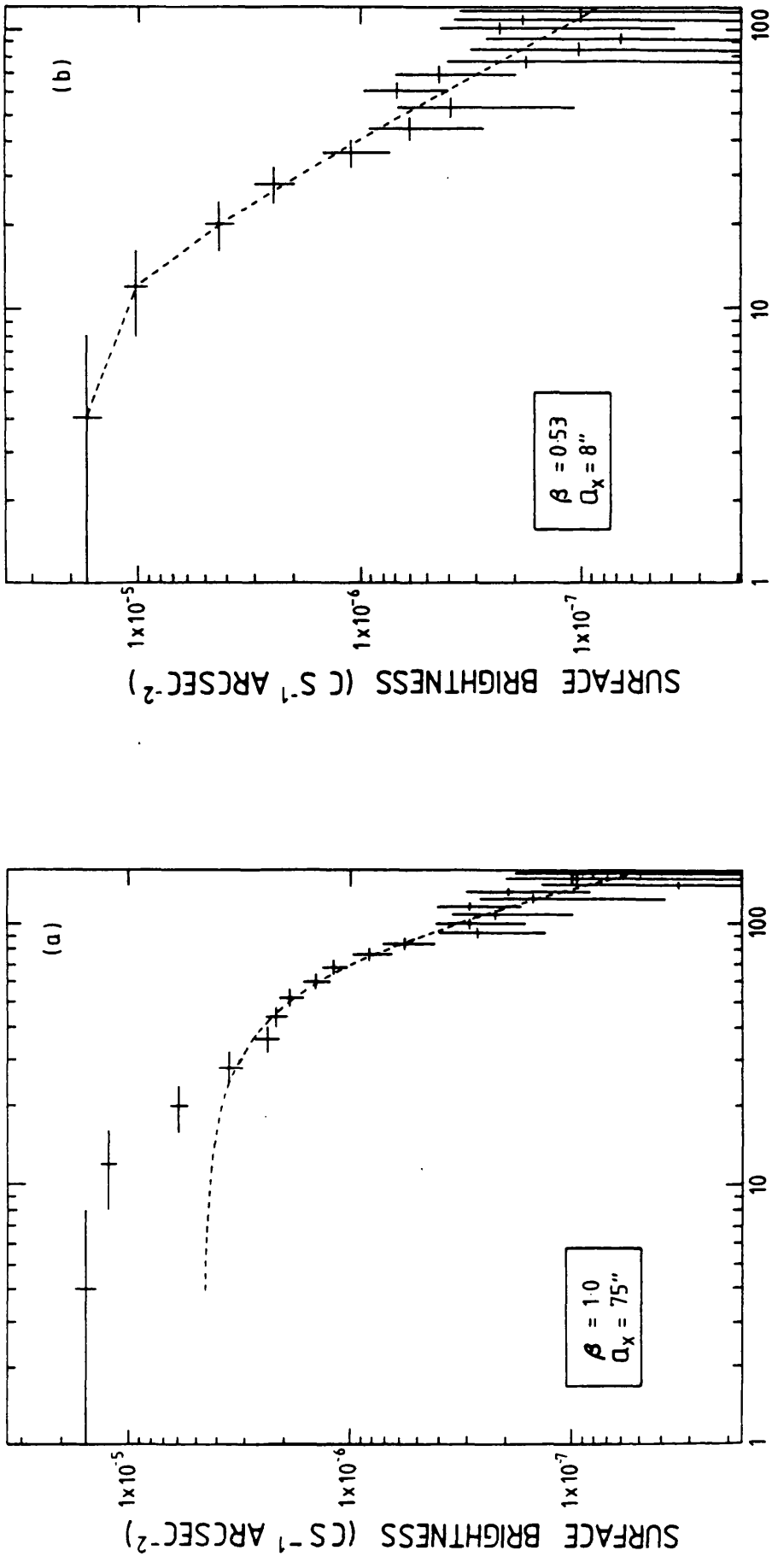

Figure 6.4 Background subtracted HRI radial profiles and best-fit isothermal gas sphere models for (a) NGC 4636 and (b) NGC 4649.

arcsec^{-2}, which corresponds to 8% of the peak value and is ~3 sigma above background. All contour levels increment by ~10% of the peak value. It should be noted that the HRI observation of NGC 4649 was of a shorter duration and exhibited a 33% higher background level than the NGC 4636 observation, and is therefore correspondingly less sensitive to diffuse X-ray emission. Although NGC 4649 itself was detected, we find no evidence for either an unresolved source or extended emission associated with the companion spiral galaxy NGC 4647. We derive a formal luminosity limit of ~1x10^{40} erg s^{-1} for a hypothetical X-ray emission region of radius one arcmin associated with NGC 4647.

Unlike NGC 4636, NGC 4649 displays a relatively simple large scale X-ray morphology. There is no evidence for a sharp change in the surface brightness profile near the centre of the galaxy, and the outer contours exhibit only a very modest degree of asymmetry. Comparison between the NGC 4636 and NGC 4649 contour maps (Figure 5.1) demonstrates that the mean radius of a given absolute surface brightness level is smaller for NGC 4649, indicating that the overall extent of the X-ray emitting gas is less than in NGC 4636. Although a detailed analysis of the IPC data is required to conirm this result, it does seem probable that NGC 4649 contains a significantly smaller quantity of hot gas than NGC 4636. This is rather surprising; NGC 4649 is the more optically luminous of the two galaxies (see Table 6.1) and thus will generate correspondingly more gas from stellar evolution (~1.2 M_o yr^{-1}, compared with ~0.5 M_o yr^{-1} for NGC 4636). The obvious conclusion is that gas depletion processes are more efficient in NGC 4649 than in NGC 4636.

NGC 4649 is located at a projected distance of 1.6 cluster core radii from the centre of the Virgo Cluster. On the basis of radial velocity measurements it would appear that NGC 4649 is a relatively stationary galaxy; its radial velocity differential relative to the cluster centroid is $\sim$ 0.1 x cluster dispersion. Assuming that any tangential velocity component is also small, the galaxy's motion relative to the cluster IGM is unlikely to induce significant ram pressure stripping, particularly since the IGM is probably relatively tenuous beyond the cluster core region. Another environmental factor, namely the evaporation of hot gas associated with the outer region of a galaxy into the ambient IGM, may be more important. Bechtold et al. (1983) estimated an evaporation loss rate of $\sim$20 $M_\odot$ yr^{-1} for a galaxy situated at roughly one cluster core radius from the centre of Abell 1367 - a cluster in an evolutionary state similar to Virgo. This loss rate is reduced still further if a galaxy possesses a massive dark halo or a substantial magnetic field, thereby reducing conduction efficiency. We estimate that NGC 4649 contains $\lesssim 10^9$ $M_\odot$ of hot gas, rather than the $\gtrsim 10^{10}$ $M_\odot$ expected from stellar mass loss considerations; it is entirely possible that slow evaporation ($\sim$1 $M_\odot$ yr^{-1}) of hot gas into the cluster IGM is responsible for the discrepancy.

NGC 4649 exhibits a relatively smooth surface brightness distribution, which in comparison with NGC 4636 would seem to indicate that large scale gas flows are not present. Conceivably, the supernova rate in NGC 4649 is so high that the radiative cooling of the modest quantity of hot gas contained within the galaxy is not sufficient to maintain a general cooling flow outside the core. In this scenario the X-ray

emitting gas is probably isothermal throughout much of the galaxy, and confined in a static distribution by an extensive dark halo, but subject to depletion by evaporation into the cluster IGM. Without an accurate measurement of the gas temperature profile we are unable to exclude cooling flow scenarios, however. The slight E-W asymmetry evident in the X-ray isophotes of NGC 4649 is not reflected in the distribution of optical light (Figures 6.1b and 6.2b). The implied distortion in the spatial distribution of the hot gas could be caused by tidal interaction with the companion spiral galaxy, which itself shows evidence of distortion (Schanberg 1973).

Finally, the azimuthally averaged radial surface brightness profile for NGC 4649 (Figure 6.4b) is well fitted by a simple isothermal gas sphere model over the full radial range of the data. The derived joint 90% confidence parameter ranges are $a_x = 8^{+8}_{-4}$ arcsec and $\beta = 0.53^{+0.2}_{-0.1}$. Theoretically, $\beta = \mu m_H \sigma^2 / kT_{gas}$, assuming the rotational energy of the stellar component is negligible compared with the kinetic energy of random motion. For NGC 4649 the velocity dispersion is $\sigma = 341$ km s^{-1} (Tonry and Davis 1981), therefore $T_{gas} \sim 1.6 \times 10^7$K is required if the predicted value of β is to equate with the observed value.

6.2.3 Small Scale Morphology

To facilitate the study of small scale X-ray structure in the central regions of the two galaxies we have smoothed the unbinned (0.5 arcsec pixel) HRI images with a 2-D representation of the HRI point response function. This technique provides fair suppression of photon noise and achieves angular resolution close to the instrumental limit.

Contour maps of the central regions of NGC 4636 and NGC 4649 are displayed in Figures 6.5 and 6.6 respectively; the ~4 arcsec resolution corresponds to a scale size of ~0.3 kpc. Outside the mapped regions the X-ray surface brightness is too low to support the study of fine structure, and even within the bright central regions some of the features may be attributable to photon noise.

NGC 4636

The mapped region in Figure 6.5 includes ~700 source photons. All contour levels increment by 10% of the peak surface brightness; the lowest contour level corresponds to 4.8×10^{-6} ct s^{-1} arcsec^{-2} (27% of the peak value), or ~10 sigma above background. It is apparent that the morphology of the central X-ray emission region of NGC 4636 is quite complex. The outermost contours exhibit a roughly circular symmetry; the peak surface brightness region is, however, a well defined plateau, elongated in the E-W direction with dimensions ~1.3x0.6 kpc. If the observed emission is predominantly due to hot gas, the implied departures from a quasi-spheroidal gas distribution probably indicate the presence of anisotropic gas flows in the core region of this galaxy. It is interesting to speculate as to whether this might be linked to the anisotropic stellar velocity distributions inferred to exist in some elliptical galaxies (eg. Illingworth 1983).

Several local surface brightness maxima are apparent in Figure 6.5. To test whether these maxima are statistically significant, we have utilized the cross-correlation technique discussed in Appendix A.4 to search for unresolved X-ray "sources" in the mapped region. This technique located seven discrete sources, each with a statistical significance $\geq$ 5 sigma; their positions have been superimposed upon

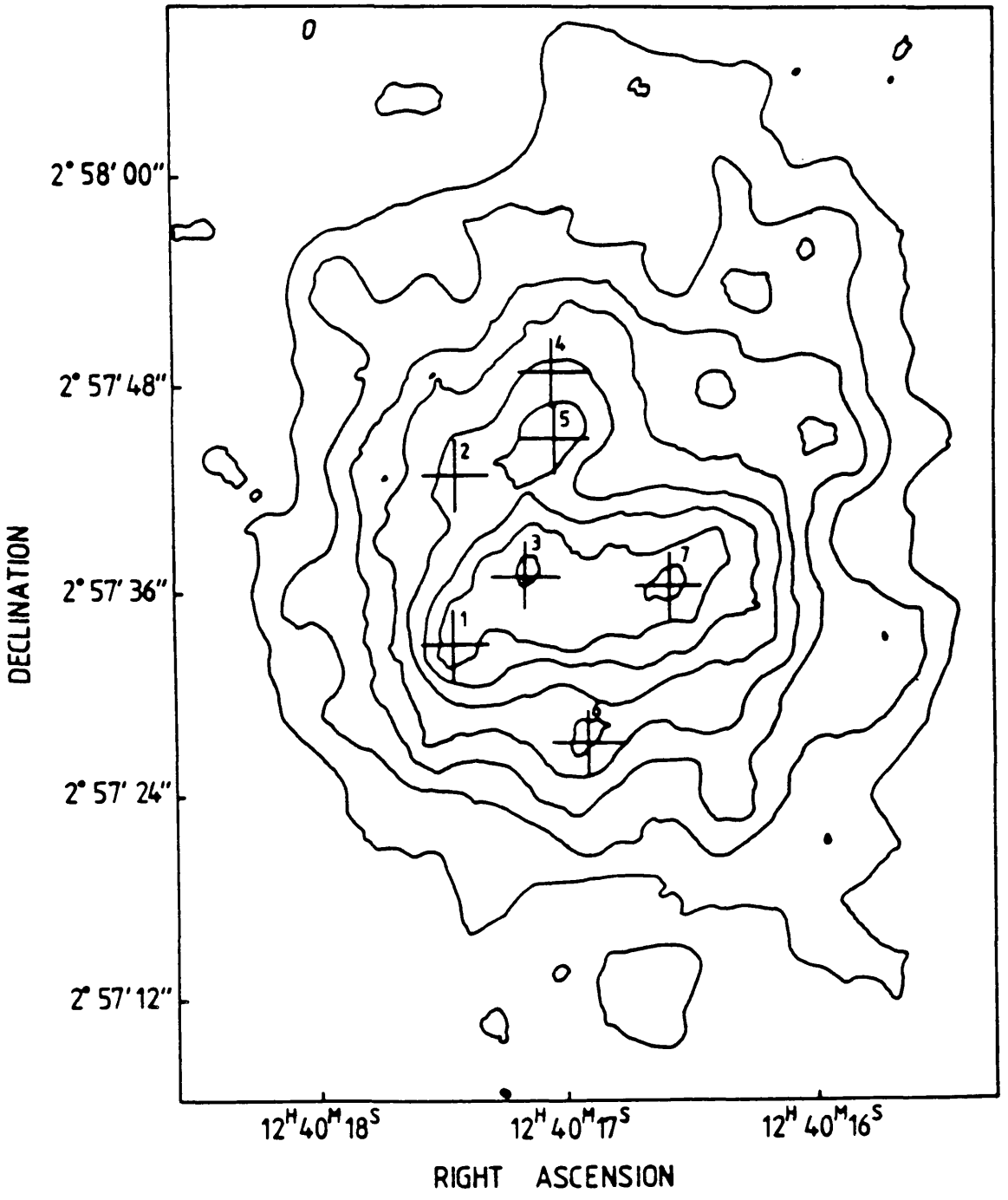

Figure 6.5 Contour map of the central region of the NGC 4636 HRI image. The data has been smoothed with the instrumental PRF, and the locations of possible unresolved sources are superimposed upon the map.

the contour map of the smoothed image (Figure 6.5). At least two sources (#4 and #5) are so close together that they are probably only marginally resolved. We have examined 1-D surface brightness slices through the central regions of the unsmoothed data, and conclude that sources #2 and #4 are probably spurious. Even a relatively sophisticated source detection technique such as the cross-correlation algorithm should not be used in isolation, since it is susceptible to resolution effects (ie. source confusion) and photon noise.

Have we actually located genuine discrete X-ray emitting objects, or are the local maxima simply representative of small scale structure in the ambient hot gas? The detected sources have count rates $\gtrsim 6\times10^{-4}$ ct s^{-1}, corresponding to $L_X \gtrsim 2\times10^{39}$ erg s^{-1}. Although high mass binary systems may occasionally attain such extreme luminosities (see Chapter Three, 3.4.1), they are most unlikely to be found among the low mass stellar population of NGC 4636. One SNR is known to have $L_X \sim 10^{39}$ s^{-1}, but such objects are extremely rare (Blair et al. 1983). Low mass X-ray binaries are certain to be present in NGC 4636, just as they are in the bulge regions of our galaxy and M31, but known examples of such systems have X-ray luminosities at least a factor of ten lower than the hypothetical objects in NGC 4636 (eg. Bradt and McClintock 1983; for a possible exception, see Chapter Three, 3.3.3). Scenarios involving the clumping together of a large number of less luminous objects in a small region of the galaxy are not excluded by the data, but suffer from an obvious artificiality and a complete lack of independent supporting evidence. A much simpler explanation does, of course, exist: local X-ray maxima could simply indicate regions where the density of the ambient hot gas is abnormally high. The

effective luminosity of such a feature is essentially proportional to the square of the gas density, so the required density fluctuations are not dramatic, although they would have to persist over a scale of $\sim$0.3 kpc. Such density fluctuations are a likely consequence of the competing heating and cooling processes within a cooling flow. Observations with considerably improved sensitivity and resolution are required if we are to distinguish between the ultra-luminous binary and gas density fluctuation hypotheses for the nature of the X-ray maxima.

NGC 4649

The mapped region in Figure 6.6 includes 300 source counts. All contour levels increment by 10% of the peak surface brightness; the lowest contour level corresponds to 5.4×10^{-6} ct s^{-1} arcsec^{-2} (25% of the peak value), or $\sim$7 sigma above background. The central region of NGC 4649 is at least as complex as that of NGC 4636. Isophotes of X-ray surface brightness extend much further to the West than the East, indicating a striking asymmetry in the spatial distribution of hot gas. (We have already noted a similar, but less pronounced, asymmetry on larger scales.) It is possible that the ambient hot gas responds to a non-isotropic gravitational potential field, or is incorporated in a complex system of flows.

Although the contour map of the smoothed data gives an impression of clumpiness, application of the cross-correlation algorithm to the raw data resulted in the detection of only two "sources", perhaps reflecting the poorer counting statistics compared to NGC 4636. Both sources were detected at a formal statistical significance $>$ 5 sigma,

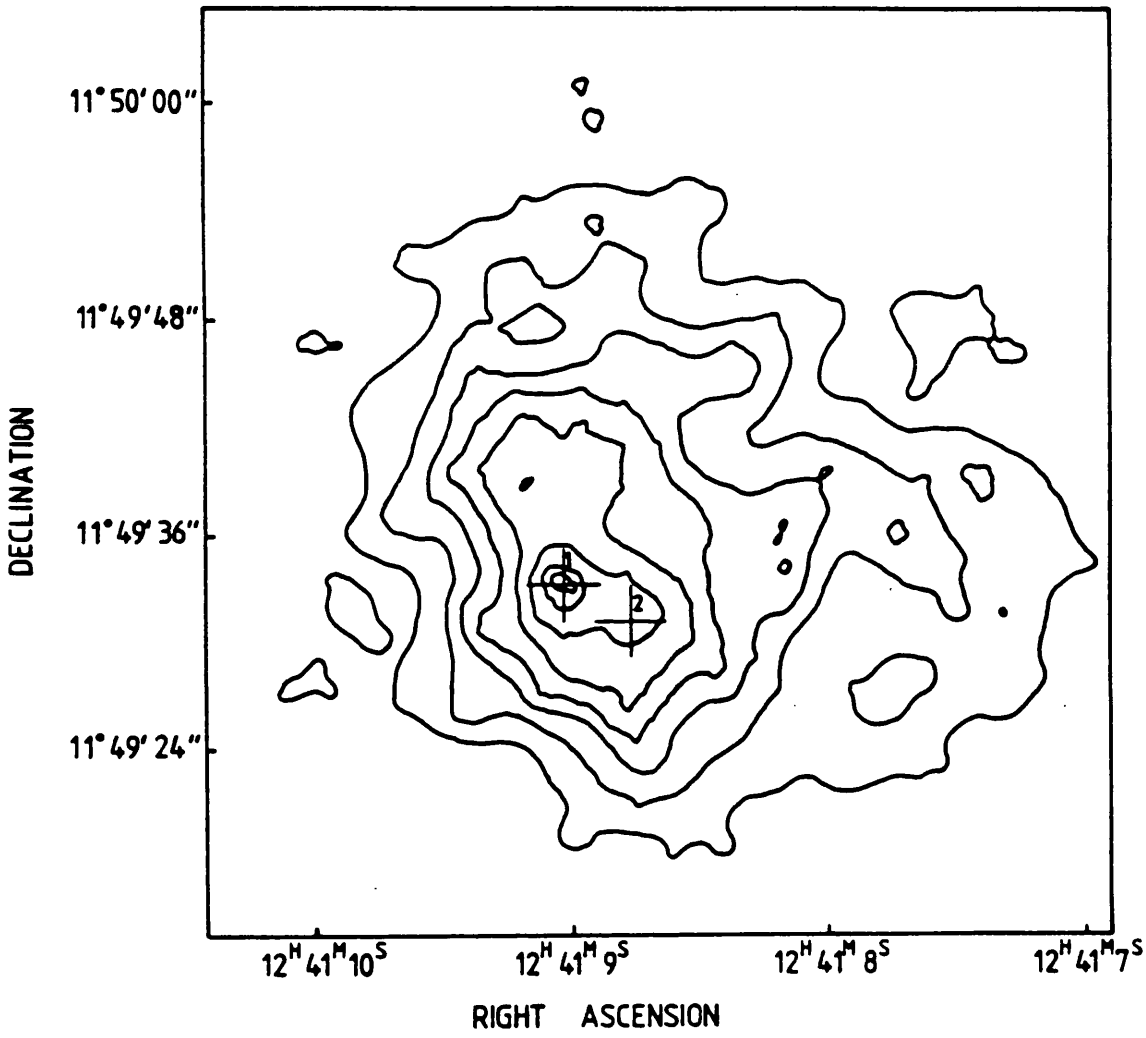

Figure 6.6 Contour map of the central region of the NGC 4649 HRI image. The data has been smoothed with the instrumental PRF, and the locations of possible unresolved sources are superimposed upon the map.

and their locations are superimposed on the smoothed contour map (Figure 6.6). It is clear that the two sources are only marginally resolved, and indeed source #2 is probably spurious. Source #1 is very prominent, and its position is consistent (within the HRI pointing uncertainty) with that of the optical nucleus of the galaxy. It is therefore tempting to attribute source #1 to a low luminosity AGN rather than an ultra-luminous X-ray binary or region of abnormally dense gas, although this assertion can certainly not be independently verified at present.

6.2.4 Simple Cooling Flow Models for NGC 4636 and NGC 4649

The radiative cooling times derived for the hot gas associated with early type galaxies are invariably short compared with the Hubble timescale. If the integrated supernova rate within a galaxy is not sufficient to counteract the effects of radiative cooling, a global cooling flow is likely to occur. Direct proof of the existence of cooling flows in early type galaxies will require X-ray observations with both high angular resolution and good spectral discrimination, thus enabling the detection of the central gas temperature inversion which is characteristic of a cooling flow (cf. M87, Lea et al. 1982, Canizares et al. 1982). Indirect evidence in the case of NGC 4636 derives from those characteristics it shares with clusters of galaxies which display evidence of cooling flows, namely a sharply rising X-ray surface brightness profile near the core region and the presence of modest nuclear activity (eg. radio emission at GHz frequencies and line emission in the optical spectrum). The large scale X-ray morphology of NGC 4636 could also be interpreted as evidence for large scale gas flows, albeit possibly disrupted by the effects of heating.

Evidence for a cooling flow in NGC 4649 is less compelling at present; the global gas temperature is currently unknown, so other gas paarameters are also undetermined, and the galaxy exhibits only one classical cooling flow signature - nuclear radio emission. Nevertheless, we will apply the same type of cooling flow model to both galaxies, and in the case of NGC 4649 check for any obvious internal inconsistencies.

Our ultimate aim is to study the relationship between cooling flows and nuclear activity; we therefore need to establish physically meaningful quantities such as mass flow rates and the thermal pressure exerted by hot gas; the HRI data must therefore be used to derive estimates for $T(r)$ and $n_e(r)$. Fabian et al. (1981) used an iterative deprojection technqiue to analyse an HRI image of NGC 1275. The radial profile of the X-ray emission was geometrically deprojected under the assumption that the X-ray emitting gas was distributed in concentric spherical shells. An additional assumption that the gas was in hydrostatic equilibrium with the galaxy's gravitational potential field enabled the derivation of $T(r)$ and $n_e(r)$, consistency being ensured by testing the results to see if they reproduced the IPC-derived spectral hardness profile, $H(r)$. Since our analysis of IPC data provides only a crude estimate of the globally averaged gas temperature rather than a radial temperature or spectral hardness profile, we prefer to relax the assumption of hydrostatic equilibrium, which in any case may not be strictly applicable to a cooling flow scenario, and instead develop a simple, self-consistent model for $T(r)$.

In the absence of suitable independent constraints, we feel that it is

sensible to adopt the simplest viable model for a cooling flow. We assume that stellar mass loss balances radiative cooling (the radiative regulation model of Cowie and Binney 1977), and heating processes exert negligible influence on the properties of the flow, which is therefore stable. Adiabatic compression occurring as the gas flows through the galaxy's gravitational potential field maintains the hottest gas at a temperature:

$$T(r) \simeq GM(r)\mu m_H/kr \quad ,$$

where M(r) is the total gravitating mass within radius r (Nulsen et al. 1984). M(r) can be calculated using a simple King model;

$$\rho(r) \propto (1 + (r/a)^2)^{-3/2}$$

which is normalized via application of the Virial theorem to the galaxy core (r = a), ie.:

$$GM(a)/a \simeq 3\sigma^2 \quad ,$$

where σ is the velocity dispersion of the core. Integrating the density profile over the core and substituting for M(r) in the temperature equation leads to:

$$T(r) \simeq 17.2\mu m_H \sigma^2 f(x) y/kx \qquad (1) \quad ,$$

where $x = r/a$ and $f(x) = \ln(x+(1+x^2)^{1/2}) - (x/(1+x^2)^{1/2})$. The multiplicative constant "y" is included to allow for possible departures from the exact Virial theorem as applied to galaxy or cluster cores. In principle, y can be varied to fit T(r) to some constraint, such as an IPC-derived global temperature. We initially set y = 1.0 and adopt equation (1) in its exact form. The adiabatic compression temperature profiles for NGC 4636 (σ = 219 km s^{-1}, a = 3.16 arcsec) and NGC 4649 (σ = 341 km s^{-1}, a = 5.37 arcsec) are displayed in Figure 6.7. The adopted velocity dispersion and core

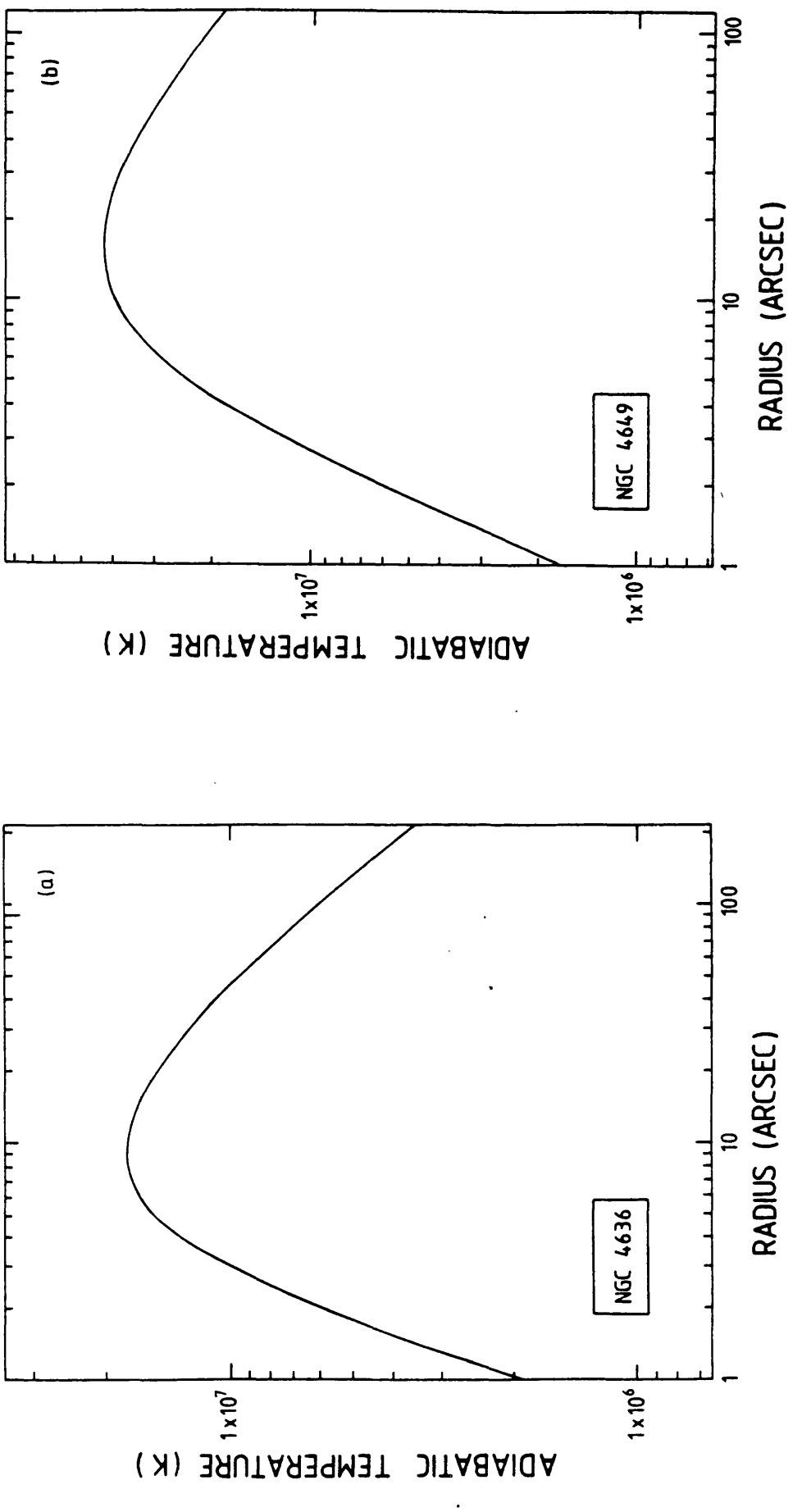

Figure 6.7 Radial dependence of adiabatic temperature in the cooling flow models applied to (a) NGC 4636 and (b) NGC 4649.

radius values are from Tonry and Davis (1981) and King (1978), respectively.

To derive the radial electron density profile we assume that all of the X-ray emission detected by the HRI is generated by an optically thin plasma, with solar element abundances, which is distributed in a set of spherically symmetric concentric shells. Each shell is assumed to have a constant gas density and to be isothermal at the temperature given by equation (1). By examining the radial dependence of gas properties we are averaging out the azimuthal asymmetry clearly present in the HRI data. Unfortunately, the counting statistics are too poor to attempt a more detailed (r, Θ) deprojection of the data, particularly in the outer regions of NGC 4636 where the asymmetry is most prominent. The assumption of spherical symmetry, and hence a gravitational potential that is a function of radius only, is probably not unreasonable for NGC 4636 and NGC 4649, since both galaxies are thought to be intrinsically quite round (King 1978).

The background subtracted radial profiles displayed in Figure 6.4 form the basic starting point of our deprojection analysis. The 8 arcsec radial bin size is sufficiently large for effects due to instrumental resolution and photon noise to be negligible. Geometrical deprojection of the radial profile data is performed using the iterative procedure described by Fabian et al. (1981) and Kriss et al. (1983); the measured surface brightness of each annulus (ct s^{-1} $arcsec^{-2}$) is converted to a deprojected volume count rate (ct s^{-1} $arcsec^{-3}$) for the equivalent spherical shell, after the application of suitable corrections for the contributions due to the outlying shells. The deprojected count rate profiles for NGC 4636 and NGC 4649 are

shown in Figure 6.8; their outer regions have been rebinned (16 or 24 arcsec bins) in order to improve counting statistics. Conversion to the electron density profile is achieved via:

$$C_v(r) = n_e(r)^2 \, F(T)/4\pi D^2 \qquad (2) \ ,$$

where $C_v(r)$ is the deprojected count rate (units: ct s^{-1} cm^{-3}) from a spherical shell at radius r; F(T) is the emissivity of an optically thin plasma with solar element abundances at a local temperature T = T(r), corrected for absorption due to the column density along the line of sight through our galaxy, and integrated over the HRI effective area function (0.1 - 4.0 keV). The derived $n_e(r)$ profiles for NGC 4636 and NGC 4649 are shown in Figure 6.9. Having determined T(r) and $n_e(r)$ we are now able to perform a detailed study of the properties of the X-ray emitting gas associated with both galaxies.

Adiabatic compression is clearly able to maintain high gas temperatures throughout both galaxies (Figure 6.7). The temperature gradient is relatively flat in the outer region of each galaxy, increasing slowly until it peaks at $r \sim 3a$ and thereafter falling rapidly towards the centre of the galaxy. Spectrally resolved X-ray observations of the core regions of NGC 4636 and NGC 4649 should reveal the presence of relatively cool gas ($T \sim 10^6$-10^7 K), if cooling flows are actually present. If supernovae heating is negligible and a steady cooling flow occurs, then equation (1) should provide a reasonably accurate representation of T(r); whereas if the heating and cooling rates are similar we would expect to find $T(r) \sim T_{global}$ (1.4×10^7 K for NGC 4636) outside the core, although a cooling flow would probably still occur within the core itself. Only if heating completely overwhelms cooling is the gas likely to be isothermal

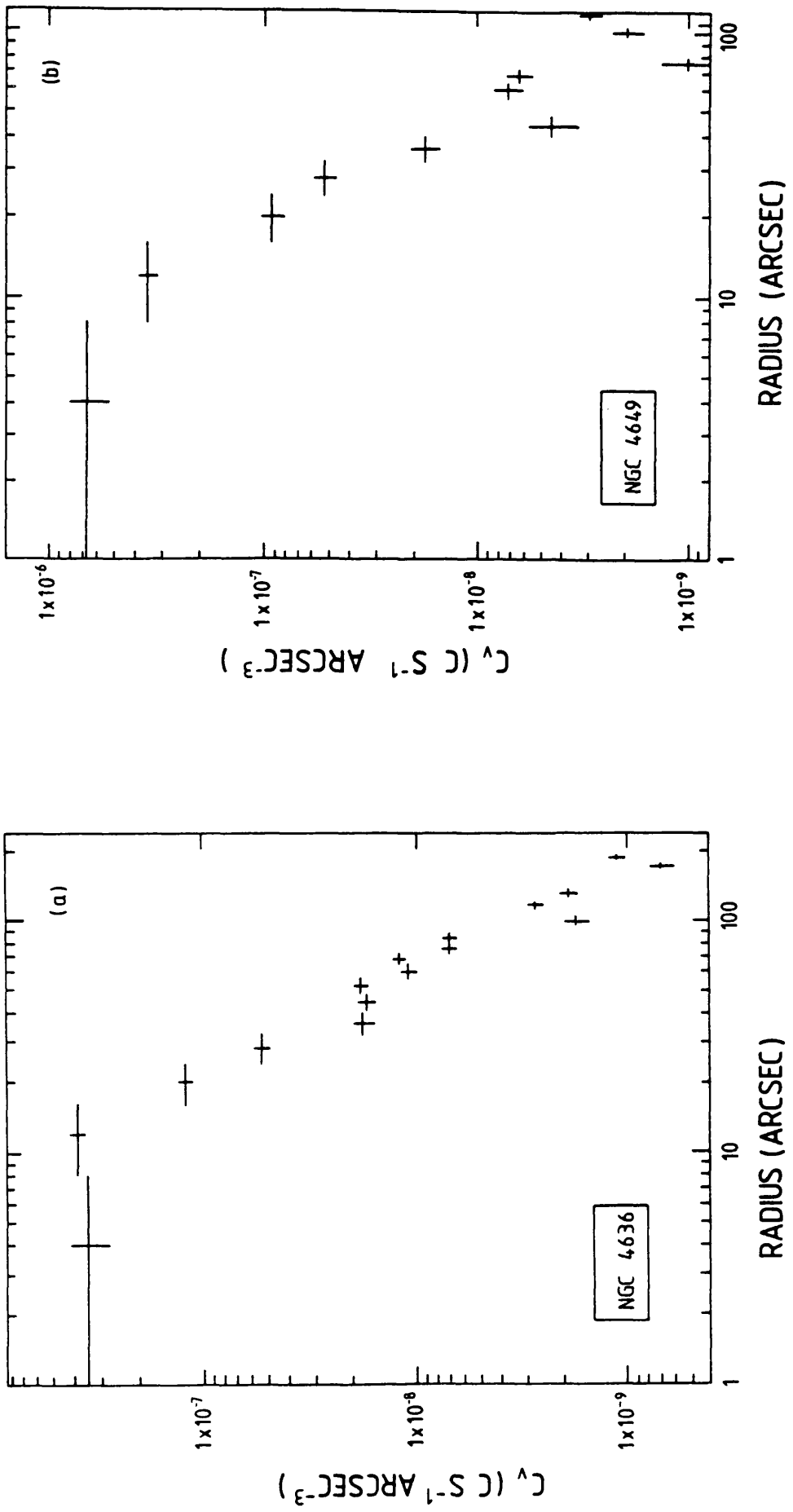

Figure 6.8 Radial dependence of deprojected volume count rate derived from HRI data for (a) NGC 4636 and (b) NGC 4649.

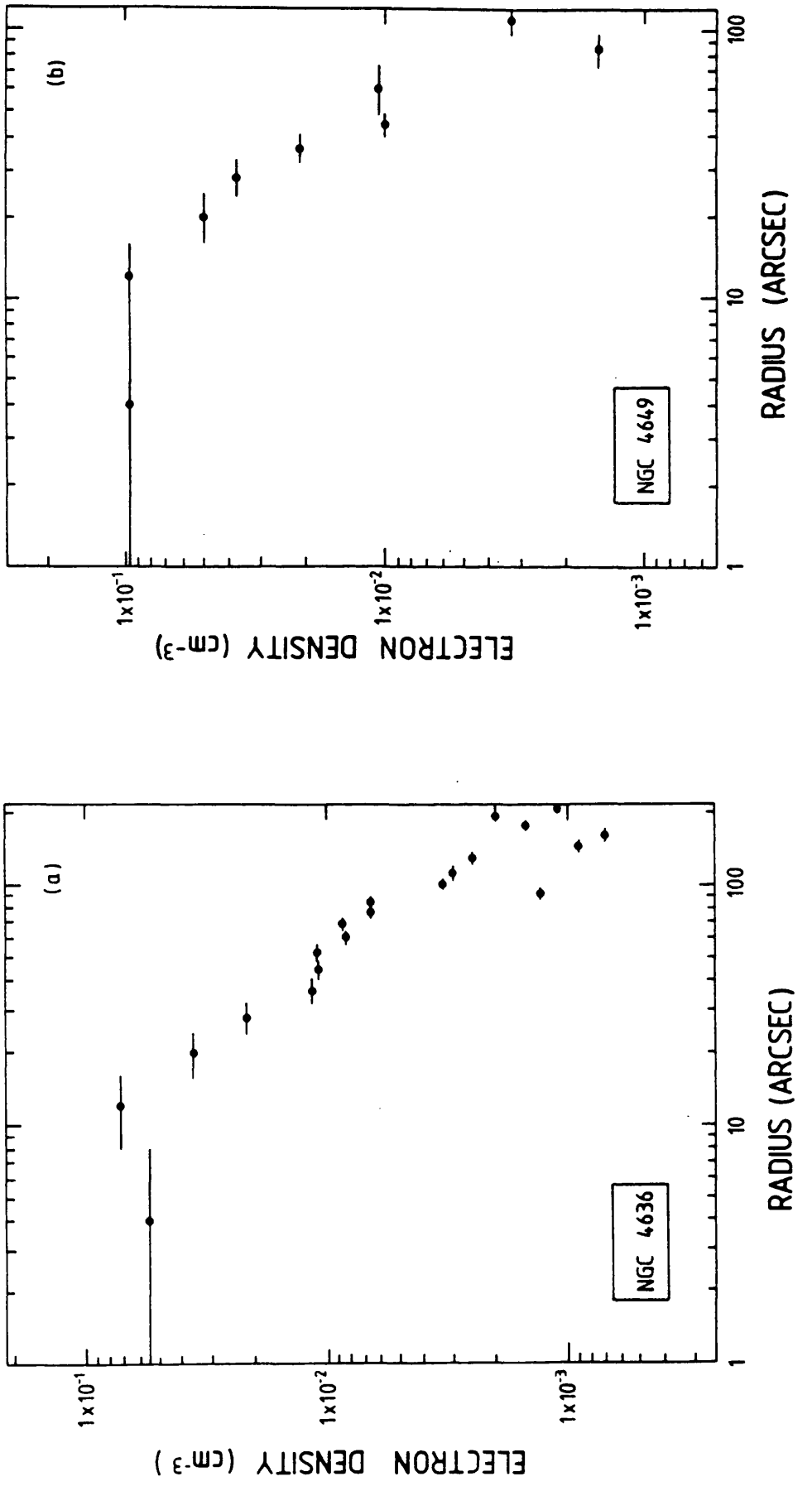

Figure 6.9 Radial dependence of electron density for (a) NGC 4636 and (b) NGC 4649.

throughout the galaxy.

Outside the core of NGC 4636 T(r) ranges from 5×10^6 to 1.8×10^7 K, in reasonable agreement with the crude IPC-derived estimate of the global gas temperature. We can derive an estimate of the globally averaged gas temperature from the adiabatic temperature profile:

$$T_{global} \simeq \sum_i C_V(i)T(i)dV(i) \;/\; \sum_i C_V(i)dV(i) \qquad (3) \;,$$

where dV(i) is the volume of the i'th shell. Summation over the region of persistent X-ray emission yields $T_{global} \sim 1.1\times10^7$ K, in good agreement with the IPC value of $\sim 1.4\times10^7$ K, hence justifying our selection of y = 1.0 in equation (1). A similar estimate made for NGC 4649 gives $T_{global} \sim 3.8\times10^7$ K, which is well in excess of the global temperatures derived for other early type galaxies using IPC data. NGC 4649 does have an exceptionally high velocity dispersion, and for this reason alone we would expect a high global temperature ($T \propto \sigma^2$). An initial examination of the crude spectral fitting performed during the automatic scientific analysis of the NGC 4649 IPC data does not, however, provide strong support for an unusually high gas temperature. It is therefore quite probable that equation (1) does not accurately describe the gas temperature profile of NGC 4649.

Relatively high gas densities ($n_e \gtrsim 5\times10^{-2}$ cm^{-3}) are required to generate the central X-ray emission in both galaxies. Beyond a few optical core radii $n_e(r)$ decreases roughly as an inverse square law. The derived density profile for NGC 4636 is fairly insensitive to the precise form of T(r) adopted; F(T) is a weak function of T for the range of interest ($T \sim 5\times10^6$ - 2×10^7 K). The electron density profile for NGC 4649 is, of course, substantially more uncertain because of

the absence of a reliable estimate of the gas temperature, and this uncertainty is reflected in further gas parameters derived for this galaxy.

In Figure 6.10 we show the radial dependence of the radiative cooling time for the hot gas in both galaxies. In the core regions of NGC 4636 and NGC 4649 the cooling times are so short ($t_{cool} \sim 10^8$ years) that supernova heating would have to occur at a prodigious rate to suppress cooling flows there. Although the cooling time increases beyond the core region of NGC 4636, it remains less than a Hubble time throughout the galaxy. Our assumption of a galaxy-wide cooling flow therefore seems reasonable (as long as the cooling rate is higher than the heating rate). The same does not appear to apply for NGC 4649; t_{cool} reaches H_o^{-1} at a radius of $\sim$80 arcsec (6 kpc), well within the optical light distribution, so a general cooling flow is unlikely.

We are able to derive the radial dependence of the thermal pressure exerted by the X-ray emitting gas within NGC 4636 and NGC 4649 ($P(r) = n_e(r)kT(r)$). The pressure profiles shown in Figure 6.11 clearly demonstrate that quite high gas pressures occur in the central 1-2 kpc of both galaxies. The slight decrease in pressure as $r \rightarrow 0$ reflects the inversion in $T(r)$, whereas the roughly inverse square law dependence beyond $r \sim 20$ arcsec reflects the similar trend exhibited by $n_e(r)$. Note that the pressures derived for NGC 4649 should be used with caution due to the previously discussed uncertainties.

Contributions from the individual shells can be summed to derive an estimate of the mass of hot gas associated with each galaxy, although such estimates are necessarily a strong function of the assumed

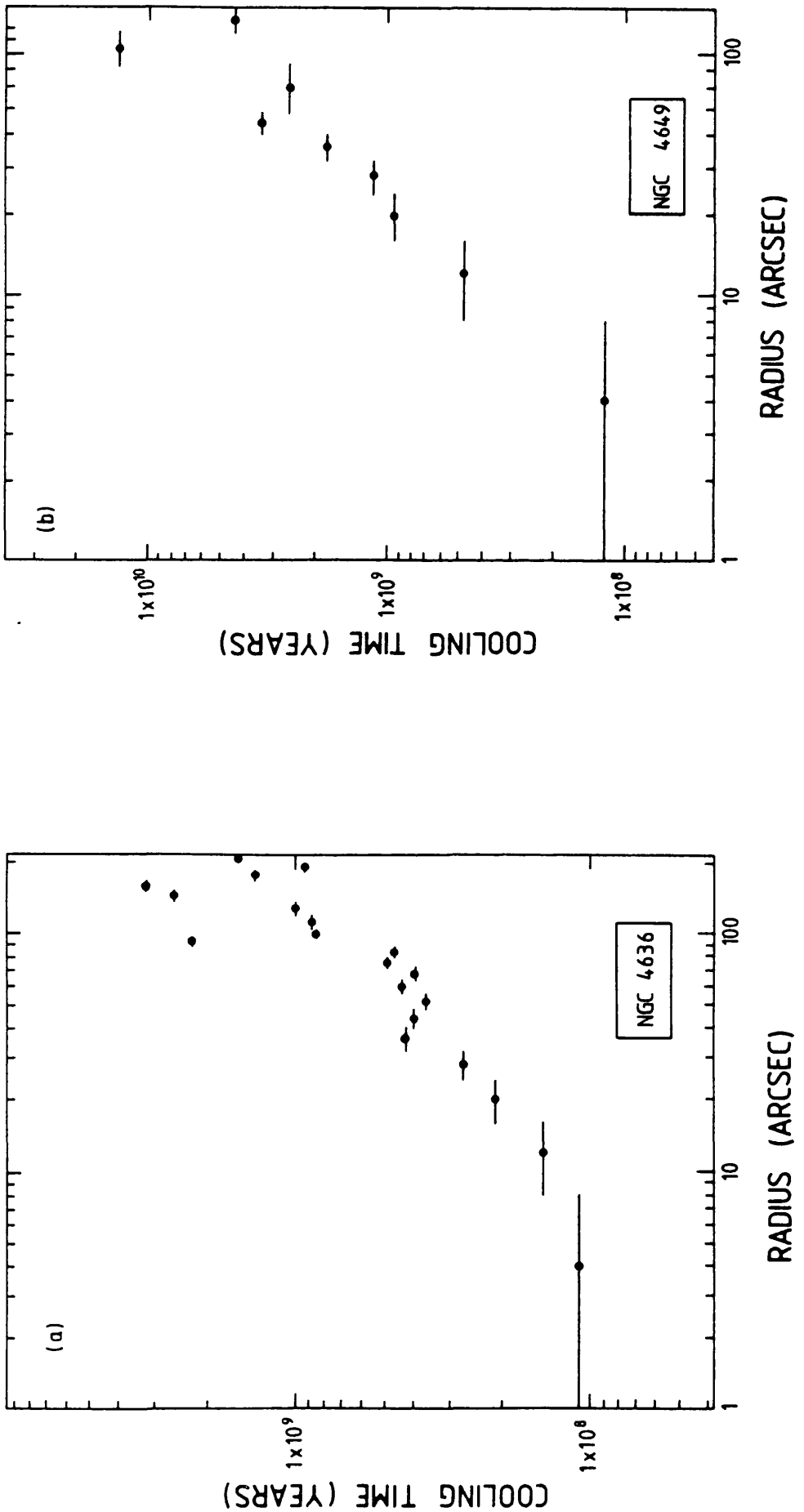

Figure 6.10 Radial dependence of radiative cooling time for (a) NGC 4636 and (b) NGC 4649.

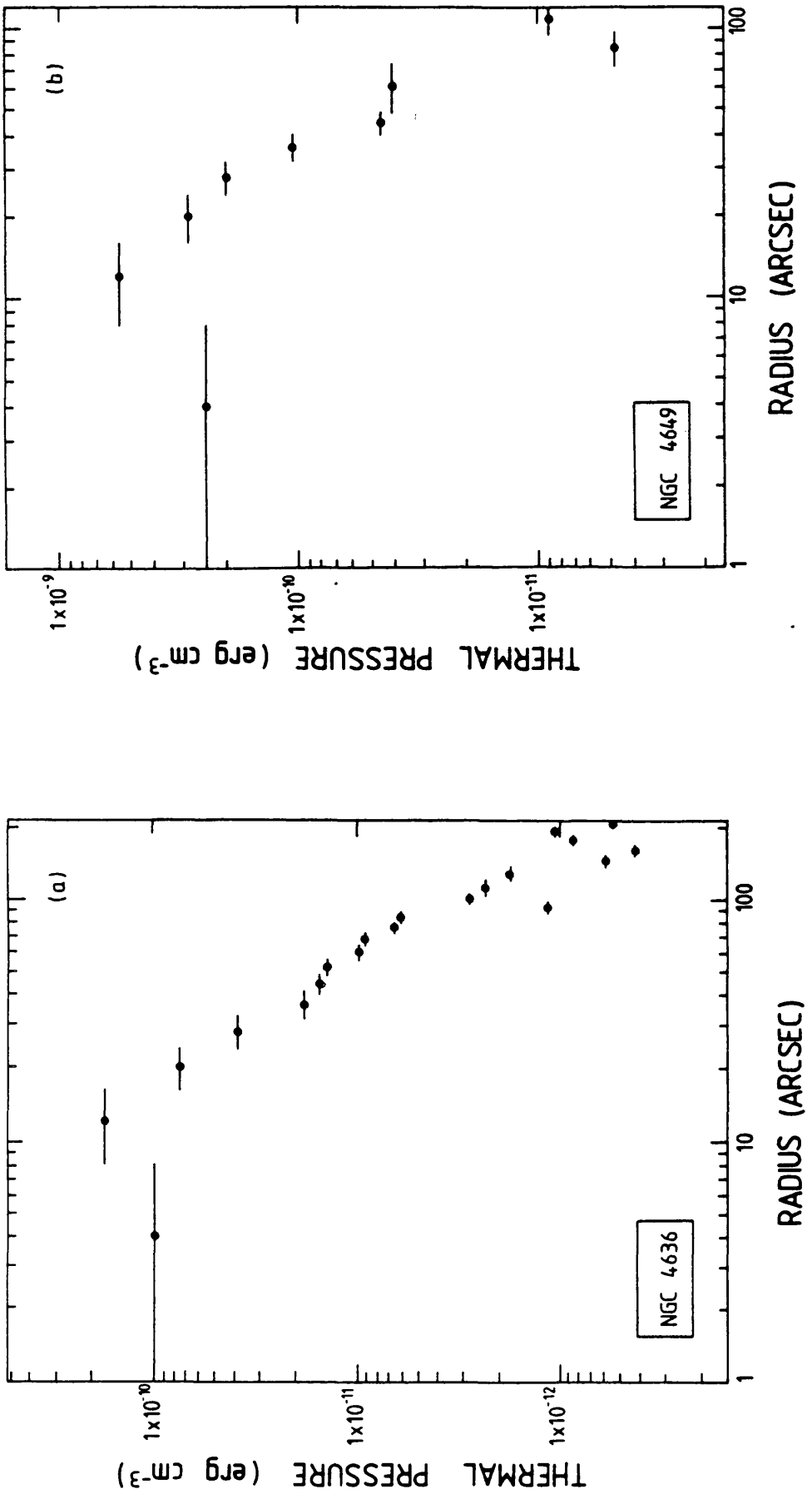

Figure 6.11 Radial dependence of thermal pressure for (a) NGC 4636 and (b) NGC 4649.

limiting radius of the distribution. For NGC 4636 we find, on the basis of HRI data alone, a radius of ~15 kpc and a mass of $\sim 4.5 \times 10^8$ $M_\odot$; the values for NGC 4649 are ~9 kpc and $\sim 2.1 \times 10^8$ $M_\odot$, respectively. Note that the IPC-derived gas mass of $\sim 1 \times 10^9$ $M_\odot$ for NGC 4636 is probably consistent with the HRI value since a larger limiting radius (20 kpc) was assumed (Chapter Five, 5.4.1).

We have established that the HRI data for NGC 4636 and NGC 4649 are consistent with cooling flows occurring within the core regions of both galaxies and throughout the whole physical extent of NGC 4636. If we apply conservation of energy to the cooling flow we find (eg. Stewart et al. 1984):

$$\dot{M}_i = L_i \, [5kT_i/2\mu m_H + (\Phi_i - \Phi_o)]^{-1} \quad ,$$

where L_i is the X-ray luminosity due to gas in the i'th shell. If the gravitational potential energy term $(\Phi_i - \Phi_o)$ is neglected, we deduce that ~ 0.01 $M_\odot$ yr^{-1} flows into the central ~1 kpc of each galaxy. The total stellar mass loss rate required to sustain a cooling flow throughout NGC 4636 is ~ 0.8 $M_\odot$ yr^{-1}, which is in reasonable agreement with the theoretical prediction of ~ 0.5 $M_\odot$ yr^{-1} from stellar evolution (Faber and Gallagher 1976). The evidence for a general cooling flow in NGC 4649 is not compelling at present; part of the predicted ~ 1.2 $M_\odot$ yr^{-1} stellar mass loss has been incorporated into what we believe is probably a static distribution of hot gas, but most has been lost from the system, perhaps via evaporation.

6.3 VLA Radio Observations of NGC 4636 and NGC 4649

6.3.1 Observation Strategy and Data Reduction

Previous radio observations of NGC 4636 and NGC 4649 have been limited to the measurement of monochromatic fluxes at various frequencies, the

angular resolution of the instrumentation being too coarse to enable detailed mapping of the radio emission (eg. Hummel et al.1983). The VLA 1465 MHz and 4885 MHz observations reported here achieved an angular resolution of ~4 arcsec, comparable to the resolution attained by the Einstein HRI in the soft X-ray band. A detailed comparison between the X-ray and radio data for these two elliptical galaxies is therefore feasible.

Our observation strategy required the mapping of both galaxies at two separate frequencies, in each case with ~4 arcsec resolution. This scheme entailed the use of two different VLA antennae configurations, which because of constraints imposed by the VLA operational cycle required the observations at different frequencies to be separated by several months. The 1465 MHz observations were performed between 1100 and 1400 LST on Jan 24 1984, with the full 27 antennae VLA in B-configuration. Both galaxies were observed in a sequence of 4x20 minute "snapshots" interleaved with observations of appropriate phase and flux calibrators. Standard celestial calibration sources were selected by the VLA staff. A basically similar strategy consisting of 2x40 minute snapshots for both galaxies was adopted for the 4885 MHz observations performed between 1000 and 1300 LST on May 9 1984.

Standard aperture synthesis techniques were employed to generate the high resolution radio maps of NGC 4636 and NGC 4649. Raw UV visibility data was corrected for known phase errors, differential zenith angle effects (eg. atmospheric absorption), and also the gain and polarization characteristics of the individual antennae. Conversion from calibrated UV data to synthesis map was accomplished

using standard FFT techniques. Positions and fluxes were determined for discrete sources identified in the synthesized data. The CLEAN algorithm (eg. Högbom 1974) was applied to sections of the data which appeared to contain complex sources or extended structure, in order to remove distortion caused by sidelobes and grating ring responses.

The resultant CLEANed 1.4 GHz and 5 GHz maps of NGC 4636 both have a resolution of 3.7x3.4 arcsec (RAxDEC, FWHM), whereas the NGC 4649 maps have a resolution of 3.7x3.9 arcsec. Absolute pointing uncertainties for CLEANed data are $\sim$0.2 arcsec at 1.4 GHz and $\sim$0.3 arcsec at 5 GHz. The largest scale structure which is theoretically fully visible in our CLEANed maps (ie. with no loss of flux) is 80 arcsec. Typical background RMS levels are $\sim$0.1 mJy/beam at both frequencies, resulting in dynamic ranges of between 50 and 200 for our VLA maps. We adopt a flux limit of $\sim$0.5 mJy as our criterion for the existence of an unresolved or slightly resolved radio source. Eight discrete sources have been identified in the synthesis maps of the NGC 4636 region; the brightest is clearly extended and located near the optical centre of the galaxy. In contrast, only one radio source is evident in the NGC 4649 synthesis maps; it too is extended and centrally located within the galaxy.

6.3.2 Discrete Radio Sources in the Vicinity of NGC 4636

The celestial coordinates and flux densities of the eight sources detected in either or both of the VLA maps of the NGC 4636 region are listed in Table 6.2. Source positions have also been superimposed schematically upon the relevant region of the PSS red plate (Figure 6.12). Sources 1, 7 and 8 lie outside the CLEANed region of the 1.4

Table 6.2 : Summary of Radio Observations of NGC 4636 and NGC 4649

NGC 4636

SOURCE	RA	DEC	FLUX (mJy)		SPECTRAL
			1465 MHz	4885 MHz	INDEX
1	$12^h40^m34.5^s$	2°57'30"	3	N.O.	?
2	12 40 22.54	2 58 21.5	N.D.	3.5	>+1.9
3 (a)	12 40 18.97	2 57 51.0	13.5	2.5	-1.41
(b)	12 40 19.10	2 57 44.5	3.6	1.0	-1.10
4 (extended)	12 40 16.68	2 57 41.4	59.3	27.3	-0.64
5	12 40 11.67	2 58 35.8	8.1	1.3	-1.50
6	12 40 7.53	2 56 47.1	6.4	N.O.	?
7	12 39 59.4	3 01 29	8	N.O.	?
8	12 39 54.1	3 00 23	16	N.O.	?

NGC 4649

SOURCE	RA	DEC	FLUX (mJy)		SPECTRAL
			1465 MHz	4885 MHz	INDEX
Core	$12^h41^m8.7^s$	11°49'34.5"	17.5	18.4	+0.04
Upper Lobe	12 41 9.2	11 49 43	2.7	1.3	-0.61
Lower Lobe	12 41 8.4	11 49 24	1.2	0.5	-0.7
Lower Lobe (Extension)	12 41 8.5	11 49 15	0.5	N.D.	?

Notes to Table 6.2

(1) Sources 1, 7 and 8 are outside the CLEANed region of the 1465 MHz map; their coordinates and fluxes are intrinsically less accurate than for the other sources.

(2) Sources 1, 6, 7 and 8 are outside the VLA FOV for the 4885 MHz observation (N.O. = Not Observed). Source 2, detected in the 4885 MHz observation, was inside the FOV of the 1465 MHz observation but not detected (N.D. in the flux column).

(3) Power Law index α, calculated assuming a continuous spectrum from 1465 MHz to 4885 MHz with the form $S_\nu \propto \nu^{\alpha}$.

(4) The coordinates of the extended lobe components of NGC 4649 and the extended source in NGC 4636 (source 4) are for the position of the centroid of emission.

Figure 6.12 (Plate)

Positions of discrete radio sources detected in the vicinity of NGC 4636 superimposed upon Palomar Sky Survey red plate. Details of positions and fluxes of radio sources are listed in Table 6.2. Plate scale is 7.7 arcsec/mm, thus 1 arcmin (or 4.2 kpc) corresponds to 7.8 mm.

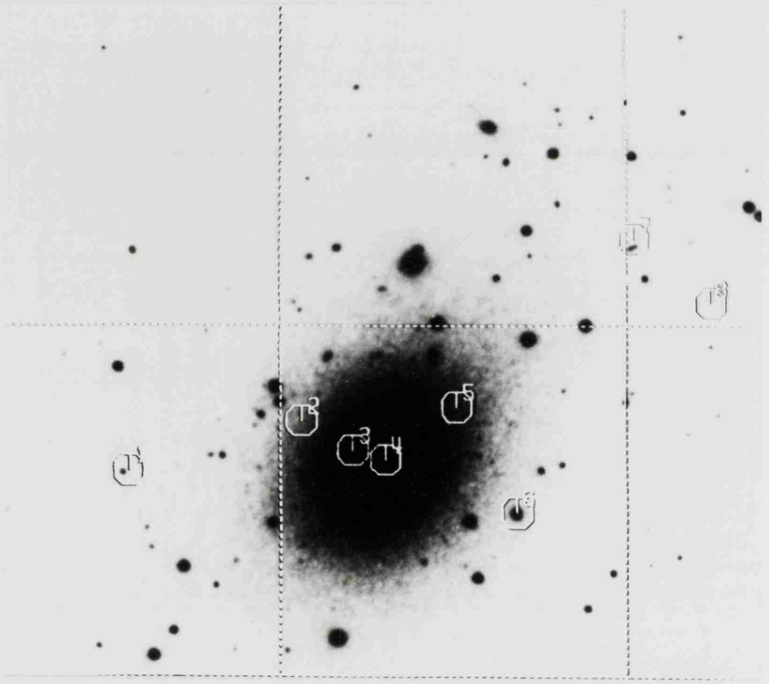

GHz map, hence their positions and fluxes are less accurate than those of the other sources. Unfortunately, sources 1 and 6-8 are beyond the limits of the 5 GHz synthsis map, so we are unable to even crudely determine their spectral parameters. Of the inner sources, 1 and 3-5 have been independently detected at both frequencies, but source 2 has only been detected at 5 GHz. Sources 1,2 and 5-8 are completely unresolved, whereas source 3 has a well defined double morphology which is consistent with two marginally resolved, point-like components. Source 4 is extended and exhibits a rather unusual morphology; we defer a detailed study of its properties to section 6.3.3.

Sources 1 and 6-8 are situated well beyond the optical bounds of NGC 4636 and are unlikely to be physically related to the galaxy. No X-ray counterparts are evident in either the IPC or HRI data, although examination of red and blue PSS plates (eg. Figure 6.12) reveals possible optical counterparts for sources 1, 6 and 7. The counterparts of sources 1 and 6 have a stellar appearance and are visible on both the red and blue plates; we estimate red magnitudes of $\sim 16.5^m$ and $\sim 13.5^m$ respectively. The counterpart of source 7 has a double morphology, possibly due to two components with magnitudes $\sim 18^m$ and $\sim 19^m$. Deep plates and accurate spectra are obviously required in order to confirm the validity of the optical identifications and establish the nature of these objects, but it seems plausible that they are radio powerful QSOs fortuitously located in roughly the same line of sight as NGC 4636. The background source density observed in the 1.4 GHz data is consistent with the Log N - Log S relationship at GHz frequencies (eg. Wall, Pearson and Longair 1981). It is therefore somewhat surprising that no background sources were detected in the

equivalent NGC 4649 map.

Although sources 2,3 and 5 appear to be situated within the optical light distribution of NGC 4636 (Figure 6.12), it is by no means certain that they are physically associated with the galaxy. Examination of available plate material fails to reveal obvious optical counterparts (eg. globular clusters), and analysis of the relevant regions of the HRI X-ray image yields a similarly negative result. Extrapolation of the log N - log S relationship for GHz frequencies to fluxes in the range 1-10 mJy leads to a prediction of roughly one background radio source within the optical bounds of NGC 4636 (eg. Wall, Pearson and Longair 1980, 1981; Wall et al. 1982). We therefore can not exclude the possibility that one or more of these radio sources are background objects. The 1.4-5 GHz spectral indices of sources 3 and 5 are relatively steep compared with typical QSOs and radio galaxies, which tend to have indices in the range -0.4 to -1.2 (eg. Kellerman et al. 1969). We are unable to rule out the background source hypothesis, since the derived spectral indices are subject to uncertainties due to possible luminosity fluctuations over the four month period between the 1.4 GHz and 5 GHz observations. The non-detection of source 2 during the 1.4 GHz observation implies either dramatic variability during this period or a strongly inverted spectrum (cf. QSO 4C 39.25, Kellermann 1974).

Alternatively, if these sources are members of the NGC 4636 system they have monochromatic radio luminosities in the range $L_{1.4} \sim 1\text{-}3 \times 10^{27}$ erg s^{-1} Hz^{-1}. This exceeds the luminosity of the galactic SNR CAS A by a factor of ~ 50. The SNR hypothesis should not be rejected on luminosity grounds alone, however, since considerably more luminous

examples probably exist, eg. the radio hotspot 41.9+58 in M82 (Kronberg and Wilkinson 1975). Ultra-luminous SNRs are to be expected in a galaxy rich in Population I objects and star formation activity, but are unlikely to occur in a relatively normal elliptical galaxy (unless the existence of such objects is favoured by the conditions prevailing in a cooling flow). In this context it is worth noting that in 1939 a supernova was observed in NGC 4636; its location (RA = $12^h\ 40^m\ 18^s$, DEC = 2° 58' 00") places it roughly 15 arcsec from radio source 3. The SNR hypothesis for sources 2, 3 and 5 can probably be rejected on the basis of their spectral indices, which under this hypothesis are quite well determined since SNRs do not vary in luminosity on timescales of months; SNRs generally have spectral indices in the range ~ -0.1 to -0.8, whereas sources 3 and 5 have considerably steeper spectral slopes. In conclusion, we believe it probable that sources 2, 3 and 5 are unrelated to NGC 4636. We therefore tentatively classify them as background objects, the exact nature of which can only be determined by detailed radio and optical studies.

6.3.3 Extended Radio Sources in NGC 4636 and NGC 4649

A detailed 1465 MHz map of the extended radio source which is situated near the centre of NGC 4636 is displayed in Figure 6.13. The contour levels correspond to 5, 10, 20, 35, 70 and 90% of the peak flux; the lowest level (0.57 mJy/beam) is ~5 x background RMS. We prefer to use the 1465 MHz data for display purposes because its dynamic range (~100) is a factor of two superior to that of the 4885 MHz data. The morphology and angular size of the source appears to be virtually identical at both frequencies, implying negligible spectral variation

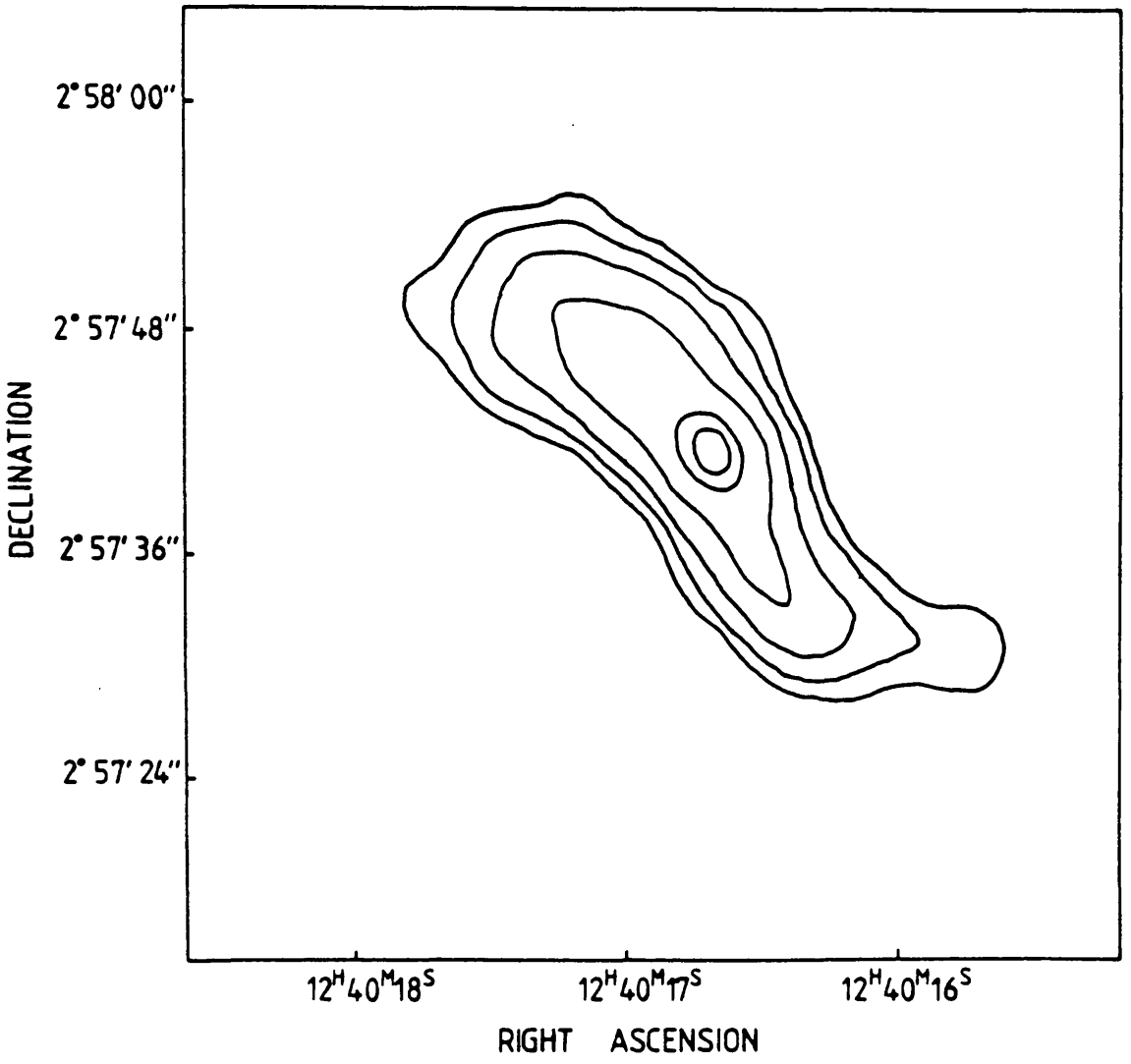

Figure 6.13 1.4 GHz VLA map of the extended radio source situated near the centre of NGC 4636. The lowest contour level corresponds to 5% of the peak surface brightness.

over the source; we derive $\alpha \sim -0.6$ for the 1.4 - 5 GHz frequency range. The source has approximate dimensions of 36 x 12 arcsec measured at the 5% surface brightness level, corresponding to a spatial scale of 2.5 x 0.8 kpc.

Extended radio structures have been observed in a number of elliptical galaxies (eg. Jenkins 1982), although they usually exhibit a fairly well defined core plus double lobe morphology. In contrast, NGC 4636 possesses a rather amorphous radio source which lacks any obvious nucleus but still displays a degree of collimation. Higher resolution radio observations may eventually reveal the existence of a central radio core, although it can only contribute a small proportion of the flux observed at GHz frequencies. Perhaps the most striking aspect of the morphology of the radio emission is the pronounced twist or curve along its major axis. If, as most authors agree, the extended radio structures associated with elliptical galaxies are due to beams of relativistic particles ejected from a central "engine", then precession of this engine (and hence the collimated beams) could be the cause of the twisted radio emission. Alternatively, differential pressure due to the ambient hot gas in the central region of NGC 4636 might cause the distortion (see also section 6.3.6).

The VLA observations of NGC 4649 have revealed the presence of an extended radio source located at the centre of the galaxy; unlike the NGC 4636 source it displays the classical morphology consisting of an unresolved core plus two collimated lobes of extended emission (Figure 6.14). The contour levels of the 1465 MHz map represent 2, 4, 8, 16, 32 and 64% of the peak surface brightness; the lowest

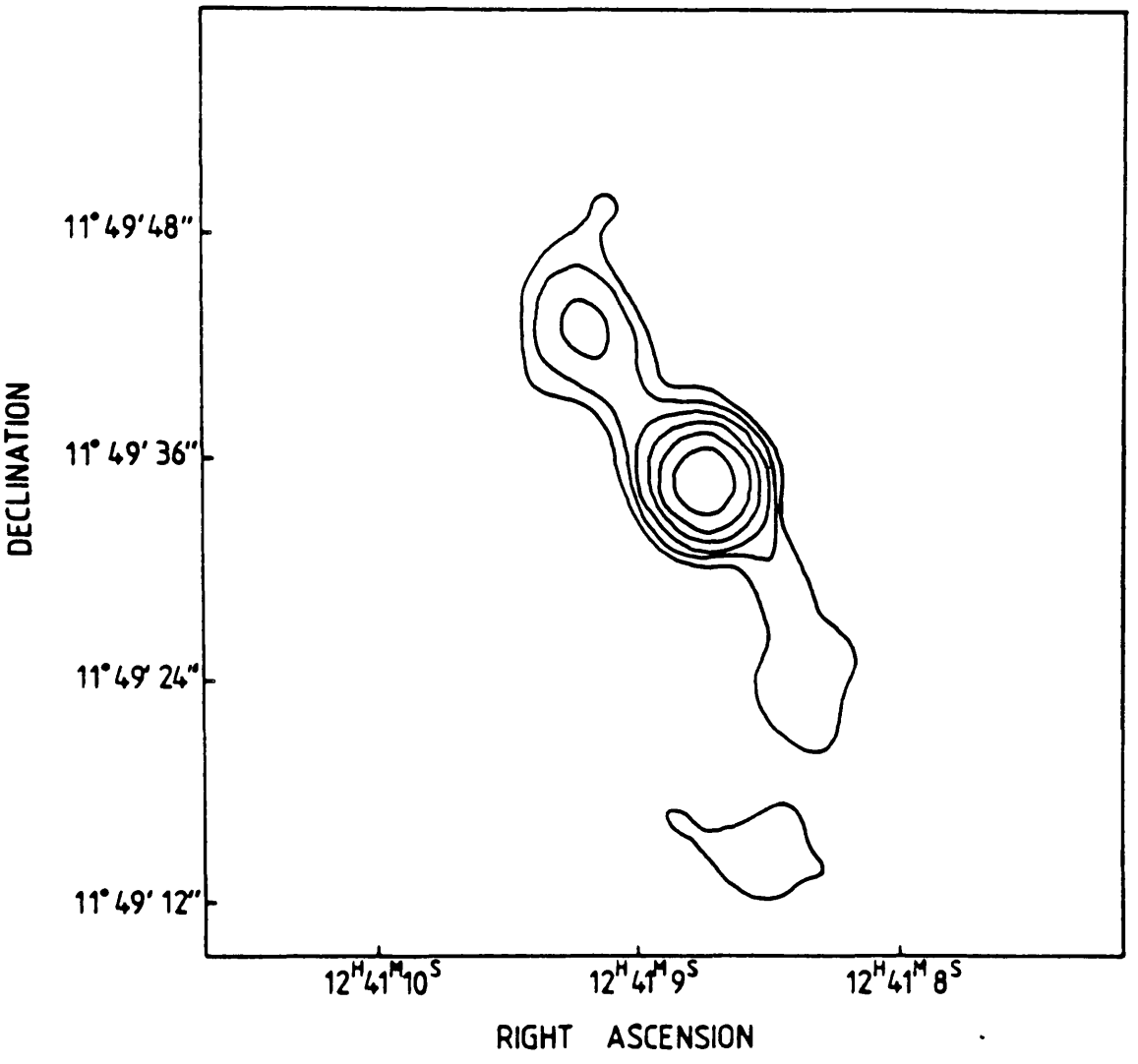

Figure 6.14 1.4 GHz VLA map of the extended radio source situated at the centre of NGC 4649. The lowest contour level corresponds to 2% of the peak surface brightness.

level corresponds to 0.35 mJy/beam, or ~4 x background RMS. Compared with the extended radio structure in NGC 4636, the radio lobes of NGC 4649 are relatively faint, contributing only ~20% of the total 1465 MHz flux from the source. Indeed, they are only marginally detectable in the 4885 MHz map, which implies $\alpha \sim -0.6$, essentially identical to the spectral index of the extended radio source in NGC 4636. Detailed analysis of the data at both frequencies demonstrates that the core component is completely unresolved; its very flat spectrum ($\alpha = +0.04$, inferred from observations separated by four months) is quite typical for such sources (eg. Jenkins 1982). Although the main radio lobe structure is roughly symmetric, the upper lobe is substantially more powerful. The lower lobe appears to have a faint, semi-detached extension, the location of which relative to the axis of symmetry again suggests precession of the particle beams ejected from the central engine, or perhaps distortion caused by differential pressure effects due to the ambient hot gas.

6.3.4 Relationships Between Central Radio Sources and Discrete X-ray Features

We have superimposed the radio contours displayed in Figures 6.13 and 6.14 upon the high resolution maps of the central X-ray emission regions of NGC 4636 and NGC 4649; the results are displayed in Figure 6.15. Although both the X-ray and radio data have virtually the same angular resolution (~4 arcsec), the dynamic range and absolute pointing accuracy of the radio data are superior. We estimate that the joint pointing uncertainty for the combined X-ray and radio maps is ~ 4 arcsec, or one resolution element.

The most noteworthy feature of the NGC 4636 map is that the

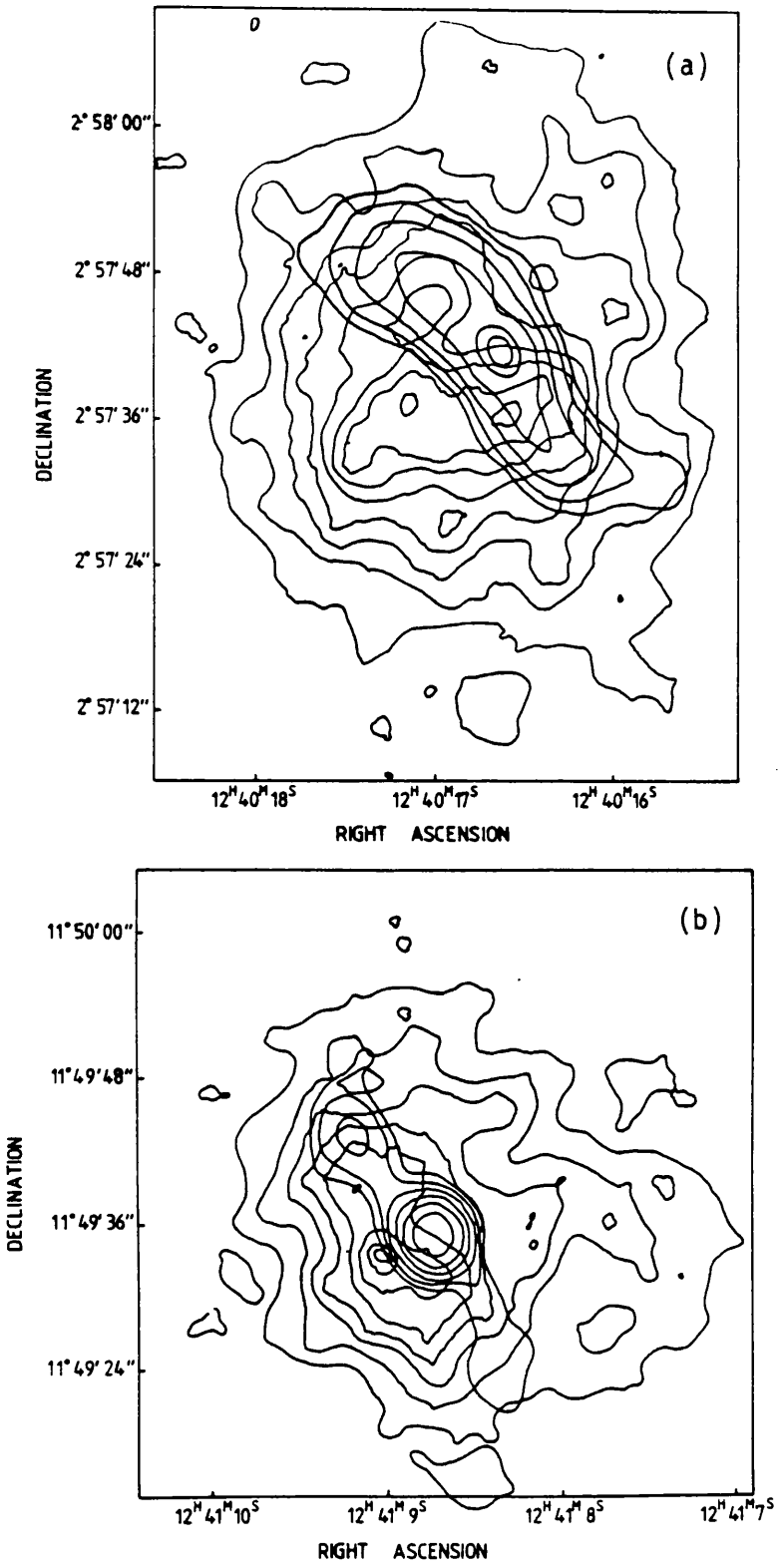

Figure 6.15 1.4 GHz VLA contours superimposed upon HRI maps of central regions of (a) NGC 4636 and (b) NGC 4649.

orientations of the elongated X-ray plateau and the extended radio structure are quite different, although their surface brightness distributions do partially overlap. Several local X-ray maxima are apparently located in the region of radio emission, although none are coincident with the peak of the radio surface brightness distribution (the nearest X-ray maxima is ~6 arcsec distant). It is conceivable that the spatial variations in gas density, indicated by the rather chaotic X-ray structure, are a consequence of local heating caused by the passage of beams of relativistic particles (ejected by the hypothetical central engine) through the ambient hot gas (eg. Tucker and Rosner 1983). The presumably complex dynamics of the hot gas in the central region of NGC 4636 may be partially responsible for the unusual morphology of the radio emission.

The angular separation between the unresolved radio core and the prominent X-ray peak (Source 1) in the central region of NGC 4649 is ~4.5 arcsec, marginally consistent with the two features being mutual counterparts (see Figure 6.15). It is entirely possible that we have found a very low luminosity, AGN-type nucleus located at the centre of this elliptical galaxy, although this is obviously not a unique interpretation of the data. Figure 6.15 clearly demonstrates that there is no direct correspondence between the morphology of the radio lobes and the spatial distribution of the X-ray emitting gas. Since the radio lobes of NGC 4649 are intrinsically less powerful than the extended radio structure in NGC 4636, we would predict that local heating of the ambient gas by relativistic particles would be less significant.

6.3.5 Cooling Flow Fueling of Radio Sources

Various authors have suggested that cooling flows are capable of fueling nuclear radio sources, both in individual galaxies (Bailey 1980, Nulsen et al. 1984) and in rich clusters of galaxies (Jones and Forman 1984, Stewart et al. 1984). Striking observational evidence for this conjecture is provided by the well defined correlation between radio luminosity and "excess" X-ray luminosity displayed by rich clusters thought to contain cooling flows in their core regions (Jones and Forman 1984). In Chapter Five we noted a similar tendency for radio sources to occur in gas-rich early type galaxies. For the purposes of discussion we will assume that NGC 4636 and NGC 4649 both contain cooling flows in their core regions; we further postulate that some of the cooled gas accretes onto a $\sim 10^8$ $M_\odot$ black hole. Nulsen et al. (1984) demonstrate that although the mass flux in a cooling flow is theoretically zero at the centre of a galaxy, the existence of a central point mass tends to suppress the thermal instabilities which remove matter from the flow (via star formation), thus allowing a finite mass flux onto the central object. These authors suggest that mass fluxes as high as 10^{-2} $M_\odot$ yr^{-1} are possible; this value is similar to the total cooling flow mass fluxes for the central ~ 1 kpc of NGC 4636 and NGC 4649 derived in section 6.2.4.

Assuming that roughly half of the central mass flux is removed by star formation, we envisage that the remaining $\sim 5\times10^{-3}$ $M_\odot$ yr^{-1} is deposited in an accretion disk around the black hole. We can estimate the total luminosity generated by the accretion process from $L \simeq \epsilon \dot{M} c^2$, where ϵ is the accretion efficiency. Although the details of the accretion process are poorly understood, it is obvious that even

relatively inefficient accretion can result in the generation of a high luminosity, eg. $\sim 3 \times 10^{42}$ erg s^{-1} for $\epsilon \sim 0.01$. Most of this output will be radiated from the accretion disk at optical and UV wavelengths, but some of the energy released by accretion will accelerate particles to relativistic velocities. Synchrotron emission from the resultant collimated particle beams gives rise to the extended radio structures observed in NGC 4636 and NGC 4649. The nature of the radio core in NGC 4649 is less clear, although the emission mechanism is also likely to be synchrotron radiation. Assuming that the spectral parameters listed in Table 6.2 are applicable over the entire 10^7-10^{10} Hz frequency range, we derive integrated radio luminosities of $\sim 1.1 \times 10^{38}$ erg s^{-1} and $\sim 6 \times 10^{37}$ erg s^{-1} for the central radio sources in NGC 4636 and NGC 4649 respectively. These luminosities are virtually negligible compared with the probable output from cooling flow - fueled accretion. The same argument also applies to the X-ray feature which may be a counterpart to the radio core in NGC 4649; its luminosity, $L_X \sim 3 \times 10^{39}$ erg s^{-1}, possibly generated by a synchrotron self-compton process, is a small fraction of the accretion output. Although the scenario we have considered is probably simplistic, it does appear that the fueling of radio sources by cooling accretion flows is a viable proposition.

6.3.6 Pressure Confinement of Extended Radio Sources

The extended radio sources in the central regions of NGC 4636 and NGC 4649 have linear dimensions of ~ 2 kpc and hence coexist with substantial quantities of hot gas (as well as the cool gas which probably fuels them). In Section 6.2.4 we derived a crude estimate of the thermal pressure of the X-ray emitting gas as a function of

radius for both galaxies. It is obviously of interest to determine whether the ambient gas exerts sufficient pressure to physically confine the radio sources.

In order to determine the energy density within the extended radio sources we have adopted the methodology of Willis et al. (1981). Using the measured flux densities and ~GHz frequency spectral indices, we have calculated integrated surface brightnesses for the extended radio features over the frequency range 10^7-10^{10} Hz (see Table 6.3). Assumption of equipartition conditions allows the derivation of the energy-minimizing magnetic field strength, which can be conveniently expressed as:

$$B_{min} \simeq [6\pi K' I_{int}(1+K)/L \sin|\psi|^{3/2}]^{2/7}$$ (Perley et al. 1979),

where I_{int} is the integrated surface brightness, L the path length through the source (assumed to be roughly the observed width of the feature), K is the ratio of proton and electron energies (assumed to be unity), K' is a constant, and ψ the angle between the line of sight and the magnetic field vector (generally assumed to be 90°). The internal energy density in particles and fields is given by $U_{min} = 7B^2_{min}/24\pi$. B_{min} and U_{min} for various regions of interest are listed in Table 6.3, as are our estimates for the local thermal pressure due to hot gas. Our estimates of U_{min} and $P_{thermal}$ are highly uncertain; the former because exact equipartition need not necessarily apply; the latter because T(r) falls rapidly within the core region of each galaxy and is in any case not well established for NGC 4649. It is clear, however, that the thermal pressure exerted by the hot gas in the central regions of NGC 4636 and NGC 4649 is more than sufficient to confine the observed extended radio structures. Indeed, similar

Table 6.3 : Energy Densities for Radio Components

Feature	Area (Sq. arcsec)	1.4 GHz Flux (mJy)	I_{int} (erg $cm^{-2}s^{-1}sterad^{-1}$)	B_{min} (gauss)	U_{min} (erg cm^{-3})	$P_{thermal}$ (erg cm^{-3})
NGC 4636 Extended Source	250	59.3	7.5×10^{-7}	1.2×10^{-5}	1.2×10^{-11}	$1\text{-}2\times10^{-10}$
NGC 4649 Radio Core	$\lesssim 3$	17.5	$\gtrsim 2.4\times10^{-5}$	$\sim 6\times10^{-5}$	$\sim 3\times10^{-10}$	1×10^{-10}
NGC 4649 Upper Lobe	60	2.7	1.4×10^{-7}	6.1×10^{-6}	3.5×10^{-12}	4×10^{-10}
NGC 4649 Lower Lobe	35	1.2	1.1×10^{-7}	6.1×10^{-6}	3.5×10^{-12}	5×10^{-10}
NGC 4649 Lower Lobe (Extension)	25	0.5	6.3×10^{-8}	7.7×10^{-6}	5.5×10^{-12}	3×10^{-10}

Notes to Table 6.3

(1) Area of radio components estimated from ~5% contour.

(2) Intensity of radio features (I_{int}) calculated using fluxes and spectral parameters listed in Table 6.2, integrated over full 10^7-10^{10} Hz frequency range.

(3) Derivation of B_{min} and U_{min} is detailed in the text. The values for the radio core of NGC 4649 are very uncertain, since the true angular size of the source is unknown; we have assumed a radius limit of ~1 arcsec.

(4) $P_{thermal}$ values have been calculated by estimating the radial distance of a particular feature from the centroid of the X-ray emission and reading off T(r) and $n_e(r)$ from Figures 6.7 and 6.9. The pressure values for NGC 4649 are highly uncertain since the temperature values are very poorly determined. Since the cooling flow model temperatures are probably unrealistically high for NGC 4649, the pressures listed in the table could be systematically too high by a factor of ~2.

features would be confined as far out as $r \sim 50$ arcsec (3.6 kpc), as Figure 6.11 indicates. A similar calculation for the unresolved radio core in NGC 4649, assuming a source size $\lesssim$ 1 arcsec, yields $U_{min} \sim 10^{-10}$ erg cm^{-3}, which is quite similar to the ambient gas pressure. None of the above analysis constitutes a proof that pressure confinement determines the size and morphology of the radio sources in NGC 4636 and NGC 4649, although the results are suggestive of it. Differential pressure effects due to the possibly complex dynamics of the ambient gas may give rise to the curved morphology exhibited by the NGC 4636 radio source, although this feature could equally well reflect the intrinsic properties of the particle beams ejected from the hypothetical central engine.

6.4 The Evolution of Cooling Flows

6.4.1 Star Formation and Supernova Heating

Our analysis of the HRI X-ray data has led us to conclude that cooling flows are present in the central regions of NGC 4636 and NGC 4649, and possibly throughout the whole stellar system of NGC 4636. If a steady cooling flow has existed in NGC 4636 for much of its lifetime, then an easily detectable quantity of cooled gas ($\gtrsim 10^9$ $M_\odot$) will have been deposited throughout the galaxy. Sensitive HI observations limit the current mass of neutral hydrogen to $\lesssim 3 \times 10^7$ $M_\odot$, and contributions from gas in other relatively cool phases are also negligible. The fueling of nuclear activity requires an almost negligible proportion of the "missing" gas, leaving star formation as the only viable alternative for a gas sink.

Many authors have noted that an elliptical galaxy, such as NGC 4636, which is undergoing continuous star formation with a normal (ie. solar

neighbourhood) initial mass function, would exhibit anomalously blue colours due to the relative over-abundance of high mass stars (eg. Faber and Gallagher 1976). NGC 4636 is not anomalously blue; its colours are quite typical for an E0 galaxy. Star formation initiated by the cooling flow must therefore occur with an IMF which is either very steep or suitably truncated at high stellar masses (eg. Sarazin and O'Connell 1983). Support for this scenario is provided by a consideration of the critical (Jeans) mass for the gravitational collapse of a non-rotating blob of cool gas. Spitzer (1978) derives $m_J \simeq 0.64\ (T_c/10K)^2 (P_c/10^7 k)^{-1/2}$, where T_c and P_c are the temperature and pressure of the cool gas. If the cool blob is in rough pressure equilibrium with the surrounding hot gas, then $P_c \simeq n_e kT \sim 10^6 k$, hence $m_J \sim 2\ M_o$. The exact relationship between m_J and the IMF of the subsequently formed stars is unknown, but stars with masses $\gtrsim 2\ M_o$ would not be expected to form in the central regions of NGC 4636 and NGC 4649.

The situation is more complicated than it initially appears to be. Nulsen et al. (1984) demonstrate that stellar mass loss injected into a cooling flow at radius r will decouple from the flow by the time it reaches radius $\sim r/2$. Star formation therefore occurs diffusely throughout the galaxy in question. At a distance of 5 kpc from the centre of NGC 4636 the thermal pressure exerted by the X-ray emitting gas is only $\sim 6 \times 10^4 k$, hence the Jeans mass increases to $\sim 8\ M_o$. Higher mass stars are likely to form preferentially in the outer regions of a cooling flow, if it extends throughout a galaxy. The total mass of stars generated as a consequence of a cooling flow in NGC 4636 during a Hubble time probably does not exceed a few percent of the galaxy's

visible mass, hence any radial colour gradient caused by the effects of a differential IMF would be difficult to detect.

Optical emission line regions have been observed in the nuclear regions of a number of elliptical galaxies, and have been interpreted as evidence for shocks associated with thermal instabilities occurring within a cooling flow (Nulsen et al. 1984). NGC 4636 is one such galaxy; a detailed examination of the spatial and velocity structure of the optical emission line region(s) should provide useful information relating to the properties of cooling flows, since the shocks which give rise to the line emission are linked to the thermal instabilities which initiate the star formation.

Since the cooling flow in NGC 4636 contributes very little to the galaxy's mass, it also contributes very little to the integrated supernova rate. The best available empirical estimates for elliptical galaxies predict supernova rates of $\sim 5\times10^{-3}$ yr^{-1} for NGC 4636 and $\sim 1.2\times10^{-2}$ yr^{-1} for NGC 4649 (Tammann 1982). Blair (1982) deduced a mean value for the energy released per supernova of $\sim 3\times10^{50}$ erg. On this basis we predict that $\sim 4.8\times10^{40}$ erg s^{-1} of supernova-induced heating is potentially available in NGC 4636, and $\sim 1.1\times10^{41}$ erg s^{-1} in NGC 4649, corresponding to ~30% and ~90% of their respective X-ray luminosities (ie. cooling rates). A quasi-steady cooling flow probably exists in NGC 4636, although heating may disrupt the outer regions (see section 6.2.2 and Figure 6.1). NGC 4649 is most unlikely to maintain a steady cooling flow, except in its dense core region. Our estimates of heating rates are, of course, dependent on the assumed supernova parameters, which are highly uncertain. The

efficiency with which energy released by a supernova is injected into, and transported through, a hot medium which is subject to radiative cooling, is also not well established.

6.4.2 Other Heating Processes

Supernova heating is not the only process capable of disrupting a cooling flow. Tucker and Rosner (1983) constructed a model of the hot gas surrounding M87 which incorporated non-thermal heating due to relativistic electrons (present in the radio lobes) and thermal conduction from the hotter outer parts of the halo. These authors find no need to invoke radiative accretion of the gas, and claim that conduction over a large scale tends to isothermalize the halo; conduction therefore suppresses the cooling flow process. Canizares et al. (1984) and Stewart et al. (1984) have criticized the conduction scenario of Tucker and Rosner, suggesting that plausible thermal conduction models are most unlikely to equilibriate with radiative cooling losses on large physical scales. If their views are confirmed it seems probable that thermal conduction scenarios are unlikely to apply to a cooling flow in NGC 4636.

Non-thermal heating by relativistic electrons may well occur in the central regions of elliptical galaxies which contain nuclear radio sources. The effects are likely to be local, resulting in chaotic structure in a cooling flow. In this context it is worth recalling the possible presence of local X-ray maxima within the region of extended radio emission in NGC 4636, perhaps indicating the heating of cooling flow material by relativistic electrons. Tucker and Rosner (1983) suggest that copious non-thermal heating could induce a cyclical flow: the central gas density increases until cooling is

dominant, whereupon an accretion flow is initiated causing the fueling of nuclear activity; ejected beams of relativistic particles suppress the flow via non-thermal heating, thus in turn switching off the nuclear activity and eventually allowing the cooling flow to recur. The extended radio emission in NGC 4636 and NGC 4649 is probably too weak for non-thermal heating due to the associated relativistic particles to be globally important.

6.5 Conclusions

We have performed the first detailed investigation of the X-ray and radio properties of two giant elliptical galaxies: NGC 4636 and NGC 4649. High resolution X-ray (HRI) and radio (VLA) maps have been analysed; deprojection of the former has enabled the determination of the radial dependence of gas parameters, which in turn has allowed us to examine the physics of fueling and confining the observed central radio sources. All the available data are consistent with the occurrence of a quasi-steady cooling flow throughout NGC 4636, although supernova heating may well disrupt the flow in the outer regions of the galaxy. A cooling flow is unlikely to occur outside the core region of NGC 4649. The cooling flow interpretation is not unique, however, and requires confirmation by sensitive observations in all wavebands.

CHAPTER SEVEN : GENERAL CONCLUSIONS AND FUTURE PROSPECTS

7.1 Introduction

In this final chapter our primary objective is to place the major results presented in Chapters Three to Six in an appropriate general context, thus allowing us to delineate the scope for further observational work using both currently available and proposed astronomical facilities. Our principal conclusions regarding the X-ray properties of M82 and early type galaxies are reiterated in terms of their wider implications for the general properties of all galaxies in section 7.2; this leads to a discussion about the possible priorities and requirements for future X-ray observation programmes. Section 7.3 is devoted to a detailed examination of the capabilities of present and future X-ray observatories, including EXOSAT, ROSAT and AXAF; we also assess their likely impact on galaxy research. Finally, in section 7.4 we outline the scope for complementary observations in other wavebands, with particular emphasis on the possibilities presented by "state of the art" facilities such as IRAS, VLA and Space Telescope.

7.2 Basic Results: A General Context and Implications for Further Research

The fundamental theme which unifies all of the research presented in this thesis is that the X-ray properties of a galaxy which does not display AGN characteristics are linked, both directly and indirectly, to the properties and evolution of its stellar population(s) and associated diffuse matter. In a seminal work, Vaiana et al. (1981) reported the results of an extensive stellar X-ray survey; their

findings clearly demonstrate that main sequence stars constitute a pervasive class of low luminosity X-ray sources. A characteristic stellar population therefore contributes directly to the X-ray luminosity of its parent galaxy. Examples drawn from our work include giant associations of O-B stars in the nuclear region of M82, each cluster of $\sim 10^5$ stars contributing roughly 10^{38} erg s^{-1} to the X-ray luminosity of the galaxy, and the enormous populations of low-mass dwarf stars which are the basic constituents of early type galaxies; a 10^{11} $M_\odot$ elliptical galaxy generating as much as $\sim 10^{38.5}$ erg s^{-1} of X-ray emission from its main sequence stellar component alone. Furthermore, at any stage of the evolution of a particular stellar population there will exist a characteristic set of evolved objects, namely SNRs and X-ray binary systems, which although rare are considerably more X-ray luminous than individual main sequence stars. Several of the X-ray sources we detected in the nuclear region of M82 are probably high-mass X-ray binaries; their soft X-ray luminosities exceed $\sim 10^{38.5}$ erg s^{-1}, thus each individual system contributes $\sim 1\%$ of M82's X-ray luminosity.

Obviously, the X-ray luminosity of any galaxy is at minimum the sum of the contributions from its populations of main sequence stars and associated evolved objects. In Chapter Five we derived a crude estimate of the minimum X-ray luminosity for a typical early type galaxy: L_X (0.5-3.0 keV) $\simeq 3 \times 10^{-5} L_V$. Although this empirical relationship accurately describes the lower bound of the luminosity function for our sample of early type galaxies, it does not necessarily apply to other classes of galaxies. For example, spiral galaxies exhibit several distinct stellar populations, each with a

different characteristic age, mass function and chemical composition. The bulge population is essentially similar to the stellar population of an early type galaxy and therefore probably follows the same stellar X-ray luminosity function, whereas the younger populations associated with the disk and spiral arm regions will have completely different luminosity functions.

Although stellar X-ray emission is obviously a property common to all galaxies, we have nevertheless identified several cases where its overall contribution to the integrated X-ray luminosity of a galaxy is relatively unimportant. Thermal emission from hot, tenuous gas (eg. $T \sim 10^7$ K, $\langle n_e \rangle \sim 10^{-2}$ cm^{-3}) provides the dominant contribution to the X-ray luminosities of many normal early type galaxies; NGC 4636 being the most notable example. The same mechanism is also responsible for the X-ray emission from the halo region of the starburst galaxy M82. Despite displaying similar physical properties, the hot gas distributions associated with M82 and NGC 4636 do not share a common origin and are subject to radically different evolutionary processes. Intense star formation activity in the nuclear region of M82 has given rise to an exceptionally high integrated supernova rate, and consequently a mass outflow along the minor axis of the galaxy. The passage of supernovae shocks outward through the inner region of the halo causes the shock-heating of ambient gas to X-ray emitting temperatures. The energy input into the halo gas from supernova heating greatly exceeds losses from radiative cooling, thus the bulk of the hot gas escapes from the galaxy before it can cool significantly. NGC 253 is another example of a nearby galaxy undergoing a violent burst of star formation; it likewise exhibits a

region of shock-heated, X-ray emitting gas (Fabbiano and Trinchieri 1984). In contrast, the hot gas observed in early type galaxies is directly linked to normal stellar evolution. Gas ejected from low mass stars at late evolutionary phases is collisionally heated to a temperature consistent with the random stellar motion within the galaxy ($T \sim 10^6 - 10^7$ K). Further heating by supernovae may result in the expulsion of the gas from the system as a continuous hot wind, in which case the X-ray luminosity of the galaxy is simply comprised of contributions from stellar X-ray sources. Many galaxies do retain substantial quantities of hot gas, possibly due to gravitational confinement by extensive dark haloes, and in such cases the balance between supernova heating and radiative cooling appears to be quite close. NGC 4636 is an example of an early type galaxy where cooling processes are probably dominant; the hot gas becomes incorporated into a radiatively driven cooling flow, and the cooled gas deposited by the flow initiates low mass star formation throughout the galaxy and fuels weak activity in its nuclear region.

Do other classes of galaxies also generate the bulk of their X-ray luminosity via thermal emission from hot gas? This is certainly a valid question since all galaxies generate gas as a consequence of stellar evolution, and late type species have retained a substantial quantity of primordial matter, so far unused in star formation. Fabbiano et al. (1984) examined the global properties of a sample of 14 nearby spiral galaxies and concluded that, with the exception of systems undergoing starbursts, their X-ray emission properties are consistent with contributions from stellar sources only. High resolution observations have also failed to reveal any diffuse X-ray

emission which could be associated with presence of substantial quantities of hot gas in spiral galaxies (eg. M100, Palumbo et al., 1981). Although spiral galaxies have significantly higher integrated supernova rates than early type galaxies of similar optical luminosity, the extra energy released is dissipated within their extensive, relatively cool interstellar material. Only if the supernova rate is exceptionally high, as in the starburst galaxies M82 and NGC 253, does shock-heating become important and substantial quantities of gas are heated to X-ray emitting temperatures.

Einstein observed approximately two hundred normal or weakly active galaxies. This constitutes a rather small sample - particularly since a significant fraction of the galaxies were not detected - and certainly restricts our ability to perform detailed studies of the dependence of X-ray luminosity on optical luminosity, galaxy morphology or stellar population characteristics. Widely based studies of this nature require large, unbiased galaxy samples. There is an obvious observational requirement for an all-sky survey at a source detection sensitivity similar to that achieved by Einstein for individual pointings. The data base generated by such a survey would yield X-ray detections for upwards of a thousand normal and weakly active (non-AGN) galaxies, thus allowing the compilation of complete, X-ray flux limited samples of galaxies. A large number of scientifically valid research programmes can be envisaged; two with particular relevance to the work presented in this thesis are outlined below.

(1) Starburst Galaxies. Late type systems undergoing intense bursts of star formation generate copious quantities of radio, IR and X-ray

emission. An all-sky X-ray survey at Einstein sensitivity levels would detect starburst galaxies with X-ray properties similar to M82 out to a distance of ~50 Mpc, thus allowing a reasonably large sample of X-ray detected starburst systems to be established. A study of the correlation between X-ray and radio luminosities should prove particularly illuminating, since both are at least partially linked to the supernovae generated by the bursts of star formation. (In M82 the outflow of hot, X-ray emitting gas is maintained by supernova heating, and young SNRs are responsible for the bulk of the nuclear region radio emission.) IRAS has detected a large number of IR-excess galaxies, many of which appear to be undergoing intense star-formation activity. Analysis of a joint X-ray - IR luminosity function should provide further information relating to the properties and physics of starbursts.

(2) Early Type Galaxies. The type of X-ray survey we have envisaged would detect NGC 4636 at a distance of ~100 Mpc, we can therefore expect to construct an X-ray selected sample of several hundred early type galaxies. Derivation of a trivariate X-ray - optical - radio luminosity function for early type galaxies in general, and elliptical and lenticular species separately, should allow us to perform a detailed study of their hot gas content, and its relationship to the degree of clustering experienced by these systems. Furthermore, a detailed analysis of the luminosity function should enable the identification of those galaxies where cooling flows are fueling nuclear radio sources. Confirmation of the existence of cooling flows within individual galaxies will provide important constraints for the properties and evolution of the parent stellar populations (eg.

stellar mass loss rates, supernova rates and low mass star formation).

The richness of information that can be derived from the analysis of high resolution X-ray observations of individual galaxies has been amply demonstrated in Chapters Three and Six of this thesis. There is considerable scope for further morphological studies of normal and weakly active galaxies, since the total number of such objects observed by the Einstein HRI was rather small (about 30). Perhaps the most important use of high resolution observations is to identify and map regions of hot gas associated with individual galaxies. It is important to stress that a detailed determination of the properties and evolutionary state of the gas can only be accomplished by the analysis of imaging X-ray data which possesses both high angular resolution and good spectral discrimination. Spectrally resolved X-ray maps are undoubtedly the key to understanding the detailed balance between heating and cooling processes in gas-rich galaxies, whether the gas is outflowing as in the halo region of M82, or static or inflowing as in early type galaxies.

7.3 The Observational Capabilities of Current and Proposed X-ray Astronomy Facilities

7.3.1 General Comments

When the complete data base of Einstein observations finally becomes available in late 1985 there will be considerable scope for further research along lines similar to the work presented in this thesis. One of the principal aims of this concluding chapter is to help stimulate new investigations into the characteristic X-ray properties of galaxies; with this in mind we will examine the observational

capabilities of current and "next-generation" X-ray astronomy facilities, and the new research possibilities which may consequently arise. The detailed study of the X-ray properties of galaxies certainly requires the analysis of high sensitivity X-ray image data, thus we will exclude from this discussion those X-ray astronomy satellites which do not include imaging instrumentation (eg. Tenma, Astro-C). EXOSAT is the only currently operational satellite which incorporates an imaging X-ray telescope in its payload. ROSAT and AXAF are dedicated X-ray imaging missions planned for launch in 1987 and 1992 respectively.

The fundamental observational capabilities of the various imaging X-ray instruments which will be available to the astronomy community during the next ten years are summarized in Table 7.1. Detection sensitivities should be used with caution, since the various instruments operate in different energy bands; and furthermore the designs for the ROSAT and AXAF instrumentation are not yet completely finalized. Sensitivity values have been calculated in terms of equivalent Uhuru count rates for an X-ray source which exhibits a power law spectrum with photon index ~2.0 and negligible low energy absorption (ie. located at high galactic latitude). A 1.0 Uhuru ct s^{-1} source yields energy fluxes of 5.6×10^{-11} erg cm^{-2} s^{-1} in the 0.1-2.0 keV band, 3.0×10^{-11} erg cm^{-2} s^{-1} in the 0.5-3.0 keV band and 2.4×10^{-11} erg cm^{-2} s^{-1} in the 2.0-10.0 keV band, for the adopted spectrum. Sensitivities for pointed observations have been calculated assuming a 3×10^{4} sec exposure time, whereas sensitivities for the sky surveys are based on the estimated mean on-source time. The enormous improvement in detection sensitivity achieved by ROSAT and AXAF relative to their

Table 7.1 - Relative Performance of X-ray Instrumentation

Satellite	Instrument	Generic Type	FOV Diameter	Angular Resolution	Energy Range keV	Energy Resolution $E/\Delta E$	Flux Sensitivity (5σ, Uhuru ct s^{-1})
UHURU [1]	PC	Collimated Proportional Counter (Non Imaging)	10°x10° 1°x10° (collimated)	0.5°	2 - 6	-	1 (Survey)
EINSTEIN [2]	IPC	Imaging Proportional Counter	1°	60"	0.2 - 4.5	1 (at 1 keV)	$3x10^{-3}$
	HRI	Microchannel Plate Detector	24'	4"	0.1 - 3.0	-	$4x10^{-3}$
EXOSAT [3]	CMA	Microchannel Plate	2.2°	18"	0.04 - 2.0	3 Filter Photometry	$2x10^{-2}$
ROSAT [4]	PSPC	Imaging Proportional Counter	2°	60" (Survey)	0.1 - 2.0	2 (at 1 keV)	$7x10^{-3}$ (Survey)
	"	"	"	30" (Pointed)	"	"	$7x10^{-4}$ (Pointed)
	HRI	Microchannel Plate Detector	36'	5"	0.1 - 2.0	-	$1-2x10^{-3}$
AXAF [5,6,7]	IPC	Imaging Proportional Counter	1°	<10"	0.1 - 10.0	5 (at 6 keV)	$<1x10^{-4}$
	HRC	Microchannel Plate Detector	32'	0.5"	0.1 - 8.0	1 (at 1 keV)	$3x10^{-5}$
	HRIS	CCD	12'	0.5"	0.5 - 8.0	10 (at 1 keV)	$3x10^{-5}$

References

1 Giacconi et al. (1977) 2 Giacconi et al. (1979a) 3 ESA (1982) 4 Trumper (1982)
5 Zombeck (1982) 6 (Schwartz et al. (1984) 7 Murray et al. (1984)

predecessors (Uhuru and Einstein) is readily apparent from Table 7.1 and the sensitivity curves displayed in Figure 7.1. For example, a deep AXAF observation will detect X-ray sources with fluxes below 10^{-15} erg cm^{-2} s^{-1} (2-10 keV), which corresponds to the X-ray luminosity of our own galaxy viewed from a distance of 130 Mpc.

7.3.2 EXOSAT

Although EXOSAT has contributed to advances in many areas of observational X-ray astronomy, most notably in the field of variability studies of X-ray binary systems, it is not well suited to determining the properties of faint extragalactic objects. Launched in May 1983, EXOSAT includes in its complement of instruments two low energy imaging telescopes, each equipped with a position sensitive detector (PSD, roughly equivalent to the Einstein IPC) and a charge multiplier array (CMA, a micro-channel plate device broadly similar to the Einstein HRI). Both PSDs and one CMA failed during the early stages of the mission. The remaining CMA has a detection sensitivity roughly a factor of six worse than the Einstein IPC or HRI, and an angular resolution intermediate between the two. Use of various filters allows a very modest degree of spectral discrimination in the 0.04-2.0 keV band.

The relative insensitivity of the EXOSAT CMA is such that observations of normal galaxies are of rather limited value, unless they have not previously been observed by Einstein. Even a relatively bright extragalactic object like M82 yields a rather low count rate, ie. $\sim 10^{-2}$ CMA ct s^{-1} (Biermann 1984, private communication), and thus requires an extremely long observation, ie. $\gtrsim 10^5$ secs, if scientifically useful data is to be obtained. It is obvious that the

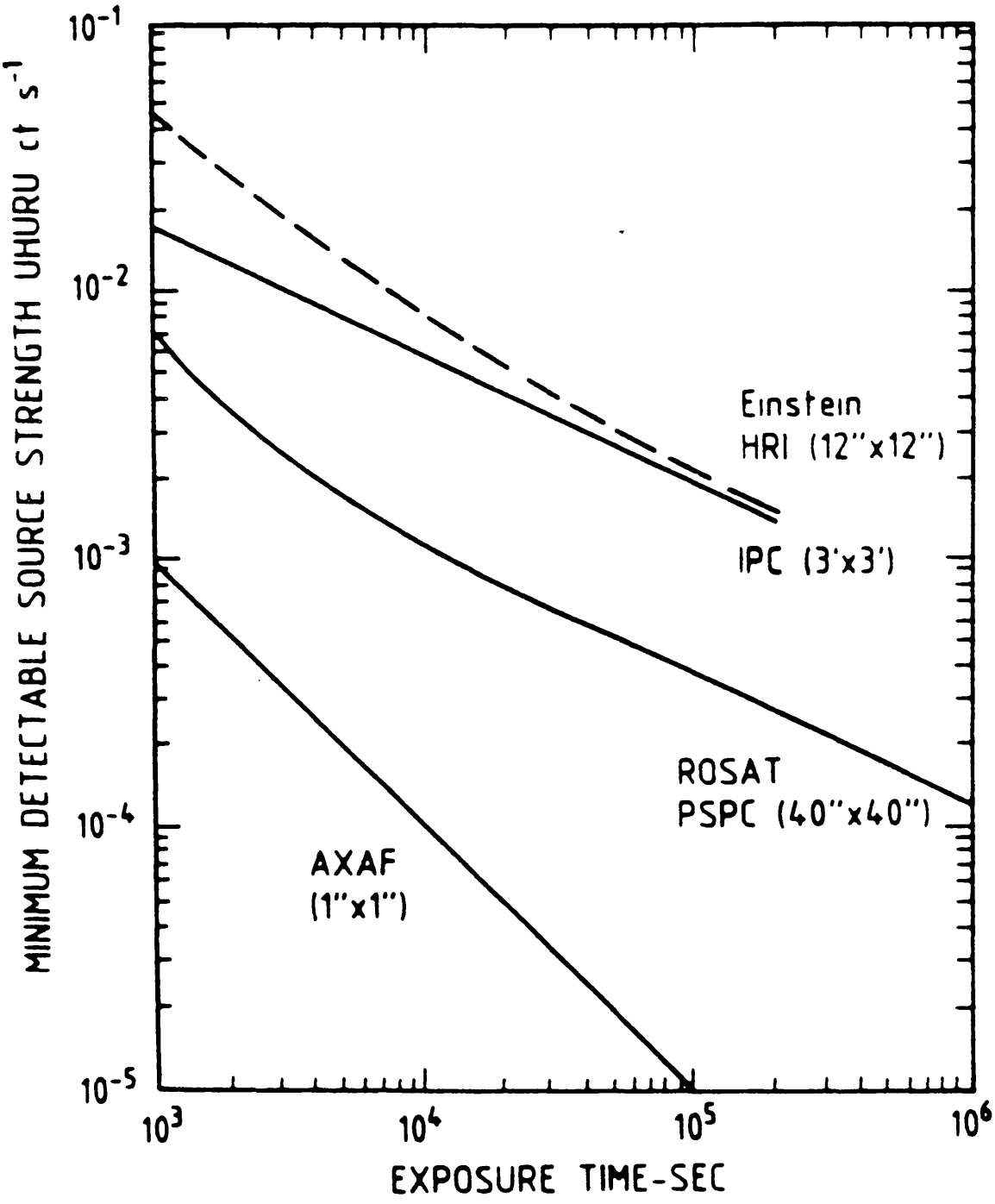

Figure 7.1 The relative sensitivities of Einstein, ROSAT and AXAF for the detection of point sources as a function of observing time. Detection cell dimensions are indicated.

number of galaxies for which detailed studies can be performed is very small. Extensive surveys of faint extragalactic X-ray sources are clearly not a cost-effective use of EXOSAT observing time.

7.3.3 ROSAT

A project instigated by West Germany, the ROSAT X-ray astronomy satellite is scheduled for launch in 1987. The primary scientific objective of the mission is to perform the first all-sky survey by means of an imaging X-ray telescope. It is anticipated that the 100-fold improvement in sensitivity relative to previous surveys will result in the detection of $\sim 10^5$ extragalactic X-ray sources, each with an absolute positional uncertainty of $\lesssim 1$ arcminute. After the six month survey phase is complete, pointed observations of selected sources will be performed.

The ROSAT telescope assembly consists of a four-nested, Wolter type-I mirror system with three focal plane instruments: two position sensitive proportional counters (PSPC), one of which will be the dedicated survey phase instrument, and a high resolution imager. Both types of imaging detector will operate in the 0.1-2.0 keV energy band, which is softer than the Einstein band and thus more susceptible to the influence of galactic absorption. In virtually all other respects the ROSAT instruments are superior to their Einstein counterparts. The angular resolution and spectral discrimination of the PSPC both display a factor of two improvement relative to the Einstein IPC, and for deep pointed-phase observations the PSPC is four times more sensitive. During the survey phase of the ROSAT mission potential X-ray sources will be in the FOV of the PSPC for $\sim 10^3$ secs of integrated

exposure time; sources as faint as $\sim 7 \times 10^{-3}$ Uhuru ct s^{-1} will be detected, similar to the limit achieved by a 6×10^{3} sec Einstein IPC observation. The angular resolution of the ROSAT HRI is limited by mirror design constraints to $\sim$5 arcsec (FWHM), slightly inferior to its Einstein counterpart, but this is compensated by the fact that the ROSAT instrument is at least a factor of two more sensitive. This improvement is due to the higher collecting area of the ROSAT mirror; an additional two-fold sensitivity enhancement becomes feasible if the front plate of the HRI is coated with caesium iodide instead of the traditional magnesium fluoride photocathode (Pounds 1984, private communication).

The desirability of performing a sensitive all-sky X-ray survey is obvious, and we have already noted some of the benefits for galaxy research in section 7.2. Such a survey should result in the detection of at least 10^{3} non-AGN galaxies, sufficient to establish well defined samples for detailed statistical studies. Pointed phase observations will also prove valuable. The PSPC has sufficient angular and spectral resolution to discriminate the X-ray halo of M82 from the nuclear emission, thus enabling the first reliable determination of the global temperature of the halo gas. Although not offering an improvement in angular resolution, the ROSAT HRI will generate a considerably more sensitive map of the halo region than its Einstein counterpart, and will also detect intrinsically less luminous sources in the nuclear region of M82. PSPC observations of high L_X early type galaxies (eg. M86 and NGC 4636) will enable a crude determination of the radial temperature profiles for the hot gas contained within these systems. HRI observations of similar galaxies not observed with the

Einstein instrument would also be valuable, since we could then assess whether the asymmetric and sharply peaked gas distribution exhibited by NGC 4636 is a common feature of gas-rich early type galaxies. The above examples have been highlighted because they are directly linked to the work presented in this thesis, but it is clear that ROSAT data will provide an immensely useful tool for all types of galaxy research.

7.3.4 AXAF

The NASA funded AXAF mission is due to be launched during 1992, and for a period of at least ten years will provide an observational facility capable of sub-arcsec imaging in the 0.1-10.0 keV band. AXAF will utilize a six-nested, Wolter type-I X-ray mirror system and a focal plane assembly which may comprise of as many as six instruments. Although the exact complement of instruments and their performance characteristics are not finalized as of late 1984, they are certain to encompass high angular resolution imaging, high resolution spectroscopy (dispersive and non-dispersive) and polarimetry. We have listed plausible candidates for AXAF imaging instruments in Table 7.1.

The IPC is likely to be a much upgraded version of the instrument flown on Einstein, achieving better than 10 arcsec resolution over the entire AXAF field of view (1° diameter) and moderate energy resolution ($E/\Delta E \sim 5$ at 6 keV) over the full 0.1-10.0 keV AXAF energy band. The high resolution camera (HRC) is generically similar to the Einstein HRI, but will attain a mirror-limited angular resolution of 0.5 arcsec within 5 arcmin of the telescope axis. Use of a CsI photocathode ensures a very high quantum efficiency throughout the 0.1-8.0 keV band, and enables the instrument to be used in a configuration which

yields a modest degree of energy resolution ($E/\Delta E \sim 1$). The high resolution imaging spectrometer (HRIS) is, as its name implies, a qualitatively new X-ray instrument. Based on CCD technology, the HRIS should achieve mirror-limited angular resolution (0.5 arcsec) within its 14x10 arcmin FOV. Energy resolution will be $\sim \pm 0.1$ keV throughout the instrument's 0.5-8.0 keV energy range, sufficient to distinguish individual emission lines within the iron line complex at 6-7 keV. Sensitivity estimates for all three instruments are rather crude, since they are based on the relatively limited information which is currently available. The values listed in Table 7.1 may well prove to be rather conservative.

With such a powerful array of instrumentation available, the demand for AXAF observing time is likely to be very heavy, consequently extensive surveys are likely to be rejected as too costly unless the class of object in question has not previously been satisfactorily observed. Observing time constraints will ensure the need for very careful selection of candidate objects for detailed AXAF studies, and in this respect the ROSAT survey results will prove invaluable. Although there are obviously a large number of scientifically valid observation programs which we could consider, we will limit this discussion to projects which are relevant to the work presented in this thesis.

A generous quantity of AXAF observing time is certain to be allocated to M82. HRC and HRIS observations will resolve the nuclear region into several hundred discrete sources; objects with X-ray luminosities as low as $\sim 10^{36}$ erg s^{-1} will be detectable, and spectral and temporal

properties will be determined for many of the brighter sources. Individual SNRs should be resolved (0.5 arcsec corresponds to $\sim$8 pc), and the total number observed will provide an estimate of the current supernova rate in the nuclear region, thus constraining the properties of the starburst. HRIS observations should also enable the derivation of the temperature and density structure of the hot gas in the halo region of M82; its energy budget, relationship to the Hα filaments and links with the nuclear region activity can then be investigated in detail. Other starburst galaxies, particularly those identified in the IRAS and ROSAT surveys, would also be excellent candidates for AXAF observations.

AXAF observations of early type galaxies will allow a number of outstanding problems to be addressed. Individual X-ray sources with $L_X \gtrsim 10^{37}$ erg s^{-1} will be detectable in early type galaxies located in the Virgo Cluster, hence the high L_X region of the X-ray source luminosity distribution can be examined in detail and compared with the equivalent distribution for spiral galaxies. IPC, HRC and HRIS observations of gas-rich galaxies like M86 and NGC 4636 will enable the derivation of detailed gas temperature and density profiles, thus allowing the following problems to be addressed: (1) Do gas-rich early type galaxies contain relatively cool gas in their core regions? The presence of a central temperature inversion would imply the existence of a steady cooling flow. (2) Is the ambient hot gas in NGC 4636 (and similar galaxies) gravitationally confined by a massive dark halo? Evidence for this hypothesis will come from a detailed measurement of the properties of any hot gas which is situated beyond the stellar component of the parent galaxy. It should, in principle,

be possible to measure the mass of a dark halo, which when combined with data about the frequency with which the phenomenon occurs may provide information relating to the properties of the universe as a whole (eg. the missing mass problem, mean density of the gravitating matter in the universe).

7.4 Future Observations in Other Wavebands

Sensitive observations at all available wavelengths are essential if we are to successfully interpret AXAF and ROSAT results. Countless worthwhile observation programs could be proposed, but here we will restrict our attention to a few possibilities arising from the use of current or near-future observational facilities, and which complement the X-ray studies of galaxies suggested in sections 7.2 and 7.3.

The Very Large Array is the most sensitive radio astronomy facility available to the general community. Observations can be performed at four frequencies and in four different array configurations, thus allowing discrete sources and extended structures to be studied over a wide range of angular scales. In Chapter Six we presented high resolution VLA maps of NGC 4636 and NGC 4649; both of these giant elliptical galaxies exhibit extended radio structures with scale sizes of about 2 kpc. Our observations achieved a sensitivity of $\sim$0.5 mJy/beam and a resolution of $\sim$ 4 arcsec, considerably superior to the $\sim$10 mJy/beam sensitivity and $\sim$30 arcsec resolution of typical surveys published to date (eg. Hummel et al. 1983). We therefore suggest that an extensive survey of early type galaxies with the VLA would produce results which could be usefully compared with the X-ray data from the ROSAT survey. In particular, it would allow us to investigate the possibility that the weak, jet-like radio structures

in early type galaxies are fueled by cooling flows and interact with the ambient hot gas, in a considerably more general manner than we could accomplish in Chapter Six. We also note that similar surveys of spiral and irregular galaxies are an efficient means of identifying starburst galaxies with characteristics similar to M82.

Although the IRAS satellite is now defunct, during the course of its eleven month mission it completed the first high sensitivity all-sky survey at far-IR wavelengths (λ = 10-100μ). The IRAS database will soon be available to the general astronomical community, and its impact upon galaxy research is certain to be significant. Early results are beginning to appear in the literature (eg. De Jong et al. 1984), and for example indicate that morphologically normal elliptical galaxies do not emit detectably in the far-IR band, presumably due to the absence of significant quantities of dust. There are, however, examples of HI-rich elliptical galaxies which <u>are</u> 10μ IR sources and are also strong radio sources (eg. NGC 1052, Rieke and Low 1972). Do other examples exist, and are they rich in dust? This question is particularly interesting in relation to NGC 1052, since this elliptical galaxy probably contains a substantial quantity of hot gas (see Chapter Five), which would tend to destroy the dust by sputtering. M82 and other starburst galaxies emit copiously in the IR band ($L_{IR} \sim 10^{44}$ erg s^{-1} for M82), thus a detailed analysis of the IRAS data for these galaxies should provide a great deal of useful information about the properties of their hyperactive bursts of star formation.

Perhaps the most striking advance in observational capability during

the next decade will occur at optical wavelengths; we are, of course, referring to the Space Telescope, expected to be operational in the late 1980's. The ~0.1 arcsec angular resolution and enormous improvement in sensitivity relative to ground based instruments should allow detailed studies of the properties of all types of stellar population to be performed. A detailed knowledge of the properties and evolution of the basic stellar population(s) and associated diffuse matter is essential if the X-ray properties of a normal galaxy are to be successfully interpreted. Another potentially important ST observation program is the study of the dynamics of the extensive families of globular clusters which surround several of the giant elliptical galaxies in the Virgo Cluster. Such studies may provide an independent estimate of the mass and physical size of a typical dark halo, if these systems do indeed exist, and thus a useful comparison with the results from X-ray studies of the confined hot gas. Perhaps the most fundamental project for ST will be observations of Cepheid variables in Virgo Cluster galaxies. The results should yield the first unambiguous derivation of H_0, thus providing a reliable extragalactic distance scale and, as a consequence, accurate luminosity values for individual galaxies.

7.5 Concluding Remarks

In this chapter we have attempted to summarize the most important general aspects of the work presented in this thesis. The study of the characteristic X-ray properties of galaxies has only recently started to gain momentum, but the enormous scope for further research using the extraordinary capabilities of the next generation of X-ray astronomy facilities should hopefully be evident to all.

APPENDIX : X-RAY ASTRONOMY DATA ANALYSIS TECHNIQUES

A.1 Introduction

Although the work presented in this thesis is primarily concerned with the analysis and interpretation of Einstein X-ray data, we feel that it would not be appropriate to provide a complete guide to all of the data analysis techniques that have been adopted. In this brief appendix we will instead emphasize several specialized procedures which have proved to be of fundamental importance to our data analysis scheme; various useful definitions and items of nomenclature will also be established. A definitive guide to X-ray astronomy data analysis techniques has yet to be published, thus any expertise in the subject simply reflects the application of common sense and the received wisdom of other, more experienced workers in this field. Two important sources of information, which have directly influenced much of the work presented herein, are the "Einstein Observatory User's Manual" and "The Einstein Cookbook". Both documents are available from the Harvard-Smithsonian Center for Astrophysics, and are essential reading for anyone attempting to analyse Einstein data.

A.2 Observation Processing Status and Automatic Scientific Analysis

Routine processing of all Einstein IPC, HRI and MPC observations is performed by the High Energy Astrophysics Division of CFA. The raw data from each observation is reduced into sorted data file form and subjected to an automatic scientific analysis. A sorted data file is fundamentally a list of detected X-ray photons. Each photon is time-tagged, and depending on the characteristics of the particular instrument may also be assigned a pulse-height channel and/or an

instrumental pixel position. Subsiduary data files, suitable for use in a detailed analysis, are constructed by selecting appropriate pixel, pulse-height channel and temporal windows.

The processing of Einstein observations at CFA has proved to be a lengthy, multi-stage operation. Final reprocessing of HRI and MPC observations is now complete, thus all data obtained from these instruments, and presented in the preceding chapters, are in their definitive form. The reprocessing of IPC observations, which commenced during 1983 and is not complete as of December 1984, is considerably more complex than for the other instruments, principally because of the corrections necessitated by the IPC's variable gain. All IPC observations discussed in this thesis are in a preliminary processed form, ie. they incorporate first-order gain corrections. Harnden et al. (1984) have recently published a detailed specification for the ultimate observation processing and automatic scientific analysis scheme now being routinely implemented for all IPC observations.

As we have already noted, an automatic scientific analysis is performed for each completed Einstein observation. The results summary generated by this procedure provides an excellent basis for more detailed studies, but should not be used in isolation since most of the data analysis algorithms are of necessity optimized for ease and speed of execution rather than precision of results. The primary aim of the automatic scientific analysis of an observation is to detect and parameterize all statistically significant X-ray sources contained within the FOV of the relevant instrument. A sliding-box algorithm is used to test an array of uniformly spaced pixel locations

within an IPC or HRI image for statistically significant excesses above the local image background level (see Giacconi et al. 1979b). The algorithm proceeds iteratively, continually updating the map of the background and sources until a consistent solution is obtained, whereupon maximum likelihood techniques are implemented in order to estimate the intensity and locate the centroid of each detected source. Even relatively sophisticated source detection methods, such as the sliding-box algorithm, can produce spurious results when applied to image regions which exhibit a high source density or patchy diffuse emission. Use of an independent method of source detection is strongly recommended (for an example, see A.4). Detection thresholds for the sliding-box algorithm are determined using artificial data and are always consistent with the expectation of detecting no more than one spurious source per field (ie. an artefact of counting statistics). Throughout this thesis we have adopted a more severe five sigma criterion for independent source existence (ie. $S/(S + B)^{1/2} \geqslant 5$, where S + B is the number of counts in a detection cell expected to contain B background counts), or a weaker three sigma criterion if the celestial position of the source corresponds to an identifiable optical counterpart. X-ray source detection is conceptually simpler for MPC data. Only one source per FOV can be directly distinguished by the MPC because of its non-imaging characteristics, hence a simple statistical test of the measured count rate versus the predicted background level is sufficient.

The automatic scientific analysis software filters the source detection results and selects those X-ray sources which are sufficiently strong for more detailed studies; these include spectral

analysis (IPC and MPC), determination of angular extent (IPC and HRI), and analysis of temporal characteristics (IPC, HRI and MPC). This analysis is necessarily limited to procedures which are relatively simple to implement; it is in no sense a thorough and complete determination of the properties of a detected source. Comprehensive analysis of Einstein data is invariably performed off-line, using the automatic analysis results as a guide.

A.3 Analysis of X-ray Spectra using IPC and MPC Data

The IPC does possess a rather limited spectral capability, so it is in principle possible to derive information about the spectral properties of a detected X-ray source. In practice, a satisfactory spectral analysis of IPC data is difficult to achieve. The instrument's coarse energy resolution and restricted energy range severely limit its effectiveness as an X-ray spectrometer. In addition, temporal and spatial gain variations introduce further uncertainties into results derived from non-reprocessed data. Spectral analysis of MPC data is conceptually similar, but easier to implement because the data is in a definitive form and the instrument is fully calibrated. Like the IPC, the MPC does suffer from rather coarse energy resolution: 8 pulse-height channels between 1 and 20 keV. Of greater practical importance is the fact that due to its non-imaging nature the MPC is relatively insensitive; useful spectral information can be obtained only for sources brighter than $\sim$0.3 Uhuru ct s^{-1} (Halpern 1982).

The minimum requirement for useful spectral analysis of IPC data is that the detected source yields at least 100 net counts. If this criterion is satisfied the following procedure can be adopted. A

pulse-height spectrum is constructed from all of the X-ray photons detected within a suitable cell which encompasses the X-ray source. The shape and size of the cell should be optimized to match the morphology and angular size of the source. For example, an unresolved source situated at the centre of the IPC FOV would require a 3 arcmin radius cell. An equivalent background pulse-height spectrum is constructed using a nearby source-free region of the image (usually concentric with the source cell). The observed background spectrum is used to estimate the background contribution to each pulse-height channel in the source cell spectrum. This is a complex process, requiring the application of corrections for (a) spatial and temporal variations in instrumental gain, (b) instrumental dead time, (c) mirror vignetting, and (d) energy-dependent scattering of source photons beyond the cell boundaries. Standard chi-squared fitting techniques are then used to compare model X-ray spectra with the background subtracted source spectrum. A sequence of parameterized models are convolved with the gain-dependent IPC effective area and energy resolution functions, and tested against the data via the chi-squared statistic. For non-reprocessed IPC data the instrumental gain, represented by the parameter BAL, is ill-determined. Spectral fits are therefore usually performed for a range of IPC gains, eg. BAL $\pm$ 1.5, to cover possible uncertainties. Allowed ranges for model parameters are derived using the prescription of Lampton et al. (1976). Models with more than two fitted paramters are not generally warranted by the quality of the IPC spectral data. Spectral fitting is usually limited to those pulse-height channels which form a contiguous set with each channel having S/N $\geqslant$ 2. For X-ray sources fainter than $\sim$ 0.3 IPC ct s^{-1} this useful channel range usually

corresponds to roughly 0.5 to 3.0 keV. A high proportion of the measured IPC counts above and below these energy limits are due to the instrumental calibration source and cosmic soft X-ray background, respectively.

Although spectral fits to IPC data rarely allow tight constraints to be derived for model parameters, they do at least allow energy fluxes to be calculated (accurate to $\lesssim \pm 20\%$ for on-axis, unresolved sources). For weak sources fluxes are simply calculated by convolving a "best-guess" spectrum with the IPC effective area and normalizing with the observed count rate. An identical procedure is adopted for the calculation of fluxes for sources detected in HRI images.

Spectral analysis of MPC data is performed using procedures exactly equivalent to those used for IPC data. Due to the instrument's non-imaging nature, no direct measurement of the background contribution to an observed spectrum is available. A reliable model of the background contribution is derived from correlations between satellite orbital characteristics (eg. sun angle, position relative to radiation belts) and measured instrumental parameters during the observation (see Halpern 1982). After background subtraction the signal to noise in the two highest energy channels is usually very low, thus restricting the useful energy range for spectral model fitting to 1-10 keV. This is sufficient to allow a reasonably accurate determination of the shape of the X-ray continuum of a relatively bright X-ray source at energies beyond the range of the IPC.

A.4 The Cross-Correlation Algorithm for Point Source Detection

This algorithm, formulated by R. Willingale at Leicester University

and first used in the analysis of an IPC image of the galactic centre (Watson et al. 1981), has been extensively utilized in the course of this thesis and therefore warrants further discussion. The cross-correlation algorithm is designed to locate and parameterize unresolved X-ray sources in IPC and HRI images. It is superior to the sliding-box algorithm because the instrumental response is directly incorporated into the source detection procedure, and is therefore less likely to yield spurious results when applied to image regions which exhibit complex structure or high source density. The algorithm essentially iterates a model of a smooth image background (which incorporates the gross structure of any extended X-ray emission) upon which unresolved sources are superimposed. An initial estimate of the image background is constructed from a five-fold smoothing of the raw image (via a cross-correlation with the instrumental PRF). This smooth model of the background is subtracted from the raw image, and the residual smoothed once. A least squares analysis converts the smooth background model into a crude statistical significance map (ie. RMS scatter as a function of pixel location). This smoothed residual is divided by the RMS map in order to generate a map of statistically significant X-ray sources, ie. features which accurately mimic the PRF. The detected sources are subtracted from the raw data, which is then re-smoothed to form an updated model of the image background. This procedure is iterated until a consistent solution is obtained. Two maps are eventually generated; one containing the locations of the detected sources (their celestial coordinates and intensities are also derived), the other displaying the gross structure of the image background and any diffuse emission.

A.5 Image Restoration and Display Techniques

Unlike radio or optical images, the X-ray images generated by the IPC and HRI contain relatively few photons. Only long exposures of very bright sources can be considered to be true images, in the sense that the number of counts in a particular pixel accurately labels the local surface brightness. For the majority of observations a pixel is simply a box which may contain a photon or two. The data is therefore severely limited by the effects of counting statistics (photon noise).

The simplest solution to this formidable data processing problem is to rebin groups of pixels together in order to locally improve counting statistics, albeit at the expense of resolution. This solution is unsatisfactory, however, because discrete features evident in a rebinned image alter significantly if the rebinning origin is shifted by one or more pixels. Image restoration can, in principle, be best achieved by the use of an algebraic deconvolution technique to remove effects due to counting statistics and instrumental response (eg. the MEM, Willingale 1981). Such techniques are difficult to implement for X-ray images, primarily due to the lack of a suitable statistic to test the deconvolved solution against the data, and hence drive the algorithm towards a convergent solution. Chi-squared statistics are inappropriate for the typically low counts per pixel levels, and even cumulative distribution statistics (eg. D^2) tend to be inadequate because of the very limited dynamic range of the data. MEM deconvolutions of some of the HRI images discussed in this thesis have been attempted, but invariably yielded statistically unacceptable solutions.

In practice the only reliable and easily implemented restoration

technique for X-ray images consists of convolving the raw data with a suitable 2-D smoothing function. This technique at least suppresses photon noise, albeit usually at the expense of resolution. Large scale structure can be examined by smoothing an image with a gaussian function: $\exp -(r^2/2\sigma^2)$, with $\sigma >> PRF$. Fine detail can be studied at the best attainable resolution by smoothing the data with the appropriate instrumental PRF. Real features of differing angular size become evident when the data is smoothed with a wide range of 2-D functions.

The most useful methods of displaying smoothed images are grey scale plots and contour diagrams. Careful choice of surface brightness levels allow specific features to be selectively enhanced. A crude estimate of the statistical significance of a particular surface brightness level can be established by calculating the mean RMS scatter per pixel of source-free regions of the smoothed image. A contour level corresponding to C counts per pixel above background can be considered to be essentially n-sigma if $C = n \times RMS$. This definition applies to all grey scale diagrams and contour maps presented in this thesis.

References

Abbreviations

Ap.J.	Astrophysical Journal
A.J.	Astronomical Journal
MNRAS	Monthly Notices of the Royal Astronomical Society
Astr.Ap	Astronomy and Astrophysics
Adv.Space.Res.	Advances in Space Research
Ann.Rev.Astr.Ap.	Annual Review of Astronomy and Astrophysics
BAAS	Bulletin of the American Astronomical Society

Axon, D.J., and Taylor, K. 1978, Nature, 274, 37.

Bailey, M.E. 1980, MNRAS, 191, 195.

Balkowski, C. 1979, Astr.Ap., 78, 190.

Bechtold, J., Forman, W., Giacconi, R., Jones, C., Schwarz, J., Tucker, W., and Van Speybroeck, L. 1983, Ap.J., 265, 26.

Bertola, F., Capaccioli, M., and Oke, J.B. 1982, Ap.J., 254, 494.

Bieging, J.H., and Biermann, P. 1977, Astr.Ap., 60, 361.

Biermann, P., Clarke, J.N., and Fricke, K.J. 1979, Astr.Ap., 75, 7.

Biermann, P., Kronberg, P.P., and Madore, B.F. 1982, Ap.J. (Letters), 256, L37.

Biermann, P., and Kronberg, P.P. 1983, Ap.J. (Letters), 268, L69.

Bignami, G.F., Caraveo, P.A., and Lamb, R.C. 1983, Ap.J. (Letters), 272, L9.

Bingham, R.C., McMullen, D., Pallister, W.S., White, C., Axon, D.J., and Scarrott, S.M. 1976, Nature, 259, 463.

Blair, W.P. 1981, in Supernovae (p475), ed. Rees, M.J., and Stoneham, R.

Blair, W.P., Kirshner, R.P., and Winkler, P.F. 1983, Ap.J., 272, 84.

Bottinelli, L., and Gouguenheim, L. 1978, Astr.Ap., 64, L3.

Bradt, H.V., and McClintock, J.E. 1983, Ann.Rev.Astr.Ap., 21, 13.

Bregman, J.N. 1978, Ap.J., 224, 768.

Bregman, J.N. 1980, Ap.J., 237, 681.

Burbidge, E.M., Burbridge, G., and Rubin, V.C. 1964, Ap.J., 140, 942.

Burstein, D., and Heiles, C. 1982, A.J., 87, 1165.

Caldwell, N. 1982, Ph.D. thesis, Yale University.

Canizares, C.R., Clark, G.W., Jernigan, J.G., and Markert, T.H. 1982, Ap.J., 262, 33.

Canizares, C.R., Stewart, G.C., and Fabian, A.C. 1983, Ap.J., 272, 449.

Clark, D.H., Doxsey, R., Li, R., Jernigan, J.G., and van Paradijs, J. 1978, Ap.J. (Letters), 221, L37.

Cottrell, G.A. 1976, MNRAS, 174, 455.

Cottrell, G.A. 1977, MNRAS, 178, 577.

Cowie, L.L., and Binney, J. 1977, Ap.J., 215, 723.

Cox, D.P. 1972, Ap.J., 178, 143.

de Jong, T., et al. 1984, Ap.J. (Letters), 278, L67.

de Vaucouleurs, G. 1975, Stars and Stellar Systems, Vol IX, p566, Univ. Chicago Press.

de Vaucouleurs, G., de Vaucouleurs, A., and Corwin, H.G. 1976, Second Reference Catalogue of Bright Galaxies, Texas Press, Austin.

Disney, M.J., and Wall, J.V. 1977, MNRAS, 179, 235.

Disney, M.J., Sparks, W.D., and Wall, J.V. 1984, MNRAS, 206, 899.

Draine, B.T., and Saltpeter, E.E. 1979, Ap.J., 231, 77.

Dressel, L.L., and Condon, J.J. 1978, Ap.J.Suppl., 36, 53.

Dressel, L.L., Bania, T.M., and O'Connell, R.W. 1982, Ap.J., 259, 55.

Dressel, L.L., and Wilson, A.S. 1983, BAAS, 15, 913.

Ekers, R.D., Goss, W.M., Wellington, K.J., Bosma, A., Smith, R.M., and Schweizer, F. 1983, Astr.Ap., 127, 361.

Elvis, M., and Van Speybroeck, L. 1982, Ap.J., 257, L51.

Elvis, M., Soltan, A., and Keel, W.C. 1984, Ap.J., 283, 479.

ESA 1982, Exosat Observers Guide Part II: Exosat Observers Handbook.

Fabbiano, G., Fiegelson, E., and Zamorani, G. 1982, Ap.J., 256, 397.

Fabbiano, G., Trinchieri, G., and Macdonald, A. 1984, Ap.J., 284, 65.

Fabbiano, G., and Trinchieri, G. 1984, Preprint, CFA.

Faber, S.M., and Gallagher, J.S. 1976, Ap.J., 204, 365.

Fabian, A.C., and Nulsen, P.E.J. 1977, MNRAS, 180, 479.

Fabian, A.C., Schwarz, J., and Forman, W. 1980, MNRAS, 192, 135.

Fabian, A.C., Hu, E.M., Cowie, L.L., and Grindlay, J. 1981, Ap.J., 248, 47.

Fabricant, D., Branduardi, G., Gorenstein, P., and Zamorani, G. 1979, BAAS, 11, 784.

Forman, W., et al. 1978, Ap.J.Suppl., 38, 357.

Forman, W., Schwarz, J., Jones, C., Liller, W., and Fabian, A.C. 1979, Ap.J. (Letters), 234, L27.

Forman, W., Bechtold, J., Blair, W., and Jones, C. 1981, in X-ray Astronomy with the Einstein Satellite, p187, Reidel.

Forman, W., Jones, C., Tucker, W.H. 1983, proc. Trieste Meeting on Clusters, in press.

Fosbury, R.A.E., Mebold, U., Goss, W.M., and Dopita, M.A. 1978, MNRAS, 183, 549.

Fried, P.J., Nousek, J.A., Sanders, W.T., and Kraushaar, W.L. 1980, Ap.J., 242, 987.

Gallagher, J.S., Faber, S.M., and Balick, B. 1975, Ap.J., 202, 7.

Giacconi, R., Kellogg, E., Gorenstein, P., Gursky, H., and Tananbaum, H. 1971, Ap.J. (Letters), 165, L27.

Giacconi, R., et al. 1979a, Ap.J., 230, 540.

Giacconi, R., et al. 1979b, Ap.J. (Letters), 234, L1.

Gisler, G.R. 1976, Astr.Ap., 51, 137.

Griffiths, R.E., Johnston, M.D., Schwartz, D.A., Schwarz, J., and Blades, J.C. 1979, Ap.J. (Letters), 230, L21.

Griffiths, R.E., et al. 1983, Ap.J., 269, 375.

Halpern, J. 1982, Ph.D. thesis, Harvard University.

Hargrave, P.J. 1974, MNRAS, 168, 491.

Harnden, F.R., Fabricant, D.G., Harris, D.E., and Schwarz, J. 1984, Smithsonian Astrophysical Observatory, Special Report 393.

Heiles, C. 1975, Astr.Ap.Suppl., 20, 37.

Heiles, C., and Cleary, M.N. 1979, Austr.J.Physics, Astrophys.Suppl., 47, 1.

Hodge, P.W. 1973, Ap.J., 182, 671.

Hogbom, J.A. 1974, Astr.Ap.Suppl., 15, 417.

Hubble, E. 1936, The Realm of the Nebulae, Yale University Press.

Hummel, E. 1980, Astr.Ap.Suppl., 41, 151.

Hummel, E., and Kotanyi, C.G. 1982, Astr.Ap., 106, 183.

Hummel, E., Kotanyi, C.G., and Ekers, R.D. 1983, Astr.Ap., 127, 205.

Illingworth, G. 1983, in Internal Kinematics and Dynamics of Galaxies, p257, Riedel.

Jenkins, C.R. 1982, MNRAS, 200, 705.

Jenkins, C.R. 1983, MNRAS, 205, 1321.

Jenkins, E.B., and Savage, B.D. 1974, Ap.J., 187, 243.

Jones, C., and Forman, W. 1984, Ap.J., 276, 38.

Jones, D.L., Wrobel, J.M., and Shaffer, D.B. 1984, Ap.J., 276, 480.

Kellermann, K.I., Pauliny-Toth, I.I.K., and Williams, P.J.S. 1969, Ap.J., 157, 1.

Kellermann, K.I. 1974. Galactic and Extra-Galactic Radio Astronomy, p332, Springer-Verlag, New York.

King, I.R. 1978, Ap.J., 222, 1.

Knapp, G.R., Kerr, F.J., and Williams, B.A. 1978, Ap.J., 222, 800.

Knapp, G.R., and Gunn, J.E. 1982, A.J., 87, 1634.

Kriss, G.A., Cioffi, D.F., and Canizares, C.R. 1983, Ap.J., 272, 439.

Kronberg, P.P., Pritchet, C.J., and van den Bergh, S. 1972, Ap.J. (Letters), 173, L47.

Kronberg, P.P., and Wilkinson, P.M. 1975, Ap.J., 200, 430.

Kronberg, P.P., and Clarke, J.N. 1978, Ap.J. (Letters), 224, L51.

Kronberg, P.P., Biermann, P., and Schwab, F.R. 1981, Ap.J., 246, 751.

Kronberg, P.P., and Biermann, P. 1983, in Supernova Remnants and their X-ray Emission, p583, IAU.

Lampton, M., Margon, B., and Bowyer, S. 1976, Ap.J., 208, 177.

Lea, S.M., Silk, J., Kellogg, E., and Murray, S. 1973, Ap.J. (Letters), 184, L105.

Lea, S.M., Mushotzky, R.F., and Holt, S.S. 1982, Ap.J., 262, 24.

Long, K.S., and Helfand, D.J. 1979, Ap.J. (Letters), 235, L77.

Long, K.S., and Van Speybroeck, L. 1983, in Accretion Driven Stellar X-ray Sources, eds. Lewin, W.H.G., and van den Heuvel, E.P.J., Cambridge Univ Press.

Lynds, C.R., and Sandage, A.R. 1963, Ap.J., 137, 1005.

MacDonald, J., and Bailey, M.E. 1981, MNRAS, 197, 995.

Mathews, W.G., and Baker, J.C. 1971, Ap.J., 170, 241.

McHardy, I.M., et al. 1981, MNRAS, 197, 893.

Murray, S.S., et al. 1984, Proposal to NASA for HRC on AXAF.

Mushtozky, R.F., Marshall, F.E., Boldt, E.A., Holt, S.S., and Serlemitsos, P.J. 1980, Ap.J., 235, 361.

Nulsen, P.E.J., Stewart, G.C., and Fabian, A.C. 1984, MNRAS, 208, 185.

O'Connell, R.W., and Mangano, J.J. 1978, Ap.J., 221, 62.

Palumbo, G.G.C., Maccacaro, T., Zamorani, G., Panagia, N., and Vettolani, G. 1981, Ap.J., 247, 484.

Patterson, J. 1981, Nature, 292, 810.

Perley, R.A., Willis, A.G., and Scott, J.S. 1979, Nature, 281, 437.

Raimond, E., Faber, S.M., Gallagher, J.S., and Knapp, G.R. 1981, Ap.J., 246, 708.

Raymond, J.C., and Smith, B.W. 1977, Ap.J.Suppl., 35, 419.

Rieke, G.H., and Low, F.J. 1972, Ap.J. (Letters), 176, L95.

Rieke, G.H., Lebofsky, M.J., Thompson, R.I., Low, F.J., and Tokunaga, A.T. 1980, Ap.J., 238, 24.

Sadler, E.M. 1984, A.J., 89, 53.

Sandage, A.R. 1961, The Hubble Atlas of Galaxies.

Sandage, A.R, and Tammann, G.A. 1975, Ap.J., 196, 313.

Sanders, R.H. 1980, Ap.J., 242, 931.

Sanders, R.H. 1981, Ap.J., 244, 820.

Sarazin, C.L., and O'Connell, R.W. 1983, Ap.J., 268, 552.

Schanberg, B.C. 1973, Ap.J.Suppl., 26, 115.

Schwartz, D.A., et al. 1984, Proposal to NASA for HRIS on AXAF.

Seaton, M.J. 1979, MNRAS, 187, 785.

Serlemitsos, P.J., Smith, B.W., Boldt, E.A., Holt, S.S., and Swank, J.H. 1977, Ap.J. (Letters), 211, L63.

Seward, F.D., and Mitchell, M. 1981, Ap.J., 253, 736.

Shapiro, P.R., and Field, G.B. 1976, Ap.J., 205, 762.

Solinger, A., Morrison, P., and Markert, T. 1977, Ap.J., 211, 707.

Spitzer, L. 1978, Physical Processes in the Interstellar Medium, Wiley.

Stewart, G.C., Canizares, C.R., Fabian, A.C., and Nulsen, P.E.J. 1984, Ap.J., 278, 536.

Stewart, G.C., Fabian, A.C., Jones, C., and Forman, W. 1984, Ap.J., 285, 1.

Stocke, J., et al. 1983, Ap.J., 273, 458.

Tammann, G.A., and Sandage, A.R. 1968, Ap.J., 151, 825.

Tammann, G.A. 1981, in Supernovae (p371), ed. Rees, M.J., and Stoneham, R., Reidel.

Thonnard, N. 1982, in The Comparative HI Content of Normal Galaxies (p65), Proceedings of a Green Bank Workshop.

Tonry, J.L., and Davis, M. 1981, Ap.J., 246, 666.

Trumper J. 1982, MPI preprint.

Tucker, W.H., and Rosner, R. 1983, Ap.J., 267, 547.

Unwin, S.C. 1980, MNRAS, 190, 551.

Vader, J.P., Van den Heuvel, E.P.J., Lewin, W.H.G., and Taken, R.J. 1982, Astr.Ap., 113, 328.

Vaiana, G.S., et al. 1981, Ap.J., 244, 163.

van den Bergh, S. 1976, A.J., 81, 795.

van Paradijs, J., and Verbunt, F. 1981, Space Science Rev., 30, 361.

Van Speybroeck, L., et al. 1979, Ap.J. (Letters), 234, L45.

Visvanathan, N., and Sandage, A.R. 1972, Ap.J., 176, 57.

Visvanathan, N. 1974, Ap.J., 192, 319.

Wall, J.V., Pearson, T.J., and Longair, M.S. 1980, MNRAS, 193, 683.

Wall, J.V., Pearson, T.J., and Longair, M.S. 1981, MNRAS, 196, 597.

Wall, J.V., Scheuer, P.A.G., and Pauliny-Toth, I.I.K. 1982, MNRAS, 198, 221.

Watson, M.G., Willingale, R., Grindlay, J.E., and Hertz, P. 1981, Ap.J., 250, 142.

Watson, M.G., Willingale, R., Grindlay, J.E., and Seward, F.D. 1983, Ap.J., 273, 688.

White, R.E., and Chevalier, R.A. 1983, Ap.J., 269, 102.

White, R.E., and Chevalier, R.A. 1984, Ap.J., 280, 561.

Williams, T.B., Caldwell, N., and Schommer, R.A. 1983, Preprint RU-29-83.

Willingale, R. 1981, MNRAS, 194, 359.

Willis, A.G., Strom, R.G., Bridle, A.H., and Fomalont, E.B. 1981, Astr.Ap., 95, 250.

York, D.G. 1982, Ann.Rev.Astr.Ap., 20, 221.

Zombeck, M.V. 1983, Adv.Space.Res., 2, part IV (p259).

Einstein X-ray Observations of Galaxies

by

V.J. Stanger

Abstract

The high sensitivity and precise imaging provided by the Einstein Observatory instrumentation has enabled detailed X-ray studies of a variety of astrophysical phenomena to be performed. In this thesis Einstein observations are used to investigate the characteristic X-ray properties of galaxies, thus allowing a galaxy's X-ray emission to be related to the properties and evolution of its stellar population(s).

Analysis of Einstein HRI data for M82 - an archetypal peculiar galaxy - reveals complex structure both in the "starburst" nuclear region and in the galaxy's halo. The nuclear region's X-ray morphology corresponds closely with Population I optical features, thus linking the emission directly to the intense star formation activity. Moreover, the halo of diffuse X-ray emission distributed along the minor axis of M82 indicates thermal emission from outflowing hot gas, which is maintained by starburst-induced supernova heating; rapid cooling near shock fronts probably causes the observed correlation with the famous Hα filament system.

The majority of this thesis is devoted to an investigation of the X-ray properties of early type galaxies. Analysis of luminosity correlations displayed by the class as a whole, complemented by detailed studies of individual galaxies, confirms previous suggestions that for many early type galaxies thermal emission from hot gas is the dominant X-ray emission mechanism. Supernova-driven hot winds keep some galaxies essentially gas free; their X-ray emission originates principally from stellar sources. In other galaxies hot gas generated by stellar evolution is retained and possibly incorporated into cooling flows. High resolution X-ray and radio studies of NGC 4636 and NGC 4649 confirm that cooling flow scenarios are viable for the central regions of both galaxies, thus explaining the fueling of the observed radio sources.

Finally, the possibilities for further research presented by both current and future observational facilities are discussed.